CRANFIELD UNIVERSITY

COLLEGE OF DEFENCE TECHNOLOGY
ENGINEERING SYSTEMS DEPARTMENT

PhD Thesis

Academic Year

2004 – 2005

Student Name

Matthew Paul Jevons

THE EFFECTS OF FIBRE PRE-STRESSING ON THE IMPACT PERFORMANCE OF COMPOSITE LAMINATES

Supervisors

Dr Michael J Iremonger, Professor John G Hetherington

Submitted

October 2004

This page is intentionally blank.

ACKNOWLEDGEMENTS

Most importantly I would like to thank my wife, Naomi, for her love and patience these last few years, giving up much to let me work on my thesis and supporting me in my times of need.

I would like to extend my thanks and gratitude also to my supervisors, Dr Iremonger and Professor Hetherington, for their support, advice and encouragement.

As this study was funded by the EPSRC and Cranfield University I would also like to thank these establishments for their financial support during this work.

For their help in the latter part of my work I would like to thank Mr Mike Stephens and Mr Eoin Simon and all the staff in the Composites Research department at Airbus UK, Filton, for giving so freely of their time, support and advice.

Thanks go to Dr Jenny Keeble and the staff in the Materials Analysis Department at Airbus UK for allowing me access and use of their polishing and microscopy equipment these last twelve months.

Mrs Maggie Keats and Mrs Ros Gibson also deserve mention and thanks for their administrative support but also by offering a friendly face and chat whenever needed.

I would like to thank the following people for their support and help at stages throughout the study:

Mike Teagle, Dr Julie Etches, Dr Crispin Doyle, Jim Harber, Brian Duguid, Dr Stewart McGuigan, Dr Ian Horsfall, Mrs Celia Watson

I would also like to acknowledge the following people’s involvement in making this work possible:

Dr Gerard Fernando, Dr Gurdip Kalsi

ABSTRACT

This thesis has presented the results and findings of a study carried out into the effects of fibre pre-stressing on the impact performance of composite laminates. Fibre pre-stress has been explained as a way of mechanically altering the internal residual stress state of a composite, which typically is a result of thermal, moisture and chemical expansions. It has been suggested that pre-stressing can offer potential benefits to composites by reducing or reversing the hygro-thermal stresses in a composite. It has also been suggested that the impact performance could be improved through fibre pre-stressing, which has given rise to this study.

In this study panels have been made with various levels of pre-stress. A special system was developed to apply pre-stress to the laminates and the produced laminates were tested under low- and high-velocity impact regimes. To apply these regimes, an instrumented falling weight and a gas gun were used respectively. A short finite element study was carried out to supplement the experimental study and offer further insight into the failure mechanics.

The main findings of the study were that although pre-stressing had no discernable effect on the high-velocity impact performance of the composite laminate considered, there was a noted effect on the low-velocity impact performance. Under low-velocity impacts the laminate showed an improved impact performance for increase levels of pre-stress, except at one critical pre-stress level (60 MPa), where the laminate absorbed less energy per damage area compared with unpre-stressed laminates.

This page is intentionally blank.

TABLE OF CONTENTS

LIST OF FIGURES

This page is intentionally blank.

1. LISTS OF ABBREVIATIONS, SYMBOLS AND SUB AND SUPERSCRIPTS

1.1. Abbreviations

PTFE	Poly-tetra-fluoro-ethylene
CRAG	Composites Research Advisory Group
BS	British Standards
PC	Personal computer
A/D	Analogue/digital
DSO	Digital storage oscilloscope
IFW	Instrumented falling weight
FE	Finite element
FEA	Finite element analysis
FEM	Finite element method
LSTC	Livermore Software Technology Corporation
UD	Unidirectional (refers to a composite ply where all the fibres run in the same direction)
AOPT	Material axis option (LS-DYNA orthotropic material control parameter)
MACF	Material axis change flag (LS-DYNA orthotropic material control parameter)
V1, V2, V3	Vectors in the global x, y and z directions respective (used to define material orientation in LS-DYNA)
N.A.	Neutral Axis
ALPH	Non-linear shear stress parameter (as defined in LS-DYNA)
DFAILM	Maximum strain in matrix for failure (parameter defined in LS-DYNA material types 54 and 55)
DFAILS	Maximum shear strain for failure (parameter defined in LS-DYNA material types 54 and 55)
FBRT	Softening of fibre tensile strength (parameter defined in LS-DYNA material types 54 and 55)
DFAILT	Maximum strain for fibre tension (parameter defined in LS-DYNA material types 54 and 55)

DFAILC	Maximum strain fro fibre compression (parameter defined in LS-DYNA material types 54 and 55)
EFS	Effective failure strain (parameter defined in LS-DYNA material types 54 and 55)
CRIT	Failure criterion (parameter defined in LS-DYNA material types 54 and 55)
SG, sg	Strain gauge
Temp, temp	Temperature
EN	European Norm (European Standards)

1.2. Symbols

δ	Infinitesimal change in length
L	Length, original length in strain measurement
ε	Strain
σ	Stress
V	Volume of a solid, fibre or matrix volume fraction when used with subscript f or m respectively
E	Young's Modulus
α	Coefficient of thermal expansion
Δ	Infinitesimal change (used mostly for temperature in this study)
T	[1] Temperature [2] Transfer matrix
ν	Poisson ratio
C	Component of the stiffness matrix of a material
P	Load
G	Shear modulus
K	Bulk modulus
SC	Shear strength (as defined in LS-DYNA)
XT	Tensile strength in the fibre direction (as defined in LS-DYNA)
XC	Compressive strength in the fibre direction (as defined in LS-DYNA for material types 54 and 55)
YT	Tensile strength transverse to the fibre direction (as defined in LS-DYNA)
YC	Compressive strength transverse to the fibre direction (as defined in LS-DYNA)

℄	Centre line
f	Material strength
G_{Ic}	Mode I fracture toughness
G_{IIc}	Mode II fracture toughness
N	Load vector in classical laminate analysis
M	Moment vector in classical laminate analysis
A	[1] Direct stiffness matrix in classical laminate analysis
	[2] Cross-sectional area
B	Bending-extension coupling stiffness matrix in classical laminate analysis
D	Bending stiffness matrix in classical laminate analysis
κ	Curvature vector
γ	Shear strain
θ	Angle of ply fibre direction (measured clockwise from global x-direction)
n	= sin(θ)
m	= cos(θ)

1.3. Subscripts

M, m	Refers to the matrix
F, f	Refers to the reinforcing fibres
C, c	Refers to the composite as a whole
1,2,3	Local coordinate system where 1 is in the fibre direction, 2 is in-plane and transverse to the fibre direction and 3 is out of plane and transverse to the fibre direction
11,22,33	Local coordinate system where 11 is in the fibre direction, 22 is in-plane and transverse to the fibre direction and 33 is out of plane and transverse to the fibre direction
r, z, θ	Cylindrical coordinate system, where r is in the radial direction, θ is in the circumferential direction and z is in the axial direction
t	Tensile
u	Ultimate
c	Compressive
x, y, z	Global coordinate system

1.4. Superscripts

P, p	Pre-stress
T	Thermal
Q	Reduced stiffness matrix
$\overline{Q}$	Reduced stiffness matrix in the global coordinate system
R	A residual stress/strain term

2. INTRODUCTION

The study presented in the pages of this thesis has considered the effects of pre-stressing on the impact performance of composite laminates. This chapter gives a brief introduction to the study, covering the aim of the work, a short background introduction, the method approach taken and a summary of the contents of the whole thesis.

2.1. Aim of Work

The principal aim of this study was to investigate how the low- and high-velocity impact damages induced in a composite laminate could be affected by mechanically pre-stressing its reinforcing fibres. The reasoning behind such an investigation was to evaluate how much the internal residual stress state of a composite laminate affected its impact performance and whether or not having the ability to alter the internal residual stress state could yield any benefits with regard to the impact performance.

2.2. Background

Looking at the present day aerospace, automotive, marine and renewable energy markets it quickly becomes apparent that composites are finding ever more use as primary structural components. Both Airbus and Boeing are producing aircraft with extensive use of composites in their primary structures. Mercedes-Benz have recently released the SLR together with McLaren, to produce a production car with major use of carbon composite primary structures; although other manufacturers have used composites for years, it has predominantly been as body panels fitted to metallic space-frame structures. Throughout all this extensive use of composites, the same concern has remained – that of out-of-plane impact threats to the laminate. Although

composites exhibit excellent strength properties in the plane of the laminate, through the thickness they rely solely on the strength of the matrix material. This leaves them with strengths typically an order of magnitude lower than in the in-plane directions. It comes then as no surprise that the field of science and engineering has dedicated much effort into improving the impact performance of composites over the years. Some solutions have been to improve the toughness and strength of the resin. Others have been to look into reinforcing the through-thickness direction with, for example, stitching or braiding.

Although not immediately obvious as another approach, since pre-stressing has arisen as an idea from the study of internal residual stresses, due to the cooling of a composite from curing temperature to ambient, the ability to change the internal stress state of a composite may yield benefits in the field of impact on composites. Some initial studies by Motahhari and Cameron (1997, 1998) and Fancey (2000a,b) have shown that indeed there may be some benefit. Despite there being a few limited engineering applications where the pre-stressing method becomes practical, its main benefit arises from allowing the engineer to better understand the implications of the residual stress state in a composite on the performance of the structure. Many applications of composites see the material being formed into complex shapes (aircraft belly fairings, car body panels), which can leave the composite with non-uniform in-plane stresses through the thickness of the laminate, as a result of thermal and chemical shrinkage. At the ECCM-11 in June 2004, Wisnom demonstrated that although in a flat panel thermal and chemical shrinkage have little effect in deforming the laminate out-of-plane, in highly curved laminates these residual stresses are great enough to deform the laminate out of its plane (referred to as spring-back or spring-

in). These geometric effects in highly curved laminates therefore have an effect on the internal residual stress state. A study into pre-stressing could then produce valuable insight into how much these changes could affect the mechanical performance of such a curved structure.

2.3. Method Approach

In industrial applications, the critical impacts are always considered on laminates rather than single plies or tows of fibres. It was therefore decided that in this study laminates should be tested. To make it easiest to infer any information from the panels, it was felt that flat panels should be used rather than curved ones, although it would have been easier to impart pre-stress into a cylinder by filament winding.

In laminates the most critical form of damage is delaminations – delaminations cause premature after-impact failure under in-plane compressive loading due to localised buckling of the delaminated areas. Delaminations are a result of differences in fibre orientation between plies. When a crack reaches a ply interface and the next ply has a different orientation, it has to reorient itself with the new fibre direction or with the ply interface. Orienting itself with the ply interface requires less energy, and therefore the crack follows this path. The more extreme the difference in fibre direction between plies, the more likely it is for a delamination to occur. It was therefore decided to choose a 0/90 type layup, as this would encourage the most delamination. Having more delamination when the differences in delamination were to be measured was then a desirable attribute to have in the laminates. It was hoped that with more delaminations the variation in delamination would be more measurable.

When studying the effects of pre-stressing on the impact performance of composites laminates, having more than one impact regime would be desirable, since they would represent different failure mechanisms. Having more than one mechanism of failure would help in determining what failure modes were affected by pre-stressing. Drop weight and gas gun impacts were chosen as they represented two different impact regimes, allowing the effect of pre-stressing to be measured under two different conditions.

Finally, to further understand the effect of pre-stressing on composite impact performance, analysis methods would also be of use. It was therefore decided to use both classical lamination theory to predict the residual stress states of the laminates and the finite element method to simulate the impact events. The classical laminate analysis was adapted to include pre-stressing terms, which allowed the ply residual stresses and strains to be calculated.

Although the finite element method is used extensively in research to carry out detail modelling of composite behaviour, it was decided to use a commercial code in this study to model the impact event using readily available models in the code and global modelling approaches, as may be found in industry. This was decided to determine, whether or not commercial failure models could adequately represent the effects of pre-stressing, or whether more consideration would be needed.

2.4. Contents of Study

This study has been broken down into eight chapters, the first of these being this introductory chapter. The second chapter gives an overview of the previous work conducted into the field of pre-stressing. Attempt has been made to cover the analysis

methods used to date in understanding pre-stress and to cover the experimental methods used to produce pre-stressed composites. The next chapter covers the experimental methods used in this study. Details have been given of the method used to produce pre-stressed laminates, the various test methods employed and the finite element approach used to supplement the experiments. The chapter following this presents the results of the experiments and of the finite element analyses. The results are only presented at this time as the two chapters following the results chapter then attempt to discuss the results and any matters arising. The first of the discussion chapters concentrates on the pre-stressing method, critically analysing the method and the panels produced. The second of the discussion chapters covers the experimental and finite element results. Here the results are broken down to explain any findings as well as presenting any implications these findings may have. The final two chapters are respectively the conclusions chapter, where the overall findings are again presented and the discussions are brought to a close, and the future work chapter, where any work is presented, which the author feels would significantly assist in better understanding pre-stress or would advance the field of engineering.

This page is intentionally blank.

3. LITERATURE REVIEW

The composite materials as discussed in this work fall into the category of long fibre reinforced materials. That is to say that these materials are made up of continuous high strength fibrous reinforcements bound together by a lower strength matrix material. These types of composites are found in applications such as the automotive and aerospace industries (Hull and Clyne, 1996). A common form in which the reinforcements come is in mats or tows of fibres, which are then impregnated with the resin material and cured into the finished shape desired. Such long fibre reinforced composite materials exhibit highly anisotropic properties, where the properties in the fibre direction are of an order of magnitude greater than those transverse to the fibre direction. To overcome this issue, composites are often made up by stacking multiple layers on top of one another where the fibre directions are at different angles to each other. This gives rise to composite laminates, which with the right stacking sequence can exhibit in-plane orthotropic or quasi-isotropic properties. However, the through-thickness properties would still be much lower than the in-plane properties (Hull and Clyne, 1996).

One issue with such laminated composites is that they may incur damage easily when loaded in the through-thickness direction. Low-velocity out-of-plane impacts can cause such loading and induce damage within the composite. The damage caused by low-velocity impacts would be indentation of the surface at the impact location, matrix cracking in the plies, delamination between the plies, fibre failure and spalling on the back face at the impact location (Abrate, 1998).

Efforts to improve composite properties are still ongoing. A particular field of study

is that of the analysis of pre-stressing. Here, the reinforcing fibres are stressed during the curing process to gain better effective mechanical properties. Among these improved properties, it is claimed that impact resistance may also be increased (Motahhari and Cameron, 1998, Fancey, 2000a, b).

This study is involved with the investigation into the effects of this method on the low- and high-velocity impact performance of composite laminates. Therefore this chapter will look at the previously published work and literature in the field of pre-stressing and how it may relate to the study of low-velocity impact of composites.

Motahhari and Cameron, 1998, and Fancey, 2000a, b, have carried out studies into the effect of pre-stressing on the impact performance of composites. Before discussing the findings of these studies, it will be useful to cover other published work on pre-stressed composites to gain a better understanding of the basic concepts, processes and issues surrounding pre-stressed composites.

3.1. Analysis of Pre-Stress

Pre-stressing changes the apparent mechanical properties of a composite, because the mechanical stressing of the fibres prior to and during cure and the subsequent release of this fibre stress only when the finished composite has been fully cured, superimposes a further stress-state onto the thermal residual stress-state within the composite which results from the curing process. Tuttle, 1988, showed in his analysis, that with the appropriate level of pre-stress these thermal residual stresses may be negated or even reversed. He reported, that when a composite is subjected to a negative change in temperature, as may be experienced when cooling a composite from its curing temperature, the different thermal expansions of the fibre and matrix

(where the thermal expansion of the fibres is around ten times lower than that of the matrix as it may be in E-glass fibre / epoxy resin systems) would cause a tensile residual stress in the matrix and a compressive one in the fibres. These thermal residual stresses can in turn severely reduce the mechanical strengths of the finished composite (Schulte and Marissen, 1992). By using micro-mechanics and macro-mechanics, Tuttle, 1988, Rose and Whitney, 1993, and Dvorak and Suvorov, 2000, managed to predict how pre-stressing would effect these thermal residual stresses. On a micro-mechanical level, Tuttle, 1988, and Rose and Whitney, 1993, proposed different methods to determine the residual stresses in fibre and matrix after pre-stressing. Tuttle's model was simpler, in effect only considering a one-dimensional problem in the fibre direction, where perfect bonding between fibre and matrix was assumed and as a result the strains in both phases in the fibre direction had to be equal. Figure 3.1 shows a diagram detailing this principle.

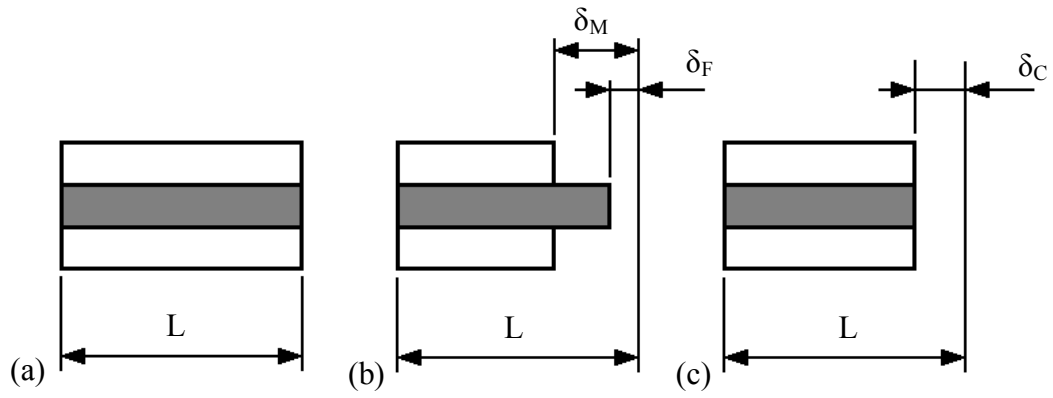

Figure 3.1 Diagram of overall strain in a cured composite unit element. (a) shows the unit element at curing temperature, (b) shows it after cooling if there were no bonding between fibres and matrix and (c) shows it after cooling with full bonding between fibres and matrix. Note that $\delta_F < \delta_C < \delta_M$.

From this, Tuttle was able to derive the following equations for the strains in the finished composite ply in the fibre direction and transverse to it as a function of

temperature and pre-stress:

$$\varepsilon_1^p = \frac{-\sigma_f^p V_f}{E_{11}} + \alpha_{11}\Delta T \qquad \textbf{(3.1)}$$

$$\varepsilon_2^p = \nu_{12}\left[\frac{\sigma_f^p V_f}{E_{11}}\right] + \alpha_{22}\Delta T \qquad \textbf{(3.2)}$$

where ν_{12} is the ply major in-plane Poisson ratio and E_{11}, α_{11} and α_{22} are given by:

$$E_{11} = V_f E_f + (1 - V_f)E_m \qquad \textbf{(3.3)}$$

$$\alpha_{11} = \frac{\alpha_f \nu_f E_f + \alpha_m (1 - V_f)E_m}{V_f E_f + (1 - V_m)E_m} \qquad \textbf{(3.4)}$$

$$\alpha_{22} = V_f \alpha_f + (1 - V_f)\alpha_m + V_f \nu_f \alpha_f + (1 - V_f)\nu_m \alpha_m - (V_f \nu_f + (1 - V_f)\nu_m)\alpha_1 \qquad \textbf{(3.5)}$$

also $\nu_{12} = V_f \nu_f + V_m \nu_m$. **(3.6)**

Tuttle was also able to derive the stresses in the fibres and the matrix due to pre-stressing with the following equations:

$$\sigma_f = E_f(\varepsilon_1^p - \alpha_f \Delta T) + \sigma_f^p \qquad \textbf{(3.7)}$$

$$\sigma_m = E_m(\varepsilon_1^p - \alpha_m \Delta T) \qquad \textbf{(3.8)}$$

Tuttle's method however did not allow for the stresses transverse to the fibre direction and around the fibre/matrix interface to be calculated. For this, the method proposed by Rose and Whitney, 1993, would have to be used. Rose and Whitney proposed to use what they called the concentric cylinder model in which the fibre and the matrix

phases would be modelled as two contacting concentric cylinders. The inner cylinder would represent the fibre phase and the outer the matrix phase. The ratio of the area of the inner to the outer would equate to the fibre volume fraction of the composite. Rose and Whitney adapted this model to incorporate pre-stress, allowing them to determine the stresses along and across the fibres and also at the fibre/matrix interface with the following equations:

$$\begin{Bmatrix} \sigma_z^m \\ \sigma_r^m \\ \sigma_\theta^m \end{Bmatrix} = \begin{bmatrix} C_{zz} & C_{zr} & C_{z\theta} \\ C_{rz} & C_{rr} & C_{r\theta} \\ C_{\theta z} & C_{\theta r} & C_{\theta\theta} \end{bmatrix}^m \begin{Bmatrix} \varepsilon_z^m - \alpha_z^m \Delta T \\ \varepsilon_r^m - \alpha_r^m \Delta T \\ \varepsilon_\theta^m - \alpha_\theta^m \Delta T \end{Bmatrix} \qquad \textbf{(3.9)}$$

$$\begin{Bmatrix} \sigma_z^f \\ \sigma_r^f \\ \sigma_\theta^f \end{Bmatrix} = \begin{bmatrix} C_{zz} & C_{zr} & C_{z\theta} \\ C_{rz} & C_{rr} & C_{r\theta} \\ C_{\theta z} & C_{\theta r} & C_{\theta\theta} \end{bmatrix}^f \begin{Bmatrix} \varepsilon_z^f + \varepsilon_p^f - \alpha_z^f \Delta T \\ \varepsilon_r^f - \nu_{12}^f \varepsilon_p^f - \alpha_r^f \Delta T \\ \varepsilon_\theta^f - \nu_{12}^f \varepsilon_p^f - \alpha_\theta^F \Delta T \end{Bmatrix} \qquad \textbf{(3.10)}$$

where the superscripts m and f refer to the matrix and fibre phases respectively, the subscripts z, r and θ refer to the axial, radial and hoop directions respectively and **C** refers to the stiffness matrix.

On a macro-mechanical or laminate level, Tuttle, 1988, Rose and Whitney, 1993, and Dvorak and Suvorov, 2000, all used the classical lamination theory. By adapting this method to include pre-stressing it allowed them to predict the overall ply and laminate strains and stresses. Both Tuttle, 1988, and Rose and Whitney, 1993, described this method only with little detail, but Dvorak and Suvorov, 2000, covered this analysis in much greater detail, presenting a clear approach and also presented their findings as first ply failure maps. Using the maximum stress criteria, their analysis showed that pre-stressing could indeed delay the onset of first ply failure to higher stress levels. In a later paper (Suvorov and Dvorak, 2002) they extended their model to include

viscoelastic stress relaxation to observe this effect on the final residual stress state of the laminate. Figure 3.2 shows failure maps from the analysis done in Dvorak and Suvorov, 2000, and in Suvorov and Dvorak, 2002. Dvorak was also involved in two further papers (Dvorak *et al.*, 1999, and Srinivas *et al.*, 1999) in which the authors analysed the effect of pre-stressing on submerged cylindrical vessels.

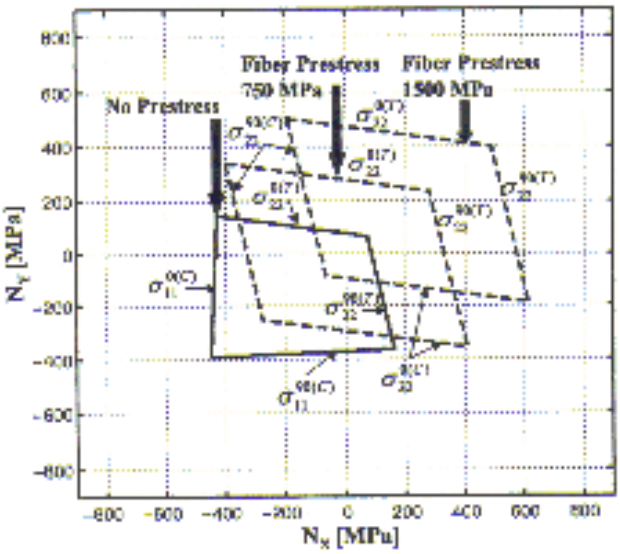

(a)

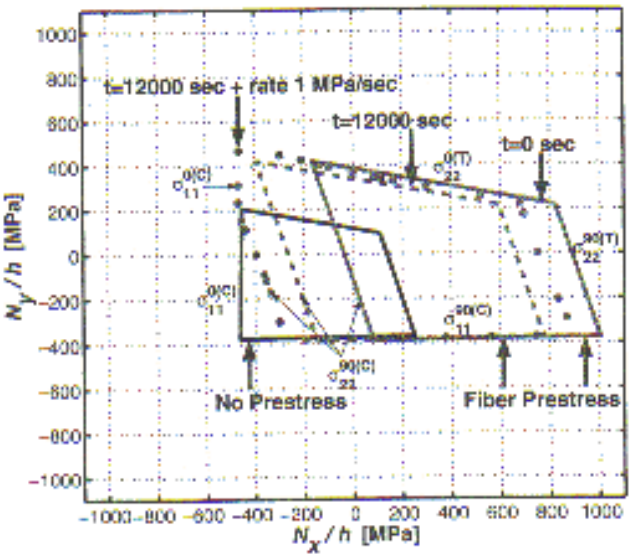

(b)

Figure 3.2 Failure maps from (a) Dvorak and Suvorov, 2000, for an S-glass/ epoxy resin system and (b) Suvorov and Dvorak, 2002, for the AS4/EPON 828 carbon fibre/epoxy resin system.

3.2. Experimental Studies

All these analytical methods present ways of predicting a composite's response to static loading conditions. No publication has been found to date, which attempts to predict the effects of pre-stressing on the transient dynamic loading of composites. Experimental publications in the investigation of pre-stressing are more numerous, however, and three of these (as detailed above) do observe the effects of pre-stressing on the low-velocity impact performance of composites.

Table 3.1 below lists the different approaches taken by authors to produce composites with pre-stress. No two authors have adopted the same method. This suggests that it is not a straightforward task. Although production methods differ a great deal, there is much less variation in the phenomena studied. Most authors chose to investigate the effect of pre-stressing on the matrix cracking behaviour. Some authors also looked at the tensile strength and modulus, impact energy absorption and balancing through-thickness variation in the hoop stress in filament wound tubes. More detail of this is given in the paragraphs following Table 3.1.

Table 3.1 List of pre-stressed composite production methods as presented by different authors.

Authors	Production Method
Schürmann, 1984	Pre-stressed pressure tubes were made by curing a 90º tube, pressurising it and wet-laying a further 0º tube on top and curing it, then releasing the pressure.
Jorge *et al.*, 1990	Fibre tows were wrapped around pins on a flat plate, tensioned, impregnated with epoxy resin and cured under another flat plate
Schulte and Marissen, 1992	A specially made rig was used to prepare prepreg panels in an oven. The rig applied the consolidation pressure and the pre-stress.
Rose and Whitney, 1993	Filament wound flat panels. Pre-stress was applied through the expansion of the mandrel at curing temperature.
Tuttle *et al.*, 1996	Flat plate prepreg panels cured in an adapted hot press.
Motahhari and Cameron, 1997, 1998	Fibre tows were tensioned and laid into a trough into which the epoxy resin was poured and cured in a tube furnace.
Fancey, 2000 a,b	Tension was imparted into Nylon 6,6 fibres and then released again. The fibres were then impregnated with resin and cured. Pre-stress was induced through the viscoelastic relaxation of the fibres.
Schlottermüller *et al.*, 2002	Filament wound tubes were made with pre-stress. A thermoplastic resin was used to quickly lock the pre-stress in.

The various methods presented above and their findings will now be discussed in the same order. Beginning with Schürmann, 1984, his method produced two-ply cylindrical tubes, which could be used in pressure tests. By first curing a 90º layer into a tube, he was then able to pressurise that tube and under pressure cure on a further 0º layer. When the pressure was subsequently removed, the elastic relaxation of the 90º tube would place the 0º layer under compression in the hoop direction. Schürmann intended for this process to prevent the matrix from cracking until higher pressures and delay the onset of weeping. He did not give details of how the resin was cured, whether it was under elevated temperature or at room temperature, nor did he give details of the materials used. He was able to demonstrate, though, that the hoop stress at the point of weeping increased with increasing levels of pre-imposed hoop stress. He also discovered that when internal pressure was removed and reapplied, although matrix cracks were present from the previous pressurisation, these cracks did not cause weeping until the previously obtained pressure was regained. This showed that not only did the pre-stressing delay the onset of weeping it also closed the cracks again until the pressure needed to cause weeping was again reached. This finding carried a significant implication with it. When a pressure vessel is produced without pre-stress, the matrix is under a tensile stress state, so not only would weeping occur prematurely, but upon re-pressurisation, the threshold weeping pressure would decrease since the tensile stress state in the matrix would keep the cracks open. As already stated, applying pre-stress allowed the pressure vessel to be loaded to the same pressure in a repeatable manner.

Jorge *et al.*, 1990, presented a method in which they ran a tow of fibres around pins along a flat panel (see Figure 3.3) and hung weights off the ends of the fibre tow to

impart pre-stress into it. To enable the pre-stress to be applied evenly across the panel the pins were lubricated. The fibres were impregnated and cured under a glass plate at room temperature, followed by a 353K (80ºC) post-cure. Jorge *et al.* claimed fibre volume fractions of 56% ± 4%, applying fibre tow pre-stress tensions of up to 100 N. Due to the small number of data points at each level of pre-stress and the scatter in volume fraction it was difficult to claim any distinctive trends, although Jorge *et al.* claimed that there was an overall increase in tensile strength and modulus. These results are both questionable. Final failure in glass epoxy composites is dominated by the fibres and not the resin. Final failure should then occur at the same load level. Stress at first sign of matrix cracking would have been more significant, since this should shift to higher stress levels due to the reduced tensile stress in the matrix as a result of pre-stressing. The modulus of the pre-stressed composites should not have changed since both fibres and epoxy resin are linear elastic brittle materials, and composites themselves exhibit linear elastic behaviour to the point of the first matrix cracking.

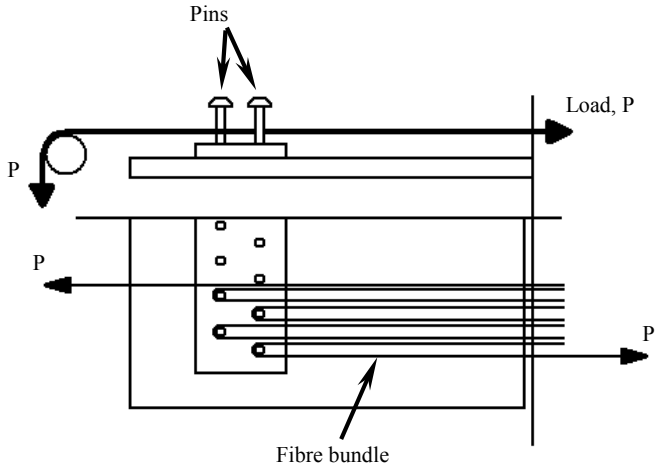

Figure 3.3 Diagram of the setup used by Jorge *et al.*, 1990, where the fibre tows were run round pins to produce panel, tensioning the fibres to impart the pre-stress.

Schulte and Marissen, 1992, on the other hand did investigate the effect of pre-stressing on the matrix cracking. They made 4-ply cross-ply laminates of $[0/90]_S$ configuration. They imparted the pre-stress into the composites by means of a V-shaped groove in a metal plate (see Figure 3.4). The 0º plies were fixed at both ends and forced into the groove near one of them. Only one level of pre-stress was thus available, but this was sufficient to show the trends sought. Their laminates were hybrid, with aramid plies in the outer 0º direction and carbon plies in the inner 90º direction. All plies were prepreg. The aramid was used for the outer plies as these fibres were very tough and could withstand being forced onto a V-groove. The carbon fibres would not have survived this as they were a lot more brittle. A covering plate was also placed onto the laminate and clamped down to produce consolidation pressure. This whole assembly was then cured in an oven. To confirm the presence of pre-stress in their panels, they produced a two-ply cross-ply laminate (which was unbalanced, with one ply in the 0º direction and the other in the 90º direction). Upon removing the panel from the plate they were able to measure the resulting curvature and derive the induced pre-stress. Schulte and Marissen chose a cross-ply laminate, since matrix cracking occurred early in the 90º plies and could be measured using X-ray technology. The method they used was to load the test specimens to a given load, remove it from the load frame, X-ray it and count the number of transverse cracks in the 90º plies. The specimens were then replaced in the load frame and taken to the next load level and the X-ray procedure repeated. This was done until final failure. They did this for a non pre-stressed and a pre-stressed specimen and found that indeed the pre-stressed panel began to show 90º ply matrix cracking later than that in the non pre-stressed one. They found though that there was no significant change in the strain to failure and the ultimate strength.

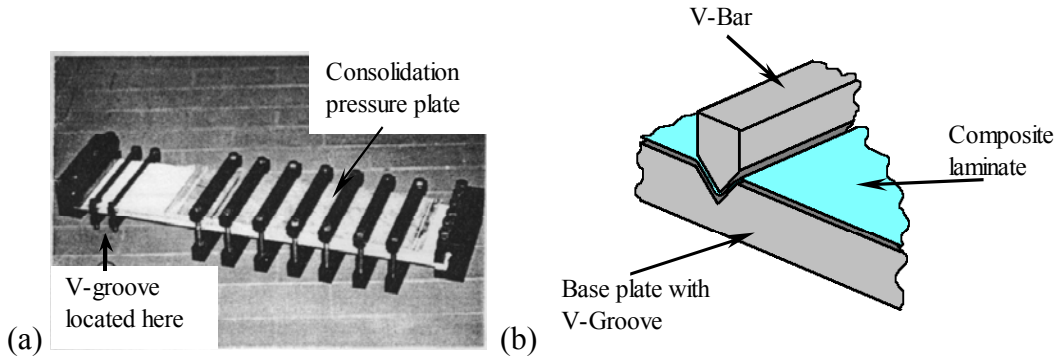

Figure 3.4 Image (a) of the setup used by Schulte and Marissen, 1992, showing the V-groove and the pressure plate in the diagram (b).

Rose and Whitney, 1993, chose to produce their pre-stressed panels by flat plate filament winding. This was a particularly good way of producing pre-stressed panels, since filament winding machines allow one to control the tension in the fibre tows being wound onto the mandrel. It was further suitable, since filament winding is a commercial technique for producing composite components. Rose and Whitney wound their panels tightly onto the mandrel and cured them in an autoclave, where the mandrel, being metallic, would cause further pre-stress in the fibres due to its greater thermal expansion over the fibres. They used a carbon/epoxy system. By rotating the mandrel through 90º, they were able to also produce cross-ply laminates. They also found that through pre-stressing the onset of first ply failure could be delayed. They also suggested that pre-stressing may find benefits in such materials as ceramic composites, where the residual stresses are high.

Tuttle *et al.*, 1996, employed yet another method to produce pre-stressed panels. They laid up carbon/epoxy prepreg laminates, which they then mounted in a loading frame. This frame attached to a hot press in which the laminates were cured. Tension in the laminates could only be applied in one direction, but could be controlled through a hydraulic foot pump and a pressure gauge. A hydraulic ram in turn applied

the tension to the laminates. Figure 3.5 illustrates this concept. Tuttle *et al.* were able to produce panels with a large variation of pre-stress – from 0 to 621 MPa. Like Schulte and Marissen, 1992, they too used curvatures of pre-stressed unsymmetrical laminates to confirm the existence and level of pre-stress in the panels. These unsymmetrical laminates were then tensile tested to determine the effect of pre-stressing on the ultimate strength and the crack generation. Again there appeared to be no effect on the ultimate strength. The crack development was however significantly affected, with the number of cracks reducing with more pre-stress.

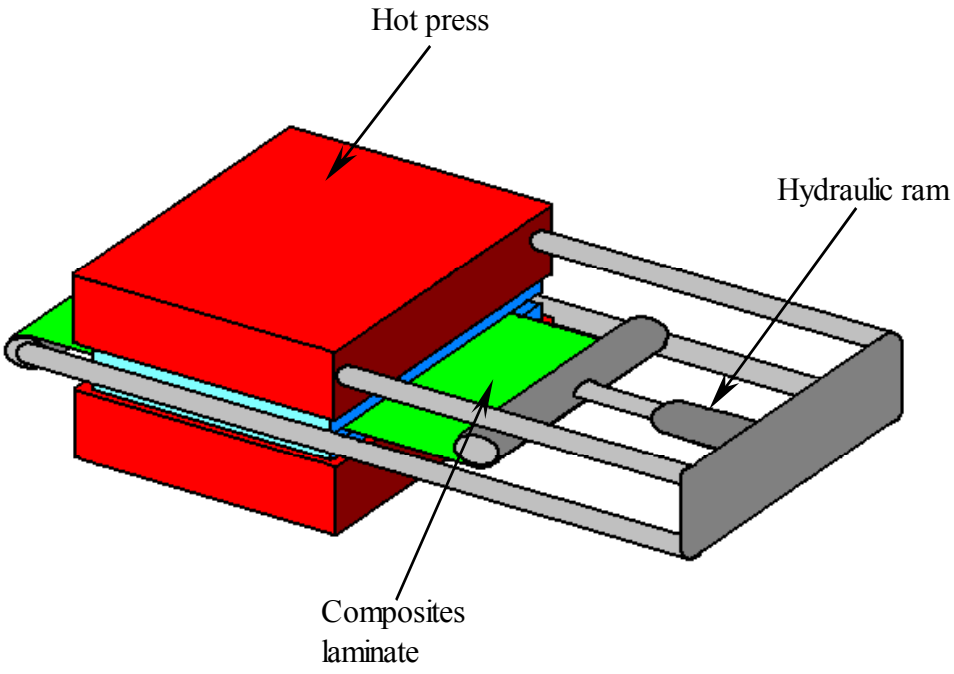

Figure 3.5 Diagram of equipment used by Tuttle *et al.*, 1996, showing the hydraulic ram, foot pump, pressure gauge and hot press.

The approaches by Motahhari and Cameron, 1997, 1998, and Fancey, 2000 a, b, were quite different from all other authors. Whereas all the others concentrated on either tubes or panels, Motahhari and Cameron and Fancey chose to produce small individual coupons for the purpose of testing in a Charpy impact test machine.

Motahhari and Cameron's approach was to load a few tows of fibres in a table-top tension test machine to the desired load, place a trough around the loaded fibres, impregnate them with an epoxy resin and cure them with the use of an adapted furnace (see Figure 3.6). By using the tensile test machine they were able to monitor the load in the fibres during the curing cycle and from that infer the level of pre-stress present in their test specimens. Their subsequent Charpy impact testing showed that pre-stressed composites could absorb up to 30% more energy than non pre-stressed ones. They also discovered that this improvement peaked at a pre-stress level of 60 MPa after which it sharply dropped off. Upon carrying out fractography they found that pre-stressed composites deflected the crack fronts to travel along the fibre-matrix interfaces, which occurred to a much lesser extent in non pre-stressed samples.

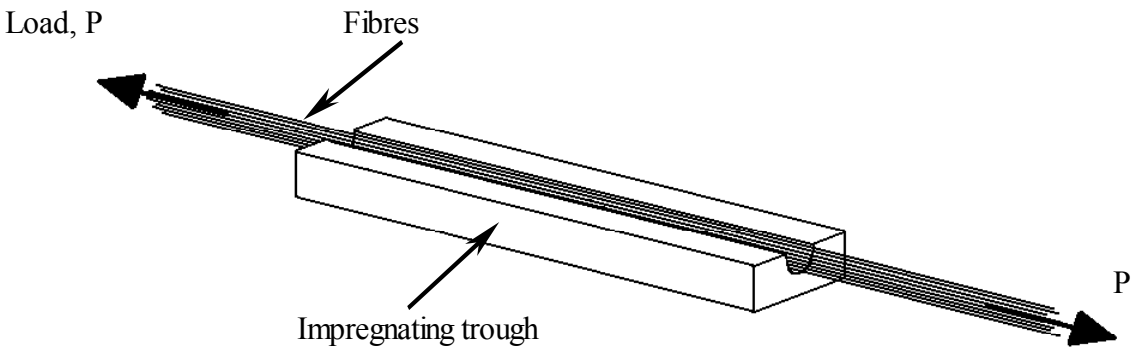

Figure 3.6 Diagram showing the way Motahhari and Cameron, 1997, 1998, produced their pre-stressed coupons.

Fancey, 2000, a, b, used Nylon 6,6 fibres in his studies. These fibres exhibited visco-elastic behaviour and so would regain their original length slowly. This allowed him to apply tension to the fibres and release it. He could then impregnate them with resin and cure them. He then carried out Charpy impact tests at given times after the curing process and observed the effect this pre-stressing would have. Like Motahhari and

Cameron, he also found that inducing pre-stress would increase the amount of energy absorbed during impact and also observed larger amounts of fibre-matrix debonding in the pre-stressed samples.

Like Schürmann, 1984, Schlottermüller *et al.*, 2002, produced tubes with pre-stress. Unlike Schürmann, Schlottermüller *et al.* produced them using the filament winding technique. Also uniquely to Schlottermüller *et al.*, was that they used a thermoplastic resin rather than a thermoset resin. The apparent advantage in using a thermoplastic resin was that it could be heated immediately before winding onto the mandrel and it would solidify very quickly once on the mandrel. This allowed the pre-stress applied to be locked in reliably without the usual problem of fibres settling closer to the mandrel. The aim of this study, which was successfully demonstrated, was to even out the hoop stresses in the radial direction of the tube.

3.3. Potential Applications of Pre-Stressing

It has been demonstrated that pre-stressing affects mechanical and impact performance of composites. It is now necessary to discuss in what areas pre-stressing may find application. Schlottermüller *et al.*, 2002, and Schürmann, 1984, both suggested that pre-stressing might find use in pressure vessels, since it can even out the hoop stresses due to working loads, prevent weeping from occurring too soon and stabilise the cracks in a pressure cylinder. Dvorak *et al.*, 1999, and Srinivas *et al.*, 1999, also suggested taking advantage of the control of the hoop stresses through the laminate thickness to produce more capable submersible cylindrical bodies. Such applications would certainly be a viable approach since filament winding would allow the necessary control of the fibre tension to impart pre-stress into the composites. No other authors have suggested specific areas where pre-stressing may be a practical

application, although Rose and Whitney, 1993, suggested it may find use in ceramic composites, although they did not present a way this may be carried out.

3.4. Conclusions

This chapter has presented all previous work found in the field of pre-stressed composites. Some authors have developed methods to predict the mechanical properties of pre-stressed composites and to understand the stresses in plies, fibres and matrix as a result of pre-stress. Other have carried out experimental studies and have on whole found that pre-stressing has no effect on tensile modulus and ultimate strength, but does have a significant effect on matrix cracking under tensile load and on the impact energy absorption properties. Some areas that have not yet been covered but would contribute significantly to the overall knowledge of pre-stressed composites would be impact, compression, compression-after-impact, fatigue, fracture mechanics and interfacial mechanics of pre-stressed composites. This study will attempt to investigate the effect of pre-stressing on the projectile low- and high-velocity impact performance of composite laminates.

4. EXPERIMENTAL

This chapter gives details of the material selected and the procedures used in this study. It is broken down into four sections, beginning with a section explaining the material selection and lamination process choices. The second section describes the process, by which pre-stress was introduced into the composites. Section three gives an account of the test measures employed to determine the effects of pre-stressing and section four describes the finite element analysis study carried out to supplement the experiments.

4.1. Material Details

4.1.1. Material Selection and Configuration

The choice of material in this study was the Hexcel Composites 913G-E-5-30 E-glass/913 epoxy resin composite UD prepreg system. Such a material allowed easy stacking to produce laminates ready for autoclave curing. Using a glass fibre system also resulted in a translucent material, which allowed ready visibility of the induced impact damage.

The chosen laminate configuration was a 16-ply, cross-ply one. This configuration has been commonly used within the Sensors and Composites Research Group and was used by Badcock, 1997. The stacking sequence was a $[0/90_2/0_2/90/0/90]_S$ symmetric lay-up. The cured ply thickness of the prepreg plies was 0.125mm each, giving a finished laminate thickness of 2mm. To cure the prepreg, the manufacturers recommended the use of a hot press or autoclave. It was suggested, though, that an autoclave would yield a better result. As such, the autoclave curing process was chosen. The cure cycle for such a process, as recommended by Hexcel Composites,

was to apply an elevated temperature of 120°C, heating at a rate of 2-10 $K.min^{-1}$, and an elevated pressure of 0.6895 $MN.m^{-2}$ (100 psi) for one hour. The heating stage was set to last half an hour (thus the heating rate of 3.33 $K.minute^{-1}$ was well within the specified range and the capabilities of the autoclave). Once at operating temperature, the pressurisation stage was started, which was also set to last half an hour. At the end of the required one-hour cure time, the depressurisation stage was again set to last half an hour, thus the overall curing cycle lasted 2.5 hours.

Storage of the prepreg was according to the manufacturer's specification at –18°C. This was achieved by keeping it in a domestic deep freezer. To prevent condensation occurring on the material, when it was removed from the freezer, it was also kept in sealed bags, containing pockets of silica gel to remove the moisture from the inside of the bags. When removed from the freezer, the sealed bags containing the prepreg were allowed to reach ambient temperature before being opened to again avoid condensation.

4.1.2. Lamination Process

The laminates were laid up by hand. For the finished laminate to fit into the pre-stress rig, each ply was cut into rectangles, 340mm long along the fibre direction and 250mm wide. Figure 4.1 gives a diagrammatic representation of the aspects of the lamination process.

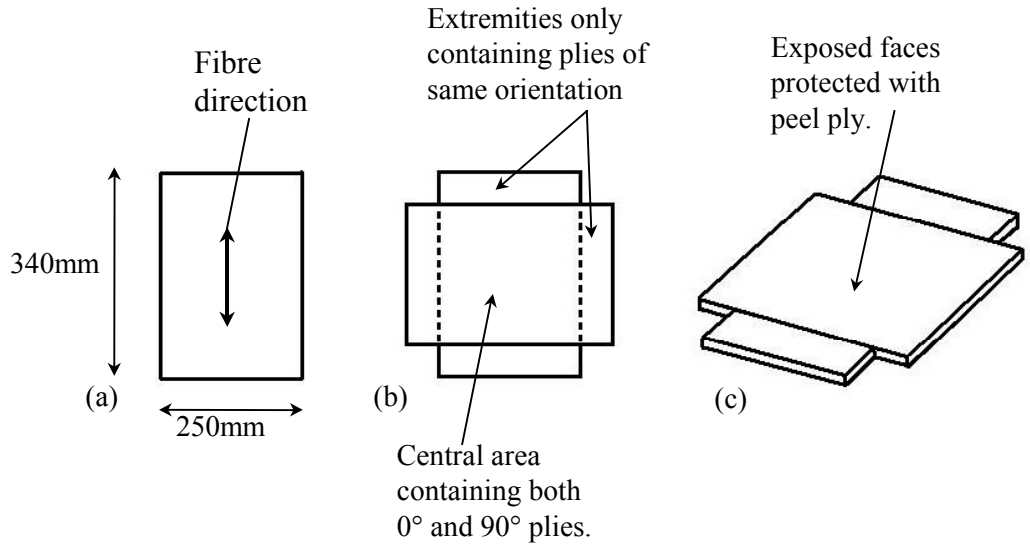

Figure 4.1 Diagrams showing aspects of the lay-up; (a) a single ply with dimensions and fibre direction shown, (b) plan shape of laminate after lay-up and (c) a 3-D representation of the final laminate.

Since the individual plies were not square, but were laid up in a cross-ply configuration, it was inevitable that there would be some areas, where there would be only eight plies of the same orientation (Figure 4.1(b)). This was intentional, since it allowed those areas to be end-tabbed as described in section 4.2.3 for the purposes of pre-stressing. To protect the finished laminate from contamination during subsequent processing stages prior to being cured, the exposed ply faces were left with their peel ply attached (Figure 4.1(c)).

4.2. Pre-Stressing

4.2.1. Philosophy to Pre-Stressing

To investigate the effect of pre-stressing on the impact performance of composite laminates, a method needed to be found, which would allow the individual plies of the laminates to be loaded prior to and during cure. Since a cross-ply configuration had been chosen, it appeared suitable to design equipment capable of pre-stressing the laminates in both the 0º and the 90º directions. Cure was achieved through the use of

an autoclave oven. This meant that the equipment had to be able to be placed inside an autoclave and be sealed inside a vacuum bag. It was therefore necessary to have a system, which was self contained during the curing process (i.e. no such items as tension test machines could be used as these would not fit into the autoclave). The autoclave used in this study was produced by Aeroform Ltd and had a working section diameter of 800mm and a floor width of 680mm (see Figure 4.2).

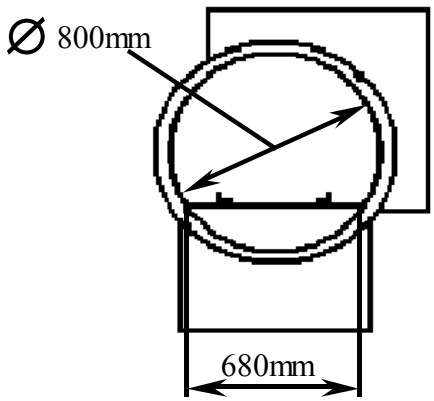

Figure 4.2 Dimensioned diagram of the Aeroform autoclave used in this study.

It was thus deemed appropriate to give the pre-stressing equipment a maximum footprint 360000mm^2 (600mm by 600mm) to allow extra space around it for vacuum bagging. Vacuum bagging required careful designing of the tooling, as sharp corners and cavities could lead to bridging and eventually bursting of the bag material. The exterior shape of the equipment thus had to be simple to allow for the vacuum bag process. As already mentioned in the literature review (section 3.2), Motahhari and Cameron, 1998, proposed a level of pre-stress of 60 MPa for optimum impact resistance. It was felt, that this level of pre-stress had to be at the very least met, even exceeded to achieve a satisfactory range of data across the spectrum of pre-stress levels. 100 MPa was chosen to be the maximum pre-stress level to be applied by the

pre-stressing equipment. A reserve factor of 2 was introduced as well, to ensure the equipment would not fail.

The existence of pre-stressing needed to be confirmed as well. A simple initial approach was to balance forces. Knowing the cross-sectional area of the eight plies in any one direction (this could be taken as the approximate cross-sectional area of the reinforcing fibres in that direction), the cross-sectional area of the load bearing frame of the pre-stressing equipment and the level of pre-stress required, the overall load required to achieve that level of pre-stress could be approximated. These forces could then be converted into direct strains in the frame and monitored using strain gauges. 3D finite element analysis was used to validate this approach (see chapter 6.2 for a more in-depth discussion).

4.2.2. Description of Equipment

The pre-stress equipment was as illustrated in Figure 4.3. It consisted of a load-bearing frame and four clamps, interconnected by two linking bolts per clamp. The frame was made from BS5950 steel 38x76 mm channel section. A finite element study was carried out to confirm the suitability of this choice (see chapter 6.2.1.2 for more details). The clamps were designed to close down over the end-tabbed ends of the laminate. Seven bolts were used to apply the clamping force. A 30 Nm torque applied to each bolt was found to give a sufficient clamping force to prevent slippage between the clamps and the end-tabs. Blanking plates were placed over the assembled equipment to simplify its shape for vacuum bagging.

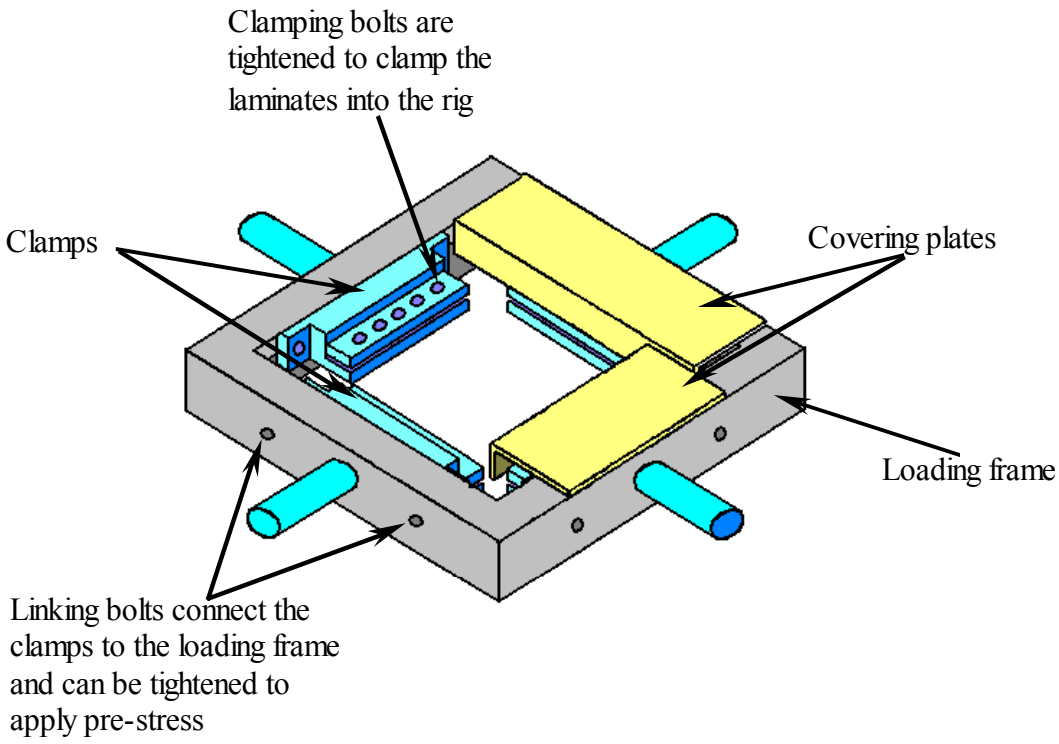

Figure 4.3 Illustration of the aspects of the pre-stressing equipment. The loading frame, clamps and covering plates are all visible.

The pre-stress was applied in a combination of two ways. The first using the thermal expansion mismatch of the steel frame and the E-glass fibres. A thermal finite element analysis showed that with no slack in the system, the composite would be pre-stressed to approximately 40 MPa, just from the expansion of the frame alone. The second process was to tighten the linking bolts beyond just removing the slack. This introduced an additional stress into the fibres and thus other pre-stress levels were attainable. These higher pre-stress levels were also attainable by loading the assembly into a tension test machine, using the loading pins on the clamps, applying a tension to the fibres and taking up the slack with the linking bolts. If lower pre-stress levels were desired than attainable by just removing the slack, slack could intentionally be introduced. This way, the expansion of the frame would first have to take up the slack before beginning to load the laminate. The strains in the frame were

monitored with strain gauges attached to it along its neutral axes. One strain gauge was also attached 5 mm off the frame's neutral axis to monitor any bending (Figure 4.4).

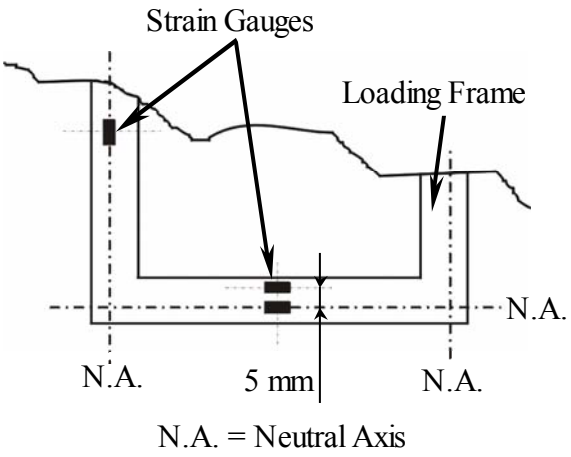

Figure 4.4 Schematic diagram of the strain gauge locations of the loading frame.

4.2.3. Pre-Stress Process

The complete process by which a pre-stressed composite panel was made has been detailed below by way of a numbered list. Where necessary, figures have been added to clarify matters.

- To begin with, the prepreg had to be removed from the freezer the night before laying up was to commence to allow the prepreg to reach ambient temperature.
- The next morning, the prepreg was removed from its sealed bag and the silica gel placed in a drying oven to remove any moisture from it.
- With the prepreg removed from its bag, the desired length was cut from the reel – typically 5 m. The remainder of the reel was then placed back into its bag and two dry pockets of silica gel were placed in with it. The bag was sealed and returned to the freezer.
- The five metres of 300 mm wide prepreg were then cut into fourteen lengths, each 340 mm long.

- These strips were trimmed to a width of 250 mm, leaving fourteen strips 340 mm long and 50 mm wide.

- The laminate was then laid up as described in section 4.1.2. The centre two plies were made up of ten of the fourteen 50 mm wide strips of prepreg to reduce the amount of waste material left over.

- The hot press was switched on and both platen temperatures were set to 120°C, the curing temperature for the prepreg.

- Eight end-tabs, 250 x 30 mm were subsequently grit-blasted. These end-tabs were also acetone-cleaned to remove any grease and debris from the bonding surfaces.

- The end-tabs were bonded onto the laminate as illustrated in Figure 4.5. The protective peel plies on the exposed surfaces of the laminate were peeled back from their extremities, and the end-tabs placed over the exposed parts of the laminate. These end-tabs were held in place with masking tape. An end-tabbed extremity of the laminate was then placed between the platen of the hot-press, using some non-porous release film to protect the platen from being covered in resin. A consolidation load of 5 tonnes was then applied. The cure time for each extremity was one hour. It was desirable not to cure any more prepreg within the laminate other than that between the end-tabs. It was found that, by placing 10 mm thick PTFE plates above and below the rest of the laminate, those areas would not be affected by the temperature of the platen as much, as when no thermal insulation was used. This process was repeated for all four extremities of the laminate.

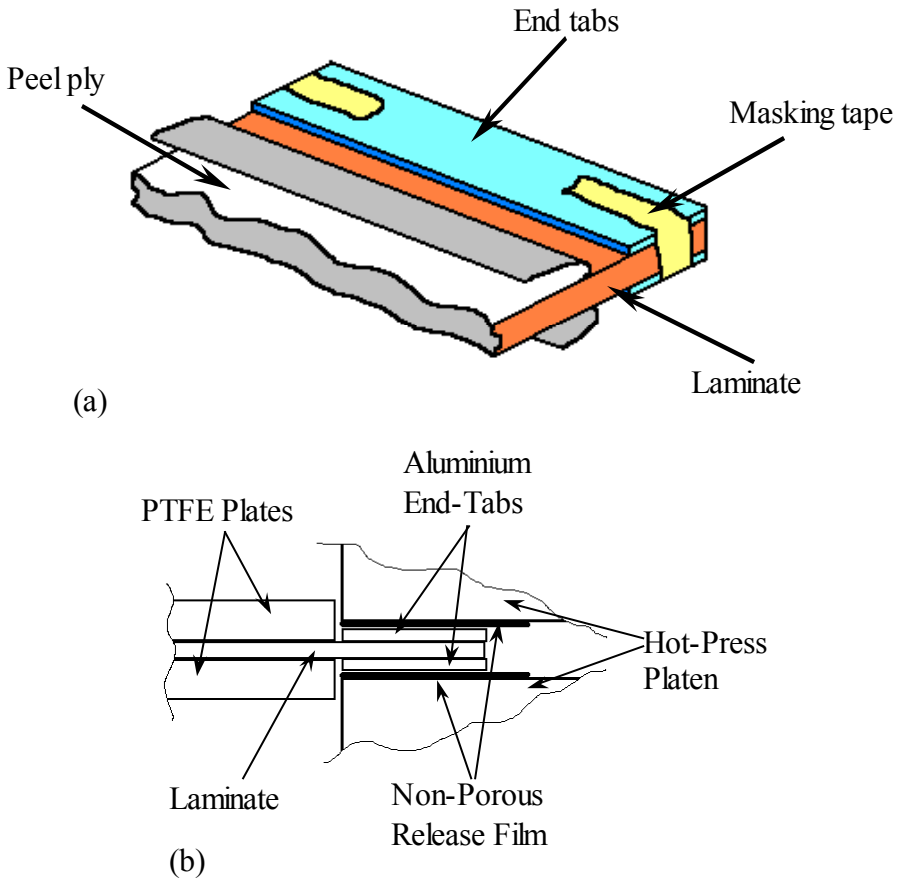

Figure 4.5 Diagrammatic illustrations of the end-tabbing process. (a) Preparation and (b) curing.

- With the end-tabs cured onto the laminate, seven 10 mm holes were drilled into each end-tabbed extremity using a specially designed drilling jig (see Figure 4.6). All the holes were deburred using a larger diameter drill bit as became necessary.

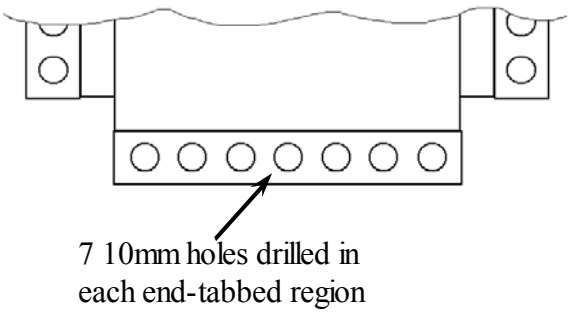

Figure 4.6 Illustration of the drilling process.

- At this stage, the laminate zero degree direction was marked onto the end-tabs using an indelible marker for later identification.
- The preparatory steps over, it was time to load the laminate into the pre-stressing equipment. First, the clamps were inserted into the frame and the laminate placed between the clamp faces.
- Next, the linking bolts were connected and the clamping bolts put into place.
- The assembly was then loaded onto the assembly stand and the clamping bolts were tightened to 30 Nm.
- The frame was rotated until it was upside-down and the peel ply was removed from the side of the laminate now facing up.
- Porous release fabric was placed over the exposed area of the laminate, followed by non-porous release film.
- The lower blanking plates were then put in place, making sure to match up the numbers on the plates to the locations on the frame. The non-porous release film was tacked in place with some high-temperature tape.
- The frame was rotated back up the other way and returned to a table.
- The peel ply was removed from this side and covered with porous release fabric, then non-porous release film.
- The upper blanking plates were put in place, again matching the numbers.
- At this stage, the strain gauge amplifier was switched on to allow it to warm up.
- Next followed the preparation for autoclave curing. The base plate of the vacuum membrane was covered in breather fabric, making sure it was at least 50 mm away from the edges of the base plate to allow the top vacuum frame to create a good seal with it.
- The assembled pre-stressing equipment was then placed onto the base plate,

which was located on top of the loading trolley and the strain gauges were connected to the wires leading to the strain gauge amplifier.

- The linking bolts were tightened to remove the slack in the system and then set to the desired level of pre-stress.

- The strain gauges were temporarily disconnected again and the pre-stress equipment was covered in breather fabric.

- Feeding the strain gauge wires from the equipment through the breech hole in the upper membrane of the vacuum frame, the frame was fitted over the pre-stressing equipment and clamped in place.

- The strain gauges were reconnected and the breech hole was sealed using tacky tape.

- The loading trolley was then connected to the autoclave using the connecting rails and the vacuum frame was pushed halfway into the autoclave to connect the vacuum hoses to the breech port.

- A vacuum was drawn and any leaks eliminated. The vacuum of 0.1 $MN.m^{-2}$ (1bar) was then left to be drawn for an hour to try to evacuate as much air as possible before the cure cycle.

- At the end of the one-hour, the frame was pushed all the way into the autoclave, the loading trolley removed from in front of it, the door shut and locked and the cure cycle was begun.

- At the end of the cure cycle, the autoclave was switched off and left to reach ambient temperature before opening the door and removing the frame back onto the loading trolley.

- Removal of the pre-stressed panel was the reverse of the above-described process.

4.3. Experimental Test Methods

4.3.1. Gas Gun Low-Velocity Impact Testing

Low mass, high-velocity impacts were achieved using a compressed air gun system (a gas gun). Figure 4.7 shows the system as was used. Ball bearings, 5.556 mm (7/32 inch) in diameter were propelled towards test coupons, 200 mm long and 20 mm wide at velocities between 0 and 130 $m.s^{-1}$. The average mass of the ball bearings was 0.707 ±0.003 g. It was decided to impact the samples at 3 Joules of energy, which equated to an incident velocity of 92 $m.s^{-1}$. This resulted in damage, which did not extend to the edges of the samples, but was large enough to be able to measure any changes in the damage due to the effect of the pre-stressing.

The target coupons were held in an adapted CRAG standards compression rig (Curtis, 1988), to which a safety enclosure was attached. The safety enclosure was put in place to retain the impactor after the impact event, stopping it from rebounding around the laboratory and causing a risk of injury to any of the room's occupants. The compression rig was loaded into an INSTRON 8032 tension-compression fatigue machine for the duration of the impact test. The use of a fatigue machine was because of previous use of the equipment, when it was used for a study of the fatigue properties of impact-damaged composites (Brooks, 2004). It allowed the impacted coupons to be mechanically tested directly after impact, although this option was not used in the present study.

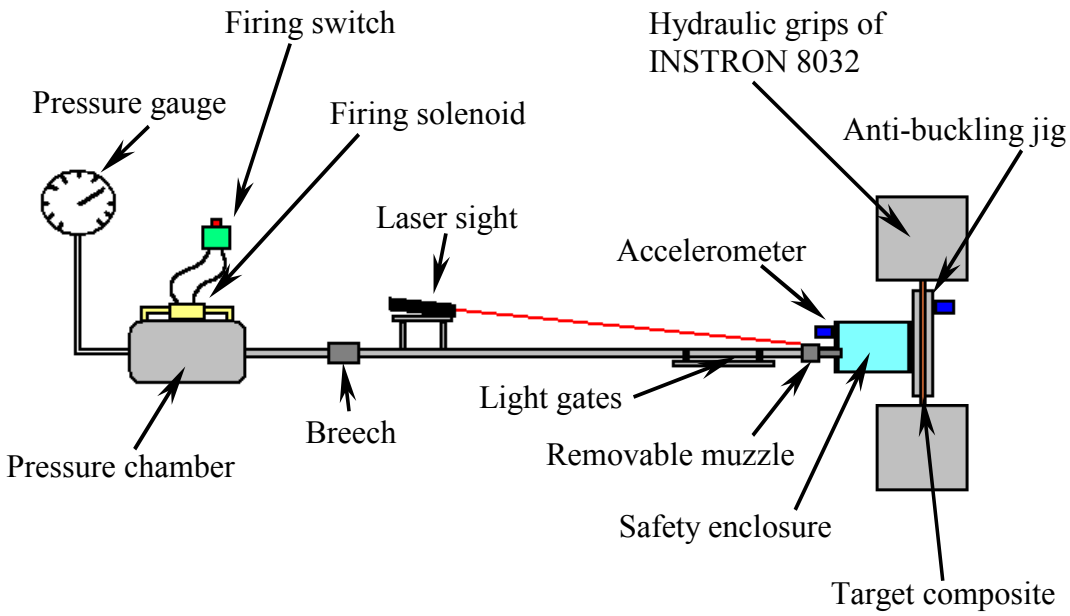

Figure 4.7 Illustration of the gas gun setup.

The gas gun was aimed at the target coupon using a laser mounted on top of the barrel near the breech (Figure 4.8(a)). The incident velocity was measured by means of two light gates mounted on the barrel near its muzzle (Figure 4.8(b)). They were spaced 100 mm apart. By measuring the time-of-flight of the impactor as it passed through the light gates, and knowing the spacing between them, the impactor's velocity could be derived (to three decimal places). Knowing the mass of the impactor also meant that the incident energy could then also be calculated (to two decimal places).

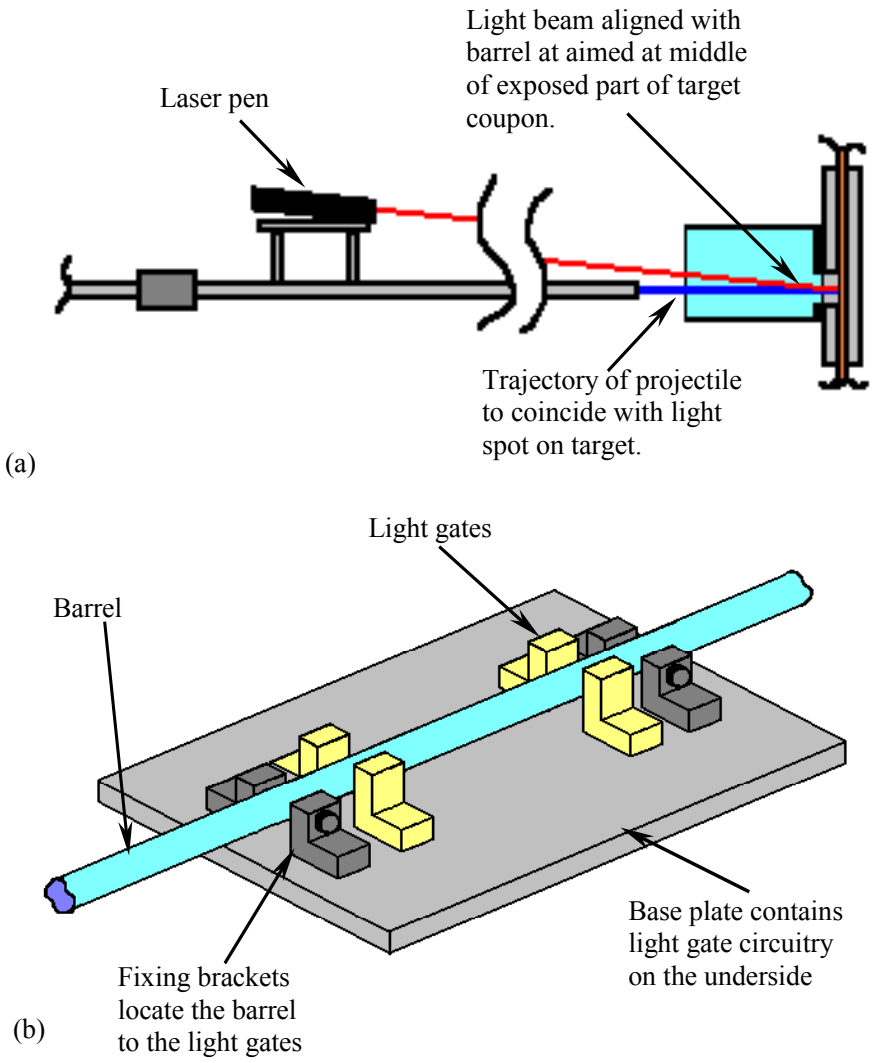

Figure 4.8 (a) Diagrammatic illustration of the laser targeting system and (b) a close-up view of the light gate assembly.

The velocity and kinetic energy of the impactor after impact was derived by again measuring the time-of-flight. Rather than using light gates, though, accelerometers were used instead. An accelerometer was mounted to the back face of the compression rig to detect the impact event against the target coupon. The impact against the front face of the safety enclosure was detected by a second accelerometer, attached to the front face (see Figure 4.9 for details). The distance between these sensors was 107 mm.

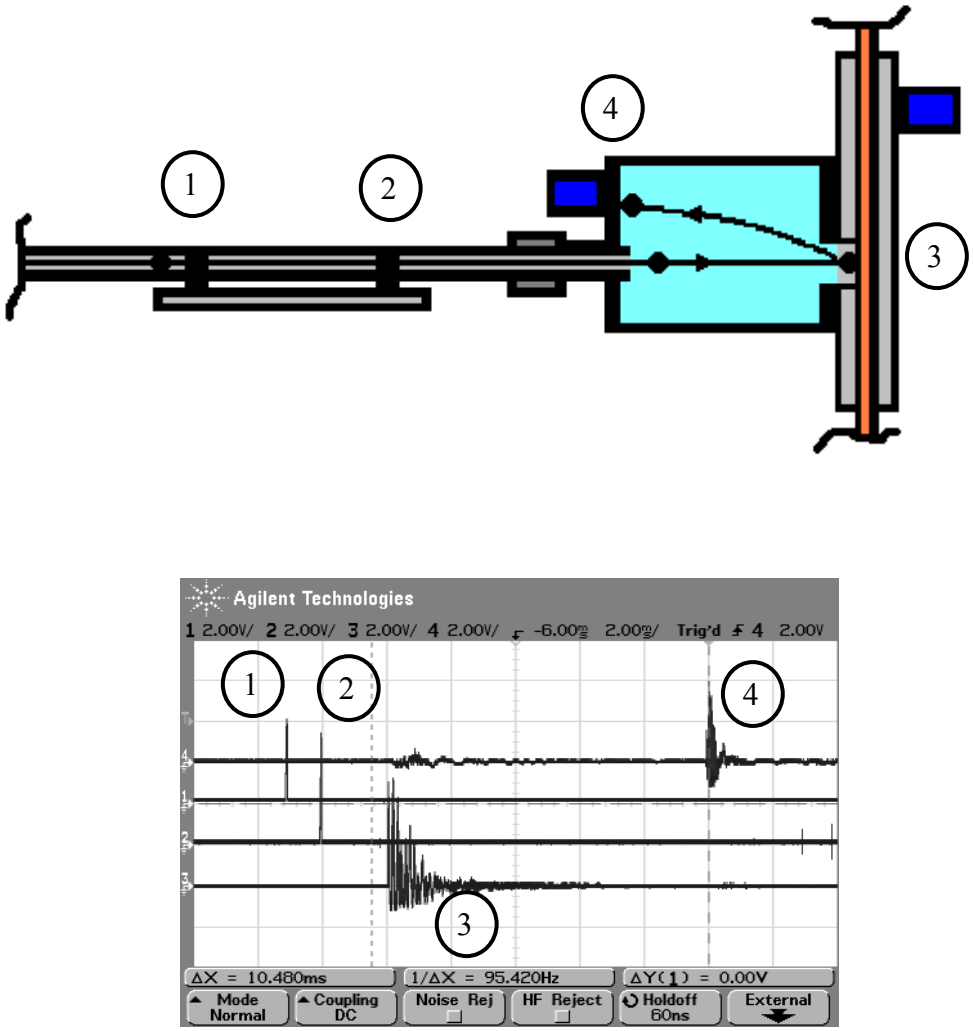

Figure 4.9 Illustration of the impact event detection using accelerometers on the safety enclosure.

4.3.1.1. Process of Gas Gun Testing

The steps required to carry out the firing of the gas gun are now described. Before beginning the firing process, all equipment needed to be switched on. This entailed switching the electrical power onto the INSTRON 8032 hydraulic power pack and control panel, the data acquisition PC, the power amplifiers for the gas gun and the signal conditioner for the light gates and accelerometers. The compressed air also needed to be fed to the gas gun system. Next the equipment needed to be left for at least half an hour to stabilise. If the hydraulic power pack had been freshly switched

on (it could have been left running overnight if other tests had been conducted on other machines in the laboratory), this would need to be left for at least an hour to warm up. Once everything was warm and stabilised, the following process could begin.

- The sample was loaded into the anti-buckling jig, with the safety enclosure attached.
- The jig was then loaded into the INSTRON 8032 with the safety enclosure facing the gas gun. Since the upper grips moved, the jig was first loaded into the lower grips, but the jaws were not tightened then. Once in the lower grips the upper grips were lowered over the upper end of the sample/jig assembly, taking care to keep all body parts out of the way of the moving parts of the INSTRON. Only when both ends of the sample/jig assembly were inside the grips were the grips tightened.
- Next, the laser was switched on and the aim of the gas gun checked. The aim of the gas gun was changed as necessary.
- Once aimed the front panel of the safety enclosure was put in place and the access hole aligned with the muzzle.
- Then the laser was switched off again.
- The pressure chamber of the gas gun was then pressurised to the level required for the desired impact energy.
- Next the projectile was loaded and the breech closed.
- With the gas gun, now ready to be fired, it was necessary to set the data acquisition going. For this the PC software was set running, the analogue/digital (A/D) converter reset button was pressed and the digital storage oscilloscope (DSO) was set to acquire.
- The gas gun was then fired.

- Results from the PC program (time of flight before and after, projectile velocity and energy before and after and percentage of absorbed energy) and the DSO (time of flight before and after) were then recorded and the trace from the DSO saved to computer.
- The breech was then opened.
- To retrieve the projectile from the safety enclosure, the front panel was carefully removed, holding a container below it to catch the projectile.
- The jig was then removed from the INSTRON and the sample from the jig. The process was then ready to be repeated.

4.3.2. Instrumented Falling Weight Impact Testing

Having a tup mass of 2.61 kg meant that the instrumented falling weight (IFW) test produced low-velocity impacts with long contact times, and subsequently low contact forces, relative to the gas gun impacts. Whereas the gas gun impacts were moving toward the ballistic range where damage was caused by the impact-induced stress-waves propagating through the thickness of the composite, the drop weight impact caused large deformations in the composite, which in turn caused damage by means of exceeding the maximum allowable strain across the fibre direction and the delamination propagating from the back face. This type of impact can be considered quasi-static, as very similar results can be produced by static indentation tests (Abrate, 1998).

Three different impact energy levels were chosen for this test: 3, 10 and 50 Joules. These values were those set in the machine, but differed slightly during the actual testing. A 3-Joule impact corresponded to the energy level used in the gas gun tests, but meant operating the drop weight equipment at the lowest achievable velocities, whereas the 10- and 50-Joule impacts were well within the operating range of the

equipment and as such would yield more accurate results. Three impacts were carried out at each energy level for each given pre-stress level (0, 40, 60, 80 and 100 MPa). Figure 4.10 shows an image of the impact damage in the 60 MPa pre-stressed panel to illustrate how the impacts were spread over the area of the target panel.

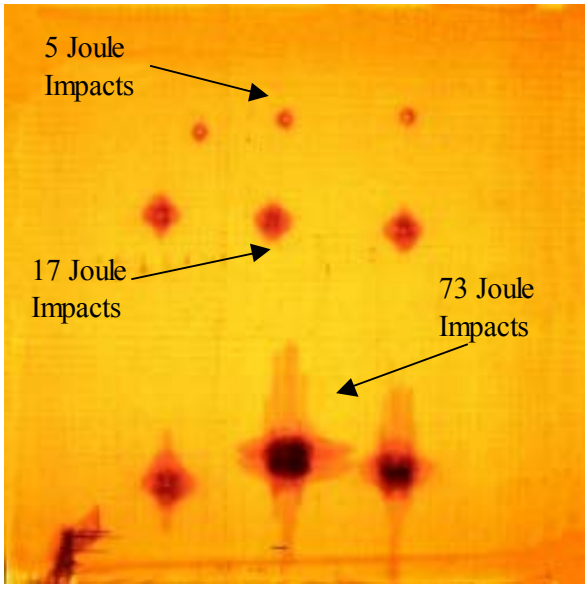

Figure 4.10 Picture of the 60MPa pre-stressed IFW test panel.

The equipment used in the instrumented falling weight impact tests was a Rosand IFW machine. The setup for these tests was as follows. The overall tup mass was, as already mentioned, 2.61 kg with a hemispherical tip of 20 mm diameter. A pneumatic clamping assembly was used to secure the target composites into place. A square clamping geometry was used with an internal dimension of 134 mm. The pneumatic pressure used to clamp the target was set to 0.2 MPa (2 bar). The principal fibre directions (0° and 90°) were aligned so they were parallel to the clamp walls. Figure 4.11 illustrates this. The instrumented falling weight meant that the incident velocity and the force-time data could be collected. The force-time data for each impact could then be used to determine the force-displacement behaviour and the absorbed energy for each pre-stressed panel.

This is discussed in more detail in chapter 5.2.2. Since the clamping system isolated any part of the composite panels from the impact event, it was not necessary to cut the produced pre-stressed panels into smaller samples, allowing them to be used immediately after removal from the autoclave with no further processing other than C-scanning them for quality control purposes.

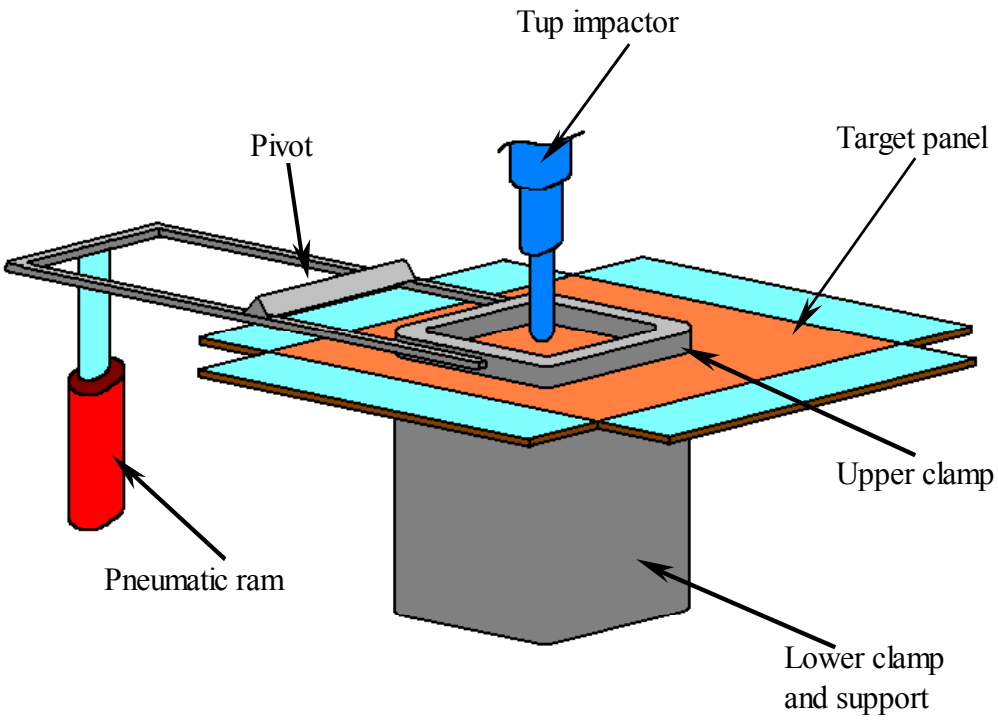

Figure 4.11 Diagrammatic illustration of the clamping arrangement.

The resulting delaminations were digitally recorded using the backlighting method (as illustrated in Figure 4.12) and quantified using the Leica QWin image analysis software.

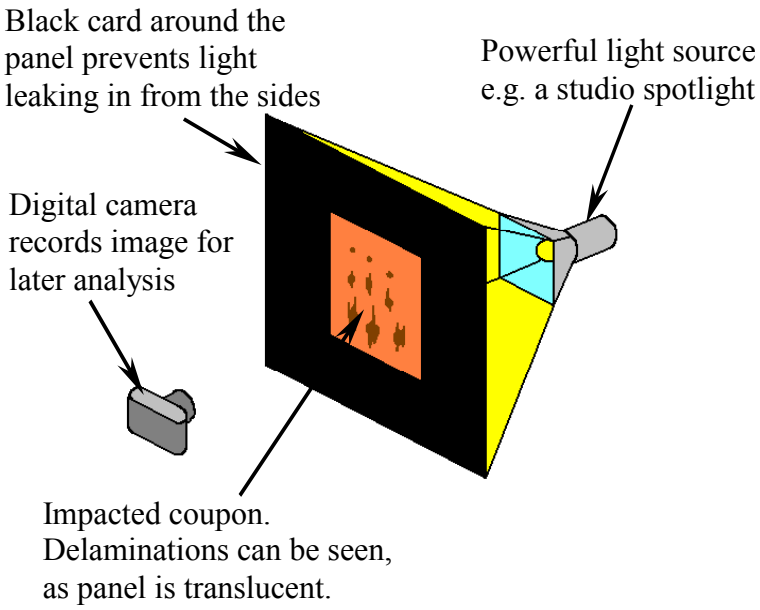

Figure 4.12 Illustration of the backlighting method.

4.3.2.1. Process of Instrumented Falling Weight Testing

The sequence for carrying out a falling weight test is now listed.

- Firstly, the test panel was located on the lower clamp ring.
- The panel was then clamped in place by pushing the clamp button twice. The first time to lower the clamp lightly onto the panel and the second time to apply pressure.
- The tup was then lowered onto the panel so that the tip of the tup was just touching the panel.
- The flags of the light gates were then adjusted to have both the green and the red lights on.
- In the control program the following steps were taken.
- The incident energy and velocity were set.
- The ‘zero’ button was pressed to zero the system.
- The ‘goto’ button was pressed to send the tup to its start position.

- The ‘arm system’ button was pressed to allow the test to commence.
- Then on the winch control the red button was pressed and held to release the tup. This button was held until the impact event was over.
- The tup was then raised a little and the panel unclamped.
- The panel could then be repositioned or replaced for the next test to commence.

4.4. Finite Element Study

In addition to the gas gun and IFW tests, a series of finite element (FE) tests were carried out to supplement the experimental results. This section will describe the study in detail. Using the finite element analysis methods made it possible to better understand some of the processes behind the effect of pre-stressing on the impact performance of composite laminates. This was because to define the model in FE one needed to understand the failure modes and processes to be able to represent them accurately.

4.4.1. Choice of Finite Element Analysis Code and Modelling Philosophy

The code chosen for this study was the LSTC (Livermore Software Technology Corporation) non-linear explicit code LS-DYNA, version 950d. It was chosen due to its range of different composite failure models (material types 22, 54, 55 and 59) and its reputation in crash simulation. Due to LS-DYNA not having a pre-processor, the pre-processor TrueGrid by XYZ was chosen.

The models were generated using shell elements for the target panels and solid elements for the impactor. Using shell elements for the target panels made the solution times shorter and the overall damage through the thickness of the panel was readily obtainable in the post-processor. The induced damage could subsequently be

measured in the Leica QWin image analysis program and the damage areas compared with those produced in the experimental tests. Further to this information it was possible to produce kinetic energy – time plots. In the case of the gas gun impacts, these could then again be compared with the experimental results.

To further reduce the solution times, symmetries were taken advantage of. The problems were symmetrical about two planes and therefore only a quarter of the model needed to be generated. The boundary conditions imposed for these symmetries were to fix the nodes on the symmetry planes in displacement perpendicular to and in rotation about the axes in-plane with the symmetry planes.

To model the impactor it was decided to use an elastic material model (material type 1), rather than a rigid body model. This allowed some response in the projectile itself. The actual material of the impactor was steel (material properties used in Table 4.1) and as such it was thought that plastic deformation in the projectile would be unlikely and only the target would be damaged. Using the elastic model, though, allowed the contact to be softer than if a rigid body was used.

Table 4.1 Material properties of steel projectile

Material Property	**Value**
Density ($kg.m^{-3}$)	7850
Young's Modulus (MPa)	210000
Poisson's Ratio	0.3

Since shells were used to model the target material, three material models were available for selection: types 22 (Chang-Chang failure criteria), 54 (enhanced Chang-Chang failure criteria) and 55 (Tsai-Wu failure criteria). Material type 54 did not seems to give out mesh data for shell elements, so models were created for types 22

and 55. Refer to Appendix A for a description of the three material models. Table 4.2 gives the input data to the two material types. Tensile coupon tests were carried out to determine the basic properties of the UD plies, using 8-ply unidirectional coupons.

Table 4.2 Material property input values for material types 22 and 55 (Consult the LS-DYNA Keyword Manual for more detail)

Material Type 22	
Values in **bold** are experimentally measured values and values in *italics* are approximated from Hull and Clyne, 1996.	
Density (kg.mm^{-3})	**1.9329E+03**
Young's Modulus, E_{11} (MPa)	**3.9745E+04**
Young's Modulus, E_{22} (MPa)	**1.4191E+04**
Young's Modulus, E_{33} (MPa)	*1.4191E+04*
Poisson's Ratio, ν_{21}	*8.9812E-02*
Poisson's Ratio, ν_{31}	*8.9812E-02*
Poisson's Ratio, ν_{32}	*0.4267*
Shear Modulus, G_{12} (MPa)	*3.8937E+03*
Shear Modulus, G_{23} (MPa)	*2.3859E+03*
Shear Modulus, G_{31} (MPa)	*2.3859E+03*
Bulk Modulus of Failed Material, K_{FAIL} (MPa)	2.000E+03
Material Axis Option, AOPT	3.00
Material Axis Change Flag, MACF	1.00
V1	1.00
V2	0.00
V3	0.00
Shear Strength in 12 plane, SC (MPa)	6.700E+01,
Tensile Strength, 1-axis, XT (MPa)	**1.16E+03,**
Tensile Strength, 2-axis, YT (MPa)	**3.585E+01,**
Compressive Strength, 2-axis, YC (MPa)	*7.171E+01,*
Shear Stress Parameter, ALPH	2.500E-01

Material Type 55	
Density (kg.mm^{-3})	**1.9329E+03**
Young's Modulus, E_{11} (MPa)	**3.9745E+04**
Young's Modulus, E_{22} (MPa)	**1.4191E+04**
Young's Modulus, E_{33} (MPa)	*1.4191E+04*
Poisson's Ratio, ν_{21}	*8.9812E-02*
Poisson's Ratio, ν_{31}	*8.9812E-02*
Poisson's Ratio, ν_{32}	*0.4267*
Shear Modulus, G_{12} (MPa)	*3.8937E+03*
Shear Modulus, G_{23} (MPa)	*2.3859E+03*
Shear Modulus, G_{31} (MPa)	*2.3859E+03*
Bulk Modulus of Failed Material, K_{FAIL} (MPa)	2.000E+03
Material Axis Option, AOPT	3.00
Material Axis Change Flag, MACF	1.00
V1	1.000E+00
V2	0.000E+00
V3	0.000E+00
Maximum Strain in Matrix for Failure, DFAILM	1.932E-02
Maximum Shear Strain for Failure, DFAILS	1.000E-02
Shear Stress Parameter, ALPH	2.500E-01
Softening for Fibre Tensile Strength, FBRT (XT is reduced to XT * FBRT after failure has occurred in compressive matrix mode)	0.800E+00
Maximum Strain for Fibre Tension, DFAILT	2.600E-02
Maximum Strain for Fibre Compression, DFAILC	2.500E-02
Effective Failure Strain, EFS	3.000E-02
Compressive Strength, 1-axis, XC (MPa)	*7.000E+02*
Tensile Strength, 1-axis, XT (MPa)	**1.160E+03,**
Compressive Strength, 2-axis, YC (MPa)	*7.171E+01,*
Tensile Strength, 2-axis, YT (MPa)	**3.585E+01,**
Shear Strength in 12 plane, SC (MPa)	*6.700E+01,*
Failure Criterion (type 54 or 55), CRIT	55

4.4.2. Gas Gun Model

Two components of the gas gun impacts were modelled: the impactor and the target coupon. It was assumed that the anti-buckling jig and the fatigue machine were totally rigid for the purposes of this analysis and thus did not need to be modelled, but simply represented by the relevant boundary conditions, and these were as follows. At the end-tabbed ends of the coupon all six degrees of freedom were fixed, as the grips of the fatigue machine would indeed impart these conditions. Where parts of the coupon rested on the anti-buckling jig (Figure 4.13), their respective areas in the FE idealisation were fixed in the through-thickness direction and restrained from rotating about both of the in-plane directions.

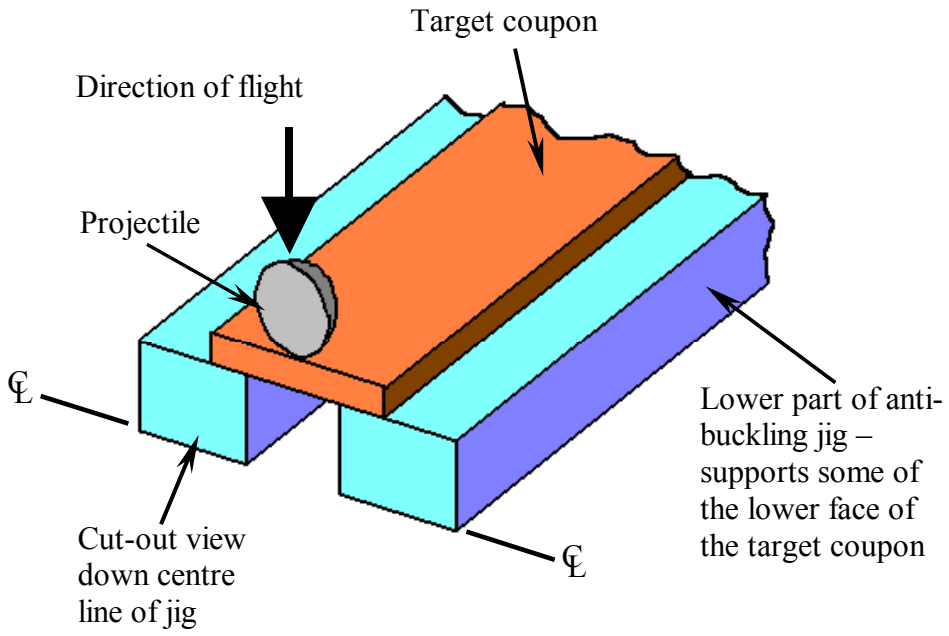

Figure 4.13 Diagram illustrating how the target coupons were restrained in the anti-buckling jig.

The actual coupons tested as described above were 200 mm long, 20 mm wide and 2 mm thick. Since the end-tabs were also 50 mm long each and would be held in the

grips, the length of the coupon that actually needed to be modelled was 100 mm long. The symmetry planes of the problem were both perpendicular to the plane of the coupon, therefore the finite element idealisation of the coupon only needed to be 50 mm long and 10 mm wide. Figure 4.14 shows the mesh as was generated. Near the impact location, a finer mesh was needed to produce better accuracy of the damage evolution, but away from the impact location, where damage did not extend to, the mesh could be made more coarse to reduce the solution time again.

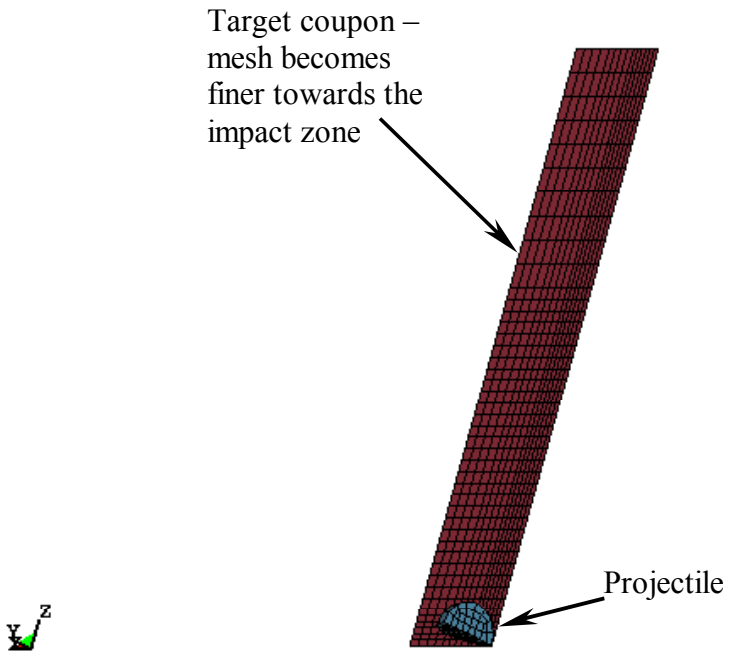

Figure 4.14 Picture of finite element mesh generated to simulate projectile impacts from a gas gun.

4.4.3. Instrumented Falling Weight Model

Again only the impactor and target were modelled. In this case, the clamp was assumed to be totally rigid and to completely clamp the panel into place. Thus, the boundary conditions around the edges of the target panel were to fix the edges in all six degrees of freedom. As was the case with the gas gun impact analysis, the area

close to the impact event was meshed more finely to get better accuracy of the damage development and meshed more coarsely away from this area to save on computation time.

The tup was not modelled exactly, but rather as a 50 mm long, 20 mm diameter steel bar with a 20 mm diameter hemispherical tip on its end. Figure 4.15 gives the details of the model used in this simulation. To account for the mass of the actual impactor, the density of the model tup was altered to achieve the same mass. Since the volume of a quarter of the model was found to be 1.4542×10^{-5} m^2, the density for a 2.61 kg heavy tup was calculated to be about 44870 $kg.m^{-3}$. The initial velocities were set to the actual impact velocities measured in the IFW tests: 1.9 $m.s^{-1}$, 3.5 $m.s^{-1}$ and 7.4 $m.s^{-1}$. In this analysis the overall damage area and the force-time plots were compared with the experimental results.

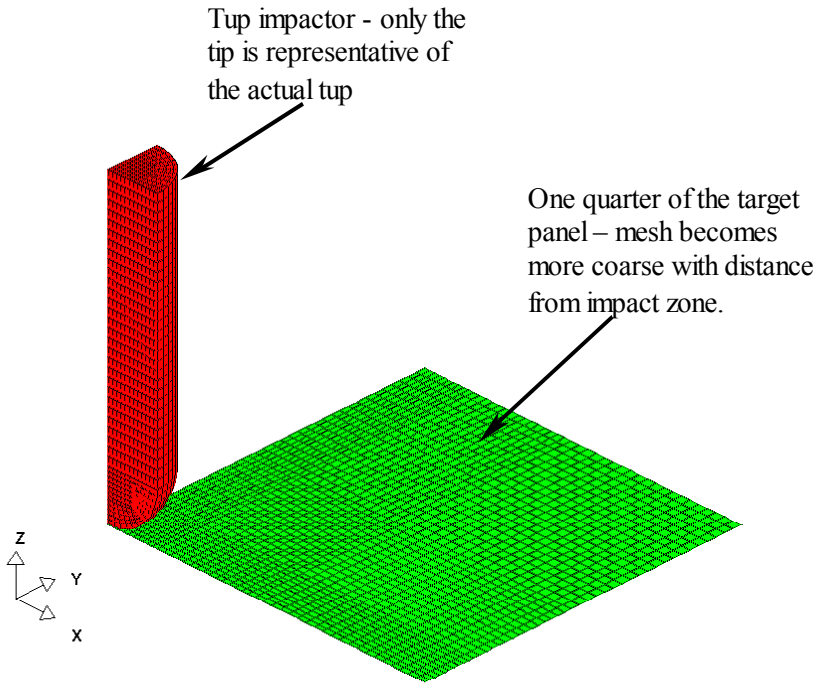

Figure 4.15 Picture showing the finite element model generated to simulate an impact from an instrumented falling weight.

This page is intentionally blank.

5. RESULTS

The results of this study have been presented in this chapter. They have been grouped into the three major aspects: panel production, experimental tests and finite element analysis. The aim of this chapter is to purely present the results and no attempt has been made to discuss them in any way. All assessments of the results can be found in subsequent chapters.

5.1. Pre-Stressed Panel Production

The results presented for the production of pre-stressed panels, are the autoclave plots, which were used to estimate the pre-stress in the panels, the C-scans, which verified the quality of the produced panels and some tensile tests, which were used to verify the existence of pre-stress. Table 5.1 lists all the panels successfully produced with their respective levels of predicted pre-stress.

Table 5.1 List of pre-stressed panels produced

Panel Number	Pre-Stress (MPa)	Panel Number	Pre-Stress (MPa)
PS01	0	PS12	100
PS02	5	PS13	70
PS03	50	PS14	200
PS04	50	PS15	40
PS05	60	PS16	100
PS06	30	US02	0
PS07	80	DT01	40
PS08	30	DT02	60
PS09	50	DT03	100
PS10	100	DT04	0
PS11	45	DT05	80

5.1.1. Autoclave Plots

The plots below show the results of the strain gauges on the pre-stressing frame, but also include the plots for mould temperature, autoclave pressure and vacuum.

Although the results have been discussed in detail in chapter 6 it would be of value to mention at this time that the results produced by the autoclave plots have been called into question as a result of difficulties encountered with the strain gauges employed for the measuring of the cure strains in the pre-stressing frame. These difficulties have also been covered in chapter 6.

In the following figures the strain gauges 1 to 5 correlate to the following locations on the frame shown in Figure 5.1

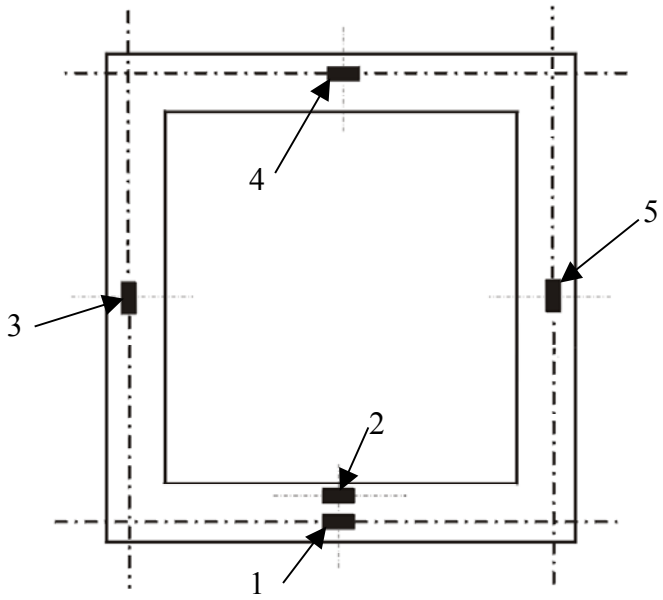

Figure 5.1 Diagram depicting the locations of the strain gauges for measuring laminate strains during cure.

To be able to negate the effects of temperature, pressure and vacuum from the strain readings, a reference run was carried out and this is shown in Figure 5.2. This run was then taken away from the actual cure cycle plots to reveal the strain in the pre-

stressing frame. The run was carried out as a fully vacuum bagged setup, but without the presence of a composite laminate to be cured and a steel blank in its place. The blank was not connected to the clamps so no strain was imparted into the frame from the blank.

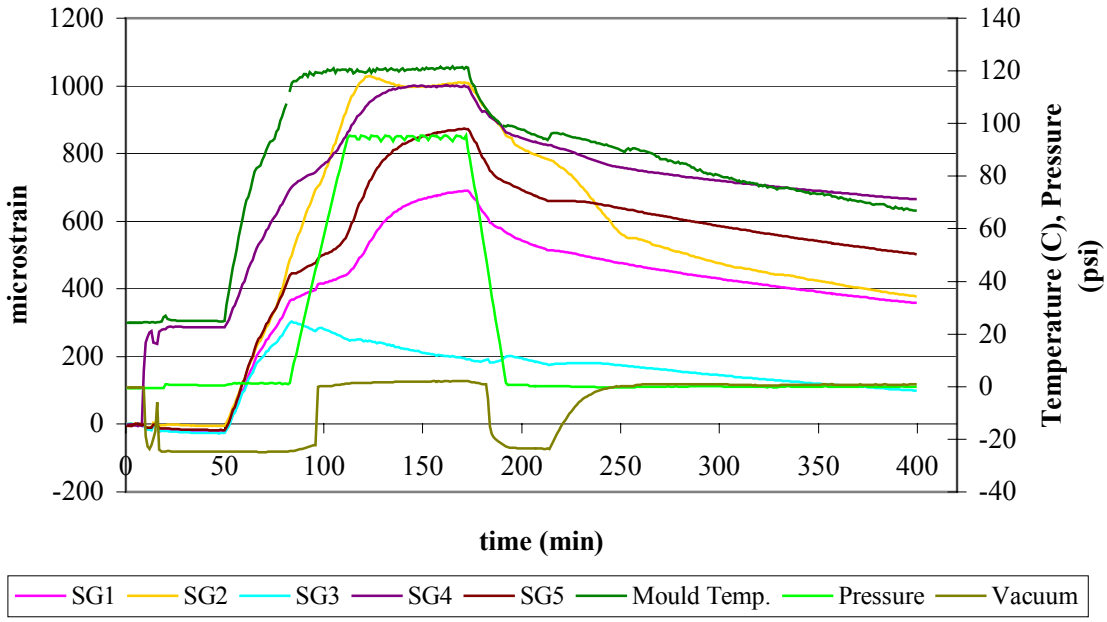

Figure 5.2 Plot of the cure cycle reference run.

Cure cycle plots were successfully generated for two panels: PS10 and PS11. These plots are shown below together with the plots where the reference run had been subtracted.

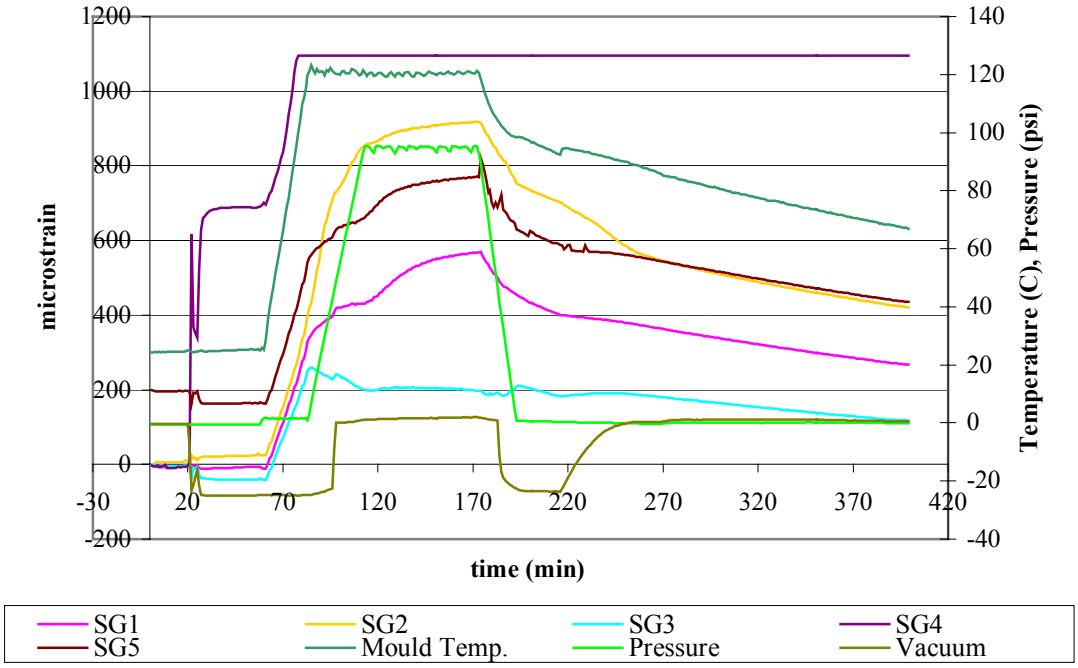

Figure 5.3 Cure cycle plot for panel PS10

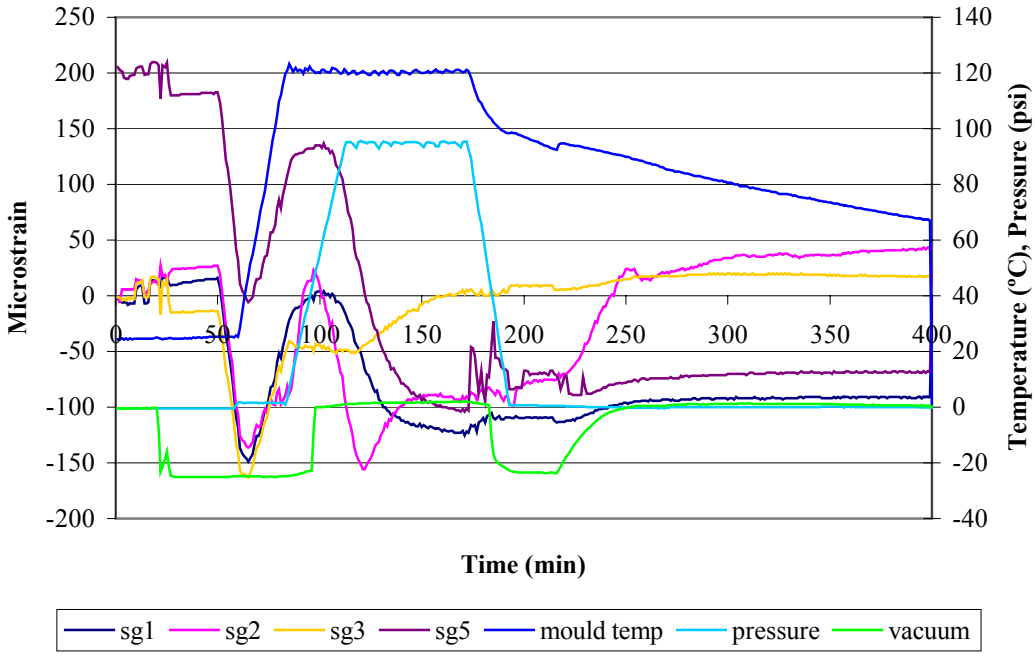

Figure 5.4 Plot of cure cycle less the reference run for panel PS10

In Figure 5.4 a linear section in the strain gauge plots (SG1, SG2, SG3 and SG5) can be seen between time 50 minutes and 66 minutes, which coincides with the heating phase of the cure cycle. This linear section is attributed to the compressive strain in

the loading frame due to the thermal mismatch between fibres and the frame. Table 5.2 lists the change in strain read by each strain gauge for this time period. The average of this was then multiplied by the Young's Modulus of the steel frame (assumed to be 210 GPa) to give the compressive stress in the frame. In turn, the load subjected to the frame could then be derived by multiplying the stress by the sectional area of the frame. This load was reacted by eight plies of the laminate (since there were eight plies in each direction). The overall width over which the load was reacted by the laminate was 250mm. Each ply was 0.125mm thick. There were eight plies in each direction, giving a laminate thickness of 1mm and a cross-sectional area of $250mm^2$. The manufacturer's quoted fibre volume fraction was 0.56 thus giving an approximate cross-sectional area for the fibres of $140mm^2$. By dividing the applied pre-stressing load by the fibre cross-sectional area, the level of pre-stress could be approximated. All this is reflected in Table 5.2.

Table 5.2 Data from frame, followed through to give fibre pre-stress, for panel PS10

Data Point	1	2	Change
Time	50	66	
Strain Gauge 1 (με)	16	-149	-165
Strain Gauge 2 (με)	27	-136	-163
Strain Gauge 3 (με)	-14	-163	-149
Strain Gauge 5 (με)	403	245	-158
Mean (με)			-159
Frame Young's Modulus (MPa)		210000	
Induced Stress in Frame (MPa)		-33.39	
Frame Cross-Sectional Area (mm^2)		856	
Pre-Stress Load (N)		57164	
Panel Width (mm)	250	Thickness of 8 plies (mm)	1
Cross-Sectional Area of 8 plies (mm^2)		250	
Fibre Volume Fraction		0.56	
Area of Fibres in one direction (mm^2)		140	
Pre-Stress in Fibres (MPa)		**408**	

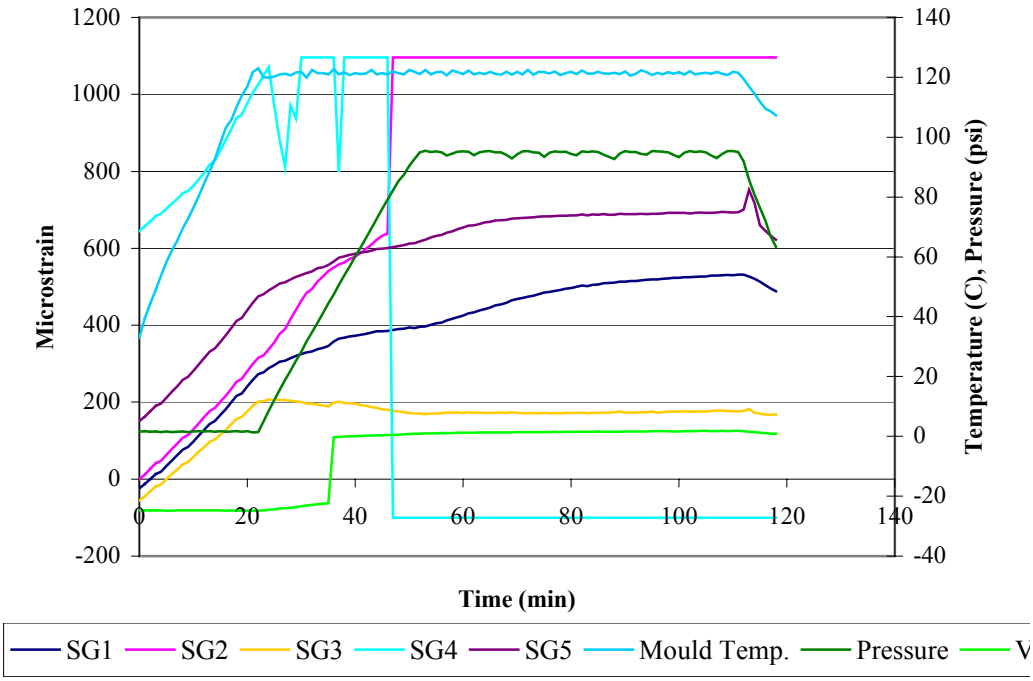

Figure 5.5 Cure cycle plot for panel PS11

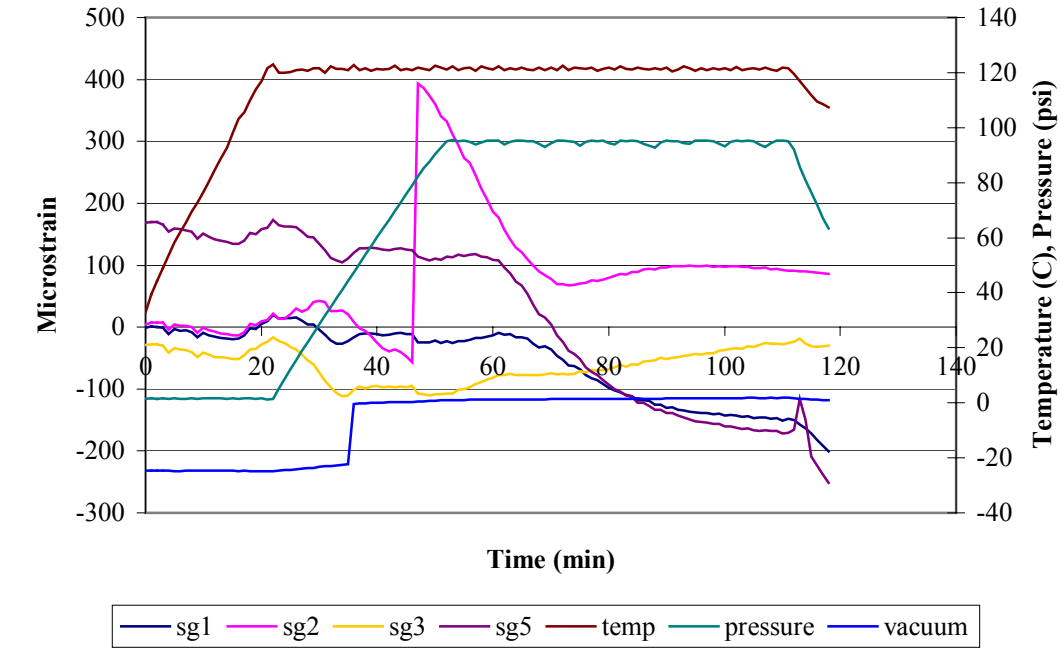

Figure 5.6 Plot of cure cycle less the reference run for panel PS11

Figure 5.6 shows the same again but for panel PS11. Again there is a linear section during the heating stage with negative slope, which can be associated with the

compressive load in the frame due to the thermal mismatch between the fibres and the frame. Table 5.3 presents the strain gauge readings for that time period again and follows them through to the resulting fibre pre-stress.

Table 5.3 Data from frame, followed through to give fibre pre-stress, for panel PS11

Data Point	1	2	Change
Time	0	15	
Strain Gauge 1 (με)	-1	-20	-19
Strain Gauge 2 (με)	4	-13	-17
Strain Gauge 3 (με)	-29	-52	-23
Strain Gauge 5 (με)	169	135	-34
Mean (με)			-23
Frame Young's Modulus (MPa)		210000	
Induced Stress in Frame (MPa)		4.83	
Frame Cross-Sectional Area (mm^2)		856	
Pre-Stress Load (N)		8269	
Panel Width (mm)	250	Thickness of 8 plies (mm)	1
Cross-Sectional Area of 8 plies (mm^2)		250	
Fibre Volume Fraction		0.56	
Area of Fibres in one direction (mm^2)		140	
Pre-Stress in Fibres (MPa)		**59**	

5.1.2. C-Scans

Each panel was C-scanned after having been removed from the pre-stress rig after cure. To set up the C-scan, the strongest signal was found on the panel using A-scan and that value was taken as the maximum. A threshold of 75% was then set and the whole panel was scanned. Figure 5.7a shows an example of an ideal panel result where the whole panel is shown in green, which means full signal all the time. Figure

5.7b shows an unacceptable panel where there are too many red areas and even some blue areas. Red represents only partial signal above the threshold and blue means no signal above the threshold. If the panel gave a reduced signal this would mean there had been some excessive attenuation. This was attributed to bad consolidation in the case of the red areas or voids in the blue areas. Figure 5.7c shows a panel, which was not ideal but acceptable.

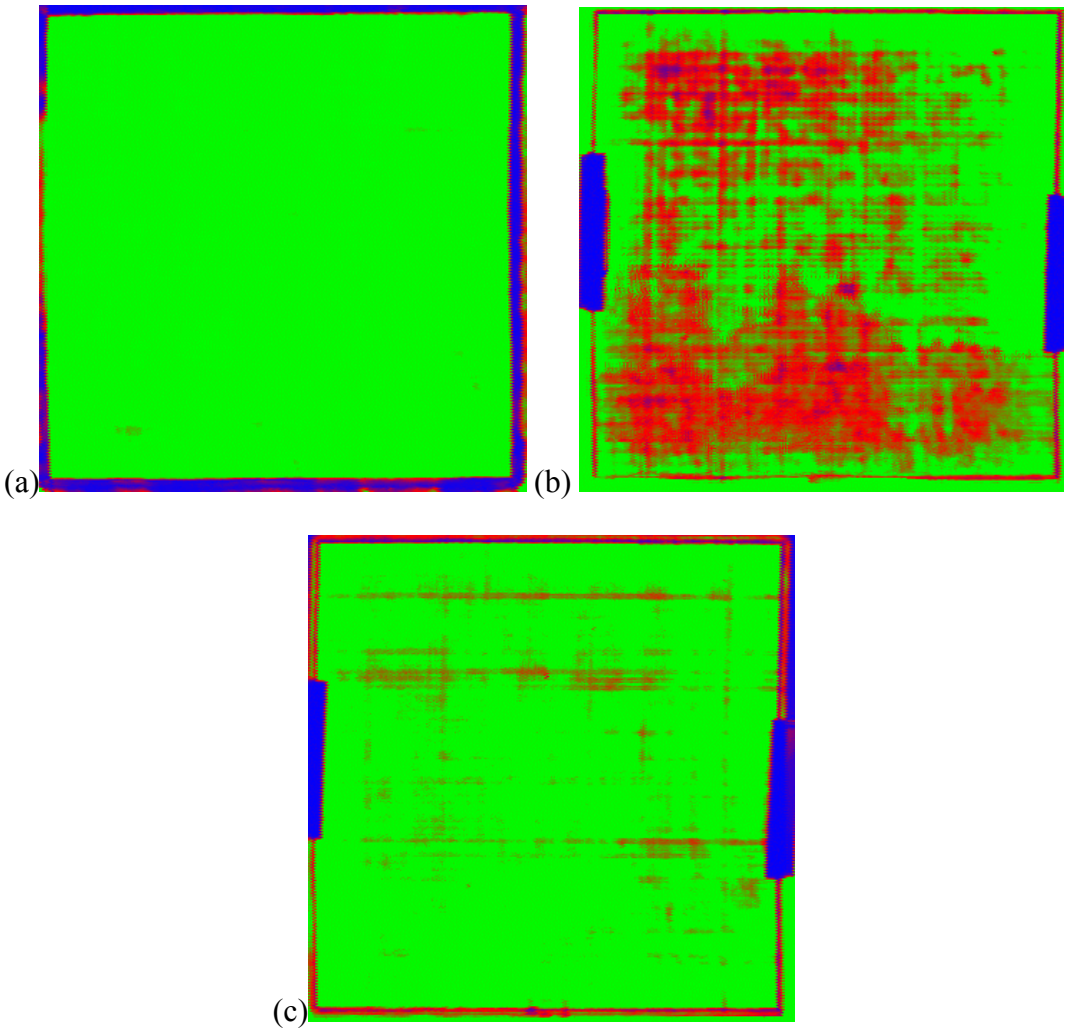

Figure 5.7 shows an (a) ideal, (b) unacceptable and (c) acceptable panel

5.1.3. Tensile Tests

A few sample coupons were taken aside for tensile testing to verify the presence of pre-stress. It was believed that the existence of pre-stress could be seen in an increase

in tensile strength in the cross-ply coupons. Figure 5.8 shows some sample stress-strain curves for the some of the pre-stressed coupons. Since the stress-strain relationship seemed only slightly non-linear with a sudden drop at the point of total failure, it was decided to take this point of total failure as the failure stress of the laminate. This failure stress was then used for comparison.

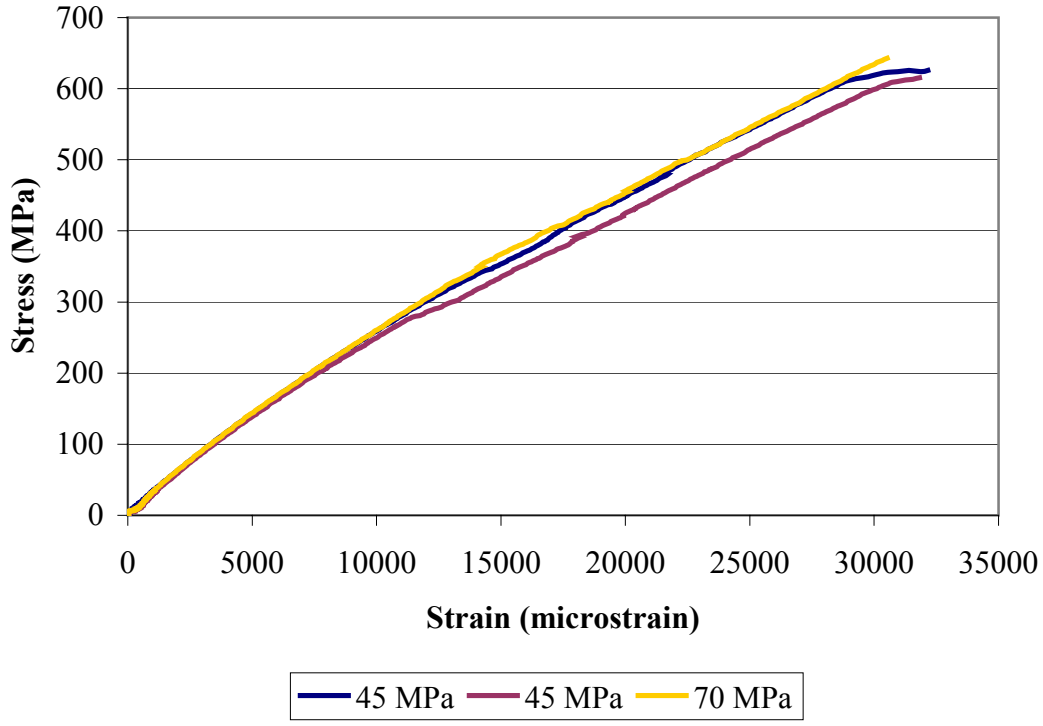

Figure 5.8 Plot of stress-strain behaviour for coupons at different levels of pre-stress

Figure 5.9 shows a comparative plot of failure stress at different levels of pre-stress. A linear fit was added to produce an approximate relationship between the laminate tensile strength and the induced pre-stress in the fibres. The resulting relationship was as follows: Failure Strength (MPa) = 1.45 x Pre-Stress (MPa) + 550.5 for the pre-stress range of 0 to 100 MPa and a 16-ply laminate with stacking sequence $[0/90_2/0_2/90/0/90]_S$. Table 5.4 also presents some predicted laminate tensile strengths

as a result of this relationship. These results and the mechanism by which tensile strength may be increased with pre-stressing are further discussed in chapter 6.

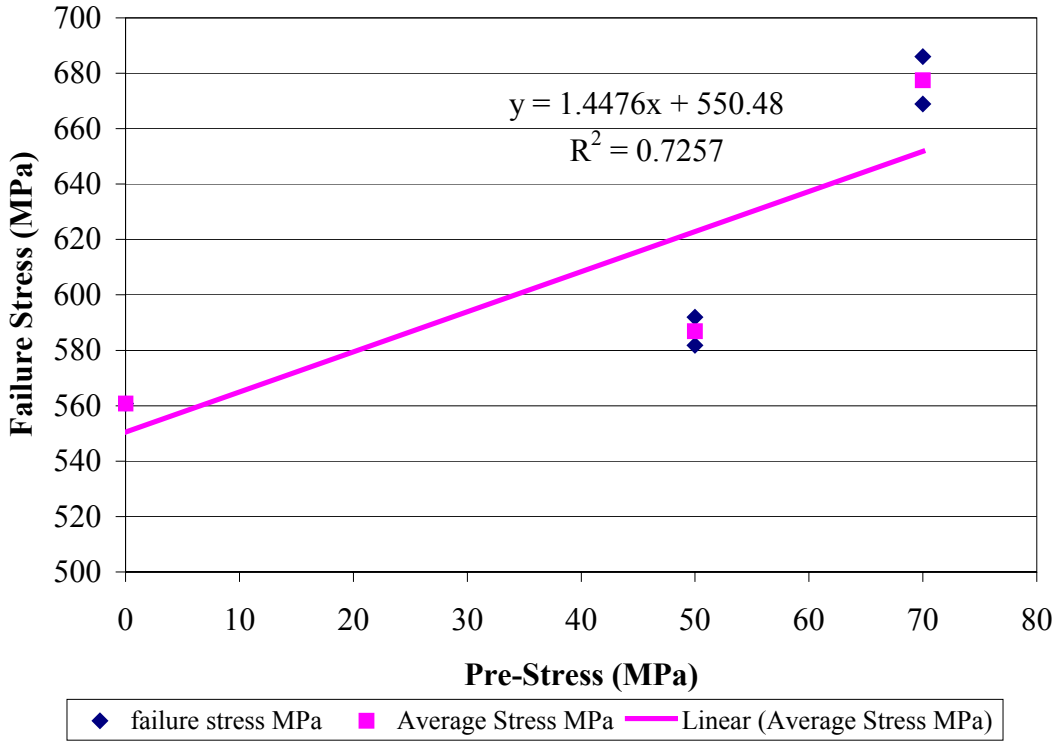

Figure 5.9 Plot of failure stress against fibre pre-stress

Table 5.4 Predicted values of laminte tensile strength for different levels of induced fibre pre-stress

Pre-Stress (MPa)	Predicted Laminate Tensile Strength (MPa)
0	550.5
30	594.0
50	623.0
60	637.5
70	652.0
80	666.5
100	695.5

5.2. Experimental Study

The results from the two experimental methods have been presented in this section, the gas gun study containing plots of absorbed energy against pre-stress levels and delamination areas against pre-stress levels and the drop weight study containing delamination areas and absorbed energy against pre-stress levels for different impact energies.

5.2.1. Gas Gun Impacts

Figure 5.11 and Figure 5.10 present the absorbed energy by the laminate against its corresponding levels of pre-stress for a 3-Joule, 93 $m.s^{-2}$ impact by a 0.707g steel sphere. No change can be observed in the absorbed energy as the pre-stress levels change. Standard deviation on the mean values is no more than 2.8%, where all but the values for 50MPa are below 2%.

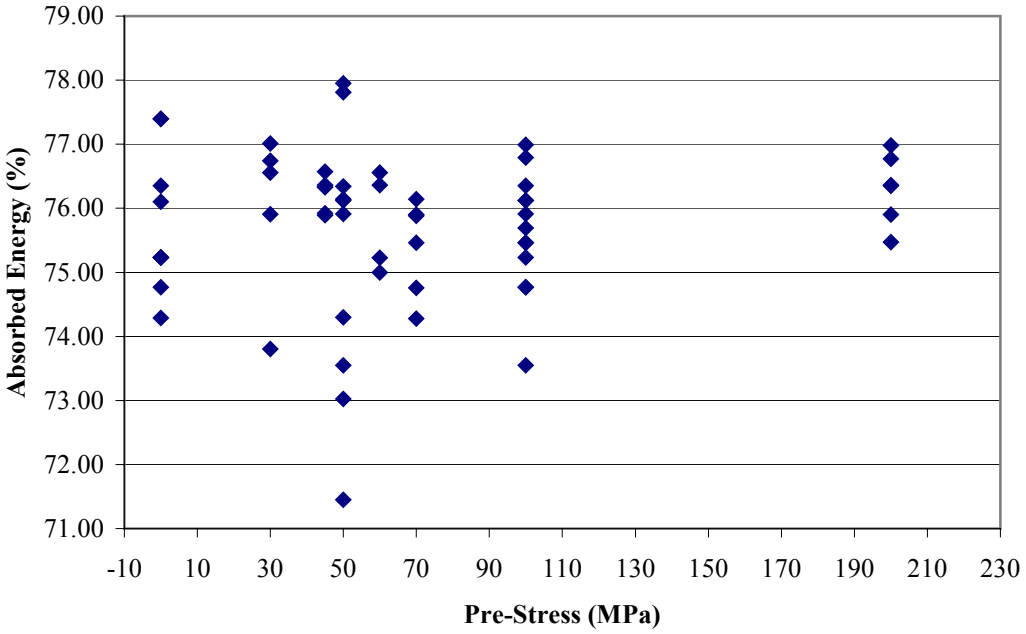

Figure 5.10 Plot of absorbed energy values against corresponding levels of pre-stress

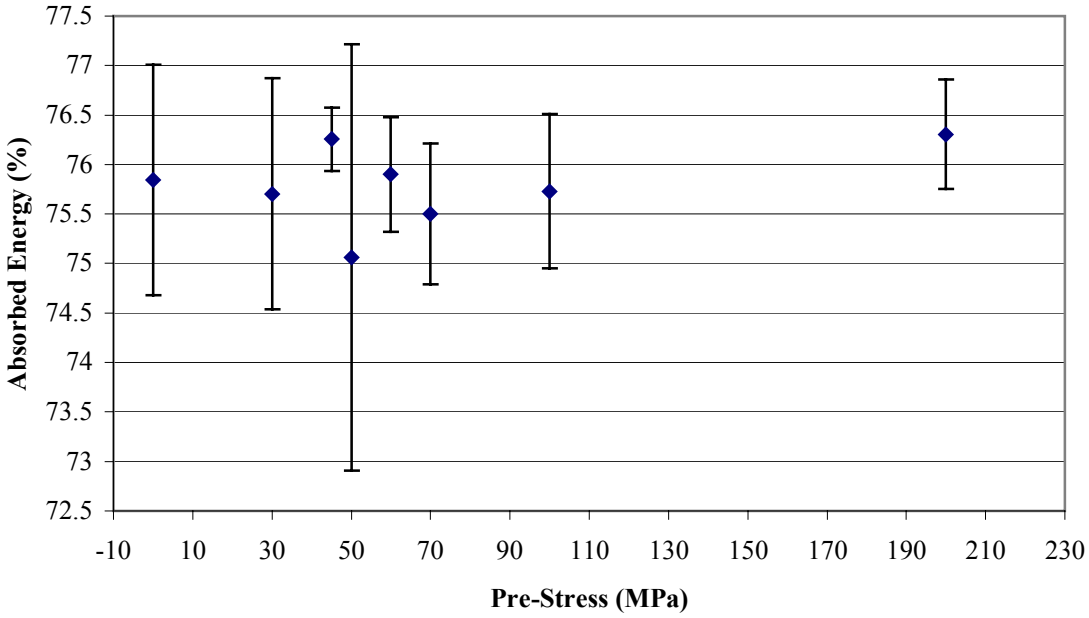

Figure 5.11 Plot showing the mean values with standard deviations for absorbed energy against corresponding levels of pre-stress

The values for absorbed energy were read directly from the gas gun impact results.

The data acquisition software, written in LabView, was able to take the time-of-flight of the projectile before and after the impact and, knowing the projectile's mass, calculate the incident and reflected impactor energies. The difference of the two gave the absorbed energy. It was assumed in this study that all energy lost by the projectile during impact would be absorbed in the laminate as damage.

Figure 5.13 and Figure 5.12 present the delamination areas in the impacted coupons using the gas gun. Again there appears to be no variation with different levels of pre-stress. Standard deviations on these mean values were between 4 and 14%.

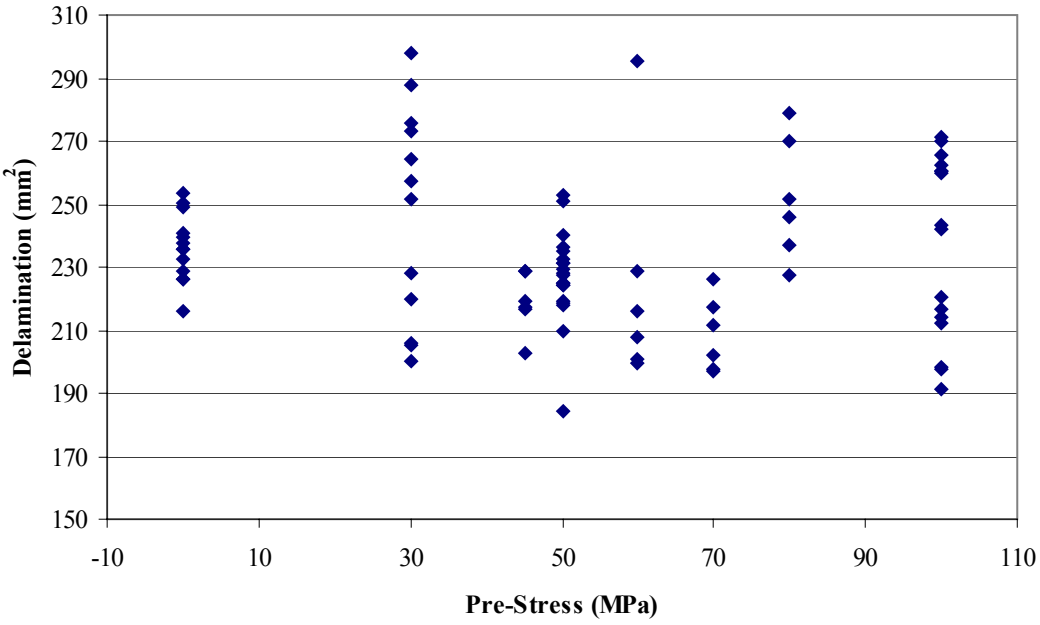

Figure 5.12 Plot of delamination areas against corresponding levels of pre-stress

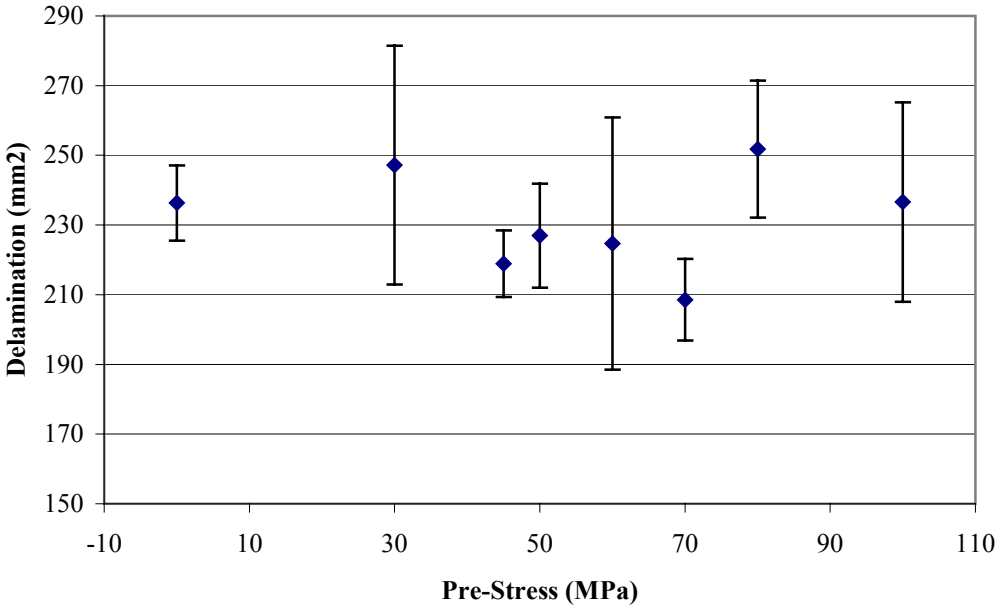

Figure 5.13 Plot of mean delamination areas against corresponding levels of pre-stress

Delamination areas for impacted coupons were determined by c-scanning them. The Leica QWin image analysis software employed thereafter to measure the value for delamination area had the capability for calculating the actual projected area of delamination for each coupon and present statistical figures (like standard deviation) for all the areas measured. To make best use of the statistical treatments, all coupons taken from one panel for gas gun impact were c-scanned together (see Figure 5.14) and run through the QWin at the same time. This meant that typically six coupons were c-scanned at the same time. The blue area in the middle of the coupon, together with its red edging was assumed to be the delamination (see Figure 5.14 for details). On such a c-scan blue signified total loss of signal as may be expected in a delaminated area. Red signified a signal of half strength. This was typically observed at the edges of panels and delaminations, where half the signal from the transducer was over the solid laminate and the other half of the signal over the void next to the coupon or the delaminated area.

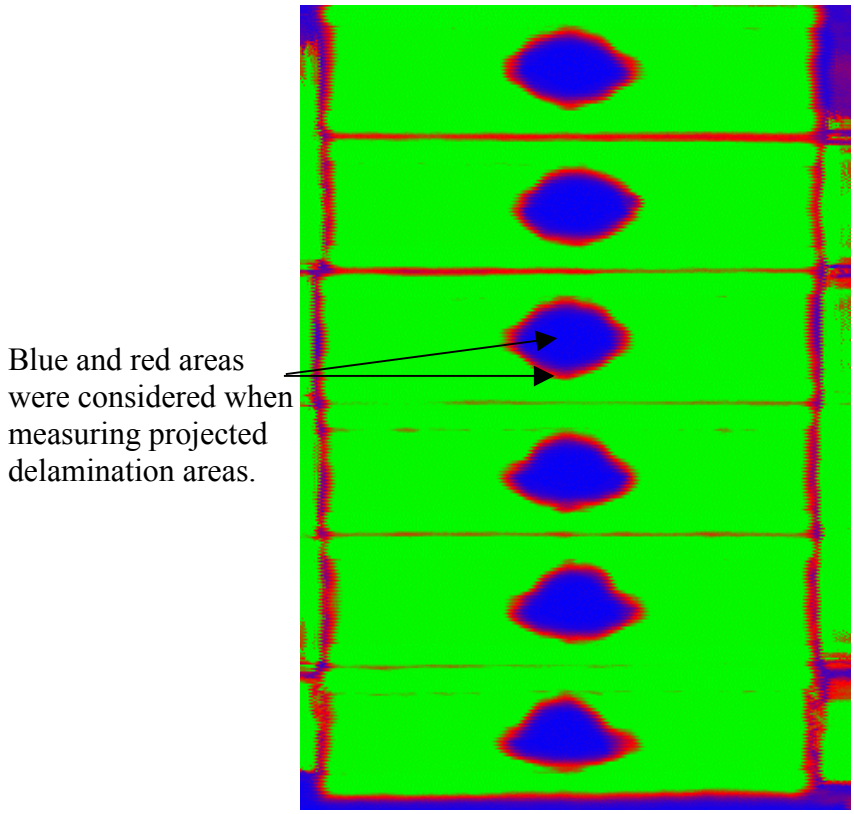

Figure 5.14 Image of a typical c-scan result for a set of six gas gun impact coupons.

Further to the above plots, Figure 5.15 and Figure 5.16 below show the typical damage through the thickness of a gas gun impacted specimen. Both figures first present the specimens as they were observed in the optical microscope (part a). In the second part of each image (part b) white lines have been added using a graphical editing program for more clarity of the delaminations.

Figure 5.15 shows a section cut across the coupon. The coupon was taken from the pre-stressed panel, PS13, which was pre-stressed to 70 MPa. The damage shows a constant delamination width through the thickness. There appears to be no delamination immediately below the impact zone stretching across the whole thickness of the laminate.

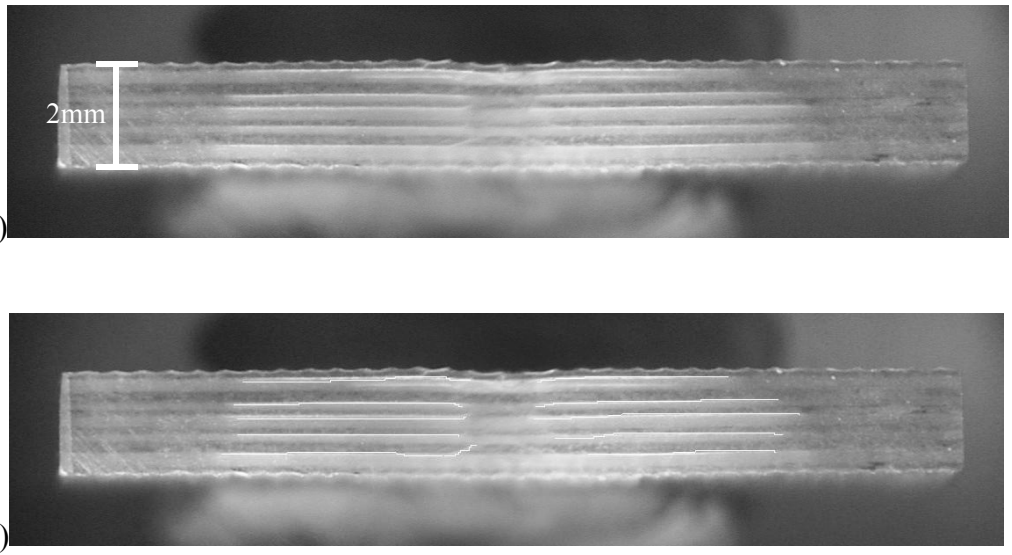

Figure 5.15 Typical Image of a delamination due to a gas gun impact. The sample has come from cutting the coupon across its length.

Figure 5.16 shows a section cut along the coupon. The coupon was taken from the pre-stressed panel, PS12, which was pre-stressed to 100 MPa. Here the damage is less constant through the thickness, but still almost constant. The same area immediately under the impact zone displays no delamination. What was not visible in Figure 5.15, though, was the backface spalling, which has become visible in the micrograph of Figure 5.16. This spalling can be seen as thick white lines on the lower surface of the micrographs.

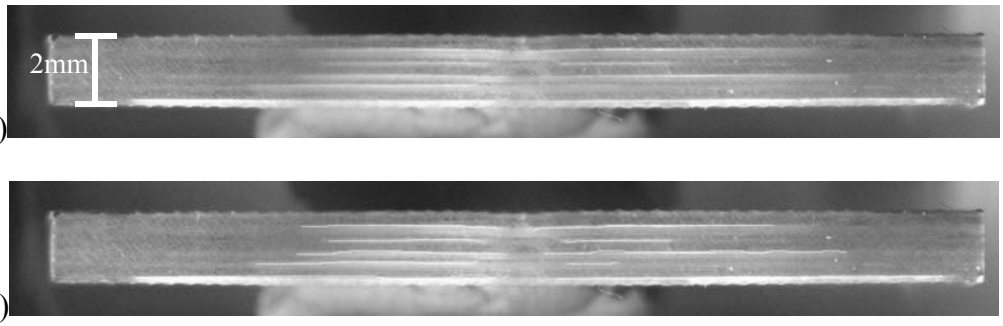

Figure 5.16 Typical Image of a delamination due to a gas gun impact. The sample has come from cutting the coupon along its length.

5.2.2. Instrumented Falling Weight Impacts

In this section the results of the instrumented falling weight impacts have been presented as delamination area against pre-stress. Due to calibration issues in the falling weight impact equipment it was not possible to derive the absorbed energies, so only the force-time curves have been presented. Figure 5.17 shows micrographs of the damage through the thickness for each pre-stress level for the 5-Joule impacts. To help see the delaminations more clearly grey lines have been added. The original micrographs can be found in Appendix B.

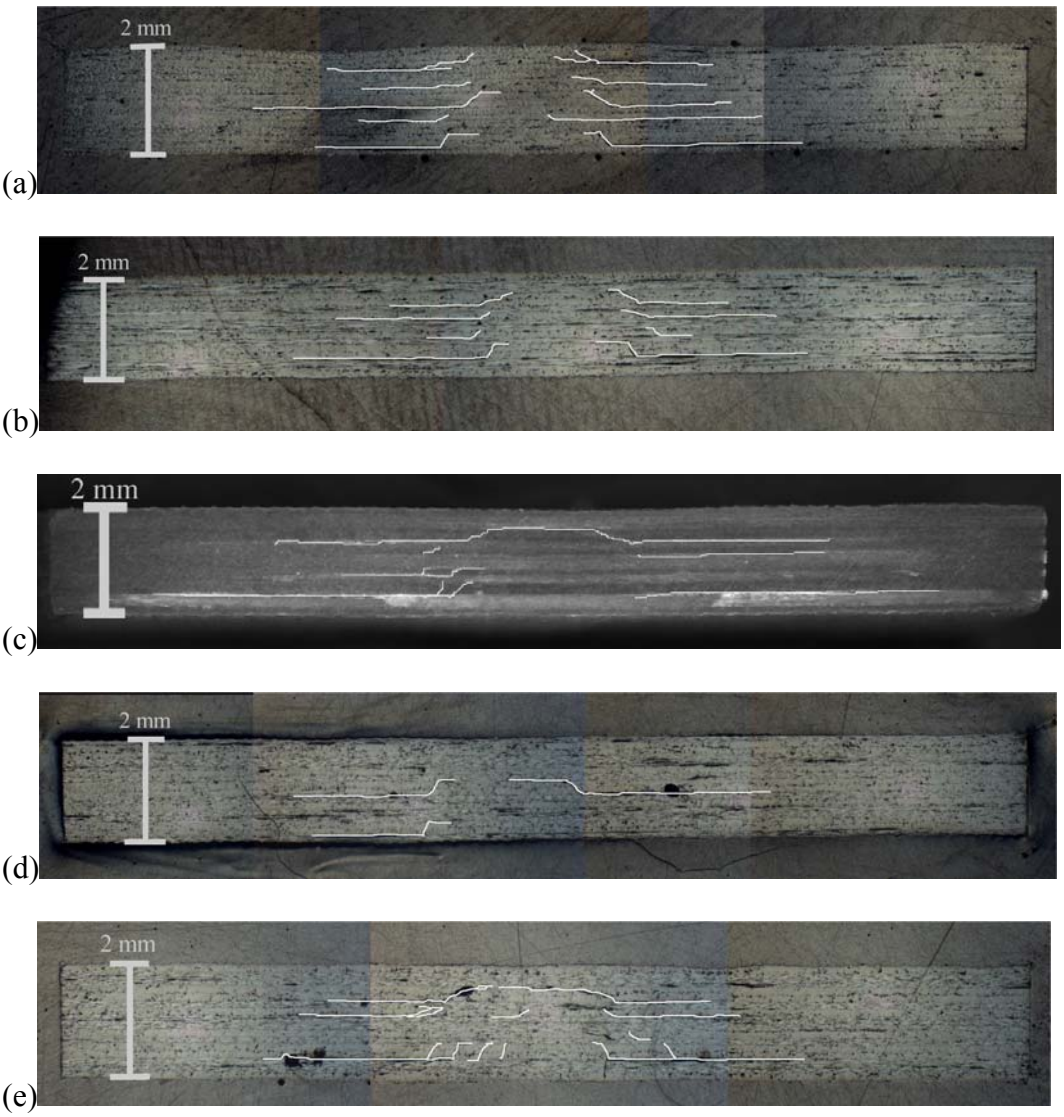

Figure 5.17 Micrographs of damage in 5-Joule impacted composites for pre-stress levels (a) 0 MPa, (b) 40 MPa, (c) 60 MPa, (d) 80 MPa and (e) 100 MPa.

The delamination areas were measured directly as described in chapter 4.3.2. All of the backlit images can however be found in Appendix B. The force-time plots for all the different levels of pre-stress are shown in Figure 5.18. In Figure 5.19 these force-time plots have been re-presented, where the value of force has been normalised against the incident velocity of the impactor. This was done to take away the variation of the incident velocity between impacts. Only representative curves are shown, rather than every curve for every impact, since three impacts were carried out

for each level of impact and each level of pre-stress. This would then give a very busy graph, from which little could be read. For purposes of readability, all force time plots have been placed in Appendix C.

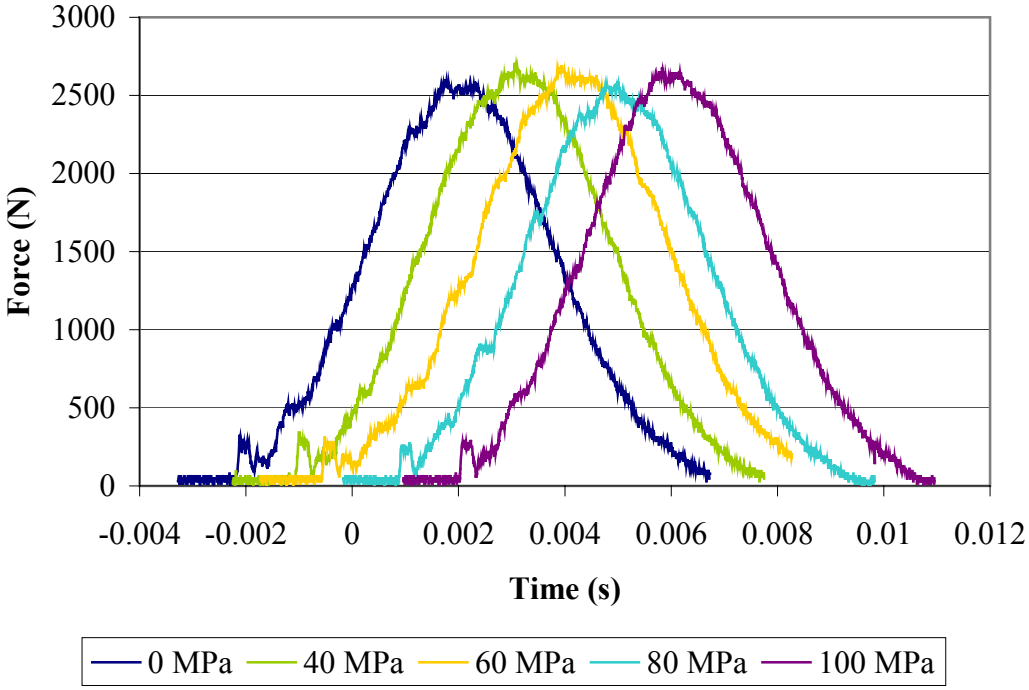

Figure 5.18 Representative force-time plots for the different levels of pre-stress impacted at 5 Joules. The various levels of pre-stress have been offset in time to allow for better clarity.

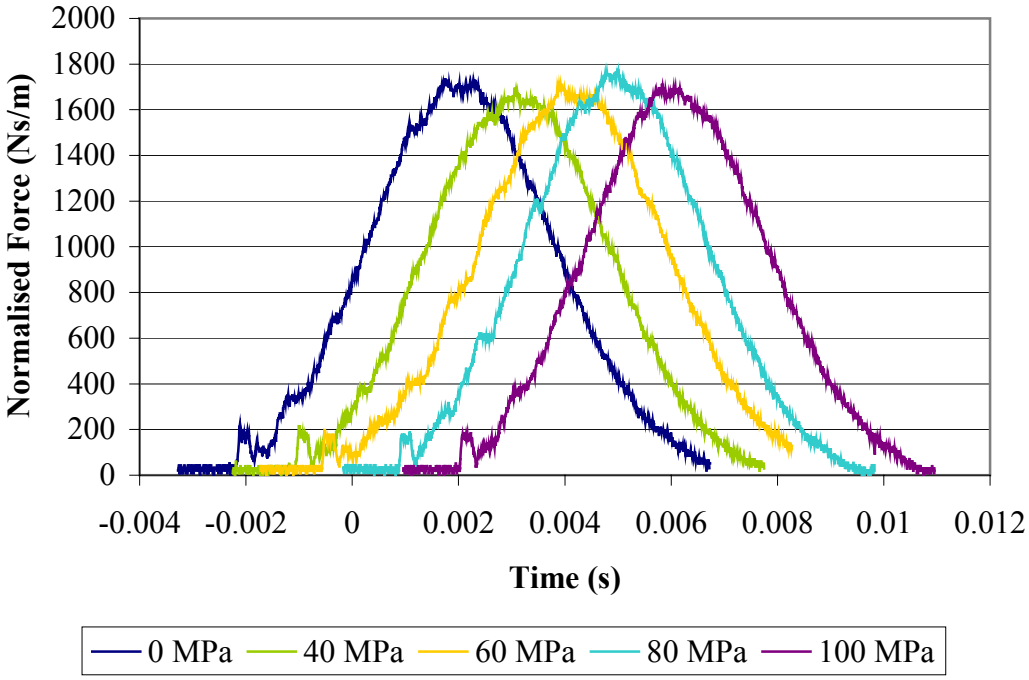

Figure 5.19 Force-Time Plots for 5-Joule impacts, where the forces have been normalised against the impact incident velocities.

The results from Figure 5.18 and Figure 5.19 show very little variation in peak force for different levels of pre-stress. For those plots of force-time relationships, where the force has not been normalised against impact velocity, there appears to be a slight increase in peak force for pre-stress levels of 40, 60 and 100 MPa against the non pre-stressed samples. The pre-stress level shows a slight drop in peak force over the non pre-stressed samples. Since the differences are, however no more that 4.6%, it may be assumed that this is random scatter.

The same can be said for the normalised force-time plots. Although the trend has now reversed itself, the variation is still no more than 2.33%, and therefore still within the bands of scatter.

The delamination areas plotted against their respective levels of pre-stress are now presented for the three different levels of impact energies. 5 Joules corresponds to a

1.9 m.s^{-1} impact by the 2.61kg tup, 17 Joules to a 3.5 m.s^{-1} impact and 73 Joules to a 6.4 m.s^{-1} impact. Figure 5.20 shows the 5-Joule impact results. There were only three data points for each level of pre-stress in each impact energy regime, so no statistical analysis could be carried out, although average values are shown for clarity. The results of these tests can therefore only be taken as giving trends and not as concrete evidence.

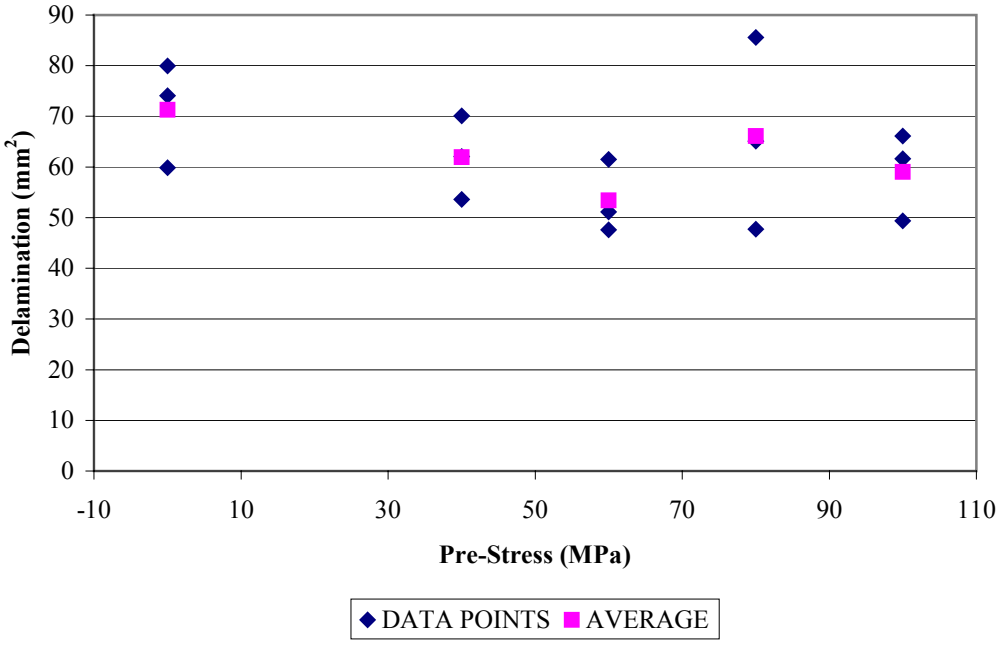

Figure 5.20 Delamination area against corresponding levels of pre-stress for the 5 Joule impact

For the 5-Joule impact, a trend was found where the delamination area dropped between no pre-stress and 60 MPa and then increased again. The drop in delamination area from no pre-stress to the 60MPa pre-stressed panel was 25%. Variation in delamination area between maximum and minimum at each level of pre-stress was between 14 and 38 mm^2, or between 13 and 29% off the average. The highest variation was found at 80 MPa of pre-stress.

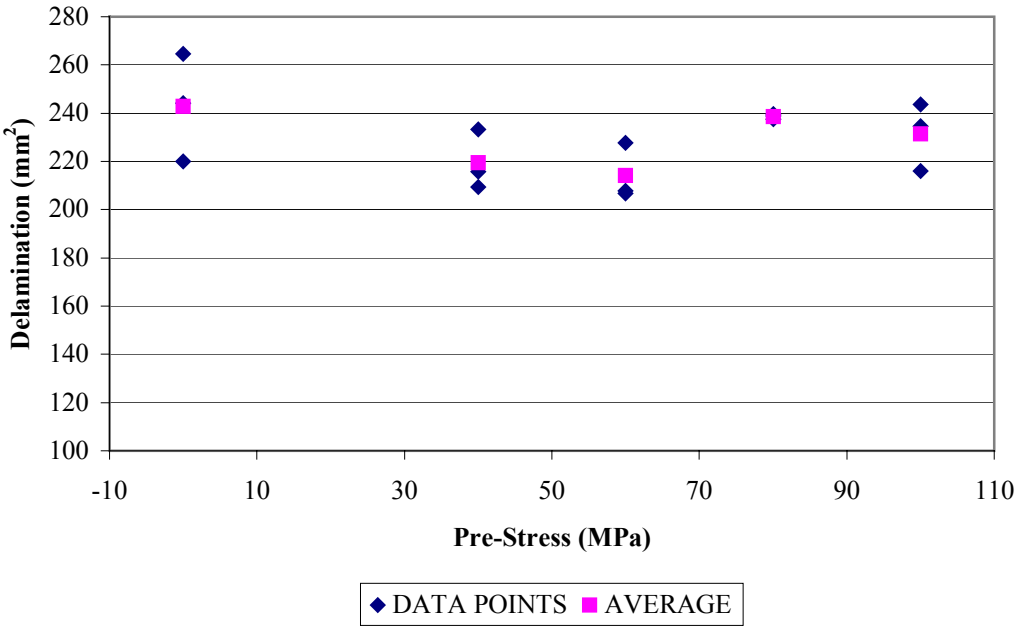

Figure 5.21 Delamination area against corresponding levels of pre-stress for the 17 Joule impact

Figure 5.21 shows the same for the 17-Joule impact, with there being a similar trend, although not as pronounced. In this case between no and 60 MPa of pre-stress there was a drop of 12% in delamination area. The variation between maximum and minimum values at each level of pre-stress was between 2 and 45 mm^2, or between 0.4 and 9% off the average. The maximum amount of variation was this time found in the panel with no pre-stress.

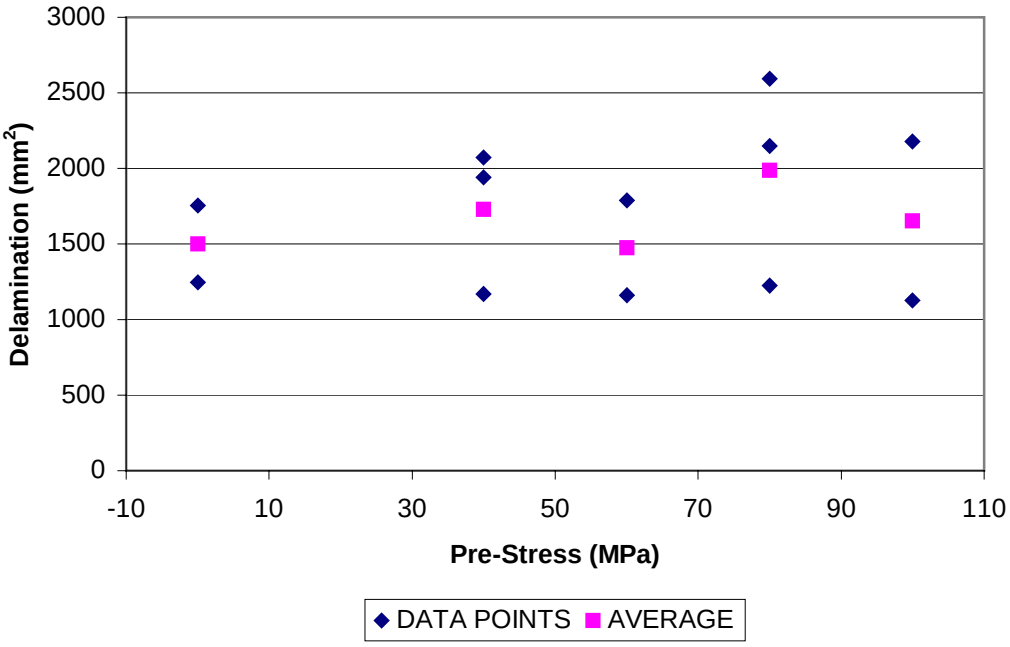

Figure 5.22 Delamination against corresponding levels of pre-stress for the 73 Joule impact

In Figure 5.22, it can be seen that the trend previously seen for delamination in both the 5-Joule and the 17-Joule impact is no longer visible. Variation for the delamination has also increased, being between 18 and 34% off the mean, or between 509 and 1367 mm^2 between maximum and minimum values.

Refer to Chapter 7.3.1 for a full discussion of the implications of these results.

5.3. Finite Element Analysis

To be able to simulate the properties of the composite laminate for different levels of pre-stress, the relationship quoted in section 5.1.3 was used. LS-DYNA calculated the laminate strengths using classical lamination theory. The equation presented in section 5.1.3 was for the whole laminate, but because it was a cross-ply laminate could be applied to the 11 and 22 ply directions of each ply. The equation was thus adapted for use in single plies, by replacing the last term (550.5 MPa) with the

respective ply strength in the direction being considered. Since no test data was available for compressive strengths, these were approximated and the same pre-stress equation was used.

The ply mechanical properties were found by carrying out coupon tensile tests on 8-ply unidirectional non pre-stressed samples. Six coupons were tested in each of the ply 11 and 22 directions. The results are presented in Table 5.5. Table 5.6 then presents the ply strength values, modified to take account of pre-stress.

Table 5.5 Coupon Test Results, showing the ply mechanical properties

Property	**Value**
Tensile Modulus, E_{11}	39745.3 ± 1036.6 MPa (± 2.6%)
Tensile Modulus, E_{22}	14191.3 ± 1475.7 MPa (± 10.4%)
Poisson Ratio, ν_{12}	0.2515 ± 0.0183 (± 7.3%)
Tensile Strength, f_{tu11}	1160 ± 118 MPa (± 10.2%)
Tensile Strength, f_{tu22}	35.85 ± 22.25 MPa (± 62.1%)

Table 5.6 Ply strength values modified for pre-stress

Pre-Stress (MPa)	**f_{ut11} (MPa)**	**f_{uc11} (MPa)**	**f_{ut22} (MPa)**	**f_{uc22} (MPa)**
0	1.16E+03	7.000E+02	3.585E+01	7.171E+01
30	1.20E+03	7.435E+02	7.935E+01	1.152E+02
50	1.23E+03	7.725E+02	1.084E+02	1.442E+02
70	1.26E+03	8.015E+02	1.374E+02	1.732E+02
100	1.31E+03	8.450E+02	1.809E+02	2.167E+02

5.3.1. Gas Gun Impacts

Images of the damage areas for MAT22 and MAT55 are shown in Figure 5.23, together with a C-scan image of a typical delamination are. The latter was added for comparison.

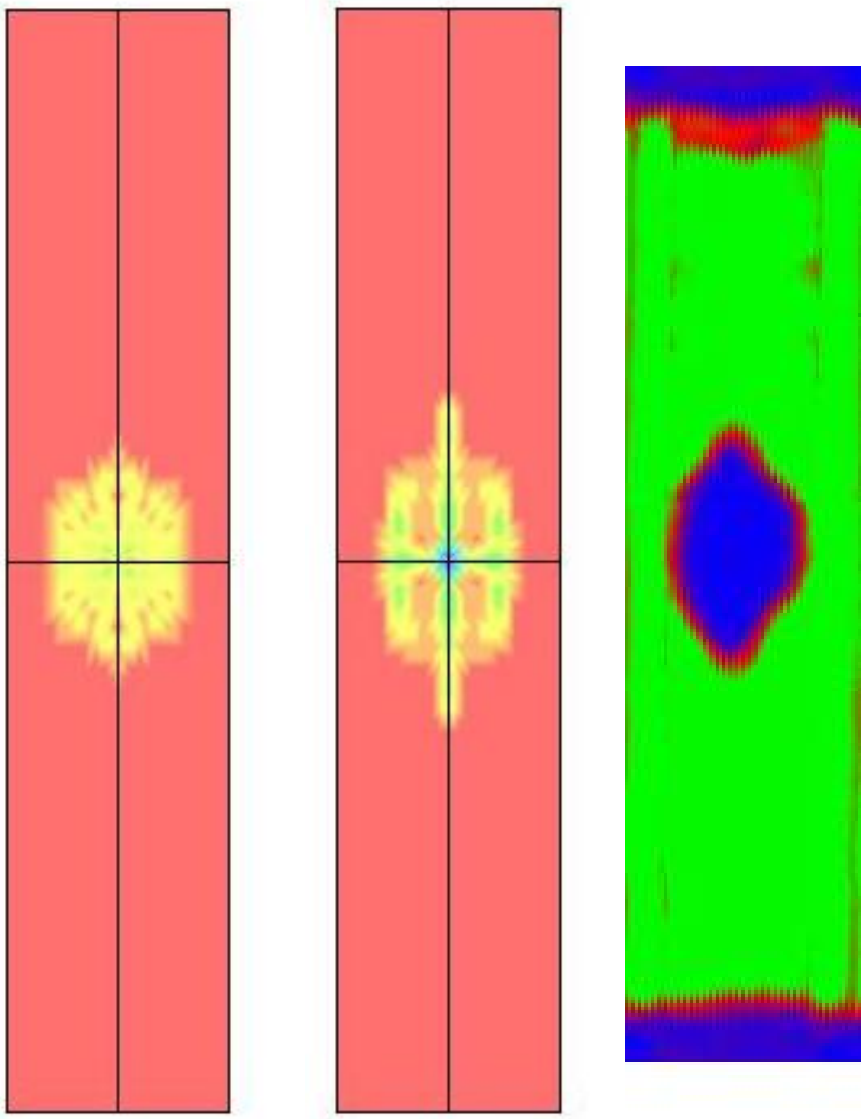

(a) (b) (c)

Figure 5.23 Impact damage area results for the finite element analyses for (a) MAT22 and (b) MAT55. (c) shows a c-scan of similar damage from experimental tests.

As with the experimental results, the absorbed energy was taken also from the finite element simulations. This was achieved by interrogating the model to give the steady-state kinetic energy of the projectile before and after the impact. This was done using the "matsum" ASCII file produced by the LS-DYNA solver. In this file the kinetic energies of all materials in the model are tabulated for each time step.

Taking the first and the last time steps, it was possible to find the initial and final kinetic energies of the projectile. The difference of the two gave the absorbed energy.

Plots of the results of the FE predictions for the gas gun impacts are presented in Figure 5.24 and Figure 5.25. They have been presented to correlate with the experimental results from section 5.2.1. Lines of best fit were also added to illustrate trends. Both material types (22 and 55) used in this study have been included in the same table to be able to draw comparisons later. Figure 5.24 shows a plot of damage areas (equivalent to the experimental C-scan results) against corresponding levels of pre-stress. Both material types exhibit a decrease in damage areas with increasing pre-stress levels, material type 55 showing a greater decrease than material type 22. Within the range presented there appears to have been no decrease in damage area, followed by a dip and eventual rise again, but a continued fall in damage area. Material type 22 displayed a linear decay in damage area, whereas the decay for material type 55 was exponential.

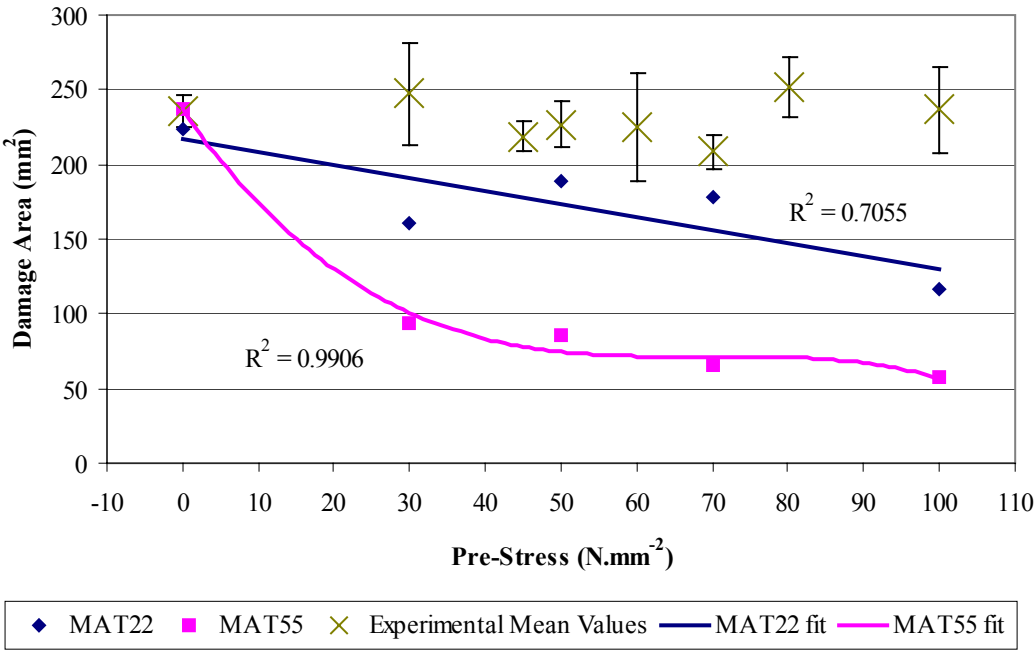

Figure 5.24 Plot showing the finite element analysis predicted damage areas against their corresponding pre-stress values. The experimental data was added for reference.

The plot in Figure 5.25 presents the variation in absorbed energy against pre-stress. Again material types 22 and 55 are shown. The results for material type 22 show an initial increase in absorbed energy, then a plateau and eventually a decline. The values for absorbed energy were also all above 90%. The results for material type 55 however show a steady linear decline in absorbed energy, beginning at 85.7% and ending at 75.4%.

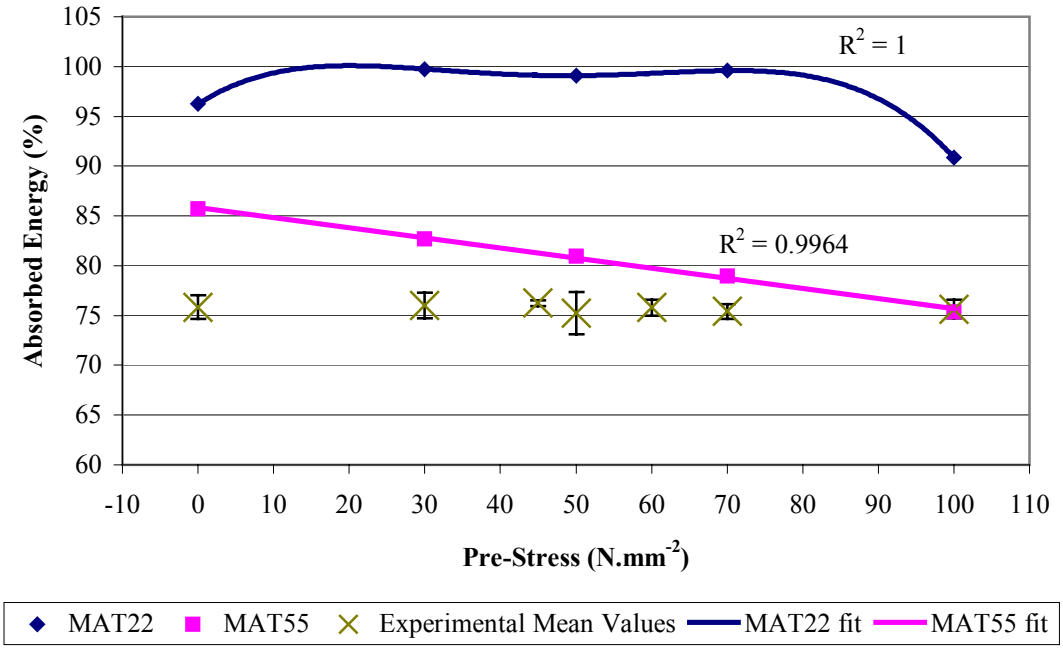

Figure 5.25 Plot of finite element analysis predicted percentage absorbed energies against their corresponding pre-stress values. The experimental results have been added for reference.

5.3.2. Drop Weight Impacts

The results of the instrumented falling weight impact have been presented in this section. In Figure 5.26, the force-time plots for each pre-stress level have been presented. Only the 5-Joule impact was modelled, as out of the three impact energies the variations in delaminations between levels of pre-stress were the greatest. Figure 5.27 supplements this result by showing peak forces from the finite element simulation plotted against those from test. The peak force in each case was determined by finding the maximum values from all the results. The finite element results were multiplied by a factor of 10 so the trends can be observed on the same scale.

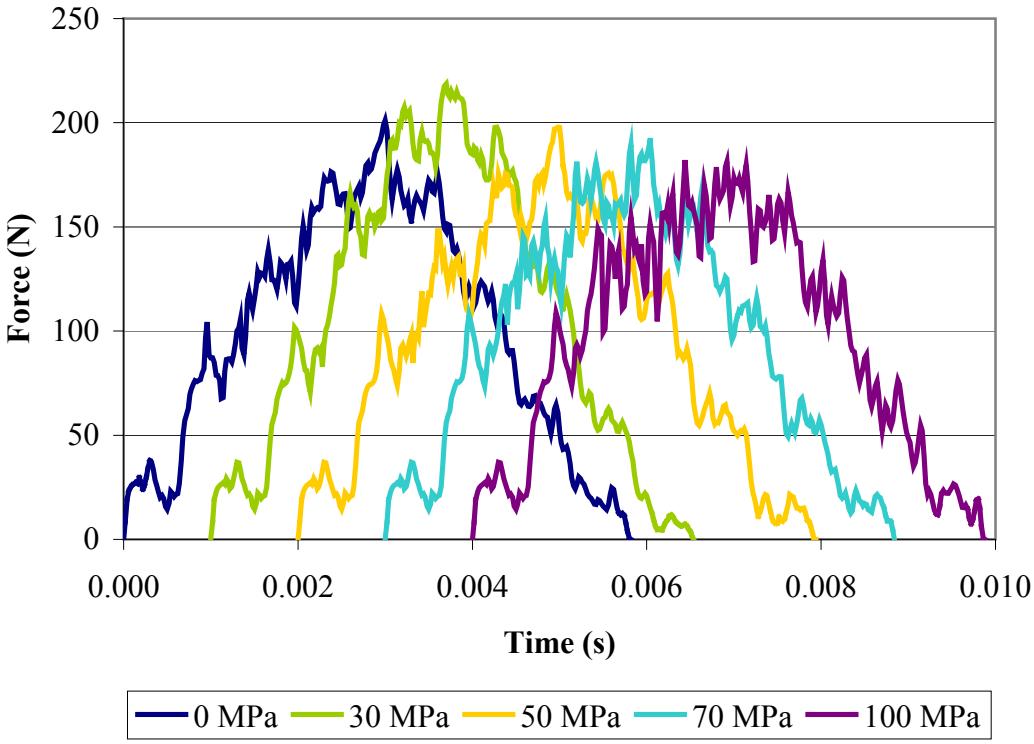

Figure 5.26 Force-Time Plots for the 5-Joule equivalent finite element simulation

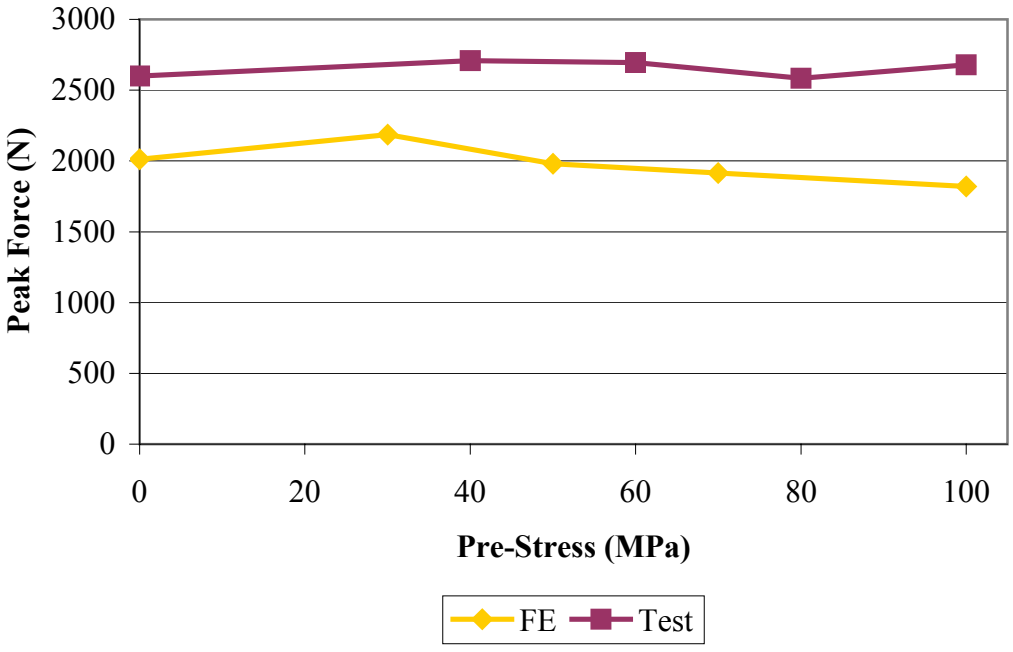

Figure 5.27 Plots of peak force against levels of pre-stress for the 5 Joule impacts.

Compared with the experimental results, the peak forces taken from the finite element

simulations (Figure 5.27) show a more pronounced trend. The peak force rises from the baseline at 0MPa pre-stress by 8% above the baseline at 30MPa and then steadily declines to 10% below the baseline at 100MPa pre-stress.

Figure 5.28 through Figure 5.32 show the damage areas in the simulated panels for the five different levels of pre-stress (0, 30, 50, 70 and 100 MPa). The width of each panel visible is 130mm – the width of the clamp setup in the instrumented falling weight. It must be noted that there appears to be a large variation in damage areas between the different levels of pre-stress and do not seem to follow any particular trend. It was therefore decided not to measure the damage areas as had been done with the gas gun tests.

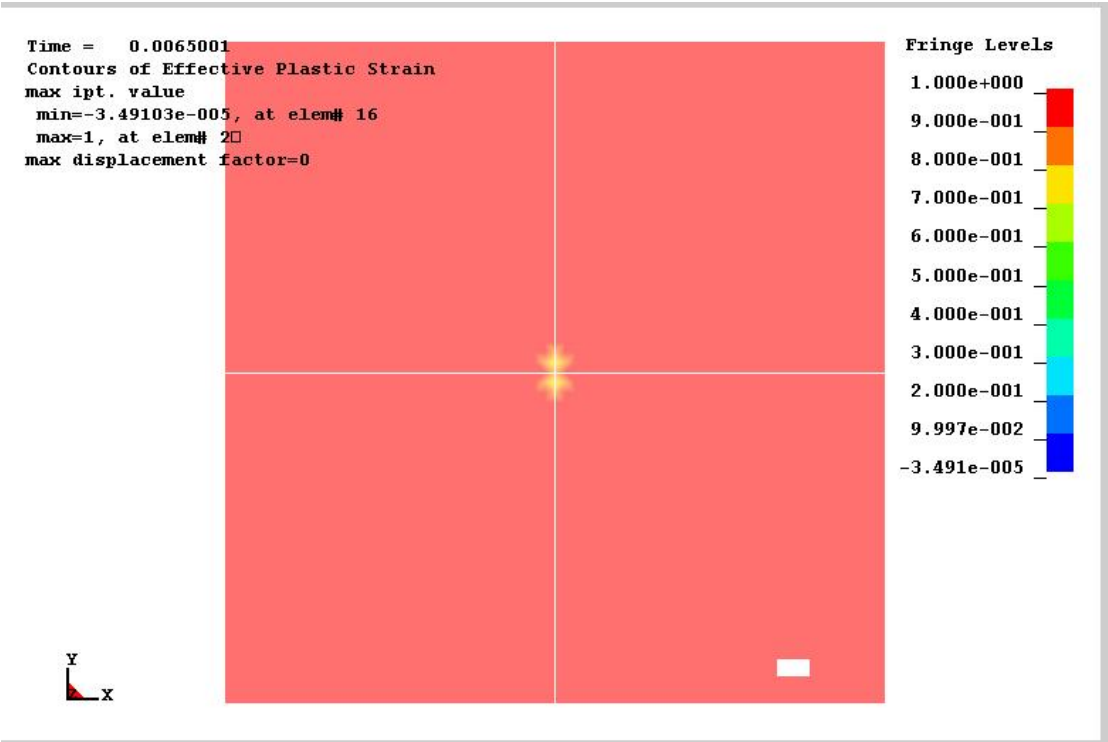

Figure 5.28 Simulation results for the panel without any pre-stressing.

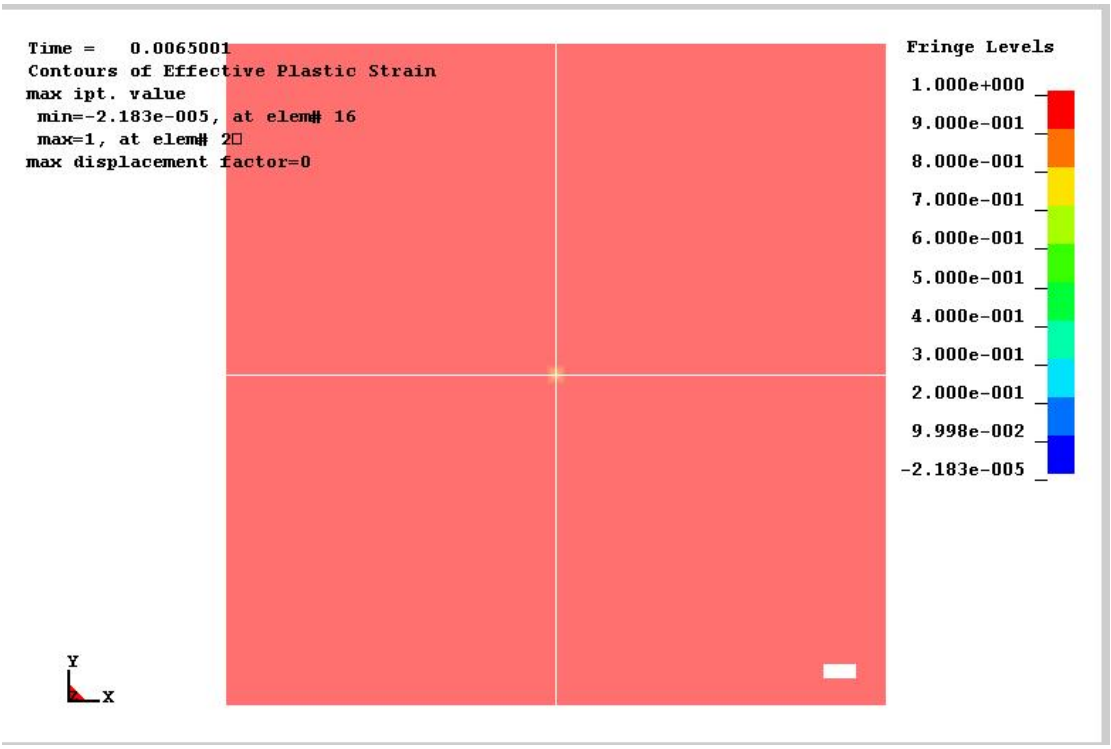

Figure 5.29 Simulation results for the panel with 30 MPa of pre-stressing.

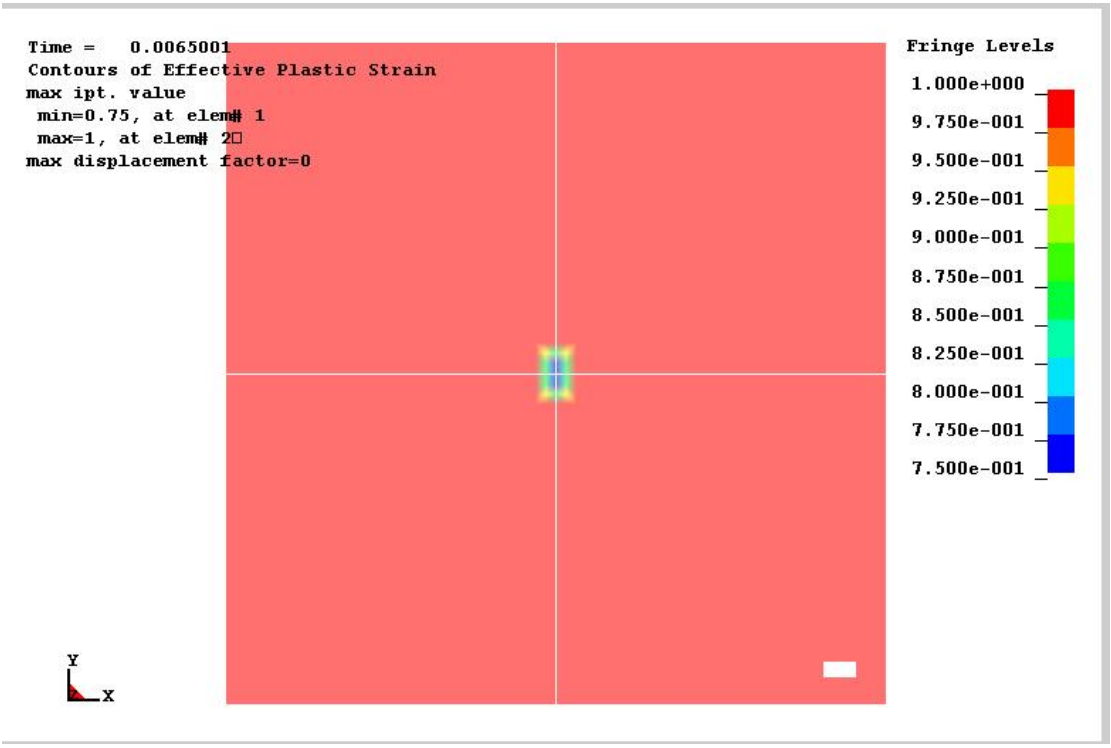

Figure 5.30 Simulation results for the panel with 50 MPa of pre-stressing.

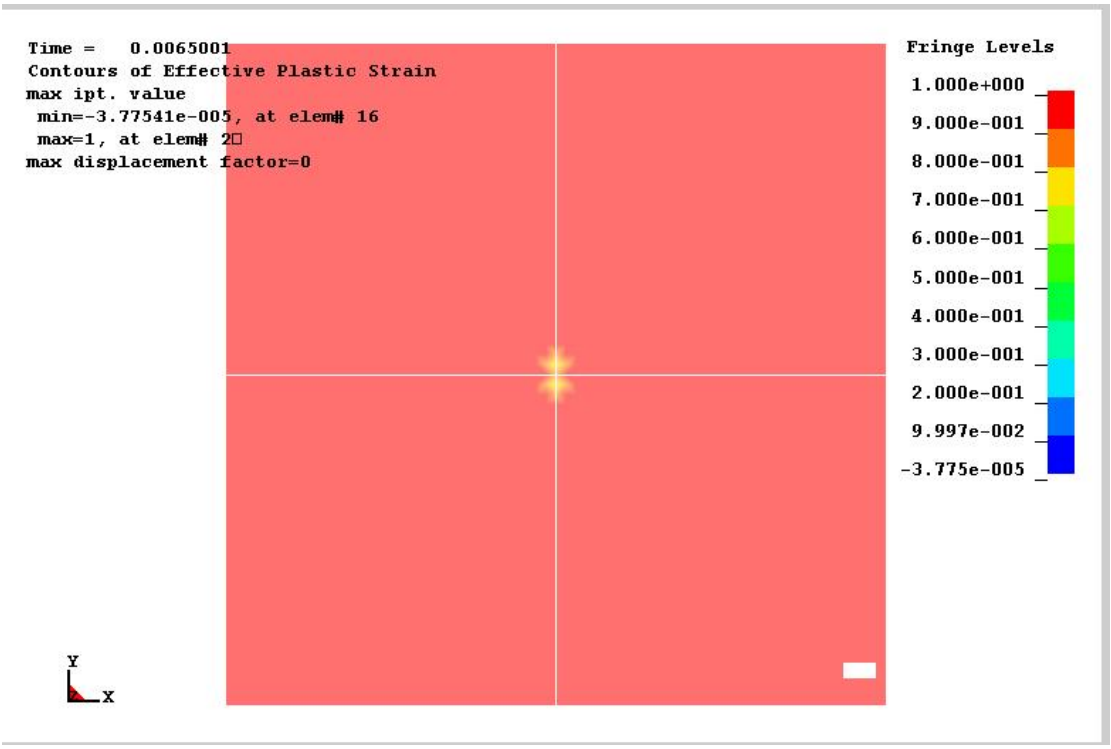

Figure 5.31 Simulation results for the panel with 70 MPa of pre-stressing.

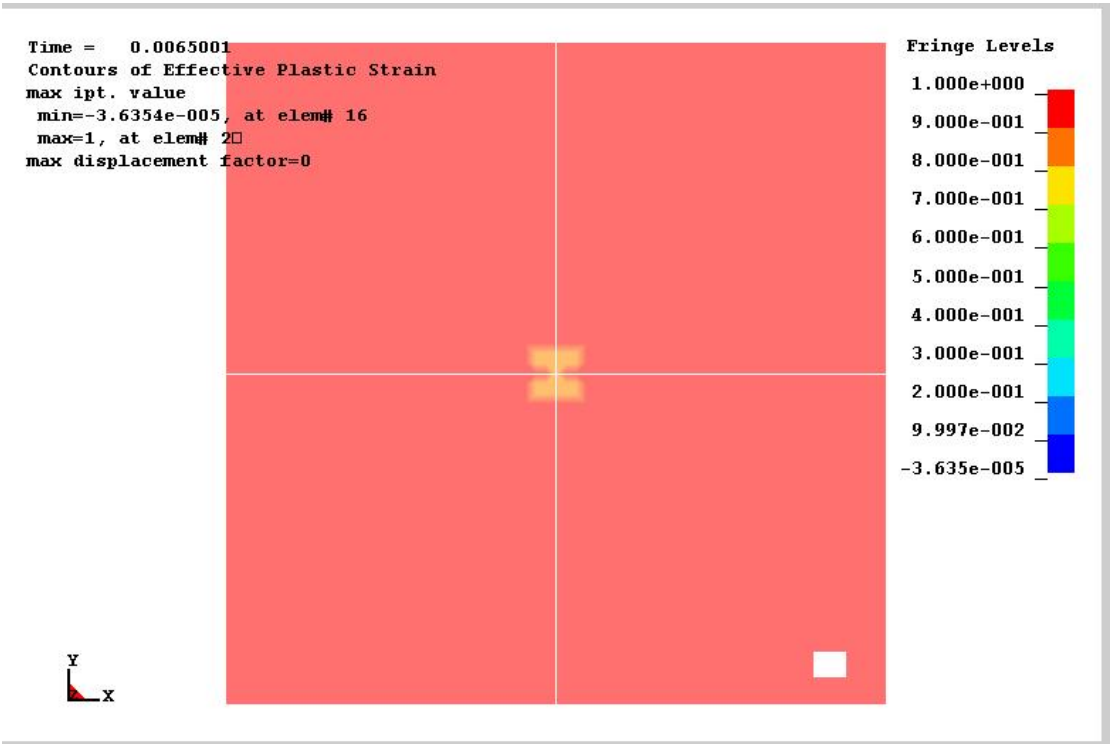

Figure 5.32 Simulation results for the panel with 100 MPa of pre-stressing.

5.4. Conclusions

This chapter has presented the results from the pre-stressed panel production (section 5.1), the experimental studies of gas gun and instrumented falling weight impacts (section 5.2) and the finite element simulations of the gas gun impacts (section 5.3). Over the last three chapters, the intention has been to be able to give an appreciation of the background, experimental procedures and their results in order to set the scene before discussing the issues encountered in this study. It is hoped that by now the reader has reached a point where they have formed their own views and discussion points and is intrigued to review the discussion about to follow. The previous three chapters have for this reason been left deliberately low in detail so the gaps may be filled during the discussions.

6. DISCUSSION – PRE-STRESS

The concepts and principles of pre-stressing, along with the process of inducing pre-stress into composites with regard to this work are discussed in this chapter. The experimental results including the impact data together with the associated discussions have been covered in chapter 0. This Chapter has been split into two main parts. The first covers the concepts and principles of pre-stressing. It also discusses the effect of pre-stressing on the internal residual stress state of a composite at a ply and laminate level. The second part discusses the method used in this study for producing pre-stressed panels. Such areas as the pitfalls and solutions to the present method and a finite element analysis of the method are covered. How pre-stressing fits into industrial applications is also discussed to give an overall appreciation of the relevance of this work.

6.1. Principles of Pre-Stressing

The principles of pre-stressing were briefly discussed in the literature review chapter, section 0. By mechanically pre-stressing the fibres before and during the cure cycle it is possible to superimpose an additional stress state onto the thermal residual stresses, which counteracts them in the matrix phase and for laminates in the ply in-plane transverse direction. Composite laminates typically fail through cracks developing along the fibre direction due to loading across it. First ply failure therefore usually occurs in the ply, which has the greatest angle from the loading direction (this will usually be the 90º ply). Thermal residual stresses leave the in-plane transverse direction of a ply under tension. Cracking is therefore likely to occur prematurely in a 90º ply with thermal residual stresses. Mechanical pre-stressing superimposes a

compressive stress in the in-plane transverse direction, thus recouping some of the transverse strength of the plies and delaying the first ply cracking to greater applied strains. This was confirmed by Dvorak and Suvorov (2000).

In the present chapter these principles will be discussed in more detail. To give the reader an appreciation of how the pre-stressing effects the stress state of the composite and how it comes about, the analysis will be carried out with a top-down approach. It will start at the laminate level and move down through to the micro-mechanical (fibre and matrix) level.

6.1.1. Assumptions

Throughout all the analysis in this chapter, a number of assumptions are applied, which make the analysis possible. The first is strain compatibility, in which it is assumed that there is perfect bonding between adjacent plies and between fibres and matrix. This results in the strains being equal in a particular direction in adjacent plies, or through the thickness of the laminate. The strains are also equal between the fibres and the matrix in the fibre directions. Figure 6.1 illustrates this concept.

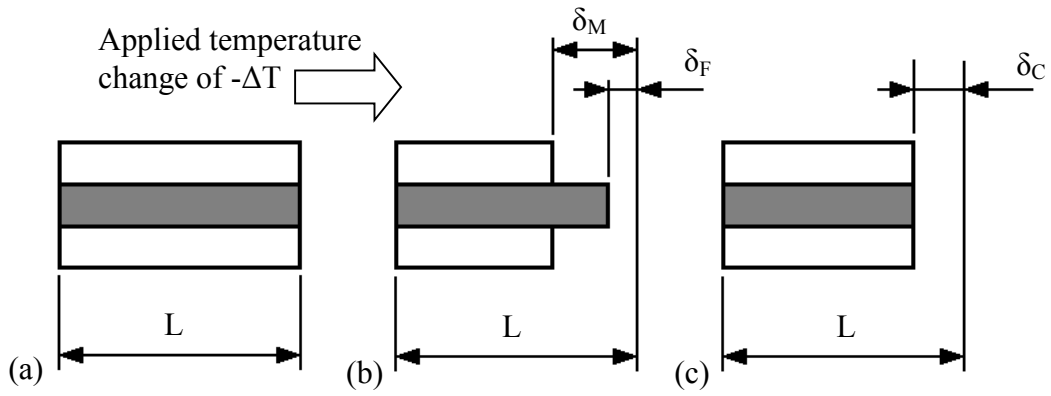

Figure 6.1 Concept of strain compatibility. (a) shows the two materials at their initial state, (b) shows their displacements if they were not connected and (c) shows them when full connectivity exists between them. It should be noted that $\delta_F<\delta_C<\delta_M$.

The second fundamental assumption is that at the point of analysis, when the residual stresses are to be calculated, no external loading is acting on the laminate. Therefore the sum of all forces must be in equilibrium and equal to zero.

It is further assumed that the stress state is steady and that there are no edge effects coming into play. Near the edges of a loaded composite laminate there exists a three-dimensional stress state. A laminate that is subject to thermal and mechanical residual stresses in the main body of the laminate, must allow these to become zero at a free boundary. Therefore, near the free edges stresses interact with the in-plane stresses to create a zero stress state. Figure 6.2 demonstrates this concept.

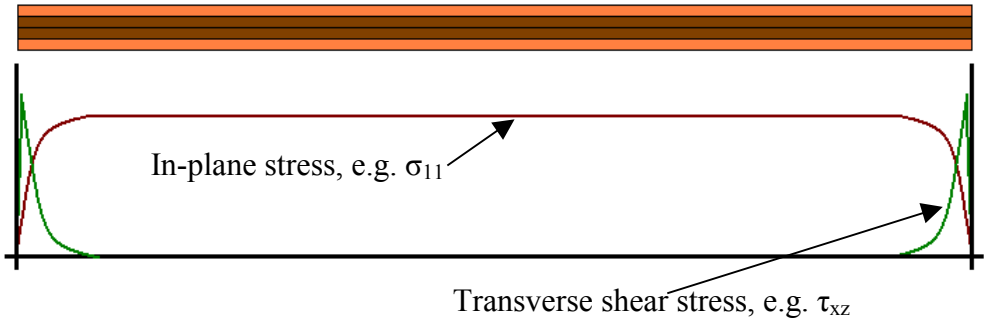

Figure 6.2 Diagram showing the locations and types of stresses at the edges of a laminate.

As a rule of thumb, it may be assumed that these stresses dissipate within one to one-and-a-half thicknesses into the laminate and after that a constant and steady stress state exists. Such edge stresses may then be ignored if the in-plane dimensions are at least ten times greater than the laminate thickness (Hull and Clyne, 1996).

For the production of pre-stressed panels this assumption has been valid, since the panels were all 250 mm square and only 2 mm thick. When panels were cut up into coupons for gas gun impact testing, new free edges were created, so the assumption had to be applied to the new dimensions of the coupons and not the dimensions of the panel. Since the coupons were 200 mm by 20 mm, in-plane, the assumption was marginal (the smaller dimension was only ten times greater than the thickness), but it was decided to continue to ignore the edge effects. Had the coupons been any smaller, this would not have been possible.

In the classical laminate analysis (Barbero, 1999) further assumptions are made specific to this study. One assumption is that the layup is balanced and symmetric. A composite layup is symmetric, when its ply stacking sequence is mirrored about its centre line (e.g. a 0/90/90/0 layup is symmetric, as is 0/+45/-45/90/90/-45/+45/0

layup). A balanced layup is one where for every +θº ply there is a corresponding –θº ply. Also for every 0º ply there is a corresponding 90º ply. Balanced laminates also have identical laminate moduli in two directions ($E_x = E_y$). This assumption is justified since the laminate in this study has a layup $[0/90_2/0_2/90/0/90]_S$, which according to the above is balanced and symmetric. The implication of this will become clear in the analysis below, but in short, it simplifies the classical laminate analysis.

Another assumption is that no bending is induced in the laminate. Again the motivation behind this is to simplify the analysis. If there is no bending applied, the bending terms can be ignored. This assumption is justified by the fact that no external loading is applied to the laminate; therefore the only source of bending may be found by each ply being pre-stressed a different amount. This would give rise to a difference in in-plane residual loading and therefore apply bending to the laminate. The pre-stress rig was designed specifically not to allow this to happen. To produce panels with varying tension in the plies in the pre-stress rig the clamps would have to sag under their own weight in the frame. Supports were put in place to prevent just that, so it may be assumed that bending was not an issue.

6.1.2. Macro-Mechanics (at a laminate level)

Classical laminate analysis links the laminate in-plane forces and moments with the in-plane strains and curvatures as follows (Barbero, 1999):

$$\begin{Bmatrix} N \\ M \end{Bmatrix} = \begin{bmatrix} A & B \\ B & D \end{bmatrix} \begin{Bmatrix} \varepsilon^0 \\ \kappa \end{Bmatrix}, \qquad \textbf{(6.1)}$$

Which expands to:

$$\begin{Bmatrix} N_x \\ N_y \\ N_{xy} \\ M_x \\ M_y \\ M_{xy} \end{Bmatrix} = \begin{bmatrix} A_{11} & A_{12} & A_{16} & B_{11} & B_{12} & B_{16} \\ A_{12} & A_{22} & A_{26} & B_{12} & B_{22} & B_{26} \\ A_{16} & A_{26} & A_{66} & B_{16} & B_{26} & B_{66} \\ B_{11} & B_{12} & B_{16} & D_{11} & D_{12} & D_{16} \\ B_{12} & B_{22} & B_{26} & D_{12} & D_{22} & D_{26} \\ B_{16} & B_{26} & B_{66} & D_{16} & D_{26} & D_{66} \end{bmatrix} \begin{Bmatrix} \varepsilon_x^0 \\ \varepsilon_y^0 \\ \gamma_{xy}^0 \\ \kappa_x \\ \kappa_x \\ \kappa_{xy} \end{Bmatrix}, \qquad \textbf{(6.2)}$$

Where N and M are the laminate direct and bending loads respectively. The **A**, **B** and **D** matrices are the in-plane stiffness, in-plane-bending coupling and bending stiffness matrices. ε^0, γ^0 and κ are the mid-plane strains, shear strains and curvatures respectively.

For a balanced and symmetric laminate, the **B** matrix will become zero, effectively decoupling the direct loading from the bending loading. Also, since there is no applied bending loading (there is no external loading and assuming pre-stress is applied evenly through the thickness of the laminate no bending will be introduced that way either), the whole of equation (6.2) can be simplified to

$$\begin{Bmatrix} N_x \\ N_y \\ N_{xy} \end{Bmatrix} = \begin{bmatrix} A_{11} & A_{12} & A_{16} \\ A_{12} & A_{22} & A_{26} \\ A_{16} & A_{26} & A_{66} \end{bmatrix} \begin{Bmatrix} \varepsilon_x^0 \\ \varepsilon_y^0 \\ \gamma_{xy}^0 \end{Bmatrix}, \qquad \textbf{(6.3)}$$

This can in turn be rewritten in term of strain.

$$\begin{Bmatrix} \varepsilon_x^0 \\ \varepsilon_y^0 \\ \gamma_{xy}^0 \end{Bmatrix} = \begin{bmatrix} \alpha_{11} & \alpha_{12} & \alpha_{16} \\ \alpha_{12} & \alpha_{22} & \alpha_{26} \\ \alpha_{16} & \alpha_{26} & \alpha_{66} \end{bmatrix} \begin{Bmatrix} N_x \\ N_y \\ N_{xy} \end{Bmatrix}. \qquad \textbf{(6.4)}$$

The **α** matrix is the direct compliance matrix.

Thermal and pre-stress terms are now introduced giving,

$$\begin{Bmatrix} \varepsilon_x^0 \\ \varepsilon_y^0 \\ \gamma_{xy}^0 \end{Bmatrix} = \begin{bmatrix} \alpha_{11} & \alpha_{12} & \alpha_{16} \\ \alpha_{12} & \alpha_{22} & \alpha_{26} \\ \alpha_{16} & \alpha_{26} & \alpha_{66} \end{bmatrix} \begin{Bmatrix} N_x - N_x^T - N_x^P \\ N_y - N_y^T - N_y^P \\ N_{xy} - N_{xy}^T - N_{xy}^P \end{Bmatrix}, \quad \textbf{(6.5)}$$

Where N^T and N^P are the mid plane effective loads for thermal and pre-stress effects respectively. These effective loads are internal loads of the laminate, which give the observed residual strains.

$$N_x^T = \sum_{k=1}^{n} \left[\overline{Q}_{11}^{(k)} \varepsilon_x^{T(k)} \left(z_k - z_{k-1} \right) + \overline{Q}_{12}^{(k)} \varepsilon_y^{T(k)} \left(z_k - z_{k-1} \right) + \overline{Q}_{16}^{(k)} \gamma_{xy}^{T(k)} \left(z_k - z_{k-1} \right) \right],$$

$$N_y^T = \sum_{k=1}^{n} \left[\overline{Q}_{12}^{(k)} \varepsilon_x^{T(k)} \left(z_k - z_{k-1} \right) + \overline{Q}_{22}^{(k)} \varepsilon_y^{T(k)} \left(z_k - z_{k-1} \right) + \overline{Q}_{26}^{(k)} \gamma_{xy}^{T(k)} \left(z_k - z_{k-1} \right) \right], \quad \textbf{(6.6)}$$

$$N_{xy}^T = \sum_{k=1}^{n} \left[\overline{Q}_{16}^{(k)} \varepsilon_x^{T(k)} \left(z_k - z_{k-1} \right) + \overline{Q}_{26}^{(k)} \varepsilon_y^{T(k)} \left(z_k - z_{k-1} \right) + \overline{Q}_{66}^{(k)} \gamma_{xy}^{T(k)} \left(z_k - z_{k-1} \right) \right].$$

$$N_x^P = \sum_{k=1}^{n} \left[\overline{Q}_{11}^{(k)} \varepsilon_x^{P(k)} \left(z_k - z_{k-1} \right) + \overline{Q}_{12}^{(k)} \varepsilon_y^{P(k)} \left(z_k - z_{k-1} \right) + \overline{Q}_{16}^{(k)} \gamma_{xy}^{P(k)} \left(z_k - z_{k-1} \right) \right],$$

$$N_y^P = \sum_{k=1}^{n} \left[\overline{Q}_{12}^{(k)} \varepsilon_x^{P(k)} \left(z_k - z_{k-1} \right) + \overline{Q}_{22}^{(k)} \varepsilon_y^{P(k)} \left(z_k - z_{k-1} \right) + \overline{Q}_{26}^{(k)} \gamma_{xy}^{P(k)} \left(z_k - z_{k-1} \right) \right], \quad \textbf{(6.7)}$$

$$N_{xy}^P = \sum_{k=1}^{n} \left[\overline{Q}_{16}^{(k)} \varepsilon_x^{P(k)} \left(z_k - z_{k-1} \right) + \overline{Q}_{26}^{(k)} \varepsilon_y^{P(k)} \left(z_k - z_{k-1} \right) + \overline{Q}_{66}^{(k)} \gamma_{xy}^{P(k)} \left(z_k - z_{k-1} \right) \right].$$

$\overline{Q}_{ij}^{(k)}$ are the reduced stiffness matrix terms in the global coordinate system for the k^{th} ply. $\varepsilon_i^{T(k)}$ and $\varepsilon_i^{P(k)}$ are the k^{th} ply strain terms in the global coordinate system for the thermal and pre-stress effects respectively. $\varepsilon_i^{T(k)}$ and $\varepsilon_i^{P(k)}$ are given by

$$\begin{Bmatrix} \varepsilon_x^{T(k)} \\ \varepsilon_y^{T(k)} \\ \frac{1}{2}\gamma_{xy}^{T(k)} \end{Bmatrix} = [T]^{-1} \begin{Bmatrix} \varepsilon_1^{T(k)} \\ \varepsilon_2^{T(k)} \\ \frac{1}{2}\gamma_{12}^{T(k)} \end{Bmatrix}, \text{ where} \qquad \textbf{(6.8)}$$

$\varepsilon_1^{T(k)} = \alpha_{11}^{(k)} \Delta T$, $\varepsilon_2^{T(k)} = \alpha_{22}^{(k)} \Delta T$ and $\gamma_{12}^{T(k)} = 0$.

$$\text{Similarly, } \begin{Bmatrix} \varepsilon_x^{P(k)} \\ \varepsilon_y^{P(k)} \\ \frac{1}{2}\gamma_{xy}^{P(k)} \end{Bmatrix} = [T]^{-1} \begin{Bmatrix} \varepsilon_1^{P(k)} \\ \varepsilon_2^{P(k)} \\ \frac{1}{2}\gamma_{12}^{P(k)} \end{Bmatrix}, \text{ where} \qquad \textbf{(6.9)}$$

$$\varepsilon_1^{P(k)} = \frac{-\sigma_f^{P(k)} V_f^{(k)}}{E_{11}^{(k)}}, \ \varepsilon_2^{P(k)} = \frac{\nu_{12}^{(k)} \sigma_f^{P(k)} V_f^{(k)}}{E_{11}^{(k)}} \text{ and } \gamma_{12}^{P(k)} = 0 .$$

α_{11} and α_{22} are the ply thermal expansion coefficients respectively in the fibre direction and the in-plane transverse direction (for a detailed derivation, refer to Appendix D). ΔT is the change in temperature from curing to ambient and is therefore always negative in value in this analysis. σ_f^P is the ply fibre pre-stress. This is the stress in the fibre applied prior to and during the curing cycle and is thus locked into each ply. V_f is the ply fibre volume fraction and E_{11} is the ply Young's Modulus in the fibre direction. $[T]^{-1}$ is the inverse of the transformation matrix,

$$[T]^{-1} = \begin{bmatrix} m^2 & n^2 & -2mn \\ n^2 & m^2 & 2mn \\ mn & -mn & m^2 - n^2 \end{bmatrix}, \text{ where} \qquad \textbf{(6.10)}$$

$m = \cos(\theta)$ and $n = \sin(\theta)$.

θ is the ply fibre angle to the global x direction, measured clockwise.

Now, knowing the laminate mid-plane strains, these can then be transformed in to the local ply coordinate system and applied to derive the ply in-plane residual stresses.

$$\begin{Bmatrix} \varepsilon_1^{(k)} \\ \varepsilon_2^{(k)} \\ \gamma_{12}^{(k)} \end{Bmatrix} = [T]^{(k)} \begin{Bmatrix} \varepsilon_x^0 \\ \varepsilon_y^0 \\ \gamma_{xy}^0 \end{Bmatrix}, \text{ and so} \qquad \textbf{(6.11)}$$

$$\begin{Bmatrix} \sigma_1^{R(k)} \\ \sigma_2^{R(k)} \\ \tau_{12}^{R(k)} \end{Bmatrix} = \begin{bmatrix} Q_{11} & Q_{12} & Q_{16} \\ Q_{12} & Q_{22} & Q_{26} \\ Q_{16} & Q_{26} & Q_{66} \end{bmatrix} \begin{Bmatrix} \varepsilon_1^{(k)} \\ \varepsilon_2^{(k)} \\ \gamma_{12}^{(k)} \end{Bmatrix}. \qquad \textbf{(6.12)}$$

$[Q_{ij}]$ is the ply reduced stiffness matrix, $\sigma_i^{R(k)}$ is the ply residual direct stress term and $\tau_{12}^{R(k)}$ is the ply residual in-plane shear stress term.

6.1.3. Micro-Mechanics (at a sub-ply level)

Once the individual ply strains have been determined as above in equation (6.11), these can then be applied in the micro-mechanical analysis of the stresses at the fibre/matrix level. Due to strain compatibility, at this level the ply strains will also be the strains in the fibres and the matrix in the fibre direction.

$$\sigma_m^{(k)} = E_m^{(k)}\left(\varepsilon_1^{(k)} - \alpha_m^{(k)}\Delta T\right), \text{ and} \qquad \textbf{(6.13)}$$

$$\sigma_f^{(k)} = E_f^{(k)}\left(\varepsilon_1^{(k)} - \alpha_f^{(k)}\Delta T\right) - \sigma_f^{P(k)}$$

6.1.4. Wrap-Up of Stress States in a Composite Laminate

This section will review what has been written above and present some graphs to illustrate the effect of fibre pre-stressing on the ply failure strengths of a laminate. The main point to come out of the above theory is that the stresses at ply and

fibre/matrix level are ultimately governed by the laminate strain response after cooling it from the curing temperature to ambient and removing the applied pre-stress loading. The fibre pre-stress, however, is applied to the reinforcing fibres only. After cure, though, the matrix has become a solid and can therefore react shear forces. It has also bonded to the fibres and is thus constraining the fibres from returning to their stress-free state. This is the process by which the pre-stress is locked into the composite. Each ply will therefore see an in-plane compressive load in the fibre direction. These compressive loads will cause the laminate strains together with the laminate thermal contraction due to cooling. The residual ply and fibre/matrix stresses result from the fact that these laminate strains do not equal the stress-free strains of the plies or fibres and matrix.

The implications of this are that when loaded, the plies will reach their failure stress at a different applied strain from that if they did not have any residual stresses. With no pre-stress applied, the residual stresses in the plies are due to the thermal contraction. These are such that the plies are under a tensile stress in the in-plane transverse direction, which can reduce the first ply failure strength of the laminate (which typically occurs in the 90º plies when these are present, thus relating to the in-plane transverse strength of a ply). Thermal residual stresses in the plies can account for around a 35% drop in in-plane transverse tensile strength of a ply compared with the measured values of a unidirectional ply not contained in a laminate (this applies for an E-glass/epoxy resin ply in a $[0/90_2/0_2/90/0/90]_S$ laminate). Since pre-stressing superimposes a compressive stress onto the thermal residual stress of the ply, this loss in strength can be relieved in this way.

Figure 6.3 shows a graph giving the percentage change in strength of a ply in the

above laminate for the ply tensile, compressive and shear strengths in and across the fibre direction. The results in Figure 6.3 have been presented for the cross-ply laminate considered in this study. The 0 MPa pre-stress level was considered the base line, so any strength changes have been measured against it. .

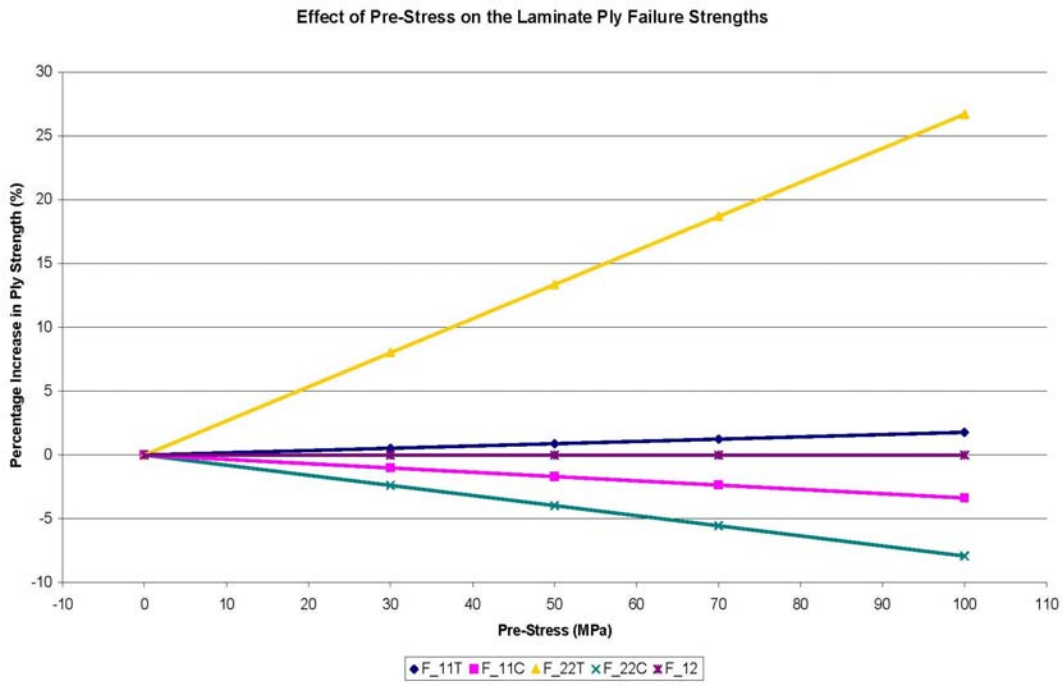

Figure 6.3 The effect of pre-stressing on the laminate ply strength. As can be seen, the in-plane transverse strength is most affected.

Figure 6.4 shows the same but compared with the measured values taken from test of a unidirectional ply. In this case the baseline was assumed to have been a UD ply with no residual stresses. Therefore, the condition of no pre-stress gave the greatest change in strength from the baseline.

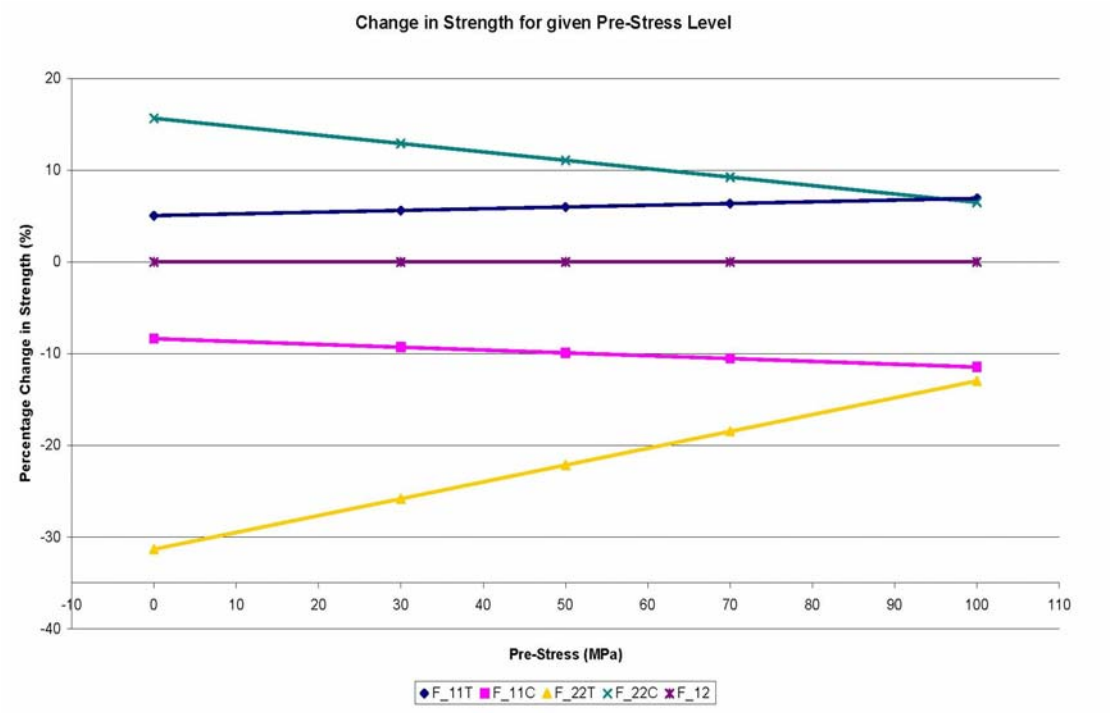

Figure 6.4 The effect of pre-stressing on the laminate ply strength, normalised against test results.

These graphs were generated from predictions made using the above classical laminate analysis in a MathCAD sheet written for this study and shown in Appendix E.

The greatest strength increase for a ply in the laminate was for the ply 22 direction; in-plane but transverse to the fibres. This was because the 22 direction had the lowest stiffness and therefore would be subject to the highest stresses for a given load. Superposition of the mechanically induced stresses (pre-stress) onto the thermal residual stresses would give the greatest effect.

The reverse was true of the transverse compressive strength of a ply. Since a compressive stress was superimposed upon the thermal residual stresses, there was less compressive strain available before failure would occur. Therefore the apparent transverse compressive strength would decrease with increasing pre-stress.

The in-plane shear strength was not affected by pre-stressing in this case, since there were no plies other than 0º and 90º. These were perpendicular to each other, and therefore none of the pre-stress was transferred through in-plane shear (1-2 plane), as would have been the case if say 45º plies had been introduced.

The classical laminate analysis predicted an increase in ply tensile strength in the fibre direction. The failure handling used in this study was the maximum strain criteria, where there is no interaction between modes of failure and therefore each ply could be treated separately with the superposition of stresses for the laminate stresses. Then considering this superposition and knowing the pre-stress was originally applied through the fibres, one may expect the tensile strength in the fibre direction to decrease rather than increase, since the pre-stressing had already taken up some of the available failure strain in the fibres, and this would dominate failure in that direction. This is contrary to the expectations for the overall tensile strength of a laminate, but that will be discussed in section 6.1.5.

The compressive strength in the fibre direction, although predicted here to decrease under pre-stress-induced residual stresses may in fact increase. This is because fibres when laid into a composite without applying pre-stress have a natural waviness to them. When these fibres are however pre-stressed they are stretched and this waviness may be removed. Under no pre-stress the fibres would fail under microbuckling when loaded in compression, caused by their waviness (Figure 6.5). When pre-stressed this waviness is reduced and microbuckling may be delayed from occurring. How the pre-stress can affect the impact performance of the laminate will be discussed in chapter 0.

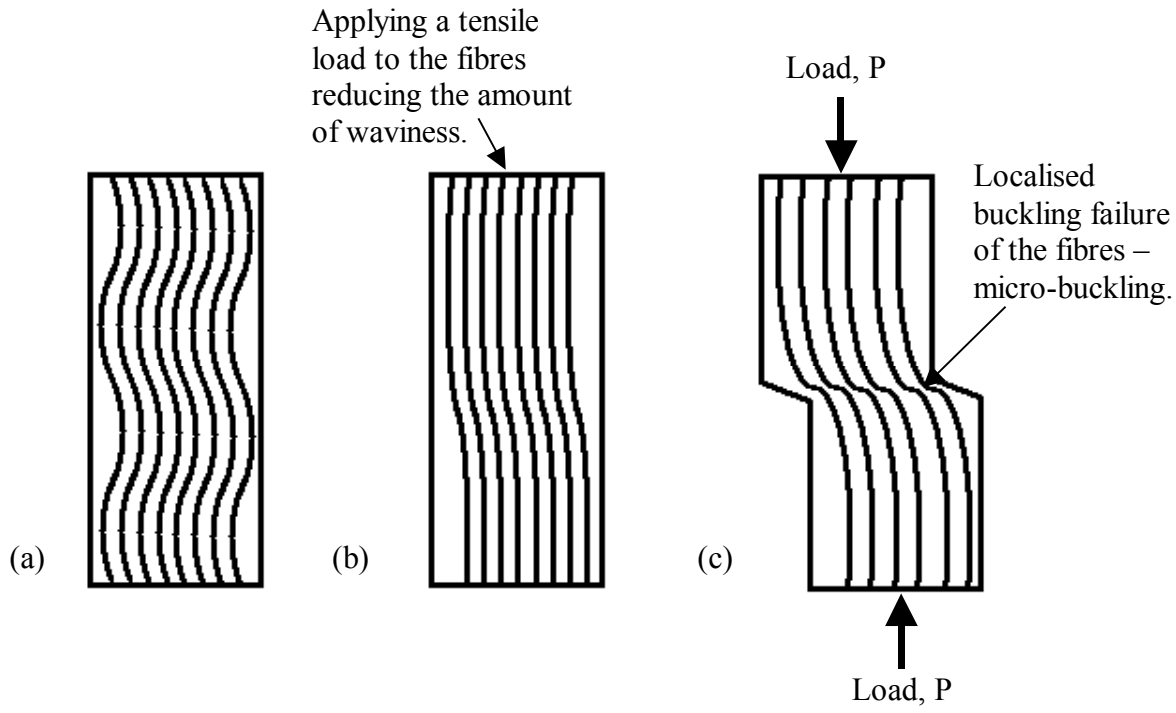

Figure 6.5 Diagrammatic representation of (a) fibre waviness, (b) the effect of pre-stress on it and (c) microbuckling.

6.1.5. Laminate Failure Mechanics under Pre-Stress Conditions

When the overall laminate is considered, plies can no longer be analysed on an individual level only. How they interact with each other in the laminate also becomes important. Some failure criteria try to account for this effect by using iterative approaches, in which the matrix failure constitutes a reduction in laminate properties, but the fibre failure dominates the final and total failure of the laminate (Barbero, 1998). Therefore, by setting matrix-dominated properties to zero in plies where matrix failure has been identified, the classical laminate analysis may be iterated through again and again until a fibre-based failure is identified.

For a cross-ply laminate under unidirectional loading it would be reasonable to assume there to be no in-plane shear interaction between plies. One could then use the maximum strain or maximum stress criteria even for this final fibre failure

iterative approach. The failure modes described in the section above would then still hold valid. This would then suggest that first ply failure could be delayed, but final fibre failure would be lower for a pre-stressed laminate, compared with a non pre-stressed one. This however was not observed in test (Figure 6.6).

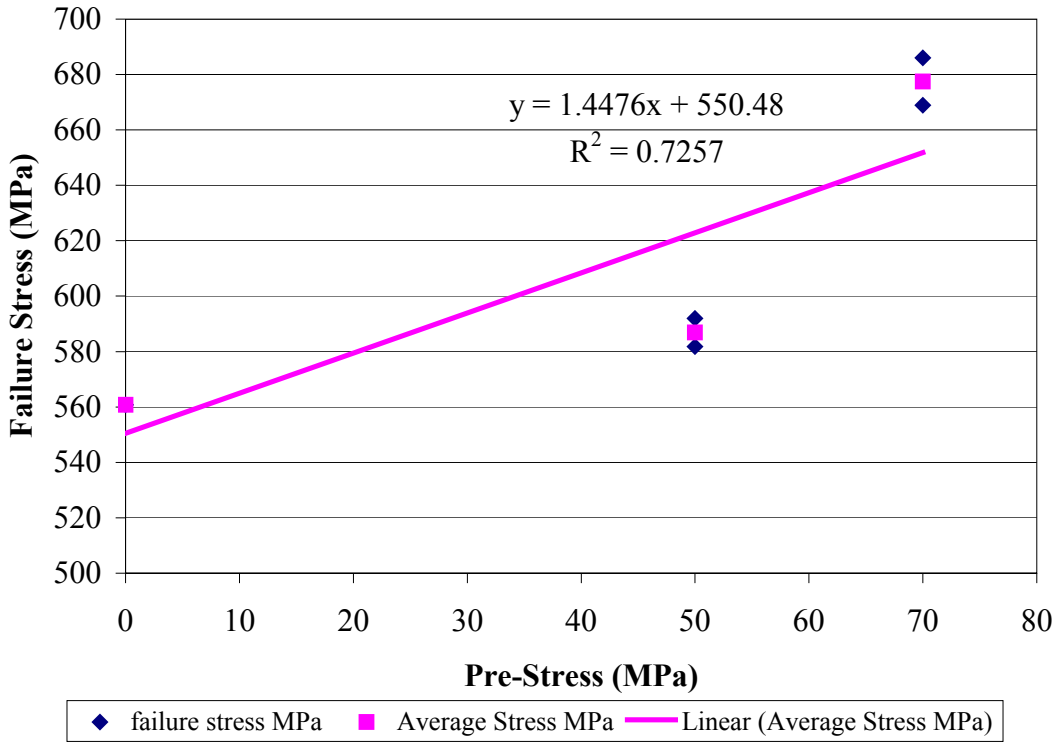

Figure 6.6 Plot of failure stress against fibre pre-stress for the tensile tests.

If, then the laminate strength increased with pre-stress another mechanism must have been acting for this to be possible. Schulte et al. (2002) presented a theory, which would explain how a pre-stressed laminate might increase in overall strength. Schulte reported that matrix type failure in the in-plane transverse direction (i.e. the 22 direction) manifests itself as microcracks through the thickness of the ply and travelling from free edges into the laminate (Figure 6.7).

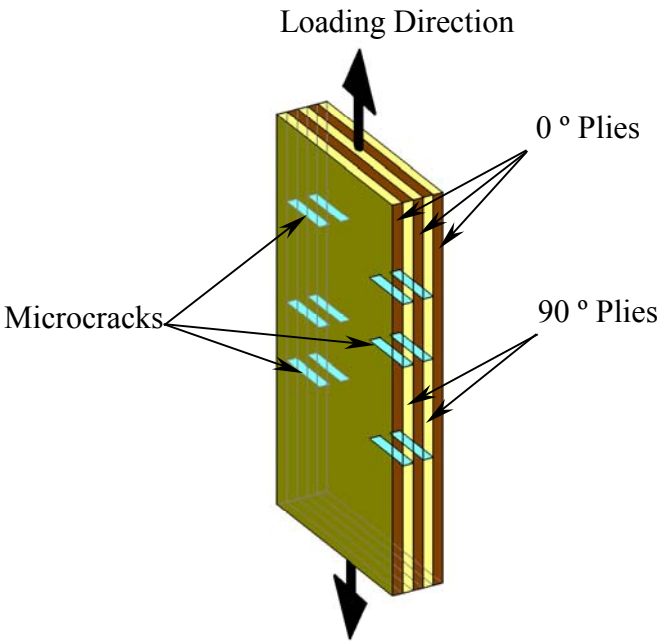

Figure 6.7 Diagram showing microcracks developing in the 90º plies of a laminate under tension in the 0º direction.

These microcracks would form stress concentrations at the boundary with adjacent plies of different orientation. When cracks became sufficient in number and the stresses at the crack tips of sufficient magnitude fibre failure would occur at the crack tip. Such fibre failure would overload the adjacent fibres and a cascade failure would ensue.

As was discussed in the previous section, a pre-stressed laminate would have increased ply strengths in the 22 direction, which in turn would delay the onset of the microcracks. Therefore, the critical number of cracks would be reached at a higher load and the laminate strength would be increased. Schulte and Marissen, 1992, did indeed show that pre-stressing would delay the onset of microcracking to higher loads.

To be able to more accurately predict laminate strengths in classical laminate analysis

then, this phenomenon of microcracking would have to be incorporated into the failure criteria.

6.2. Pre-Stressing Methodology

The above analysis of pre-stress gives the reader a good idea of how pre-stressing can affect the residual stress state in a composite. It is now important to move attention to the methodology of producing pre-stressed composites. The various methods employed by other authors were presented in the literature review chapter (chapter 0), so it remains to discuss the method used in this study. The method itself was presented in the experimental chapter (chapter 4) and the strain gauge plots from the autoclave runs in the results chapter (chapter 0).

6.2.1. Analysis of Present Method

Section 4.2.1 in the Experimental chapter (chapter 4) gave a quick overview of the validity of the choice of pre-stressing method employed in this study. This section will delve more deeply into this matter to better justify the choices made and give the reader a better understanding of the philosophy behind such a method.

On a fundamental level the choice of curing process was a simple one. The Sensors and Composites Research Group had an autoclave as a means of curing composite panels and the author had access to prepreg materials. Alternative methods such as filament winding and hot-press curing were not available to the author at the outset of the study. This made it clear that the route to take would be autoclave curing. As already described in chapter 4 this brought with it a unique set of challenges to overcome in the design of the pre-stressing method.

These were the need to have a fully self-contained method able to fit not just into the

autoclave but also into a vacuum bag to enable quality panels to be produced. The latter had the implication that the overall outer shape of the pre-stressing method has to be simple, so as not to offer up too many areas where bridging of the vacuum bag could occur, which in turn could lead to bag burst.

6.2.1.1. Concept Selection of Method and Philosophy

The main design drivers for the concept selection were cost and ease of manufacture as well as the restriction imposed on the design by the use of autoclave curing. A further design driver was that the tool would have to be handled by a single person, although this was less critical than the others. As described in chapter 4, the tool had to be capable of applying 100MPa of pre-stress to a 16-ply cross-ply laminate in both fibre directions. This level of pre-stress translated to a significant load of around 14 metric tonnes. The derivation of this load is now presented.

Level of fibre pre-stress desired = 100 MPa

Width of ply to be pre-stressed = 250 mm

Number of plies in each direction = 8

Thickness of single ply = 0.125 mm (assumed to be equal to cured-ply thickness as this is given in manufacturers' data sheet)

Fibre volume fraction = 0.56 (again assumed to be equal to the cured-ply fibre volume fraction taken from manufacturers' data sheet)

Cross-sectional Area of all plies in one direction,

$A_{plies - 0\ degrees} = 8 \times 0.125 \times 250 = 250\ mm^2$

Load carried by the fibres in these plies with a fibre pre-stress level of 100 MPa, $P_{pre\text{-}stress} = 250 \times 0.56 \times 100 = 14000$ N.

During the concept selection three candidate designs emerged, although only one presented itself as suitable. The two designs that were rejected (see Figure 6.8a and b) were done on the account they were only viable if applying pre-stress in one direction only. This however was not enough, as it had been decided to apply pre-stress in both fibre directions. Ultimately it was found that the solution was to have a load-bearing frame, connected to a series of clamps, which in turn held the laminate in place. Bolts linking the clamps to the frame were chosen, since this made it possible, by varying the torque on the bolts, to apply varying levels of pre-stress.

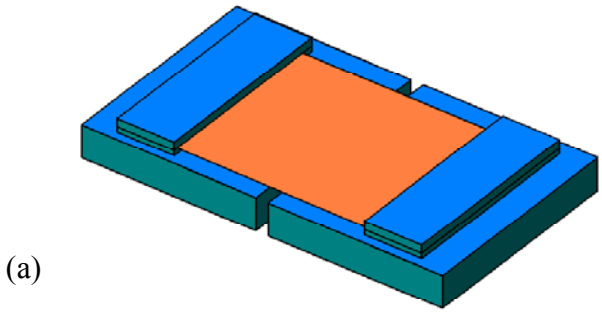

(a)

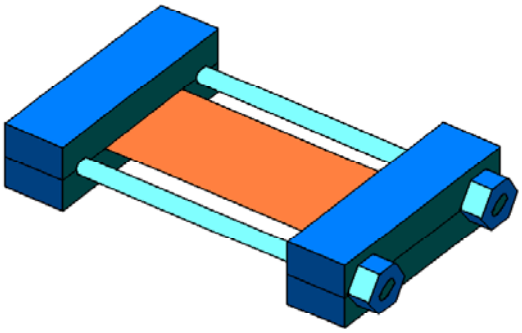

(b)

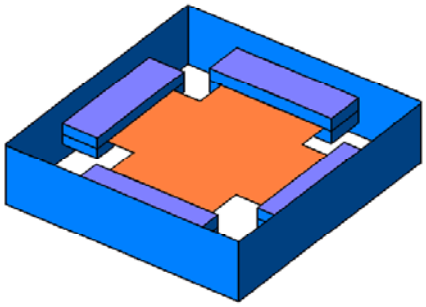

(c)

Figure 6.8 Candidate concepts designs. (a) Two base plates; the laminate is clamped at each end to one of them and the plates are forced apart to induce the pre-stress. (b) The laminate is clamped at each end and the clamps pushed apart by compressing the connecting studs to apply the pre-stress. (c) The laminate is clamped on all four sides. The clamps are connected to a load-bearing frame, using, say bolts. The bolts can be tightened to apply the pre-stress. This design was chosen.

Once the initial concept was chosen, a detailed study was carried out to obtain an optimised design based on the above design drivers. To keep cost down readily available steels were used. A finite element study was carried out to determine the best design. Figure 6.9 shows some of the designs considered. The finite element study was used to determine which designs would be capable of taking the loads, by

carrying out linear elastic simulations and determining whether or not any of the stresses reached values greater than the yield strength of the material (mild steel was assumed so the yield strength was assumed to be 280 MPa). The other criteria were that access should be available to the inside of the frame and that the frame should be the most cost-effective design in terms of manufacture.

The initial approach was to have steel bar with angle plates at the corners (Figure 6.9a), as such material would be easily available. It was found though, that this approach produced stresses above the material yield stress. Using thicker bar material for the frame alleviated the stress problem but made the frame too heavy (Figure 6.9b). By using thin steel plate material and cutting circular holes into the face plates (Figure 6.9c and d) gave solutions for which the stresses were not too high and were not too heavy either, but there were issues with access to the interior of the frame. Using a channel section material for the loading frame gave the best compromise between stress limits, weight and access (Figure 6.9e)

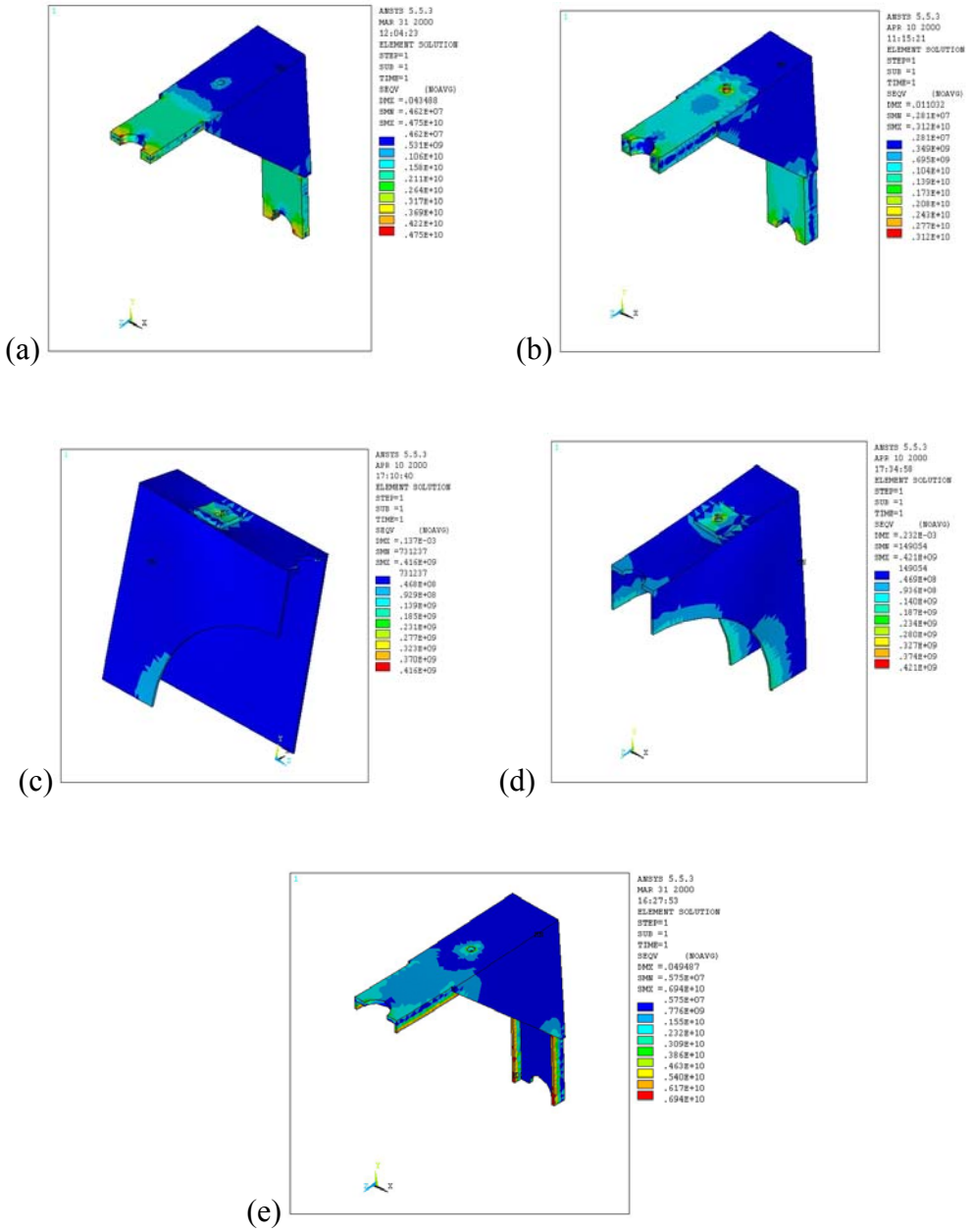

Figure 6.9 Finite element results of various frame designs carried out in ANSYS.

All the designs presented above required significant amounts of welding. In welding thin plates, as are seen in these designs, there is always a risk of warping so the final design was chosen partly to minimise the amount of welding to be done, but also to simplify the construction of the frame. The final design could be made from four sections of BS5950, 38x76 mm steel channel section, only welding them together at the corners. This reduced the risk of warping the frame and reducing the amount of

time required to make it. The clamps were machined from blocks of EN24 carbon steel and the loading pins from EN25 carbon steel. These grades were chosen for their higher strength whilst still being machineable, EN25 being stronger but only being used in the pins as these required the higher strength. The finished frame (Figure 6.10a) was capable of loading a cross-ply laminate in both fibre directions, but offered too many cavities for the vacuum bag to bridge over and burst. Therefore blanking plates (Figure 6.10b) were made to cover the cavities, thus simplifying the outer shape of the frame. These were made from 3 mm steel plate bent into shape as this thickness would be more than capable of sustaining the high pressure loads from the autoclave.

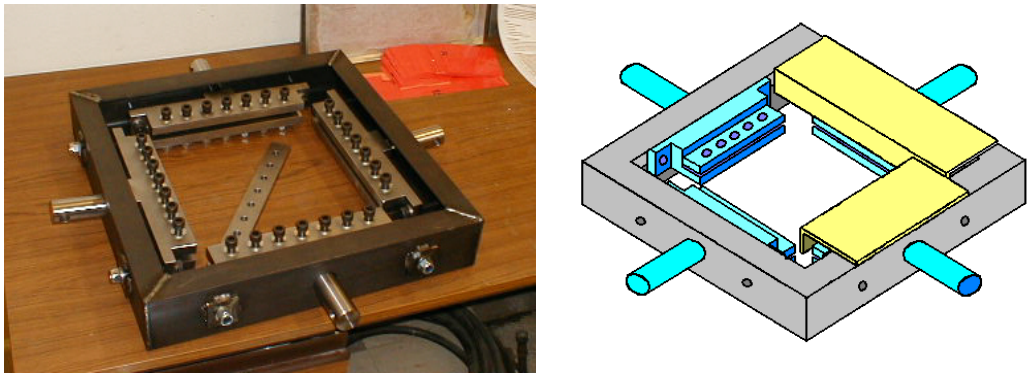

Figure 6.10 (a) Photograph of finished frame and (b) diagram showing addition of blanking plates.

In all this left the frame weighing almost 50kg, which was well over the health and safety allowed weight to be lifted by one person. Therefore a frame lifting device had to be designed, into which the unassembled frame could be mounted and the laminate, clamps and blanking plates attached. This device was made by adapting an off-the-shelf engine mount, which enabled the frame to be rotated, so both sides were accessible. From the frame lifting device it was possible to place the assembly onto a base frame to push the assembly into the autoclave with. For getting the pre-stress rig

assembly in and out of the autoclave, a trolley was adapted with rails to link up with the rails in the autoclave. It was possible for the base frame to slide over these rails giving access to the inside of the autoclave without having to lift the pre-stress rig into or out of it.

Finally, after unsuccessfully attempting to use single use vacuum bags it was decided to make a silicon membrane re-usable vacuum bag system, which could be made to the net shape of the pre-stress rig. This made it possible to vacuum bag the rig without risk of a bag burst.

6.2.1.2. Finite Element Analysis of Pre-Stress induced in a Panel by the Rig

An ABAQUS finite element study was carried out to investigate how the pre-stress rig applied stress to the composite laminate during the elevated temperature of curing. It was found that due to the different thermal expansions of the frame and the composite the frame would, without having to add further loading by tightening the bolts, apply a certain amount of pre-stress to the fibres. This was again due to strain compatibility, since the rig and laminate assembly was fully self-contained and no external loads were assumed to be acting on it. A simple one-dimensional strain compatibility analysis (Appendix F) showed that the composite would indeed be loaded by the frame in this way and that the resulting pre-stress in the fibres would be about 48 MPa. This analysis acted as a good first approximation as the frame had significantly greater stiffness and cross-sectional area than the fibres, but did not take the bending deflections of the frame into account. The frame would experience some bending as the load in the laminate would be transferred to the frame via the bolts, which were offset from the neutral axis of the frame components parallel to the loaded fibre direction (see Figure 6.11 for details).

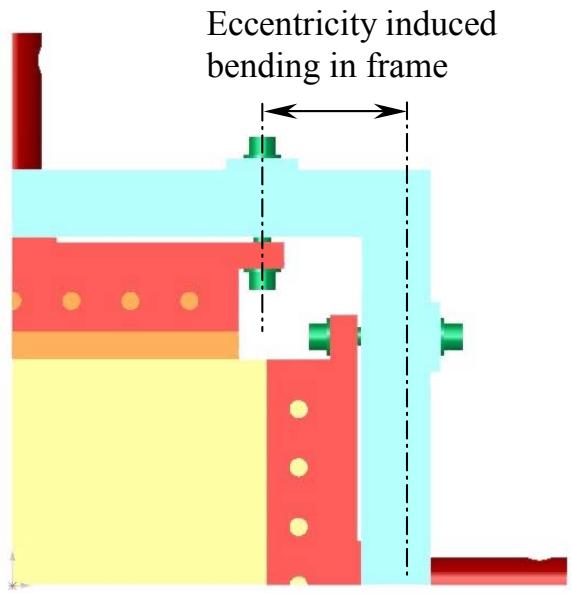

Figure 6.11 Illustration of the eccentricity of the bolt centre line from the frame neutral axis

In the finite element analysis a three-dimensional model was generated, containing all the components of the frame and laminate assembly (frame, clamps, bolts and laminate). This allowed a more detailed analysis to be carried out which took into account the bending effects of the eccentric loading of the frame as discussed above. To save on computational requirements the axes of symmetry were taken advantage of and a $1/8^{th}$-symmetry model was generated. This model is shown in Figure 6.12.

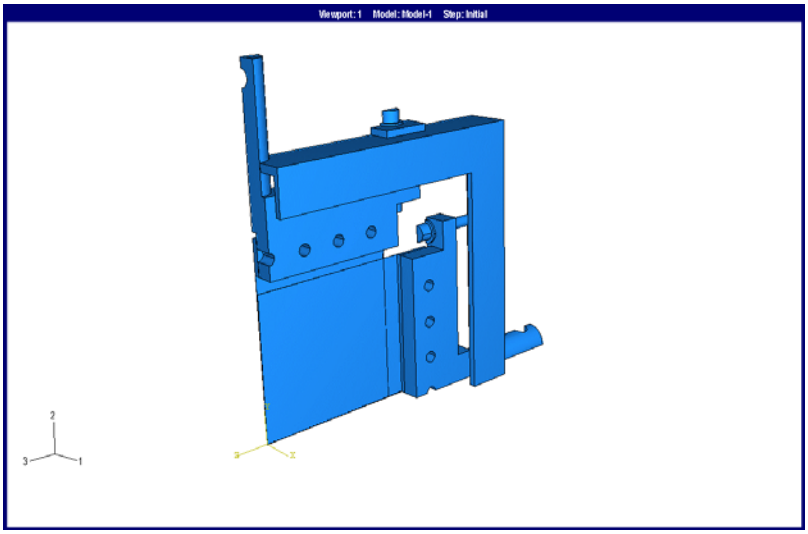

Figure 6.12 ABAQUS 1/8th-symmetry model of pre-stress frame and laminate assembly

All the steel components were modelled using an isotropic elastic material model and their respective properties. All plies in one direction were modelled as one single ply. They were, however modelled separately from the plies in the other direction. This was to simulate the fact that there was no bonding between the two ply directions before the cure was completed. The friction between the two ply-directions was therefore set to zero, to prevent any interaction between them, so they would only see uni-axial loading. Since ABAQUS is a non-linear solver and capable of solving contact problems this type of approach was possible. Furthermore all contact interactions were modelled – ply-to-ply, ply-to-clamp, clamp-to-bolt and bolt-to-frame. Three simplifications were carried out though. The first was not to model the cure-on end-tabs, but to simply thicken the plies around that area. This was acceptable as the stress-state was unimportant in this region of the plies. The next was not to model the clamping bolts, but to simply tie the plies to the clamps (infinite friction between the two surfaces). This reduced the number of components to be modelled and saved on computational requirements. The third and most important

simplification was to do with the plies. In real life before curing the matrix effectively being in a liquid state could not take shear and therefore would not contribute to the load-bearing capabilities of the plies. For true accuracy therefore only the fibres should be modelled. This however would be highly impractical as there are innumerable fibres in each ply. This would tie up unreasonable amounts of computation time. To simplify this, the plies were modelled with a cross-sectional area equal to that of the fibres in those plies and the material properties were defined based on the fibre properties, rather than the cured-ply properties. The finite element results showed that bending did indeed occur, which resulted in a lower stress being present in the fibres, compared with the one-dimensional analysis. It was found that the fibre stress was now around 40 MPa (compared with the previous 48 MPa). The two methods were therefore sufficiently close though to be able to claim the predictions were right.

6.2.2. Critical Evaluation of Present Method

According to the analyses presented above in section 6.2.1, it should have been possible to generate pre-stressed panels with the current method. The rig was designed to bear the loads of pre-stressing and it was possible to vacuum bag the assembly. Although the frame itself would put the fibres under pre-stress when the system was heated to curing temperature, the overall pre-stress in the fibres could be varied by tightening or slackening the bolts linking the clamps to the frame. Care had to be taken to tighten/slacken the bolts evenly to ensure the pre-stress in the plies was balanced along their width. This was however achievable and the graph of failure stress for different levels of pre-stress (Figure 5.9 in chapter 0) shows that it was indeed achieved.

The one problem faced in the whole system was that of monitoring the strain gauges on the frame. Two errors in the design were encountered in the use of these gauges. These were, that the change in lead wire resistance with changing temperature was not compensated for in the setup of the strain gauge system, and that unsuitable gauges were used. The ones used did not have an operating temperature high enough to deal with a cure cycle.

Although the strain gauges were located on the neutral axes of the frame and were capable of measuring the strain in the frame when the pre-stress was first being applied to the frame and the strain gauge placed 5mm off the neutral axis was able to measure bending at that time, the errors became apparent when the frame was heated. Figure 6.13 shows one of the strain gauge plots for a cure cycle in the autoclave, as already presented in chapter 0.

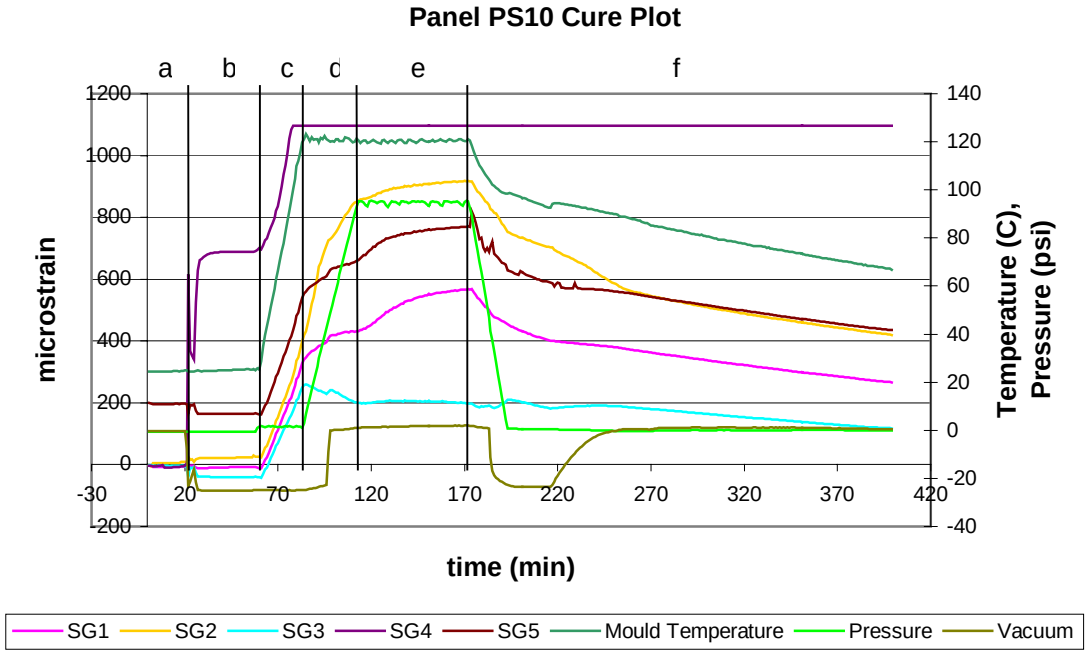

Figure 6.13 Cure cycle plot for panel PS10

The various stages of the cure cycle could be broken down into six time periods. Period (a) saw the application of pre-stress into the fibres. This particular panel was planned to have 100MPa applied to it, therefore a further 60MPa needed to be applied to the fibres mechanically as the frame would during heating apply the other 40MPa (as predicted in the above ABAQUS finite element analysis). Table 6.1 shows the strain readings required to achieve certain levels of pre-stress in the fibres before cure. These were derived at through carrying out simple force-balance calculations since each side of the frame would bear half the pre-stressing load in the fibres. Knowing the cross-sectional area of the frame and its Young's modulus the resultant strains in the frame could then be calculated from the loads. These could then be read off the strain gauge amplifier when applying the pre-stress before cure.

Table 6.1 Strain values for the frame for given levels of pre-stress before cure.

Pre-stress required in panel (MPa)	**Additional pre-stress required (MPa)**	**Load in frame (N)**	**Strain in frame (to be read off amplifier) (micro-strain)**
50	10	-982	-3
60	20	-1963.5	-5.5
70	30	-2945	-8
80	40	-3927	-11
90	50	-4909	-14
100	60	-5890	-16.5

In period (b) the vacuum was applied to debulk the laminate prior to cure. The strain gauges respond well showing the compressive load on the frame due to the pressure differential across the vacuum bag. Until the beginning of period (c) everything occurs at ambient temperature (around 25ºC). In period (c) temperature is applied up to the curing temperature of 120ºC. The strain gauges that were chosen for this work were TML FLA-2-11 temperature compensated strain gauges. These gauges were temperature compensated for steel. One would therefore assume that the strain

measured in this heating stage would correspond to the strain in the frame due to the pre-stress forces exerted on it by the fibres. This is likely not to have been the case though. Two reasons can be presented for this. The first is that only a two-wire quarter-bridge connection to the amplifier was used, which meant that the change in resistance in the lead wires from the gauges to the amplifier were not compensated for. Therefore, the strain measured in this period (c) is likely to be the change in lead wire resistance rather than the strain due to pre-stressing. To compensate for this, a three-wire quarter-bridge connection should have been used.

The other is that although the strain gauges were temperature compensated, this compensation was only really intended to cancel out temperature fluctuation in the test lab during a test and not for large temperature variations as experienced during a cure cycle. Furthermore, the maximum operating temperature of these gauges was 80ºC, which was well below the curing temperature of 120ºC. It is less likely, though, that this would have caused the strain readings in period (c), as a deviation from the temperature compensation and a departure from the operating temperature range would have caused a non-linear behaviour rather than a linear one. Since the strain readings in period (c) are linear, it is felt that the first explanation of a change in lead wire resistance is the most likely.

In time periods (d) and (e), there is no longer any change in temperature. Subsequently a significantly non-linear behaviour of the strain gauge readings can be observed. Even though in period (d) pressure is being applied the non-linearity continues throughout period (e), in which a steady-state condition is in operation (temperature and pressure are both constant). Therefore the strain gauges should reflect this in their readings. Their non-linearity in these sections could then be

explained by the fact that they are being subjected to conditions well outside the operational limits of the gauges.

In all, it must be concluded that the strain gauge system employed in this study was unsuitable for task, thus making it impossible to obtain pre-stress values for the panels produced. In hindsight this pre-stressing method could be made to work as desired though, through the use of strain gauges with higher operating temperatures and three-wire quarter-bridge connections to the amplifier. Also keeping the amplifier in a temperature controlled room would also have been advisable, as, sat next to the autoclave, it was subjected to temperature fluctuations of around 20ºC (the autoclave room would, during a cure cycle, often go from 25ºC ambient temperature to 45ºC). Such fluctuations could cause the zeroing of the amplifier to drift significantly as well.

6.2.3. Practical Application of Pre-Stressing

In commercial applications the composite components will typically become large (hundreds of millimetres to several metres in size) and also contain large numbers of plies (around 32 or more plies). Examples would be helicopter rotor blades, wind turbine blades, aircraft wing covers, aircraft control surfaces. When considering that to produce 100 MPa of pre-stress in a 16-ply composite, 250 mm wide required 14 kN of force, the forces required to induce such stresses in a much larger component would soon become impractical. Further to this, commercial components are rarely, if ever flat and this would again bring with it more complexities when trying to apply pre-stress. Pre-Stress, therefore, in the guise found in this study would not be practical in commercial applications. There is, however, an area where pre-stress could be used and some authors (Dvorak *et al.* 2001, Suvorov *et al.* 2001,

Schlottermüller et al, 2002) have suggested benefits could be found. This area would be in filament winding. When filament winding a component tension needs to be applied to the tows to ensure a good wind. This tension can typically equate to a fibre pre-stress of 100 MPa. The study of pre-stress then becomes very relevant. Also with modern winding machines it has become possible to vary the tension in the tows during winding. This has brought with it the possibility of varying pre-stress through the thickness of the components, the benefits of which are discussed in the above-mentioned authors' papers.

The issue that is raised by the above is also that although pre-stress may not have intentionally been applied to a composite components, there may in fact be some pre-stress present, due to processing parameters (as in filament winding) or due to geometric effects (e.g. spring-back). Therefore, this study may not yield a process, by which pre-stress could be commercially applied to composites, it does highlight that pre-stress may exist and therefore needs to be investigated to determine how much effect it can have on the structure's performance.

6.3. Conclusions

This chapter has shown the significance of pre-stressing and has discussed the method of producing pre-stressed panels in this study. Pre-stressing can significantly affect the laminate ply strengths, recouping some of the strength lost due to the thermal residual stresses. Practically, it can be difficult to produce pre-stressed panels, as has been shown above. Although the method used in this study experienced problems, which prevented the levels of pre-stress to be determined for the panels produced, the above analysis has shown that the concept was sound and would need only minor alterations to make it possible to return the levels of pre-stress. The actual values for

pre-stress quoted in this study had to, however, be inferred from predictions and initial strain gauge readings prior to autoclave curing, since no useful data was obtained from monitoring the strain gauges during the curing process. Finally, pre-stress is a real concern for industrial applications, since it is present already in filament wound components, and this study would also be applicable to geometrically induced residual stresses.

This page is intentionally blank.

7. DISCUSSION – EXPERIMENTAL

In this chapter the results of the experimental study have been discussed. Discussions of the different impact regimes; their corresponding target responses and resulting laminate damage have been presented with the aid of the results for the non pre-stressed composites. The effect of pre-stressing on the damage caused by the different impact regimes has then also been discussed.

Impact onto composites can result as a consequence of a range of different scenarios. When a tool is accidentally dropped onto a panel during maintenance it causes a slow response of the target. A bird striking the leading edge of an aircraft can be a very fast event, although both the target and the bird are deformable, thus softening the impact. During take-off or landing, stones or other debris can be thrown up and strike the underside of the aircraft. These projectiles can be travelling at around 100 $m.s^{-1}$ when impacting. If there is a rotor burst in a gas turbine engine during operation or if a military vehicle is fired upon the impacts will be in the ballistic range of several hundreds of metres per second. All these represent different loading regimes, for which the composite laminate will respond differently. In this study the low-velocity, tool drop type impacts as well as the high velocity runway debris impacts have been investigated and will be discussed.

It must be noted that damage in a composite laminate as a result of an impact by a foreign body is affected by a number of different variables: the mass of the projectile as well as the mass of the target, the projectile's incident velocity and the kinetic energy as well as the clamping conditions of the target. The first three variables have been discussed in section 7.1 and the clamping conditions in section 7.2. All these

variables have their own effect, but are also interlinked and affected by each other. Although each variable has been discussed individually, connections between them have also been presented where possible.

7.1. Impact Loading Regimes

The mass of the projectile has a direct effect on the magnitude and rate of load applied to the target structure. If the impacting mass is large, it will give a lower peak contact force than a smaller mass will for the same incident energy.

During non-penetrating impact the projectile has to come momentarily to rest before rebounding back in the opposite direction. In a low-velocity impact, the impactor often has large dimensions and the dynamic response is slow. In such an impact the contact is governed by the dynamic response of the target laminate. The laminate deflects to its maximum and then begins to repel the impactor. Contact ceases when the target has reached its upper maximum deflection and the impactor continues to travel away from the target (Figure 7.1). The dynamic response of the laminate can be readily defined using closed-form analytical solutions for simple loading and clamping conditions (Abrate, 1998). For more complex loading and clamping conditions, the finite element analysis can give more accurate results.

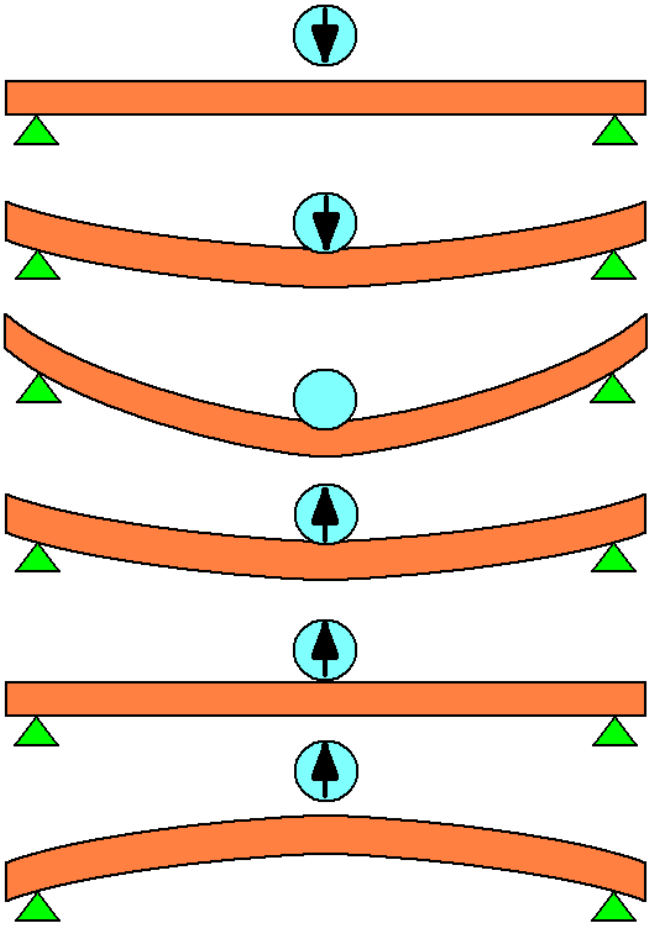

Figure 7.1 Diagrammatic representation of the target response during a low-velocity impact.

In impacts where the projectile is travelling at greater speeds - high-velocity impacts – and where the mass and dimensions of the impactor are much less than that of the target, contact is governed by the time the contact-induced stress waves take to travel to the back of the impactor and back to the contact zone. When the stress waves reach that zone contact ceases and the projectile rebounds. This more closely resembles the impact of an elastic impactor onto a rigid surface, since the target laminate does not have time to respond dynamically before the impactor rebounds. Therefore the dynamic response of the target can be assumed to be negligible until after the impact event has finished. The projectile in this case experiences the deformation during

contact and rebounds from its own elastic response (Figure 7.2).

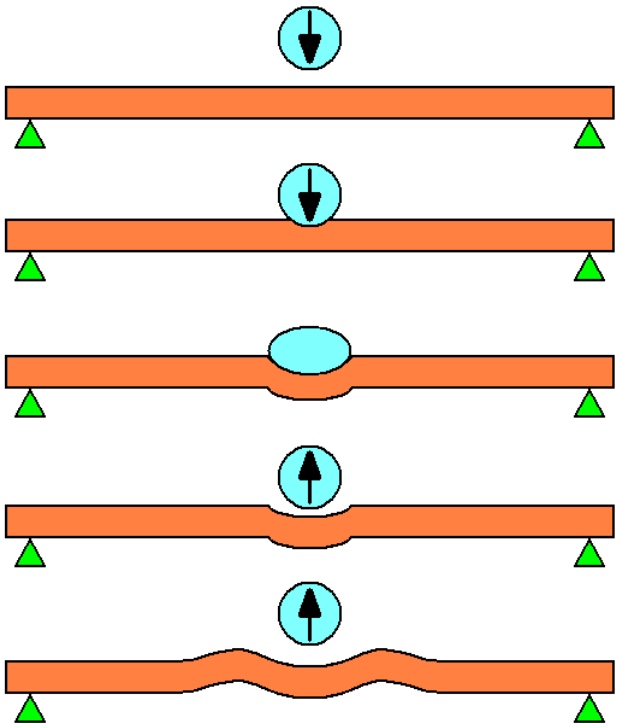

Figure 7.2 Diagrammatic representation of the target and impactor responses during a high velocity impact. Impact and target responses have been exaggerated to aid clarity.

Since in both cases described above the projectile comes to a complete halt, it can be assumed that all its kinetic energy is transferred to the target. Also, since this is a non-penetrating impact it can then be assumed that the elastic strain energy absorbed by the target is returned to the projectile at the point where contact ceases. The energy not returned to the projectile is assumed to have been lost in the creation of damage in the composite, heat and sound; for the purposes of this study, however, the energy absorbed in heat and sound will be ignored. For a given impact energy a small mass projectile will have much less time to transfer all its energy into the target than a large mass projectile would. The rate of energy transfer then has to be greater for the small mass and subsequently the peak force has to be as well.

These discussions apply if the mass of the target is significantly greater than the mass of the projectile. In most test cases this will be so, as the target will have been rigidly clamped to either large test equipment or the ground. In both cases the equipment will be orders of magnitude greater in mass than the projectile. In such a case the projectile will rebound. If the target is of equivalent or lesser mass than the projectile, the target will be propelled away from the point of impact. In this discussion such systems will however not be considered and only systems where the target is much greater in mass than the projectile will be discussed.

To achieve non-penetrating impacts with large massed projectiles, the incident velocity needs to remain low (for the 2.6 kg tup used in this study penetration was beginning to take place in the 72-Joule impacts, which were at 7.5 $m.s^{-1}$ incident velocity), whereas for lower masses, penetration can be absent even for high velocities (the 0.707g projectiles of the gas gun tests did not penetrate even at 93 $m.s^{-1}$ impact velocities). Of course, under these two different conditions the loading will be very different.

The low-velocity impact will be slow to occur, since the higher mass will ensure the impacting bodies remain in contact whilst plate motion is established. In this event the contact will be long enough for the contact-induced stress waves to propagate to the plate boundaries and back, which allows the whole plate to respond dynamically. In the high velocity impact event contact is very short as the mass is low and the longest dimension of the impactor is small. In this case the stress waves cannot propagate to the plate boundaries and back before contact ceases. This is illustrated in Figure 7.3.

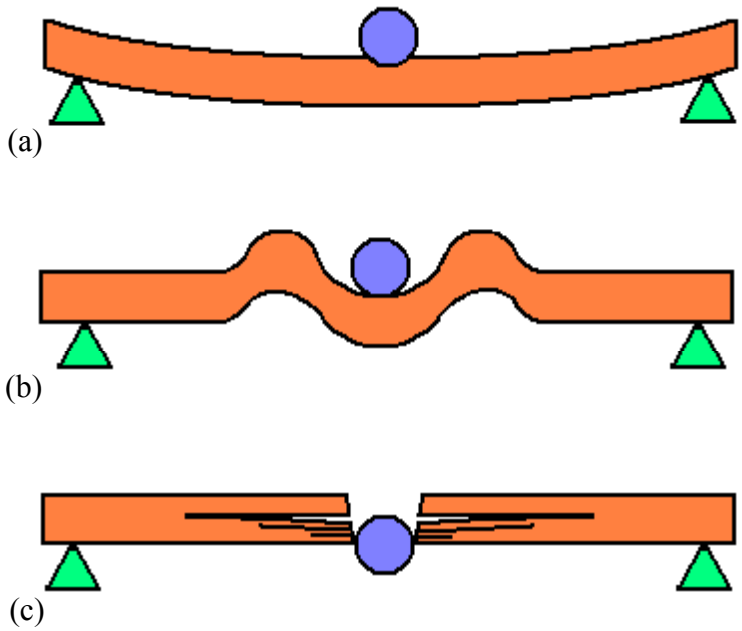

Figure 7.3 Diagrammatic representation of (a) low, (b) high and (c) ballistic type target responses.

As mentioned above during non-penetrating impact all of the projectile's kinetic energy is transferred to the target when the impactor comes to a complete stop just before it is reflected back away from the target. When contact ceases, some of the initial kinetic energy is returned to the projectile and it travels away from the target in a rebound. Not all of the energy is returned to the projectile, though. During impact some energy is lost in indenting the target, in heat and sound generation, but most of the energy not returned is used up in generating damage, which in composites is the generation of fracture surfaces. The damage generated due to low-velocity, high mass impacts is very different from that generated by high-velocity, low mass impacts. This is immediately apparent when the delamination areas of these two impact regimes at the same impact energy are compared. Delamination is much smaller if the impact velocity is less and the mass is greater.

It may have become apparent from the above discussions that impact velocity, projectile mass and target mass are inseparably linked and cannot be treated on their own. Furthermore referring to an impact by incident energy only, does not give enough information as to the type of impact occurring, since both high-velocity, low-mass impacts and low-velocity, high-mass impacts can have the same measured incident energy. In ballistics testing the term energy density is used, where the energy transferred is taken across the projectile's cross-sectional area. Therefore a larger projectile will have less intensity in transferring its energy into the target. This gives a measure of penetrability for the complete ballistic range. When reaching the bottom of the ballistic range where the non-penetrating impacts are found and moving into low-velocity impact regimes, energy density may no longer be relevant as in this region the rate effects in the impacts affect the damage progression. Again, impactors of equal cross-section will not generate the same amount of damage if they travel in different velocity regimes. It may therefore be better to use energy transfer rate in preference to other measurements as this may then be linked to the peak force reached, which has in literature been related to the amount of damage induced in the target laminates.

7.2. Boundary Conditions and Target Configurations

In addition to the effects of velocity and mass, the target support types and thickness have a significant effect on the resulting damage state in the laminates. For any given impact velocity the distance to the supports is critical, as this will determine whether plate motion due to the impact will be set up or not. For plate motion to be set up, the stress waves emanating from the impact site must be able to travel to the boundaries and back. In the case of low velocity impacts this usually is the case and therefore

predictions of the plate motion can be used. For high velocity impacts, the time during which the impacting bodies are in contact is sufficiently short for the stress waves not to be able to reach the boundaries and reflect back. In that case no plate motion is established and the target laminates deform only locally to the impact region.

If the target panel is edge supported the plate motion can be predicted using well-established methods presented in Abrate, 1998. If the support system becomes more complex, though, classical methods can no longer be used and finite element methods need to be employed instead. If the target becomes fully supported, again the analysis methods can become simpler with the analysis of an impact onto a half-space.

Laminate thickness can also have a significant effect on the impact response. During low velocity impacts, the bending stiffness resulting from the laminate thickness determines the magnitude of the deflection, thus controlling the type of damage. For a very thin laminate, the plate will deflect sufficiently to cause tensile failures in the back face and causing an inverted pine tree type delamination. Once the laminate becomes thick enough to prevent this kind of excessive bending, the failure initiates at the contact zone and propagates downwards, giving a pine tree type delamination (Figure 7.4). The figure shown is for illustration purposes only, but shows the damage observed in one of the pre-stressed laminates due to the drop-weight 5-Joule impacts (Figure 5.17 in chapter 5.2.2). The delaminations have been highlighted with grey lines to make them more visible.

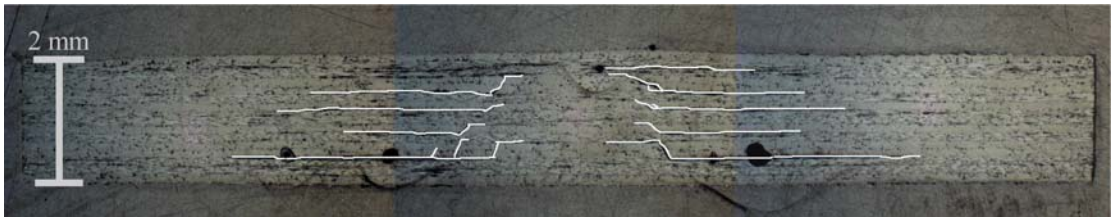

Figure 7.4 Micrograph example of a typical pine-tree type delamination in a composite laminate after a low-velocity impact

During high velocity impacts, where the deformation of the laminate is local to the impact zone, damage occurs due to an altogether different mechanism. Because the plate has no time to deform globally, only the area immediately surrounding the impact area deforms. In non-penetrating high-velocity impacts the area immediately below the impactor experiences a constant compressive strain, which is being "pushed" out the opposite face of the laminate as a shear plug (Figure 7.5). As a result high through-thickness shear stresses are set up between the shear plug and the rest of the laminate. Unlike ballistic type impacts, though, these shear stresses do not become high enough for the plug to detach from the rest of the laminate. This high through-thickness strain field does however also include high interlaminar shear stresses, which do reach high enough levels to initiate and propagate delaminations. Assuming these shear stresses to be approximately constant through the thickness of the laminate (this is based on the assumption that the shear plug has a constant and negligible direct compressive strain in the through-thickness direction), the resulting delaminations should be approximately equal in size at each interface through the thickness.

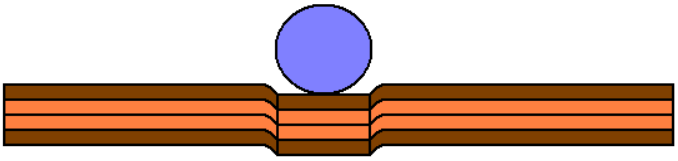

(a)

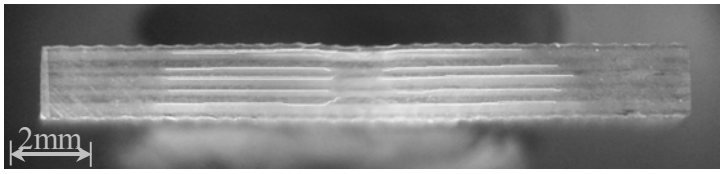

(b)

Figure 7.5 (a) a diagrammatic illustration of a shear plug developing during a high velocity impact and (b) micrograph showing the resulting damage.

7.3. Effect of Pre-Stress on the Impact Damage

The results of this study showed that there was no noticeable effect of pre-stressing on the high-velocity impact performance of the test laminates, whereas pre-stressing caused a variation in impact performance of around 25% for low-velocity impacts. The following sections analysed why this occurred.

7.3.1. Low Velocity Impacts

In the type of low velocity impacts studied here, failure started at the impact zone with ply cracking under the impactor. It propagated through the thickness by means of transverse cracks travelling through a ply, along a ply interface, through the next ply and again along the interface. This continued to the back face. As it travelled through the thickness of the laminate, the delaminations increased in diameter.

At the impact face during a low-velocity impact, the composite is locally crushed by the impactor, which in turn generates matrix cracks in that ply. Due to the shear forces present from the bending of the plate, these cracks are driven downwards. In simple terms this can be shown using beam bending. Considering a beam supported

at the ends and loaded in the middle the shear forces in any part of the beam can be shown as in Figure 7.6(b). These shear forces can be resolved into their principal components as in Figure 7.6(c) (the arrows represent the loading due to the deflection caused by the impact). It can be seen that these shear forces encourage opening of the cracks as they travel through the laminate.

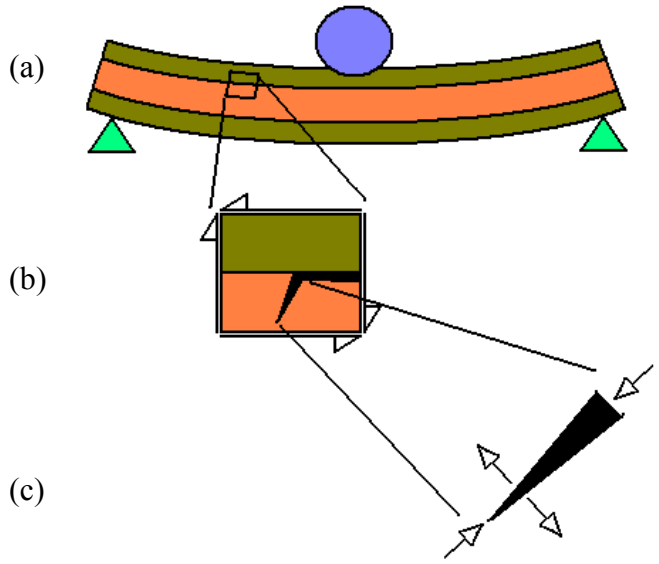

Figure 7.6 Diagrammatic representation of resolving forces at a crack tip subjected to shear due to the impact event without considering any thermal or mechanical residual stresses. (a) shows a simplified representation of a composite panel being impacted by a projectile. (b) shows stress state surrounding a propagating crack at an interface between plies and (c) shows the resolved forces at the crack tip.

At this point the plane of the crack is along the fibre direction and between normal and 45º to the plane of the panel (Figure 7.7). When the crack encounters an interface with an adjacent ply, it can no longer continue in its plane and must reorient to continue. To continue down through the laminate the crack would either have to break fibres to stay in its plane or rotate its plane to be in line with the fibres of the next ply. The latter requires less energy and to reach this plane, the crack follows the

interface between the plies until its plane is aligned with that fibre direction (Figure 7.7). In so doing, delaminations are created on the way. As the crack travels along a ply interface, its path is dominated by the fibres in the ply it is trying to align with, this gives the characteristic "peanut" shape.

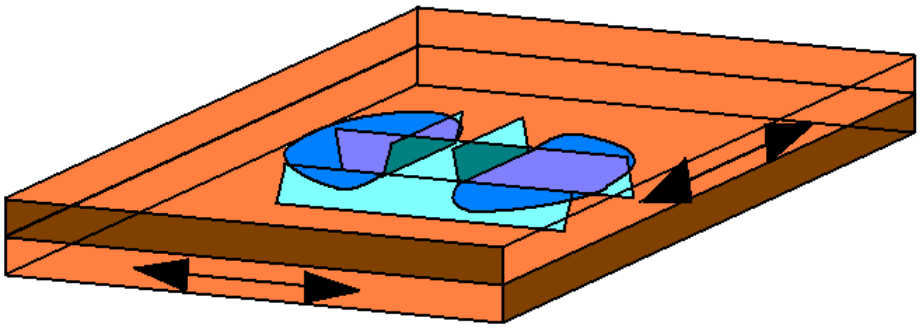

Figure 7.7 Diagram showing the crack propagation from one ply to the next and the resulting delamination. The black arrows show the fibre directions in each ply.

In Figure 7.8(b) and (c) the residual thermal stresses have been superimposed over the load-induced shear components shown in Figure 7.6. The component of the residual stresses normal to the crack also encourages crack opening therefore worsening the situation. This is where pre-stressing can be of benefit, as the pre-stressing reduces the residual in-plane stresses in the laminate, which in turn reduces the opening loads on the crack tip.

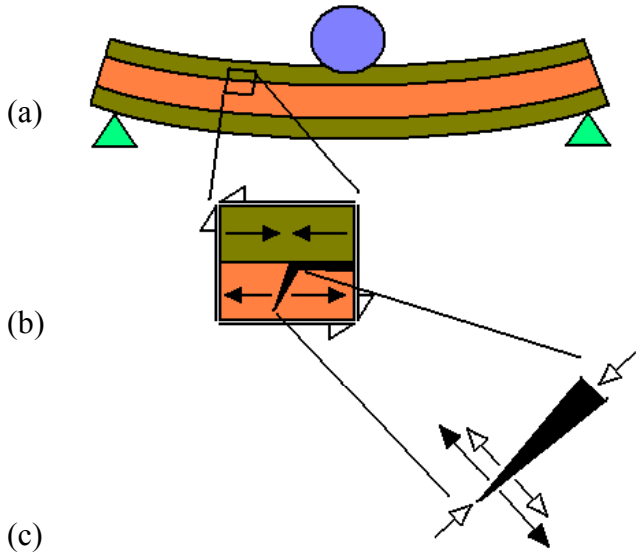

Figure 7.8 Diagrammatic representation of resolving forces at a crack tip subjected to shear due to the impact event and the thermal and mechanical residual stresses. (a) shows a simplified representation of a composite panel being impacted by a projectile. (b) shows stress state surrounding a propagating crack at an interface between plies and (c) shows the resolved forces at the crack tip.

Comparing this now with experimental results, the theory is confirmed in Figure 7.9, where the number of through-ply cracks are significantly reduced by applying 40MPa of pre-stress.

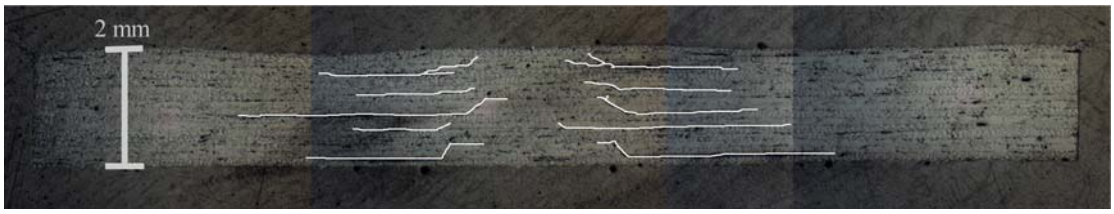

(a)

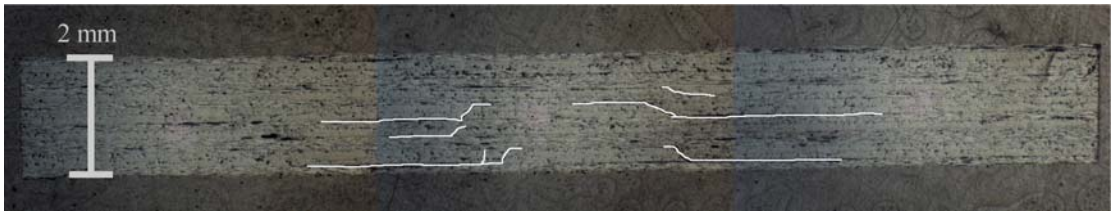

(b)

Figure 7.9 Micrographs of the damage state in (a) a composite without pre-stress and (b) a composite with 40 MPa of pre-stress

Basing ones views on the above argument, one could stipulate that for even greater pre-stress the delamination could be reduced yet further.

Interestingly, this is not the case. As pre-stress in increased further, past 60MPa, the amount of delamination begins to increase again. Figure 7.10 shows the damage state for specimens with 100 MPa of pre-stress.

Figure 7.10 Micrograph of the damage state in a laminate pre-stressed to 100 MPa and impacted at 5 Joules in the instrumented falling weight impact tester

It can be observed that between Figure 7.9 and Figure 7.10 the number of cracks travelling across plies has increased significantly. Whereas in panels pre-stressed below 60MPa there is typically a single crack travelling between delaminations, in panels pre-stressed above 60MPa more than one can be seen to be travelling between

delaminations. This observation is likely to be linked to the explanation as to why 60MPa has been found to produce the least amount of delamination.

Further study would have to be conducted to be able to fully explain the reasons for the increased numbers of microcracks. Use of micro-mechanical finite element models and fracture mechanics experiments would have to be carried out to study the effects of the pre-stress on the fracture behaviour both at a fibre-matrix level as well as at a laminate level. Only then could this phenomenon be fully explained. The scale of such an investigation would however warrant enough time to be spent as has already been done in this study.

At this stage it should suffice to give an indication as to how this observation may have come about. A composite laminate without any pre-stress in it is subject only to its thermal residual stresses as a result of having cooled it from its curing temperature to ambient conditions. As already discussed, these cause tensile stresses in each ply, perpendicular to the fibre direction. As pre-stress is applied these tensile stresses are reduced, since pre-stressing superimposes a compressive stress in this direction.

During an impact event, the propagating cracks are encouraged to propagate by the thermal residual tensile stresses in the ply, possibly giving rise to only a single crack. As pre-stress is increased, such encouragement for crack propagation is reduced, making it harder for cracks to traverse plies. At around 60 MPa of pre-stress the stresses encouraging crack propagation may have reduced so far that a single crack is no longer encouraged and multiple cracks are formed. As these traverse the plies they create more points at which delamination may start, thus allowing delamination to increase again. This postulation is only an initial suggestion and as has already been

stated would require significant amounts of more research to fully verify.

7.3.2. High Velocity Impacts

During high velocity impacts, through-thickness cracks were less apparent. All damage appeared to be at ply interfaces only. This could have been caused by high interlaminar stresses being set up due a shear plug being generated below the impactor. Unlike in ballistic impacts, the shear plug did not detach from the parent material around it, thus high through thickness shear stresses were generated, which in turn were picked up by the ply interfaces, where interlaminar shear failure took place. Assuming no significant amounts of through-thickness strain in the shear plug, the shear stresses at each ply interface through the thickness would be approximately equal, which would in turn explain the roughly equal amount of delamination at each ply interface in the tested samples.

Furthermore, since the response of laminate was mostly local to the impact zone and the contact forces were quite high, high shear forces would have only been set up around the shear plug, where failure would then have initiated at the weakest points – the ply interfaces. As the composite then began to respond dynamically to the loading, those delaminations would have grown in mode II, since locally high shear stresses would still have been dominating. The whole impact event would then have been over before the laminate could have responded quasi-statically. Figure 7.11 demonstrates this concept. These shear stresses to initiate failure must also have been sufficiently high to override any benefits pre-stressing may have offered. Therefore there was no noticeable change in delamination area or absorbed energy for this kind of impact event and for different levels of pre-stress.

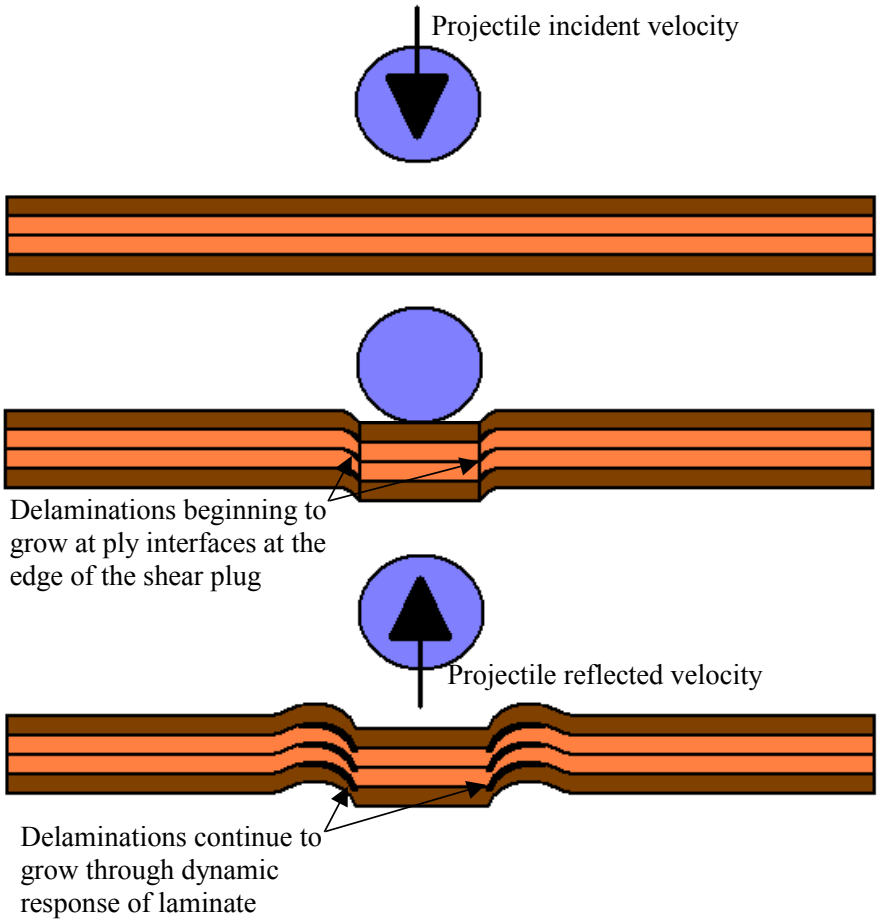

Figure 7.11 Diagrammatic representation of the creation of damage in a high velocity impact

7.4. Finite Element Simulations

When considering the results from the finite element simulations, neither the drop weight nor the gas gun impacts reflected the experimental results. There were, however differences in the damage as a result of pre-stressing between the drop weight impacts and the gas gun impacts.

7.4.1. Gas Gun Impacts

The experimental results for the gas gun impacts showed no discernable change in either absorbed energy or delamination area with different levels of pre-stress. Although the damage shapes for both material models studied compared well with

test, the plots of delamination area against pre-stress and the plots of absorbed energy against pre-stress did not reflect any correlation, neither for material type 22 or type 55. Compared with each other, however, they did show considerable difference in damage area against pre-stress (Figure 7.12).

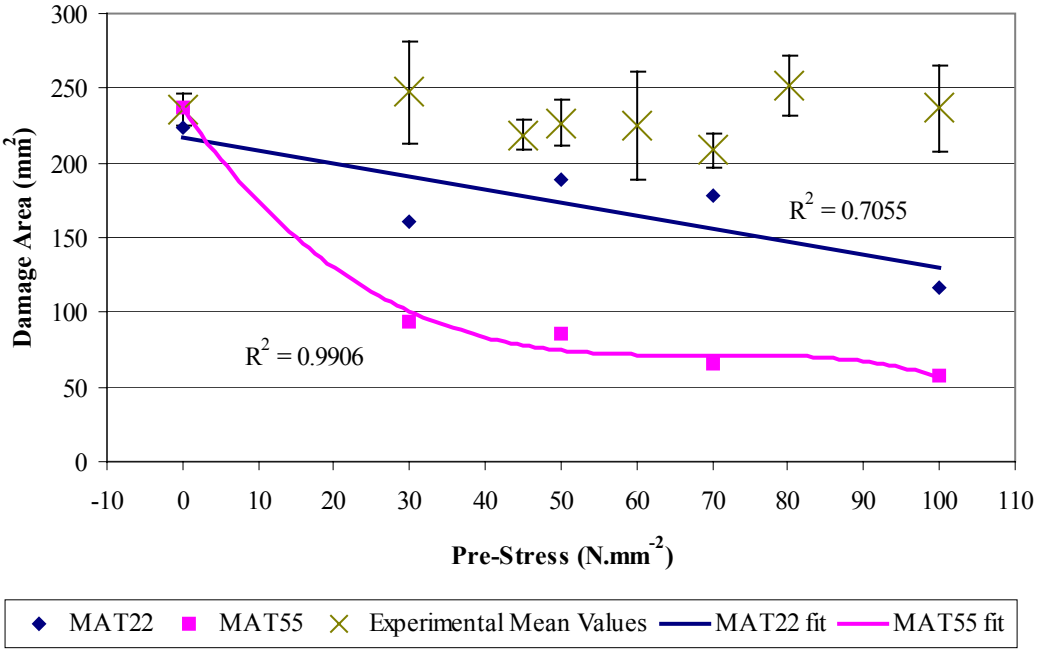

Figure 7.12 Plot showing the finite element analysis predicted damage areas against their corresponding pre-stress values. The experimental data was added for reference.

Material type 22 used the Chang-Chang failure criteria whereas material type 55 used the Tsai-Wu failure criteria. Table 7.1 shows the failure criteria for both material types and how the material properties were changed after a particular failure mode was encountered. In the case of material type 22, failure occurred if $F_{fibre}^{tensile}$, $F_{matrix}^{tensile}$ or F_{matrix}^{comp} became equal to or greater than 1. In material type 55, failure occurred if e_{ft}^2, e_{fc}^2, e_{mt}^2 or e_{mc}^2 became equal to or greater than zero.

Table 7.1 Comparison of failure models for material types 22 and 55.

Material Type 22 (Chang-Chang Criteria)	**Material Type 55 (Tsai-Wu Criteria)**
$F_{fibre}^{tensile} = \left(\frac{\sigma_1}{S_1^T}\right)^2 + \bar{\tau}$ $E_{11} = E_{22} = G_{12} = \nu_1 = \nu_2 = 0$	$e_{ft}^2 = \left(\frac{\sigma_1}{S_1^T}\right) + \beta\left(\frac{\tau_{12}}{S_{12}}\right) - 1$ $E_{11} = E_{22} = G_{12} = \nu_1 = \nu_2 = 0$
None	$e_{fc}^2 = \left(\frac{\sigma_1}{S_1^C}\right)^2 - 1$ $E_{11} = \nu_1 = \nu_2 = 0$
$F_{matrix}^{tensile} = \left(\frac{\sigma_2}{S_2^T}\right)^2 + \bar{\tau}$ $E_{22} = G_{12} = \nu_1 = \nu_2 = 0$	$e_{mt}^2 = \left(\frac{\sigma_2}{S_2^T}\right)^2 + \left(\frac{\tau_{12}}{S_{12}}\right)^2 - 1$ $E_{22} = G_{12} = \nu_2 = 0$
$F_{matrix}^{comp} = \left(\frac{\sigma_2}{2S_{12}}\right)^2 + \left[\left(\frac{S_2^C}{2S_{12}}\right)^2 - 1\right]\frac{\sigma_2}{S_2^C} + \bar{\tau}$ $E_{22} = \nu_1 = \nu_2 = 0$	$e_{mc}^2 = \frac{\sigma_2^2}{S_2^C S_2^T} + \left(\frac{\tau_{12}}{S_{12}}\right)^2 + \frac{\left(S_2^C - S_2^T\right)\sigma_2}{S_2^C S_2^T} - 1$ $E_{22} = G_{12} = \nu_1 = \nu_2 = 0$
$\bar{\tau} = \frac{\frac{\tau_{12}^2}{2G_{12}} + \frac{3}{4}\alpha\tau_{12}^4}{\frac{S_{12}^2}{2G_{12}} + \frac{3}{4}\alpha S_{12}^4}$	

Where $F_{fibre}^{tensile}$, $F_{matrix}^{tensile}$ and F_{matrix}^{comp} are the material type 22 indexes for fibre tensile, matrix tensile and matrix compressive failure modes respectively. e_{ft}^2, e_{fc}^2, e_{mt}^2 and e_{mc}^2 are the material type 55 failure indexes for fibre tensile, fibre compressive, matrix tensile and matrix compressive failure modes respectively. S_1^T, S_1^C, S_2^T, S_2^C and S_{12} are respectively the fibre direction tensile and compressive strengths, the transverse (matrix) direction tensile and compressive strengths and the in-plane shear strength. α is the non-linear shear stress parameter for the Chang-Change failure criteria and β is the weighting factor for the shear term in tensile fibre failure mode. For this study, β was set to zero.

Both models were applied to shell elements only and the failure criteria were therefore only considered for in-plane stresses and strengths.

The key difference between the two failure models was in the way they treated the in-plane shear interactions in fibre tensile and matrix tensile failure modes. The Chang-Change failure criteria of material type 22 incorporated the $\bar{\tau}$ term as defined above in Table 7.1 and the Tsai-Wu criteria used a much simpler term of $\left(\frac{\tau_{12}}{S_{12}}\right)^2$. The implications of this were that as in-plane shear increased, failure in the fibre or matrix tensile directions became dominated by the shear term. Note that because β was set to zero in the Tsai-Wu failure criteria, no shear stress terms affected the fibre tensile mode in material type 55.

Figure 7.13 demonstrates this. Shown is the percentage of the direct term (fibre tensile or matrix tensile) in the overall failure index against the ratio of shear stress to direct stress.

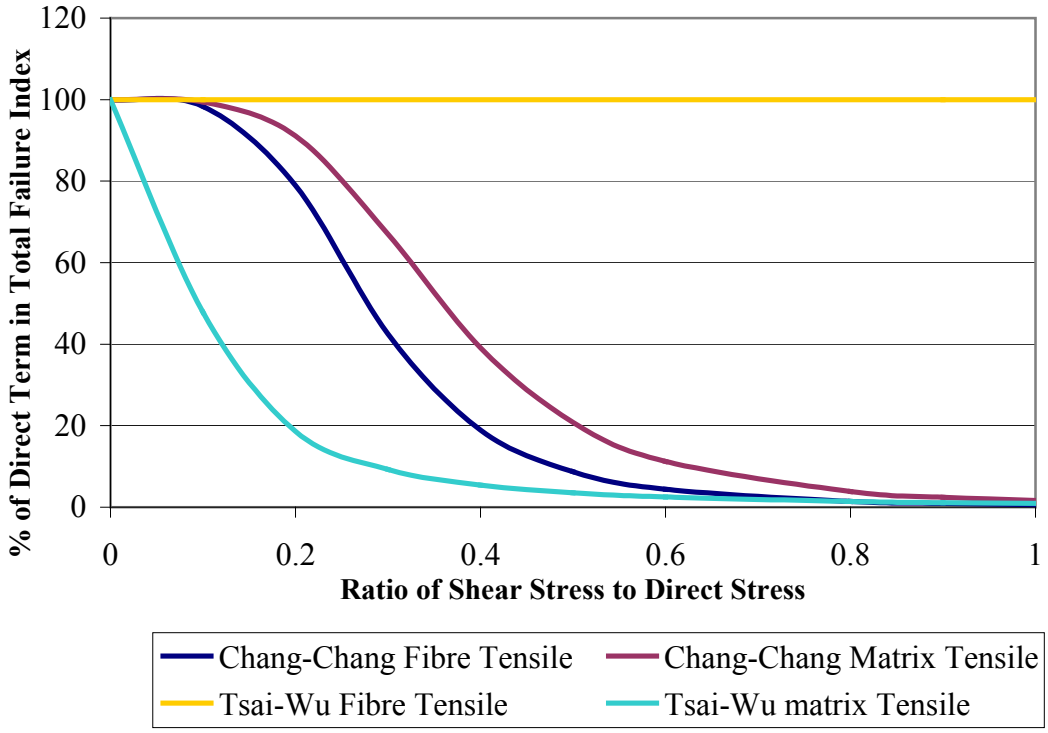

Figure 7.13 Effect of the shear term on the fibre and matrix tensile failure modes for the two different failure models.

In this study it was assumed that the shear strength was not affected by the pre-stressing, since with a cross-ply laminate there was no mechanism to affect the shear strength through pre-stress in the fibres. Therefore if the shear stresses were dominating the failure of the plies during the impact event, the benefits of the pre-stressing would have been masked.

It is therefore likely that for material type 22, the failure was mode dominated by shear terms and in material type 55 it was not. This is likely since the fibre tensile mode in material type 55 was completely unaffected by the shear term, thus potentially allowing the benefits of pre-stressing to be more readily seen.

Although these differences may have been observed, neither model matched the experimental results.

Figure 7.11 showed diagrammatically how the gas gun type impacts would affect the target laminates, where high through-thickness shear stresses caused predominantly through-thickness shear failure, leading to delamination. Neither material type 22 or type 55 in LS-DYNA could take account of these failure modes, using shell elements. It may have been possible to represent them using a model using solid element, this was however not possible in the timescales of this study. However, even using solid elements, the version of LS-DYNA available during this study would not have been able to model the delamination. In addition to this it was not possible with LS-DYNA to determine which plies had failed, and which had not. It was only possible to say that a certain proportion of the plies had failed. Therefore very little comparative information could be taken from the finite element results.

There were two useful conclusions though, which could be drawn from this finite element study. The first was to confirm that for high velocity impacts the use of shell elements could not adequately represent the event. Shell element could only take into account the in-plane failure properties of the laminate. Since only the laminate through-thickness strengths were affected by the gas gun impacts, any effects observed in the finite element simulations were wholly unrelated to the actual failure mechanics involved in high velocity impacts. And this was the second useful result; insofar this inability to represent the through-thickness failure confirmed that for high-velocity impacts failure was dominated by the through-thickness strengths.

7.4.2. Drop Weight Impacts

The experimental results for the low-velocity, drop weight impacts showed a marked effect of the pre-stressing on the impact performance of the composite laminates. Again, the finite element results did not match the experimental results. The force-time plots, although matching is basic shape, did not follow the same trend as for the experimental results. Both shape and size of damage areas did not match. Whereas there was a clear trend for delamination area against pre-stress for the experimental study, no such trends could be discerned from the finite element simulations.

The implications of these findings confirmed, though that the damage mechanics for low-velocity impacts were not related purely to the in-plane strengths. The material properties that could be varied in the finite element model were the in-plane tensile and compressive strengths, which took account of material failure for in-plane loading, but not of crack propagation. In the case of the low-velocity impacts it was postulated that the cracks were prevented from propagating through a ply as a result of in-plane residual stresses, reducing the crack tip opening stresses. Such an effect could be taken account of using an energy-based fracture mechanics method, but not by the failure models within LS-DYNA, as these only considered material failure on a static strength basis.

As with the high-velocity impact analyses above the useful findings in the low-velocity impacts were that LS-DYNA version 950 could not simulate impact events in composites to a satisfactory degree using readily contained failure models. More recently released versions of LS-DYNA may well have better material models, capable of simulating the complex nature of composite failure under impact loading. A further useful finding was that again by not matching the experimental results the

finite element results support the assumptions discussed in the experimental sections above by not disproving them.

7.5. Conclusions

In this chapter the results of the study have been analysed and discussed. Attempt has been made to best explain phenomena that have occurred, breaking them down to their fundamentals. Where possible the practical implications have also been discussed. The main findings will now be reiterated for completeness.

In terms of the low-velocity impacts it had been found that pre-stressing significantly affected the damage area. The damage reduced from no pre-stress until 60 MPa and then rose again beyond that level of pre-stress. This trend was indeed apparent in both impacts at 5 Joules and at 17 Joules.

This finding is in agreement with the findings of Motahhari and Cameron (1996, 1998) and Fancey (2000a, b), who reported that a pre-stress of 60 MPa would be the optimum level of pre-stress for minimising the amount of damage in a composite. They, however considered only unidirectional test specimens, impacted in a Charpy impact tester. This allowed them to observe the fibre-matrix failure behaviour, but not the interlaminar delamination behaviour. This study has shown that for delamination behaviour also, 60 MPa pre-stress yields the least amount of damage.

There were two major findings for the high-velocity impacts, the first being that pre-stressing did not affect the impact performance for such an impact regime. Therefore no benefits or penalties could be identified. The second was identifying the damage state in a composite laminate under high-velocity impact loading. The damage state in this loading regime pointed toward a shear plug having been set up below the

impactor, similar to that in ballistic impacts. The difference being that this shear plug did not detach from the rest of the laminate. This shear plug would have set up very high shear stresses around its perimeter, which in turn would have caused shear failure at the ply interfaces, since these ply interfaces would have presented the lowest strengths to the shear stresses. Delamination growth would then have occurred during the dynamic response of the laminate. This was rather a coincidental finding as the original aim of the work was to identify the effect of pre-stressing on the impact performance of the composite laminates. The assumption originally was made that the damage state would be that of low-velocity impacts, which was based on information from Abrate (1998).

Finally, it was also found that the finite element method studied here to simulate effects of pre-stress on the impact performance proved to be inadequate for the task. The failure models in the analysis code (LS-DYNA version 950) did not take account of suitable failure modes to be able to include the effects of pre-stressing. The finite element analyses were intended as backup simulations to supplement the experimental work. As with the high-velocity impacts, the findings however, deviated from the initial intentions to highlight other areas of interest. It would certainly now be of value to re-evaluate composite failure models used in finite element analysis to take into account the effects of internal residual stresses and also to look at more recently developed failure models, not included in this study.

This page is intentionally blank.

8. CONCLUSIONS

All work and discussions for this study have now been presented. This conclusions chapter will offer an overview of this work to complete the presentation. The chapter has been split into three sections. The first will summarise the work presented in the previous chapters. The second section will reiterate the key results and findings and the third will provide some final concluding remarks.

8.1. Work Presented

8.1.1. Review of Literature

The literature review chapter presented all publications found on the subject of pre-stressed composites. The range of authors had investigated varied aspects such as methods of producing pre-stressed composites, analysis methods to define material behaviour and performance, and testing for the mechanical properties such as static strengths and impact performance. Since this study considered the impact performance of pre-stressed composites the papers by Motahhari and Cameron (1998) and Fancey (2000a, b) were of particular interest.

It was found from the review that there existed a large range of approaches to producing pre-stressed composites from the simple approaches by Motahhari and Cameron (1997, 1998) and Fancey (2000a, b) where a single bundle of fibres was impregnated with resin whilst under applied strain, to the more complex approaches by Schulte and Marissen (1992) and Tuttle *et al.* (1996). The potentially most practical approach was presented by a range of authors, who used filament winding to produce their pre-stressed composites.

The analysis of pre-stressed composites was carried out at two levels – at the micro-mechanical level, looking at the interaction between fibres and matrix and at the laminate level, looking at the interaction between plies. At the laminate level it was shown that pre-stress could be included in the classical laminate analysis as an extra term on top of the hygro-thermal terms.

8.1.2. Experimental Procedures

All experimental procedures were presented and detailed in this chapter as well as such issues as material selection, choice of laminate stacking sequence and the lamination and pre-stressing processes. The key points in this chapter to recall were that the material chosen was a Hexcel Composites E-glass fibre, 913 epoxy resin prepreg UD tape, which was laid up in a cross-ply laminate of a $[0/90_2/0_2/90/0/90]_S$ symmetric lay-up. The laminates were cured in an autoclave at 120ºC and 0.6895 $MN.m^{-2}$ for one hour under vacuum, which was released when the autoclave pressure reached 0.3103 $MN.m^{-2}$. Pre-stress was applied in both fibre directions of the cross-ply laminate using a specially-designed pre-stressing rig, which consisted of a steel loading frame and four clamping mechanisms, linked to the frame using steel bolts. Blanking plates were used to avoid the vacuum bagging material from entering the complex shape of the frame and causing a bag burst. Strain gauges on the frame were used to monitor the fibre pre-stress during the curing process. The produced laminates were predominantly tested for high and low velocity impacts using a gas gun and an instrumented falling weight respectively. A small number of coupons were also tested in tension to confirm the presence of pre-stress. To supplement the experimental tests, finite element simulations were carried out for the high and low velocity impacts.

8.1.3. Results

Chapter 0 presented all results from the panel production, experimental tests and finite element simulations. A range of pre-stress levels were achieved between 0 and 200 MPa. The tensile tests showed a trend that confirmed the presence of pre-stress. In the impact tests it was found that pre-stressing had no effect on the high velocity impact performance of the laminates. In the low-velocity impact regimes there was, however a noted effect. The finite element analyses were found not to correlate to the experimental results.

8.1.4. Discussion of Pre-Stressing Concept and Process

The first of the discussion chapters discussed the pre-stressing method only. Within this chapter the pre-stressing concept was explained using classical laminate analysis and micro-mechanics. For the analysis some assumptions were made. Strain compatibility and balance of forces were essential in both classical laminate analysis and micro-mechanics. Assumptions specific to classical laminate analysis were also made. These were that the laminate had to be balanced and symmetric (this was justified for the lay-up chosen) and that no bending was induced in the laminate. With these assumptions given the classical laminate analysis was discussed, giving details of how the pre-stress terms could be included in the analysis. These analysis methods were used to identify the properties most affected by pre-stress. It was found that pre-stressing most affected the in-plane properties transverse to the fibre direction. It was then postulated that pre-stressing could indeed improve laminate strengths by reducing (or even reversing) the tensile residual stresses in each ply transverse to the fibre direction as a result of the thermal residual stresses. This was concluded to have an affect in increasing the first ply failure, but as the final failure

was fibre-dominated that would remain the same. It was further postulated that compressive strength could be increased through fibre pre-stressing as this process reduced the fibre waviness. This was however only an assumption as no experimental investigation was carried out into this area.

The pre-stressing methodology was also discussed, giving details of choices made in deciding the final method. Three approaches were presented of which the third was chosen, justifying this choice as it was the only configuration to pre-stress the laminates in both fibre directions. A small finite element study was also discussed, which was used to choose the best design for the final choice of loading method configuration, since after making the initial configuration choice it was then necessary to iterate through some designs.

Finally, a critical evaluation of the method used in this study was presented. In particular there were some issues with making the frame useable for use in the autoclave. Blanking plates had to be added to prevent bag bursts. In fact, in the end a reusable vacuum bag system had to be made using silicone rubber membranes as use of single-use vacuum bagging material was not possible. The frame was also found to be too heavy for one man to lift, weighing approximately 50 kg. Therefore, an engine mount was adapted to hold the frame during assembly and a trolley had to be adapted to allow the frame to be transported to the autoclave. The trolley also had the capability of linking up to the rails in the autoclave, so the frame could be slid into the autoclave without being lifted. As well as monitoring the strain gauges during the cure, simple calculations and non-linear finite element simulations were carried out to identify how pre-stress was being applied to the laminate and how much was being applied.

8.1.5. Discussion of Experimental Results

The second discussion chapter took a closer look at the results from the two impact regimes as well as the finite element results. To give the reader an appreciation of how pre-stressing may affect the impact performance the effects of the different impact regimes were discussed. In low-velocity impacts the target structure responded globally to the impact event, since the event was long and slow enough for a dynamic response to be set up. In high-velocity impacts the impact time was sufficiently short for the target laminate to only respond locally. These different types of loadings and responses meant that the laminates failed in different ways.

In low-velocity impacts damage initiated at the impacted face by way of matrix cracking. These cracks then propagated through the laminate towards the back face. When a crack reached a ply interface where the next ply had a different fibre orientation, a delamination would be set up and propagated by the interlaminar shear stresses due to the bending of the laminate. The propagating paths of the impact-induced cracks could be impeded, as the stresses transverse to the fibre direction were reduced due to pre-stressing. This would produce less impact damage, which was confirmed in the experimental results. At the critical level of 60 MPa, the residual stresses that were impeding the crack growth would have interacted with the thermal-residual stresses of an unpre-stressed laminate in such a way that the crack growth inhibition would have been negated, allowing more cracks to be formed. An increase in the number of transverse cracks would have encouraged more delamination growth. Therefore delamination was observed to increase again after the critical pre-stress level of 60 MPa.

The fact that the high-velocity impact performance of the laminate was not affected

by pre-stressing was put down to the fact that in a high-velocity impact the structure responded only locally and unlike in low-velocity impacts the damage was initiated at the ply interfaces immediately rather than as a consequence of a propagating crack. This was justified by the fact that no through-thickness cracks were observed in the high-velocity impacted samples. These delaminations were a result of the high interlaminar stresses set up around a shear plug created through the thickness of the laminate under the impactor. A combination of these interlaminar stresses being particularly high and pre-stressing having little effect on the interlaminar stresses meant that no discernable effect of the pre-stressing could be found in the high-velocity impacts.

The finite element simulations were found not to correlate with the experimental results. This was explained by the fact that the failure models in LS-DYNA version 950 did not take account of relevant failure modes or did not use an energy-based approach to predict the impact damage. This meant that the failure calculated in the finite element simulations was not that found in the experiments. Furthermore the models generated in this study used shell element to represent the target laminates, as this was the most appropriate way to represent composite laminates in LS-DYNA version 950. Using shell element for the target laminates meant that the through-thickness stresses could not be taken account of. Using solid element would have made that possible, but would have been much more time-consuming and would have detracted from the experimental work. Also the only failure model in LS-DYNA version 950 that could be used with solid element to represent composite was material type 22, which did not take account of the failure modes found to be affected by pre-stressing.

8.2. Key Results and Findings

In the literature review chapter it was found that the field of research into the effects pre-stressing on composites remains still an area of interest but receiving very little attention. Relatively few authors over the years have looked at this field of research. Of particular value to this study was that no authors had looked at the effects of pre-stressing on the impact behaviour of composite laminates. In analytical terms, it was very useful to discover that pre-stressing could easily be incorporated into classical laminate analysis as an extra term. Furthermore it was found that filament winding was the most practical way to impart pre-stressing into composites for industrial applications.

From analysing the pre-stressing method it was found that although in principle this method was capable of producing adequate quality pre-stressed composite laminates, an unfortunate choice of strain gauges meant that none of the strain gauge plots from the autoclave cures could be used to confirm the level of pre-stress in the laminates. This in turn meant that the levels had to be assumed based on predictive calculations. It was therefore felt that although in this study the strain gauges were of little use, with careful selection of special gauges, the frame could be of great value in future studies.

It is important to note that the findings in this study was in agreement with the findings of Motahhari and Cameron (1996, 1998) and Fancey (2000a, b), who reported that a pre-stress of 60 MPa would be the optimum level of pre-stress for minimising the amount of damage in a composite. They, however considered only unidirectional test specimens, impacted in a Charpy impact tester. This allowed them to observe the fibre-matrix failure behaviour, but not the interlaminar delamination

behaviour. This study has shown that for delamination behaviour also, 60 MPa pre-stress yields the least amount of damage.

The finite element simulations demonstrated above all, that in aerospace applications of the finite element method, where shell elements are typically used to represent a structure the failure models found in LS-DYNA version 950 can neither be used to take account of pre-stress or simulate impact events. Detailed solid models would have to be used to model the impact events and energy based methods and models that take account of pre-stress would have to be put into analysis codes to be able to make practical use of the finite element method.

8.3. Final Remarks

In overall conclusion of this work it can be said that although there were some difficulties encountered during the study, it was possible to report useful findings, which help to further understand the complex nature of composites. Pre-stressing can offer potential benefits to composites (unidirectional or multi-angular laminates) in terms of static properties. This study has shown that there are also potential benefits to the impact performance of not just unidirectional composite (as demonstrated by Motahhari and Cameron, 1998, and Fancey, 2000a, b) but also of multi-angular laminates, as long as careful consideration is given to the level of pre-stress chosen.

The key findings again were (in bullet form)

- The field of pre-stressed composites remains an under-researched field of study.
- Bi-axially pre-stressed composites can be produced in an autoclave but much care has to be taken in monitoring the loads in the frame during the cure cycle.

- Pre-stressing had no discernable affect on the high-velocity impact performance of composite laminates
- Delamination due to low-velocity impacts could be reduced by as much as 25% in pre-stressed laminates.
- If considering delamination area against absorbed energy for low-velocity impacts, 60 MPa of pre-stress produced the worst case in glass fibre reinforced composite laminates.
- The failure models in the finite element analysis code studied here were neither capable of taking pre-stress into account, nor model the failure mechanics accurately.
- The study of pre-stressing can give valuable insight into composites' behaviour due to residual internal stresses as well as be used to improve the performance of filament wound components.

All that remains to do now is to offer ideas as to what further studies could be carried out in the field of pre-stressed composites to increase the knowledge base of this field. This is done in the next section.

This page is intentionally blank.

9. FUTURE WORK

During this study it became apparent that pre-stressing composites was a much greater field of research, much in need of more in-depth investigations than was thought at the start of the project. The following sections detail some potential projects, which would address some of the questions raised as a result of this study.

9.1. Expansion of Results Data

The most obvious area for future work would be to carry out more of the same tests and hence to be able to carry out full statistical analyses and critically assess the conclusions obtained in this study. Since the pre-stressing equipment is now readily available together with the testing equipment it would be viable to carry out a full test programme in approximately two years. One year to produce sufficient numbers of pre-stressed panels and a further year to carry out test and conduct analyses.

For this level of investigation more levels of pre-stress in the range from 0 to 100MPa would be needed, maybe three different lay-ups and four different types of material (e.g. e-glass epoxy, carbon epoxy, e-glass with a thermoplastic matrix and carbon with a thermoplastic resin). Keeping three different levels of impact energy, also carrying out some tension after impact / compression after impact tests, a full picture could be obtained. For this level of investigation, though, time and above all funding would be required.

9.2. Finite Element Study of the Residual Stress Field within a Pre-Stressed Composite

This study, together with other work by Motahhari and Cameron (1996, 1998) and Fancey (2000a, b) has shown that pre-stressing affects composites at several levels.

At a micro-mechanical level within each ply stresses are affected in the resin, fibres and their interfaces. At the meso-mechanical level there are also interactions between plies and their interfaces, which are affected by pre-stress. To better understand the extent of these effects it would be beneficial to carry out detailed finite element simulations using the unit cell approach (similar to the approach of Schulte *et al.* 2004) at both the micro- and meso-mechanical levels.

To carry out these models, a detail mesh would need to be generated for the smallest repeatable unit of the level in question. For a micro-mechanical model this may be a small volume containing a representative cluster of fibres set in the resin matrix. For the meso-mechanical level, it may be a set of plies. The boundary conditions would then have to be defined to simulate the unit cell as set in a complete laminate. By meshing the interfaces between fibre and matrix or between plies particularly finely, the interfacial stresses may also be estimated. These stress fields could then be used in fracture mechanical analyses as described in section 9.3.

9.3. Fracture Mechanics of Pre-Stressed Composites

As a result of this study having taken a broader look at the effects of pre-stressing on the impact performance and from surveying the existing literature it has become apparent that a detailed study of the fracture behaviour of pre-stressed composites would have great benefit. This and other studies showed that pre-stressing has an effect on the damage tolerance of composites under certain conditions. It would therefore be useful to investigate which failure modes are affected by pre-stressing and how. This would quite likely have to be coupled with a detailed stress analysis of the composite configuration in question as has been suggested in section 9.2.

The fracture mechanical study would have to incorporate both analytical and experimental aspects. Either classical or finite element based analysis methods could be used or derived to investigate the fracture behaviour of pre-stressed composites. In the experimental part all forms of failure testing coupled with fractography could be employed. For example tensile tests, in-plane shear tests, mode I, mode II and mixed mode I and II tests would give useful information. As pre-stressing mostly affects the in-plane strength properties tensile and in-plane shear tests, could characterise the fracture behaviour in this type of loading. As pre-stress becomes higher, a worsening of the impact resistance was observed and attributed to excessive interfacial stresses propagating cracks readily. Using mode II testing this could be confirmed. Mode I is likely not to be affected but tests would confirm this. In impact events it is most likely that a mixed mode I and II failure would occur, so such a test should also be carried out.

Ultimately, this fracture mechanics study would further yield great value for the engineering community in clarifying the effects of residual stresses on the strength of composites.

9.4. Application of Pre-Stressing

Although most methods presented in this study and in other literature would not be suitable for commercial application of pre-stressing, the filament winding method has been proven to offer the possibility of producing pre-stressed components on a commercial scale (Rose and Whitney, 1993, Dvorak *et al.*, 1999a, b). Benefits could be found in further investigating the viability of the application of pre-stress into industrial scale components. Such an investigation would require assessment of various manufacturing methods and their suitability to pre-stressing as well as

manufacturing trials to optimise any processes identified with a view to developing commercial processes for producing pre-stressed components.

A second angle on the application of pre-stressing falls into the realm of exploiting the knowledge gained in analytical studies of pre-stress. This would be done with the view to better understanding the effects of residual stresses in composite components. Although pre-stressing may or may not be viable as a commercial process, the ability to vary the residual pre-stress can help in understanding how residual stresses affect a composite and also to develop more accurate analysis methods to be used in the structural analysis of composite components.

Both of these approaches fall within application of pre-stressing and although not entirely suitable for academic projects such as a PhD are vital to ensure exploitation and implementation into the industrial sector of composites.

9.5. Development of Finite Element Material Models for Composites

With the publication of the international failure model study (Hinton *et al.*, 2002) the composites world is in the strong position of having a comprehensive overview of the failure models available for composites. Unfortunately, although numerous methods are available these days, none represent actual failure of composites to their fullest. Again pre-stressing offers another opportunity to better understand composite behaviour by concentrating on the residual stress state and its effect on composite strength. Such knowledge could either feed into pre-existing failure models or may indeed produce an altogether new approach to this long-standing problem. Although understanding residual stress-states is not an exhaustive approach to failure analysis, it could highlight effects not otherwise identified by other methods.

The present study although not yielding the desired results from the finite element method with respect to the resultant damage state after an impact event, has highlighted potential areas of shortcomings in the present failure models implemented in the LS-DYNA code used in this study with regard to the residual stress-state and its affect on the damage state. There therefore exists an opportunity to develop failure models within the finite element method, which can take account of the residual stress state.

9.6. Post-Impact Compression and Fatigue Strengths of Pre-Stressed Composites

The logical next step after having identified the extent of damage in a composite with pre-stress would be to assess the residual properties of an impacted composite with respect to pre-stress. In particular compression after impact and fatigue after impact would be two aspects to investigate, as these are critical after-impact strengths for an aircraft structure. Compression after impact is also the strength most affected by impact-induced delamination.

Since pre-stressing has been shown to affect the impact resistance during low-velocity drop weight type impacts, it would make sense to use this method in the investigation of the residual strength of pre-stressed composites. Furthermore, drop weight type impacts lend themselves well to impacting panels and allowing coupons to be cut from them subsequently.

This page is intentionally blank.

10. REFERENCES

1999, “TrueGrid Manual”, XYZ Scientific Applications Inc.

Abrate, S, 1998, “Impact on Composite Structures”, Cambridge University Press, Cambridge.

Badcock, R.A., 1997, “Optical Fibre Sensors for Structural Strain Monitoring”, PhD Thesis, Brunel University, UK.

Barbero, E.J., 1999, “Introduction to Composite Materials Design”, Taylor and Francis, Philadelphia, USA.

Brooks, D., 2004, “Effect of Impact Damage in a Carbon Fibre Composite Material“, PhD Thesis, Brunel University, UK.

Dvorak, G.J., and Suvorov, A.P., 2000, “The effect of fiber pre-stress on residual stresses and the onset of damage in symmetric laminates”, Composites Science and Technology, Vol. 60, pp 1129-1139.

Dvorak, G.J., Prochazka, P., and Srinivas, M.V., 1999a, “Design and fabrication of submerged cylindrical laminates – I”, International Journal of Solids and Structures, Vol. 36, pp 3917-3943.

Dvorak, G.J., Prochazka, P., and Srinivas, M.V., 1999b, “Design and fabrication of submerged cylindrical laminates – II. Effect of fiber pre-stress”, International Journal of Solids and Structures, Vol. 36, pp 3945-3976.

Fancey, K.S., 2000a, “Investigation into the feasibility of viscoelastically generated pre-stress in polymeric matrix composites”, Materials Science and Engineering, Vol. A279, pp 36-41.

Fancey, K.S., 2000b, “Prestressed Polymeric Composites Produced by Viscoelastically Strained Nylon 6,6 Fibre Reinforcements”, Journal of Reinforced Plastics and Composites, Vol. 19, No. 15, pp 1251-1266.

Hallquist, J., 1999a, “LS-DYNA Keyword Manual, Version 950”, Livermore Software Technology Corporation, Livermore, California, USA.

Hallquist, J., 1999b, “LS-DYNA Theory Manual, Version 950”, Livermore Software Technology Corporation, Livermore, California, USA.

Hallquist, J., 1999c, “LS-DYNA User’s Manual, Version 950”, Livermore Software Technology Corporation, Livermore, California, USA.

Hinton, M.A., Kaddour, A.S., Soden, P.D., 2002, "A Comparison of the Predictive Capabilities of Current Failure Theories for Composite Laminates, Judged against Experimental Evidence", Composites Science and Technology, vol. 62, pp. 1725-1797

Hull, D, and Clyne, T.W., 1996, “An introduction to Composite Materials”, Second Edition, Cambridge University Press, Cambridge.

Jorge, L.D.A., Marques, A.T., De Castro, P.M.S.T., 1990, “The Influence of Prestressing on the Mechanical Behaviour of Uni-Directional Composites”, Proceedings of the Fourth European Conference on Composite Materials, Stuttgart, pp 897-902.

Motahhari, S, and Cameron, J, 1997, “Measurement of Micro-Residual Stresses in Fiber-Prestressed Composites”, Journal of Reinforced Plastics and Composites, Vol. 16, No. 12, pp 1129-1136.

Motahhari, S, and Cameron, J, 1998, “Impact Strength of Fiber Pre-Stressed Composites”, Journal of Reinforced Plastics and Composites, Vol. 17, No. 2, pp 123-130.

Rose, D.H., and Whitney, J.M., 1993, “Effect of Prestressed Fibers upon the Response of Composite Materials”, Proceedings of the American Society of Composites, Eighth Technical Conference on Composites, Lancaster, P.A., pp 489-498.

Schlottermüller, M., Schledjewski, R., and Mitschang, P., 2002, “Residual stress in thermoplastic filament wound parts”, Tenth European Conference on Composite Materials (ECCM-10), June 3-7, Brugge, Belgium.

Schulte, K, and Marissen, R, 1992, “Influence of artificial pre-stressing during curing of CFRP laminates on interfibre transverse cracking”, Composite Science and Technology, Vol. 44, pp. 361-367.

Schürmann, H., 1984, “Geziehlt eingebrachte Eigenspannungen erhöhen die Belastbarkeit von Bauteilen aus Faser-Kunststoff-Verbunden”, Kunststoffe, Vol. 74, No. 9, pp 520-526.

Suvorov, A.P., and Dvorak, G.J., 2002, “Stress Relaxation in Prestressed Composite Laminates”, Journal of Applied Mechanics, July, Vol. 69, pp 459-469.

Tuttle, M.E., 1988, “A Mechanical/Thermal Analysis of Prestressed Composite Laminates”, Journal of Composite Materials, Vol. 22, pp 780-792.

Tuttle, M.E., Koehler, R.T., and Keren, D., 1996, “Controlling Thermal Stresses in Composites by Means of Fiber Prestress”, Journal of Composite Materials, Vol. 30, No. 4, pp 486-502.

Wisnom, M.R., Ersoy, N., Gigliotti, M., Potter, K.D., 2004, “Generation of Residual Stresses and Distortion during the Cure of Polymer Matrix Composites”, Proceedings of the 11th European Conference on Composite Materials (ECCM-11), May 31 – June 3, Rhodes, Greece.

APPENDIX A

A BRIEF SUMMARY OF THE LS-DYNA MATERIAL MODELS TYPES 22, 54 AND 55

A BRIEF SUMMARY OF THE LS-DYNA MATERIAL TYPES 22,54 AND 55

The following pages are intended to give an overview of the composite failure models considered in this study. First the basic composite failure model Material Type 22 will be dealt with and then the advanced failure models types 54 and 55. In each section the failure criteria with which failure of the composite is predicted has been presented together with how progressive failure is handled to allow a way to predict final failure of a composite laminate.

Material Model 22: Chang-Chang Composite Failure Model

The Chang-Chang model can be used with solid and thick and thin shell elements (Hallquist 1999). It uses five material parameters (longitudinal tensile strength, σ_{t1}, transverse tensile strength, σ_{t2}, shear strength, τ_{f12}, transverse compressive strength, σ_{c2}, non-linear shear stress parameter, α) in three failure criteria (Chang and Chang 1987a; Chang and Chang 1987b). The three failure criteria are matrix cracking failure, matrix compressive failure and final failure due to fibre failure.

The parameters σ_{t1}, σ_{t2}, τ_{f12}, and σ_{c2} are obtained from material strength measurements of unidirectional plies. α is derived from the shear stress-strain relationship. When considering the plain strain case, strains can be given in terms of stresses as follows.

$$\begin{aligned} \varepsilon_1 &= \frac{1}{E_1}\left(\sigma_1 - \nu_1\sigma_2\right) \\ \varepsilon_2 &= \frac{1}{E_2}\left(\sigma_2 - \nu_2\sigma_1\right) \\ 2\gamma_{12} &= \frac{1}{G_{12}}\tau_{12} + \alpha\tau_{12}^3 \end{aligned} \qquad \textbf{(A.1)}$$

Where ε_1, ε_2, σ_1, σ_2, E_1, E_2, ν_1 and ν_2 are the strains, stresses Young's Moduli and Poisson's ratios in the 1 and 2 directions respectively. γ_{12}, τ_{12} and G_{12} are the shear strains, shear stresses and Shear Modulus in the 1-2 plane respectively. The third equation defines the shear stress parameter, α.

Each damage mode is also augmented by a fibre-matrix shear term:

$$\bar{\tau} = \frac{\frac{\tau_{12}^2}{2G_{12}} + \frac{3}{4}\alpha\tau_{12}^4}{\frac{\tau_{f12}^2}{2G_{12}} + \frac{3}{4}\alpha\tau_{f12}^4} \qquad \textbf{(A.2)}$$

The matrix cracking criteria is then determined from

$$F_{matrix} = \left(\frac{\sigma_2}{\sigma_{t2}}\right)^2 + \bar{\tau} \qquad \textbf{(A.3)}$$

Where failure is assumed whenever $F_{matrix}>1$. Once F_{matrix} exceeds the value of 1, then the material constants E_2, G_{12}, ν_1 and ν_2 are set to zero making the assumption that after matrix failure in a ply only the fibres of that ply can carry load.

The compressive failure criteria is determined from

$$F_{comp} = \left(\frac{\sigma_2}{2\tau_{f12}}\right)^2 + \left[\left(\frac{\sigma_{c2}}{2\tau_{f12}}\right)^2 - 1\right]\frac{\sigma_2}{\sigma_{c2}} + \bar{\tau} \qquad \textbf{(A.4)}$$

Where failure is assumed whenever $F_{comp}>1$. Once F_{comp} exceeds the value of 1, then the material constants E_2, ν_1 and ν_2 are set to zero.

The fibre breakage criteria is determined from

$$F_{fibre} = \left(\frac{\sigma_1}{\sigma_{t1}} \right)^2 + \bar{\tau} \qquad \textbf{(A.5)}$$

Where failure is assumed whenever $F_{fibre}>1$. Once F_{fibre} exceeds the value of 1, then the material constants E1, E2, G_{12}, ν_1 and ν_2 are set to zero and it is said that that ply has completely failed and is no longer able to carry any load.

The information about the status of each integration point (composite ply) can be plotted using the additional integration point variables. The number of additional integration point variables for shells written to the LS-TAURUS database is input by the *DATABASE_EXTENT_BINARY definition as the variable NEIPS.

The additional variables for this material model (22) are tabulated below:

History Variable	Description	Value	LS-TAURUS Component
1. ef(i)	Tensile fibre mode	1 – elastic 2 – failed	81
2. ec(i)	Compressive fibre mode		82
3. em(i)	Tensile matrix mode		83

These variables can be plotted in LS-TAURUS as element components 81,82, …, 80+ NEIPS.

The following components, defined by the sum of failure indicators over all through-thickness integration points, are stored as element component 7 instead of the effective plastic strain:

Description	Integration Point
$\frac{1}{nip}\sum_{i=1}^{nip} ef(i)$	1
$\frac{1}{nip}\sum_{i=1}^{nip} ec(i)$	2
$\frac{1}{nip}\sum_{i=1}^{nip} em(i)$	3

Material Models 54 and 55: Enhanced Composite Damage Model

These models are very close in their formulations. Material Model 54 uses the Chang-Chang (Chang and Chang 1987a) matrix failure criterion (as does Material Model 22), whereas Material Model 55 uses the Tsai-Wu (Tsai 1971) criterion for matrix failure. They can be used to define arbitrary orthotropic materials (e.g. unidirectional layers in composite shell structures). Depending on the model, the Chang-Chang based failure criteria (Model 54) or the Tsai-Wu based failure criteria (Model 55) can be specified. In addition to these, special measures are taken for failure under compression as given in (Matzenmiller and Schweizerhof 1991).

Material Models 54 and 55 are only valid for shell elements.

The Chang-Chang failure criteria is given as follows:

For tensile fibre failure:

$$\sigma_1 > 0 \text{ then } e_{ft}^2 = \left(\frac{\sigma_1}{\sigma_{t1}}\right)^2 + \beta\left(\frac{\tau_{12}}{\tau_f}\right) - 1 \begin{cases} \geq 0 & failed \\ < 0 & elastic \end{cases} \qquad \textbf{(A.6)}$$

$$E_1 = E_2 = G_{12} = \nu_{21} = \nu_{12} = 0 \text{ after failure}$$

where, for β=1 the results follow the original criterion by (Hashin 1980) in the tensile fibre mode. For β=0, failure follows the maximum stress criterion, which compares better with experimental results.

For compressive fibre failure:

$$\sigma_1 < 0 \text{ then } e_{fc}^2 = \left(\frac{\sigma_1}{\sigma_{c1}}\right)^2 - 1 \begin{cases} \geq 0 & failed \\ < 0 & elastic \end{cases} \qquad \textbf{(A.7)}$$

$$E_1 = \nu_{21} = \nu_{12} = 0 \text{ after failure}$$

For tensile matrix failure:

$$\sigma_2 > 0 \text{ then } e_{mt}^2 = \left(\frac{\sigma_2}{\sigma_{t2}}\right)^2 + \left(\frac{\sigma_{12}}{\tau_f}\right)^2 - 1 \begin{cases} \geq 0 & failed \\ < 0 & elastic \end{cases} \quad \textbf{(A.8)}$$

$E_2 = \nu_{21} = 0$. $\rightarrow G_{12} = 0$ after failure

For compressive matrix failure:

$\sigma_2 < 0$ then

$$e_{mc}^2 = \left(\frac{\sigma_2}{2\tau_f}\right)^2 + \left[\left(\frac{\sigma_{c2}}{2\tau_f}\right)^2 - 1\right]\frac{\sigma_2}{\sigma_{c2}} + \left(\frac{\sigma_{12}}{\tau_f}\right)^2 - 1 \begin{cases} \geq 0 & failed \\ < 0 & elastic \end{cases} \quad \textbf{(A.9)}$$

$E_2 = \nu_{12} = \nu_{21} = 0 \quad \rightarrow G_{12} = 0$ after failure

$\sigma_{c1} = 2\sigma_{c2}$ for 50% fibre volume

The Tsai-Wu fibre failure criteria are the same as the Chang-Chang for the tensile and compressive fibre failures. The failure criterion for the tensile and compressive matrix mode is given as:

$$e_{mtc}^2 = \frac{\sigma_2^2}{\sigma_{c2}\sigma_{t2}} + \left(\frac{\sigma_{12}}{S_c}\right)^2 + \frac{(\sigma_{c2} - \sigma_{t2})\sigma_2}{\sigma_{c2}\sigma_{t2}} - 1 \begin{cases} \geq 0 & failed \\ < 0 & elastic \end{cases} \quad \textbf{(A.10)}$$

Failure can occur in four different ways:

1. If DFAILT (Maximum allowable tensile fibre strain) is equal to zero, failure occurs if the Chang-Chang failure criterion is satisfied in the tensile fibre mode.

2. If DFAILT is greater than zero, failure occurs if the tensile strain is greater than DFAILT or less than DFAILC.

3. If EFS (Effective Failure Strain) is greater than zero, failure occurs if the effective

strain is greater than EFS.

4. If TFAIL is greater than zero, failure occurs according to the element timestep.

Failure can occur at individual integration points of one element. When failure has occurred at all integration points of that element (equivalent of all plies failing at the respective location on an actual composite plate), the element is deleted. Elements, which share elements with deleted elements, become "crashfront" elements and can have their strengths reduced by using the SOFT parameter (the softening reduction factor for material strength in crashfront elements), when TFAIL is set as greater than zero.

The information about the status of each integration point (composite ply) can be plotted using the additional integration point variables. The number of additional integration point variables for shells written to the LS-TAURUS database is input by the *DATABASE_EXTENT_BINARY definition as the variable NEIPS.

The additional variables for these material models (54 and 55) are tabulated below:

History Variable	Description	Value	LS-TAURUS Component
1. ef(i)	Tensile fibre mode	1 – elastic 2 – failed	81
2. ec(i)	Compressive fibre mode		82
3. em(i)	Tensile matrix mode		83
4. ed (i)	Compressive matrix mode		84
5. efail	Max[ef(ip)]		85
6. dam	Damage parameter	-1 – element intact 10^{-8} – element in crashfront 1 – element failed	86

These variables can be plotted in LS-TAURUS as element components 81,82, …, 80+ NEIPS.

The following components, defined by the sum of failure indicators over all through-thickness integration points, are stored as element component 7 instead of the effective plastic strain:

Description	Integration Point
$\frac{1}{nip}\sum_{i=1}^{nip} ef(i)$	1
$\frac{1}{nip}\sum_{i=1}^{nip} ec(i)$	2
$\frac{1}{nip}\sum_{i=1}^{nip} em(i)$	3

References

Chang, F. K. and K. Y. Chang (1987a). "A Progressive Damage Model for Laminated Composites Containing Stress-Concentrations." Journal of Composite Materials **21**(9): 834-855.

Chang, F. K. and K. Y. Chang (1987b). "Post-Failure Analysis of Bolted Composite Joints in Tension or Shear-Out Mode Failure." Journal of Composite Materials **21**: 809-833.

Hallquist, J. (1999). LS-DYNA Keyword User's Manual, Livermore Software Technology Corporation.

Hashin, Z. (1980). "Failure Criteria for Unidirectional Fiber Composites." Journal of Applied Mechanics **47**: 329.

Matzenmiller, A. and K. Schweizerhof (1991). Crashworthiness Simulations of Composite Structures - A First Step with Explicit Time Integration.

Tsai, S. W. a. W., E.M. (1971). "A General Theory of Strength for Anisotropic Materials." Journal of Composite Materials: 58-80.

Appendix Notes – Axis Definition and Nomenclature

Axis Definition

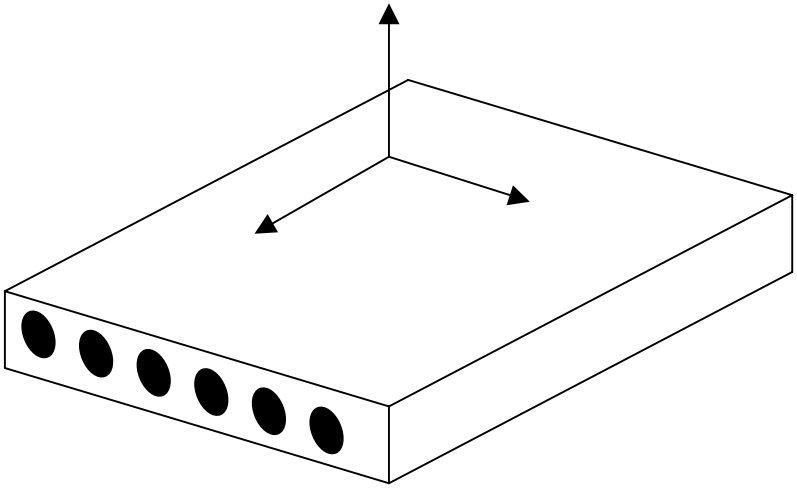

As shown in the diagram above the major axis (1-direction) is parallel to the fibres in a unidirectional composite ply. The in-plane transverse axis is the 2-direction and the through-thickness axis is the 3-direction.

Nomenclature

E	-	Young's Modulus
G	-	Shear Modulus
ν	-	Poisson Ratio
ε	-	direct strain
σ	-	direct stress
γ	-	shear strain
τ	-	shear stress
α	-	non-linear shear stress parameter
F	-	failure criterion for MAT22
e^2	-	failure criterion for MAT54 and MAT55
$\bar{\tau}$	-	fibre-matrix shear term

Subscripts

1,2 and 3	-	denote the respective axis directions
matrix, mt	-	refers to matrix tensile failures

fibre, ft	-	refers to fibre tensile failures
comp	-	refers to compressive failure
mc	-	refers to matrix compressive failure
fc	-	refers to fibre compressive failure
mtc	-	refers to matrix failure in tension or compression
t	-	denotes tensile failure strength properties
c	-	denotes compressive failure strength properties
f	-	denotes failure strength in shear

This page is intentionally blank.

APPENDIX B

BACKLIGHTING AND MICROGRAPH RESULTS FOR THE DROP WEIGHT TESTS

BACKLIGHTING RESULTS

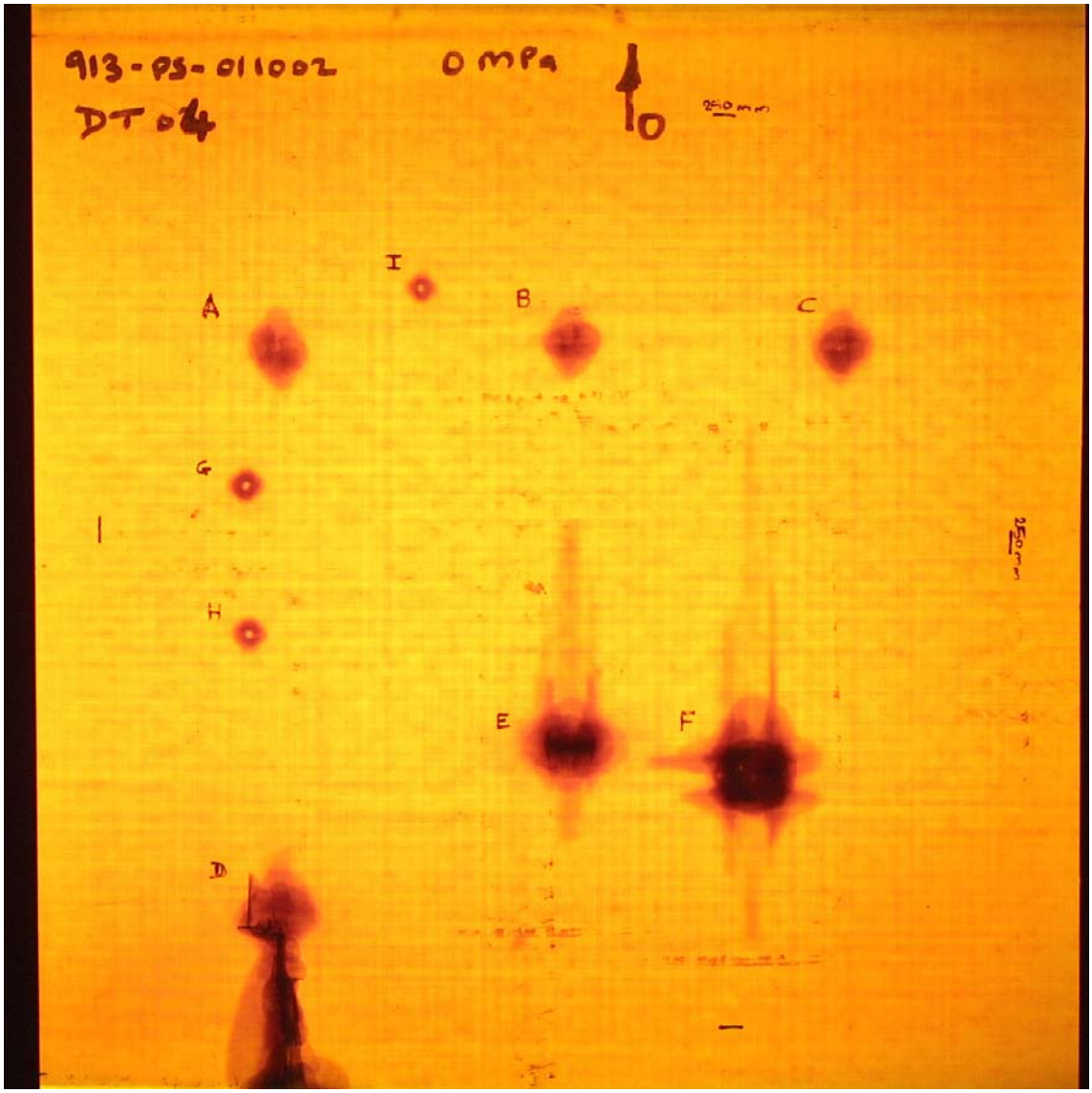

Figure B.1 Backlighting image of the impact damage in panel DT04, with 0MPa pre-stress.

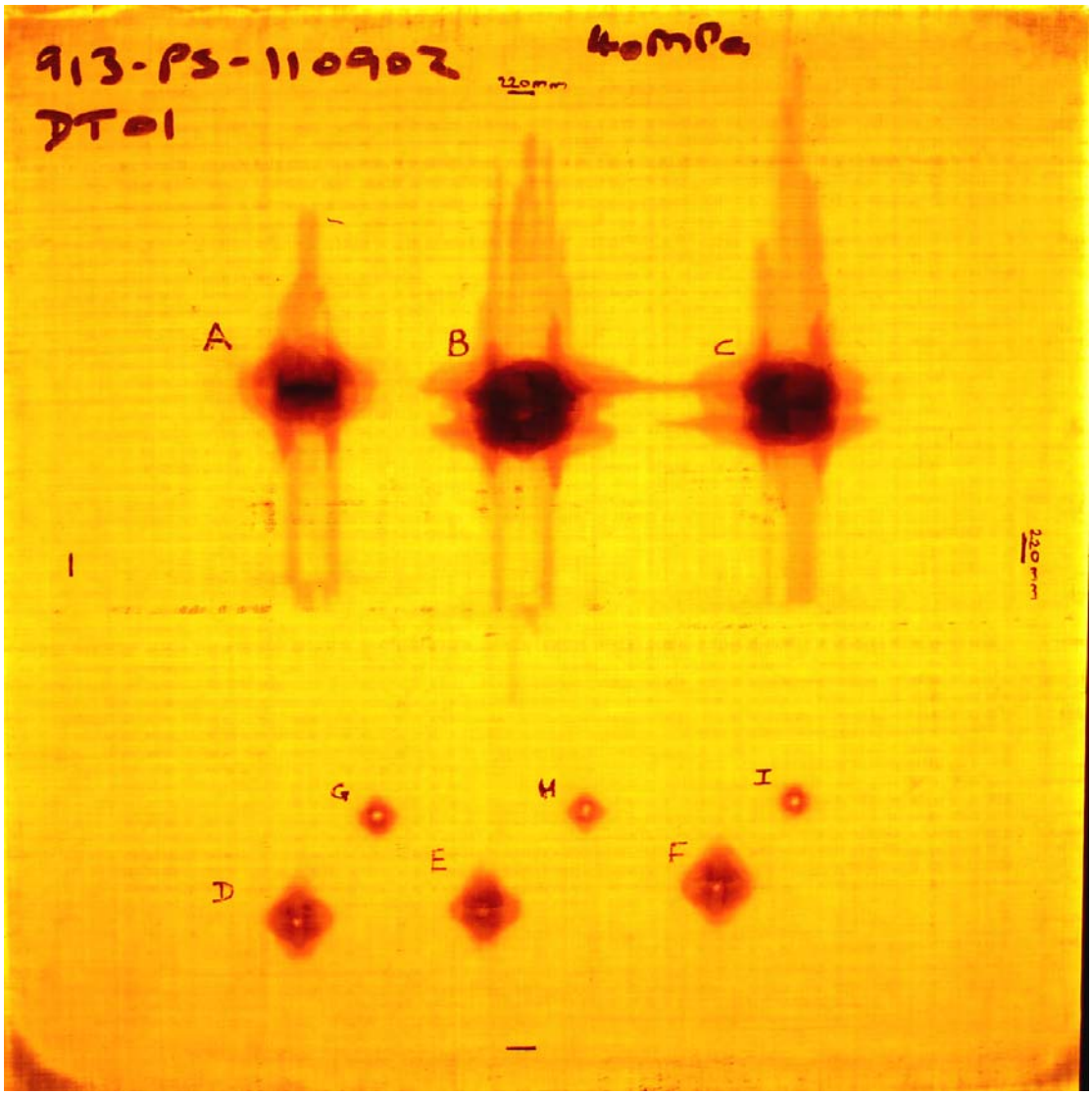

Figure B.2 Backlighting image of the impact damage in panel DT01, with 40MPa pre-stress.

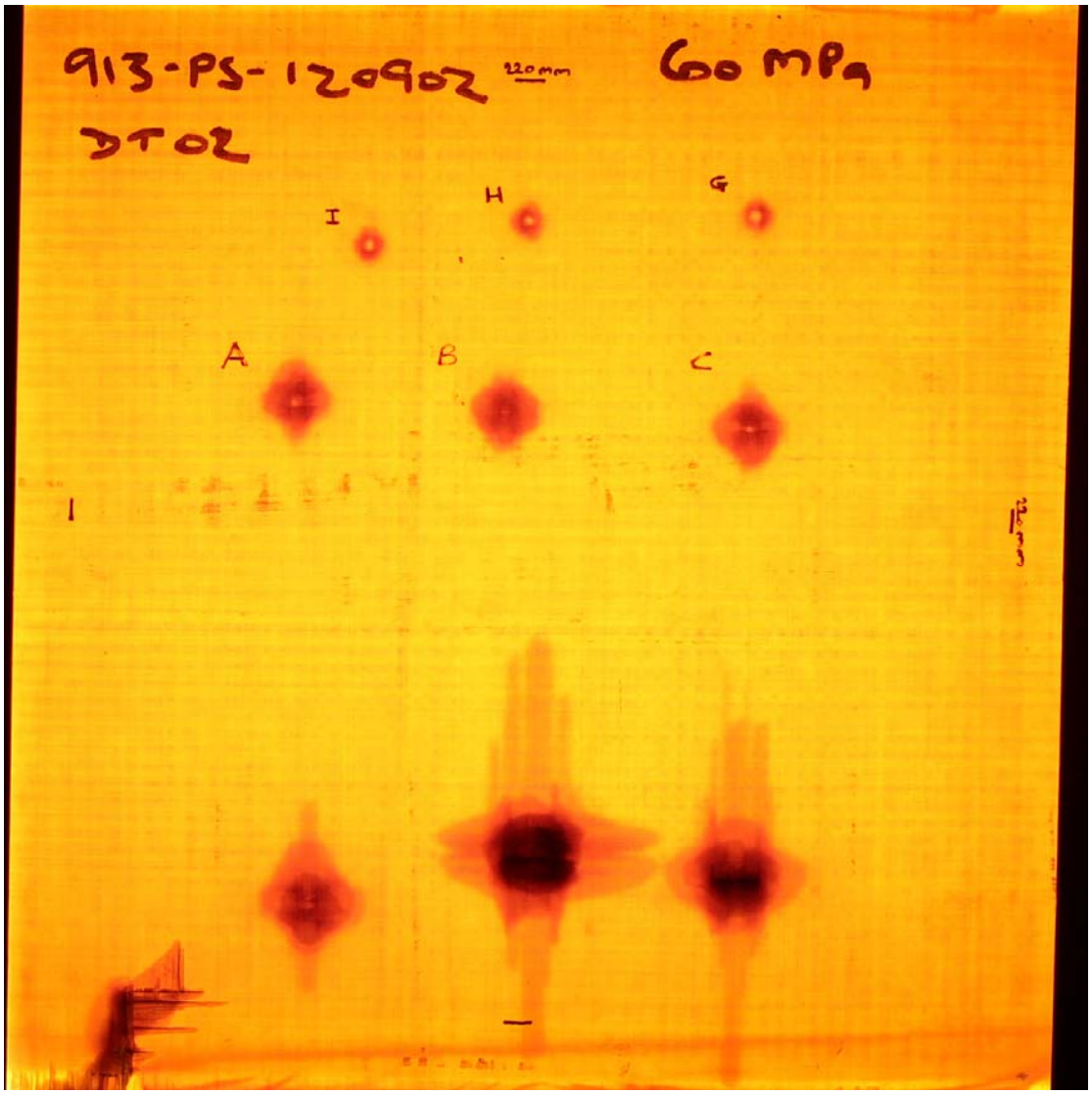

Figure B.3 Backlighting image of the impact damage in panel DT02, with 60MPa pre-stress.

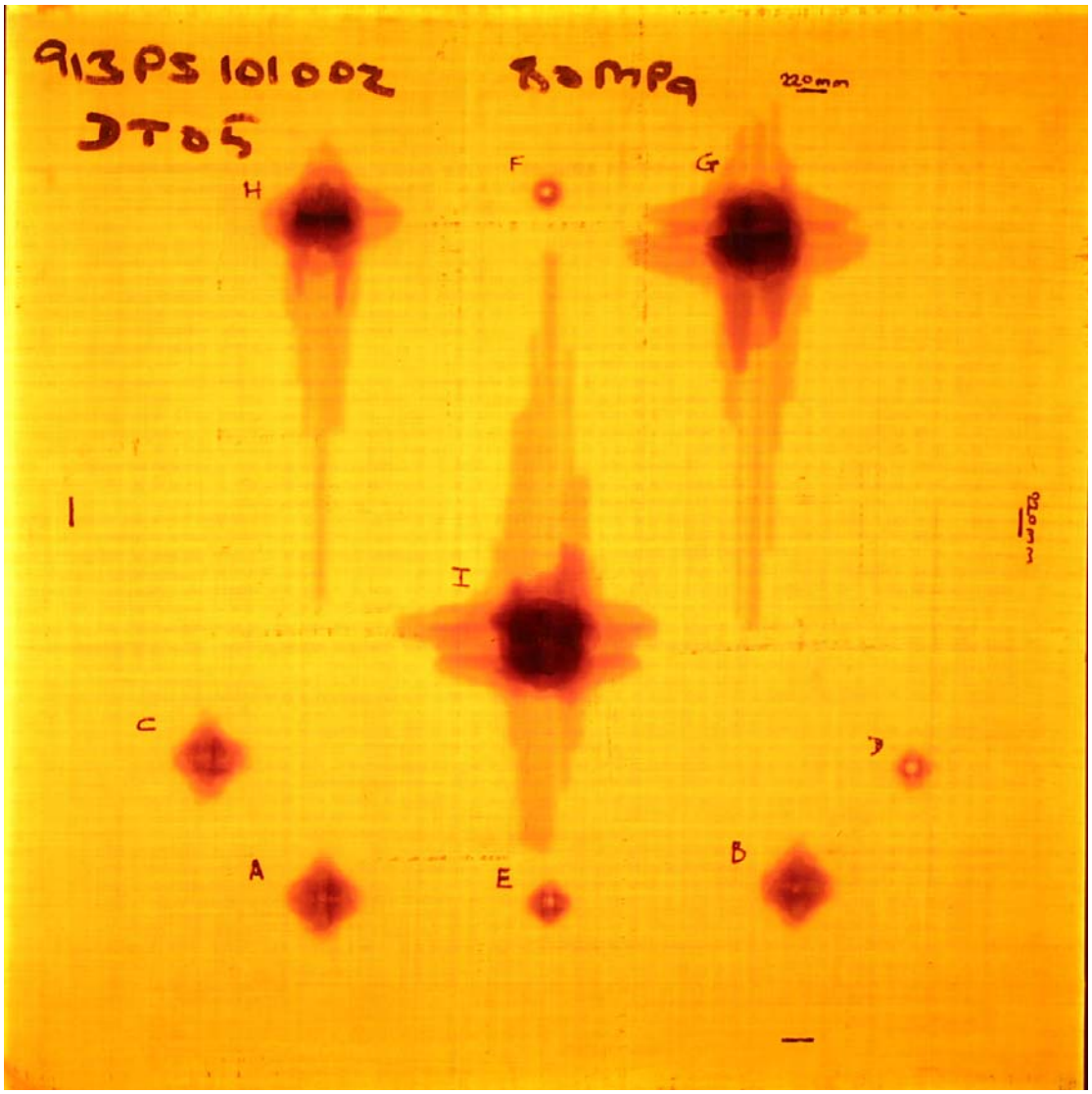

Figure B.4 Backlighting image of the impact damage in panel DT05, with 80MPa pre-stress.

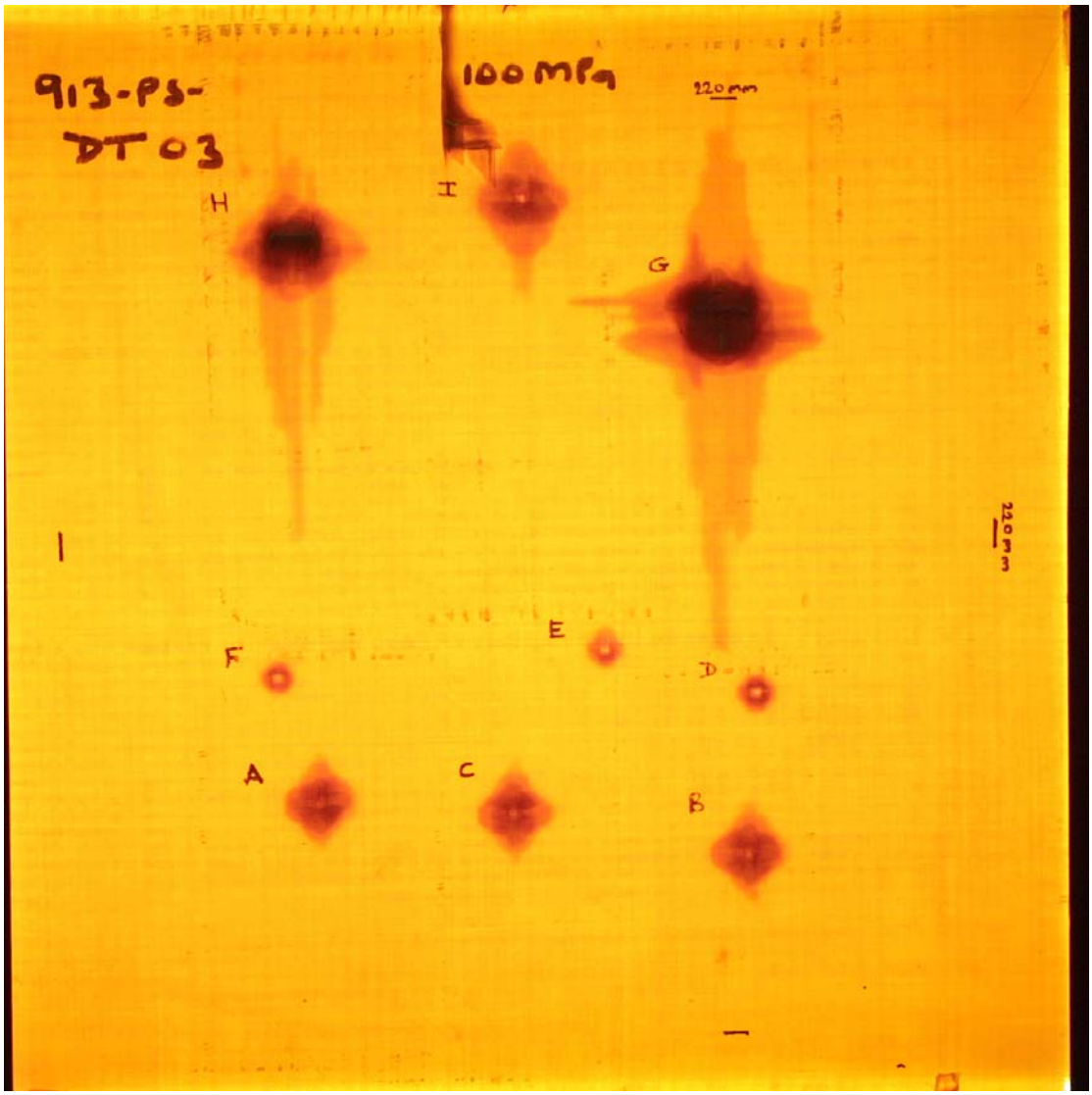

Figure B.5 Backlighting image of the impact damage in panel DT03, with 100MPa pre-stress.

MICROGRAPHS

(a)

(b)

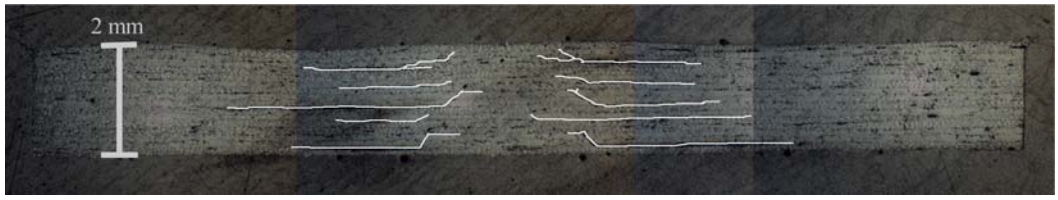

Figure B.6 Micrographs of the 5-Joule impact onto the panel DT04 with 0MPa pre-stress. (a) shows the micrograph without the delaminations highlighted and (b) shows the micrograph with the delaminations highlighted.

(a)

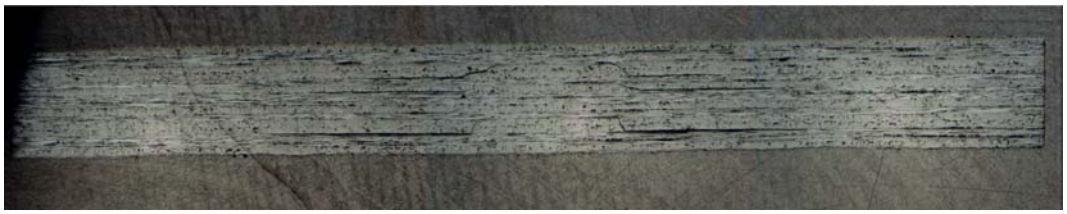

(b)

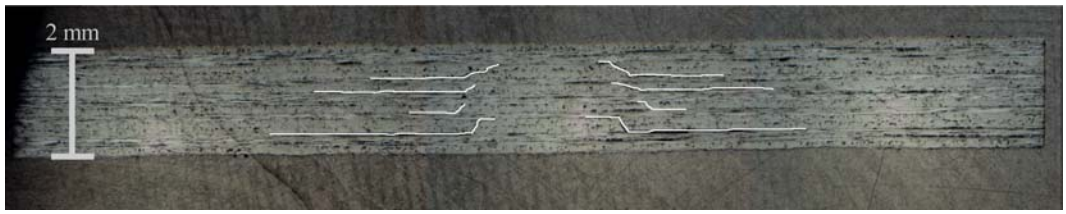

Figure B.7 Micrographs of the 5-Joule impact onto the panel DT01 with 40MPa pre-stress. (a) shows the micrograph without the delaminations highlighted and (b) shows the micrograph with the delaminations highlighted.

(a)

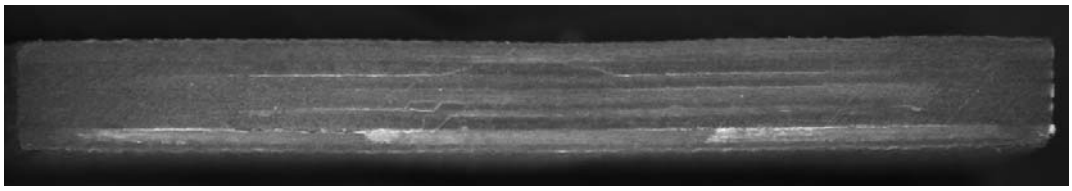

(b)

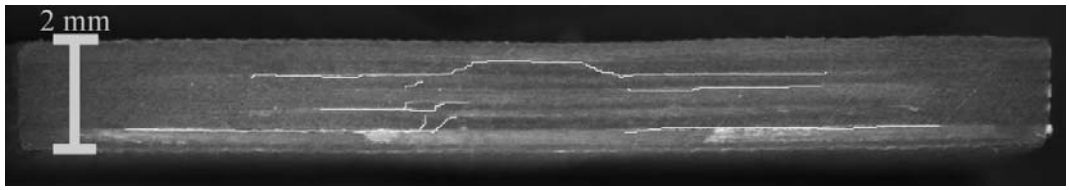

Figure B.8 Micrographs of the 5-Joule impact onto the panel DT02 with 60MPa pre-stress. (a) shows the micrograph without the delaminations highlighted and (b) shows the micrograph with the delaminations highlighted.

(a)

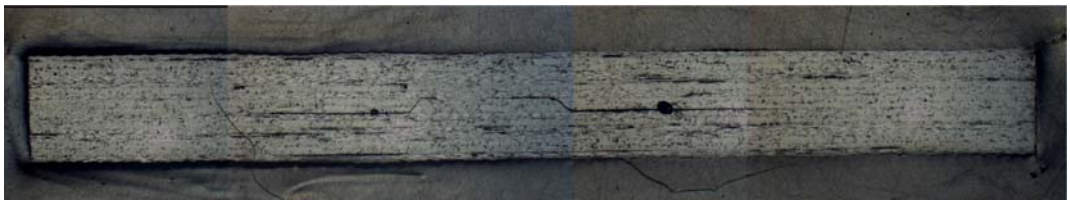

(b)

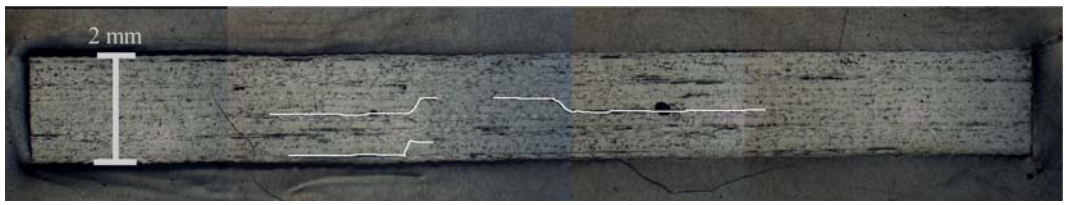

Figure B.9 Micrographs of the 5-Joule impact onto the panel DT05 with 80MPa pre-stress. (a) shows the micrograph without the delaminations highlighted and (b) shows the micrograph with the delaminations highlighted.

(a)

(b)

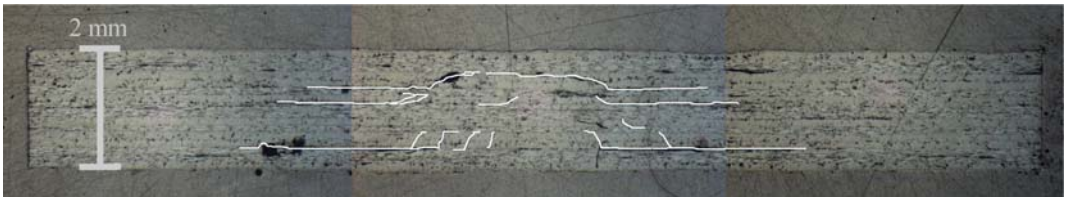

Figure B.10 Micrographs of the 5-Joule impact onto the panel DT03 with 100MPa pre-stress. (a) shows the micrograph without the delaminations highlighted and (b) shows the micrograph with the delaminations highlighted.

This page is intentionally blank.

APPENDIX C

FORCE-TIME PLOTS FOR THE DROP WEIGHT IMPACTS

5 JOULE IMPACT

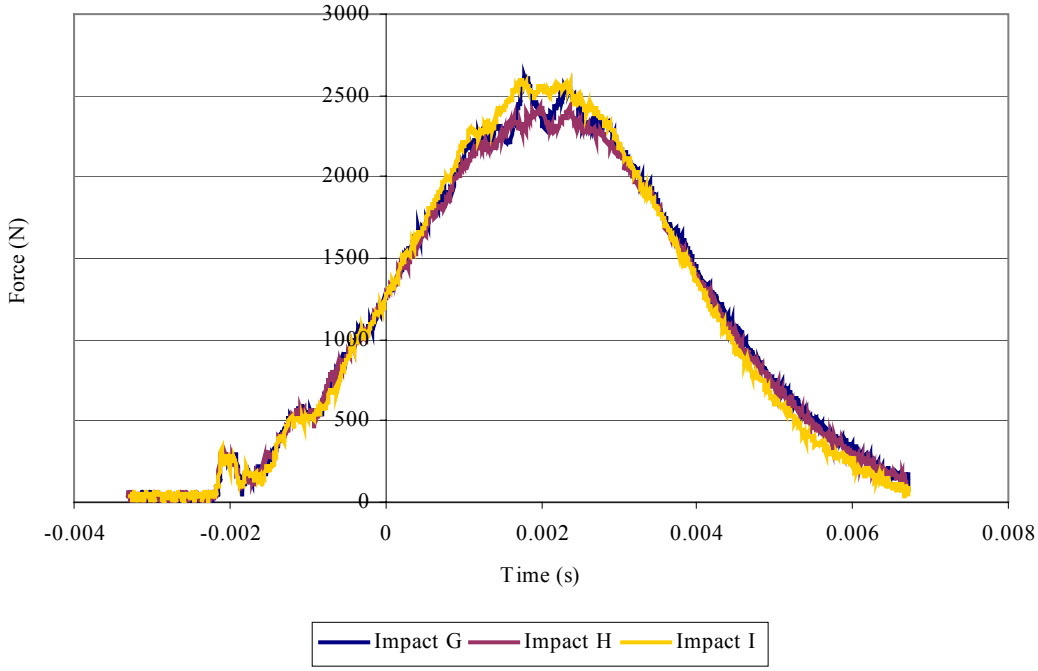

Figure C.1 Force-time plots for panels with 0MPa pre-stress.

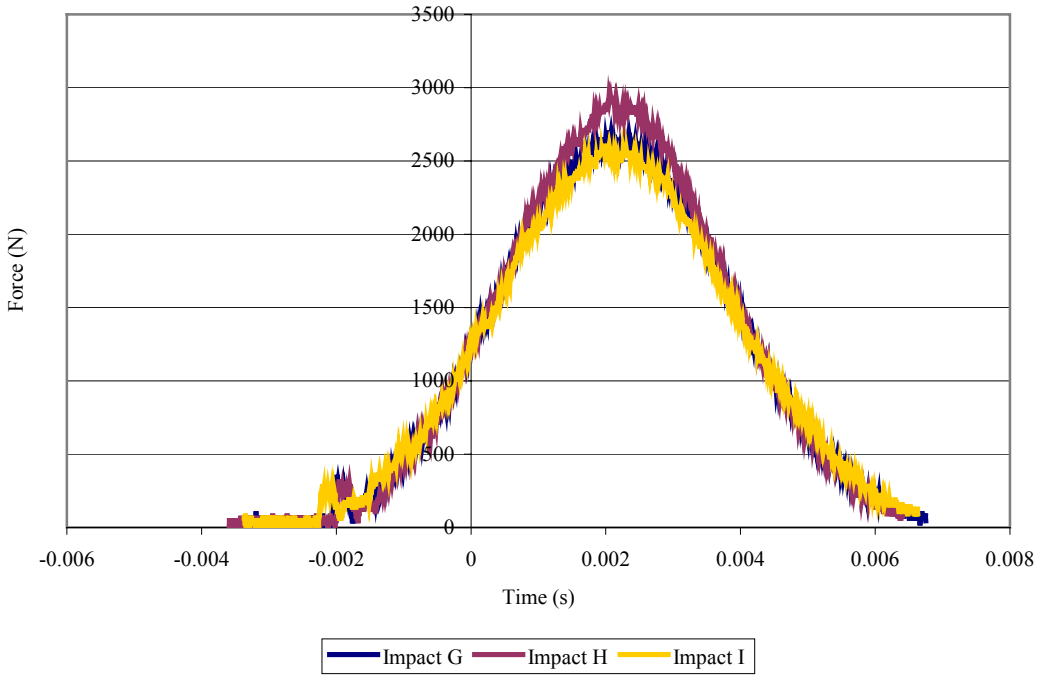

Figure C.2 Force-time plots for panels with 40MPa pre-stress.

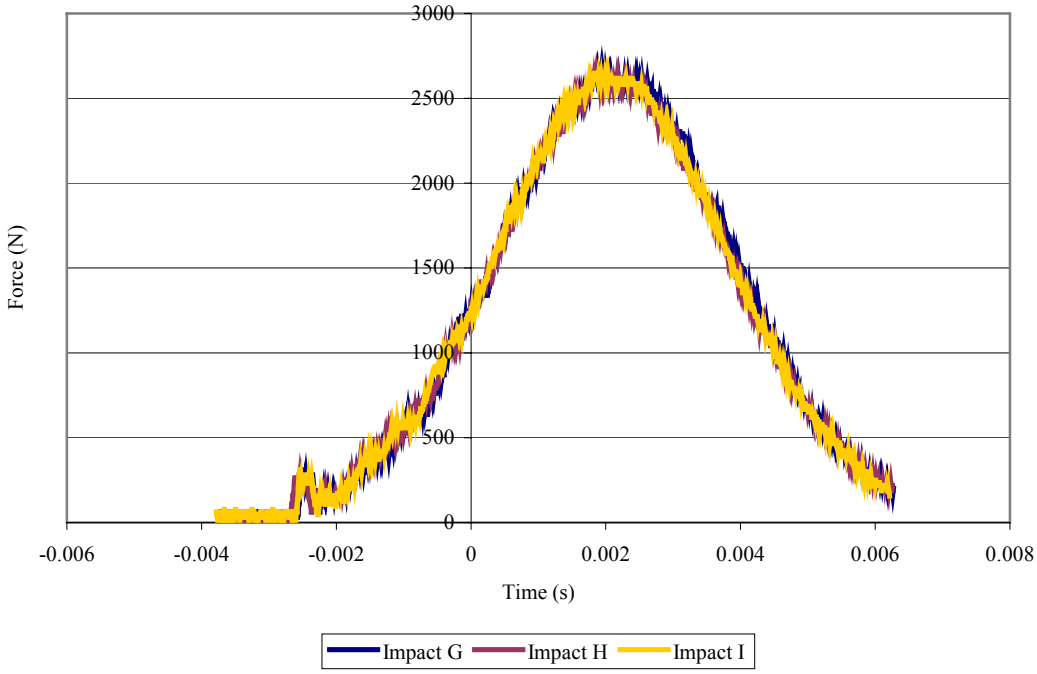

Figure C.3 Force-time plots for panels with 60MPa pre-stress.

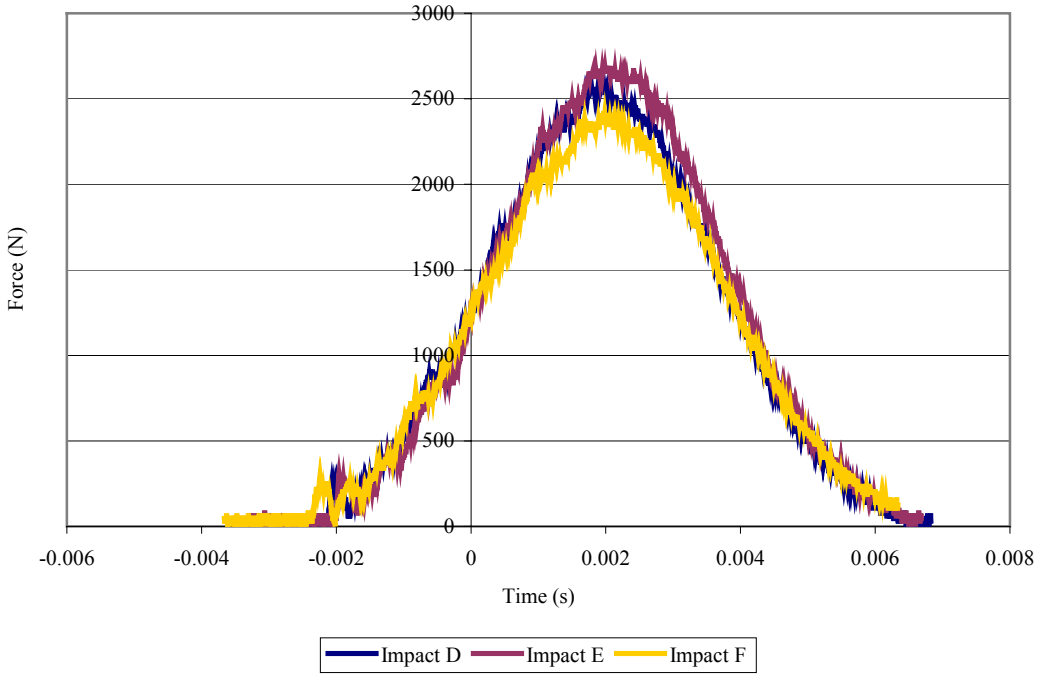

Figure C.4 Force-time plots for panels with 80MPa pre-stress.

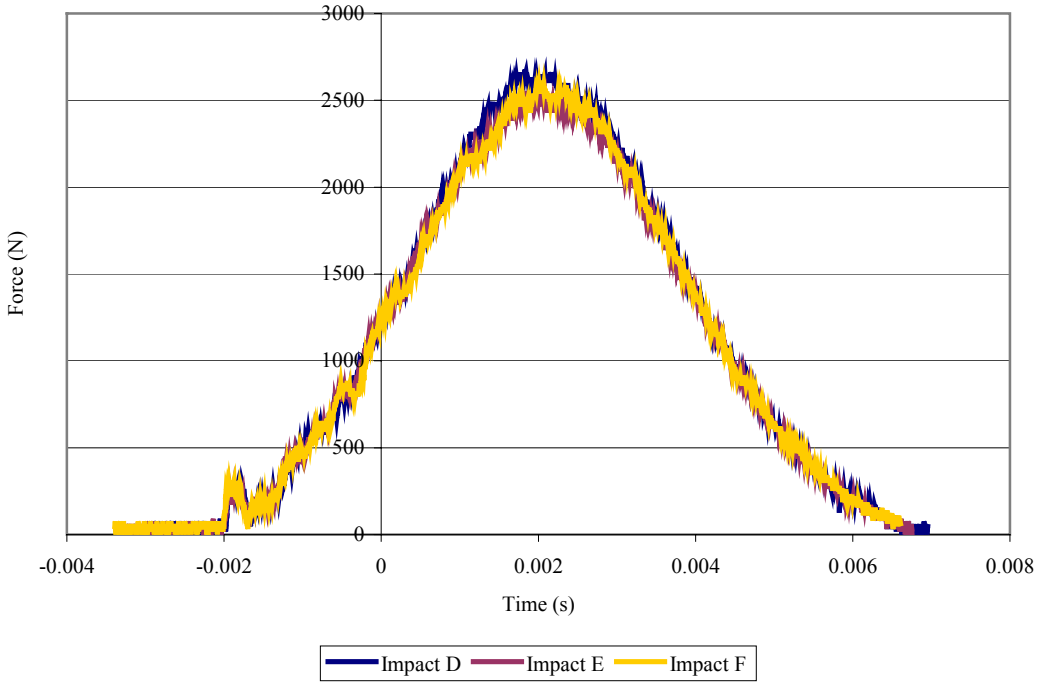

Figure C.5 Force-time plots for panels with 100MPa pre-stress.

17 JOULE IMPACTS

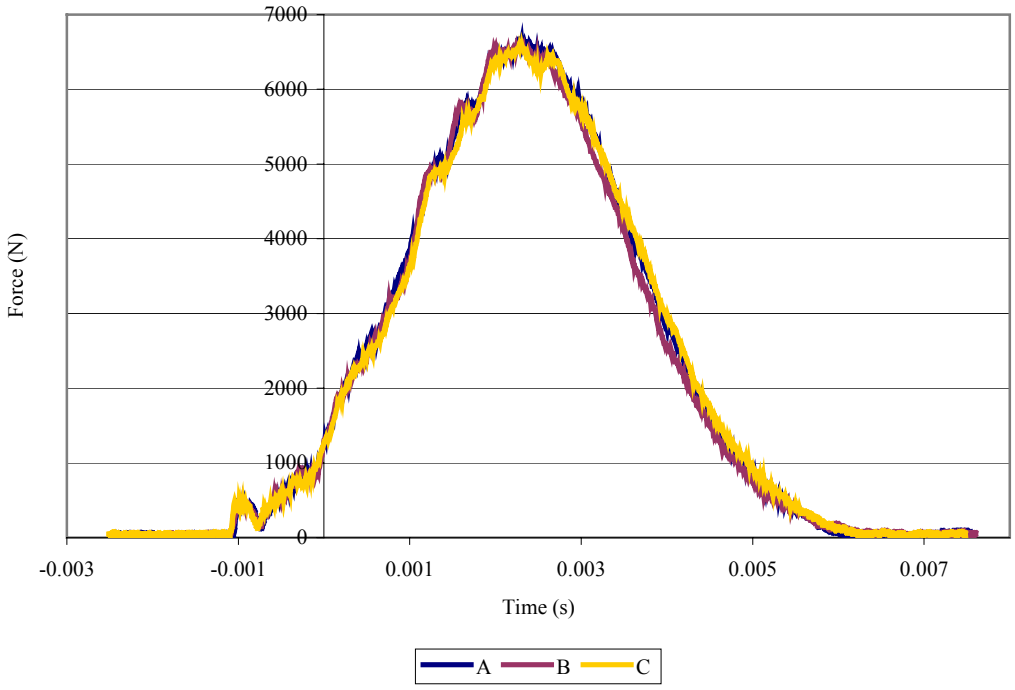

Figure C.6 Force-time plots for panels with 0MPa pre-stress.

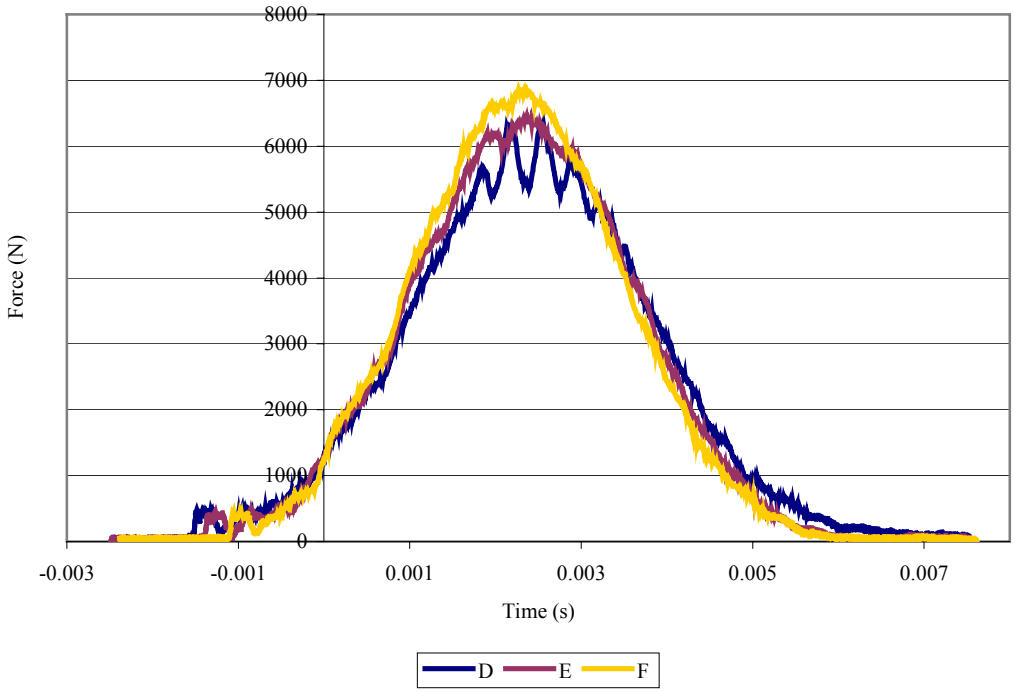

Figure C.7 Force-time plots for panels with 40MPa pre-stress.

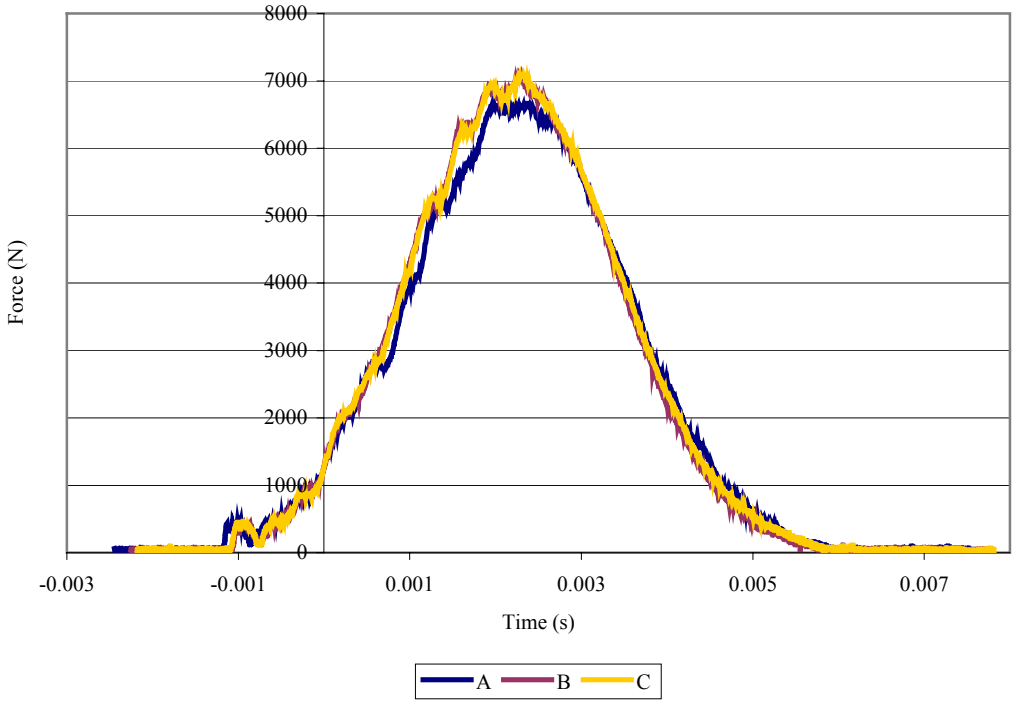

Figure C.8 Force-time plots for panels with 60MPa pre-stress.

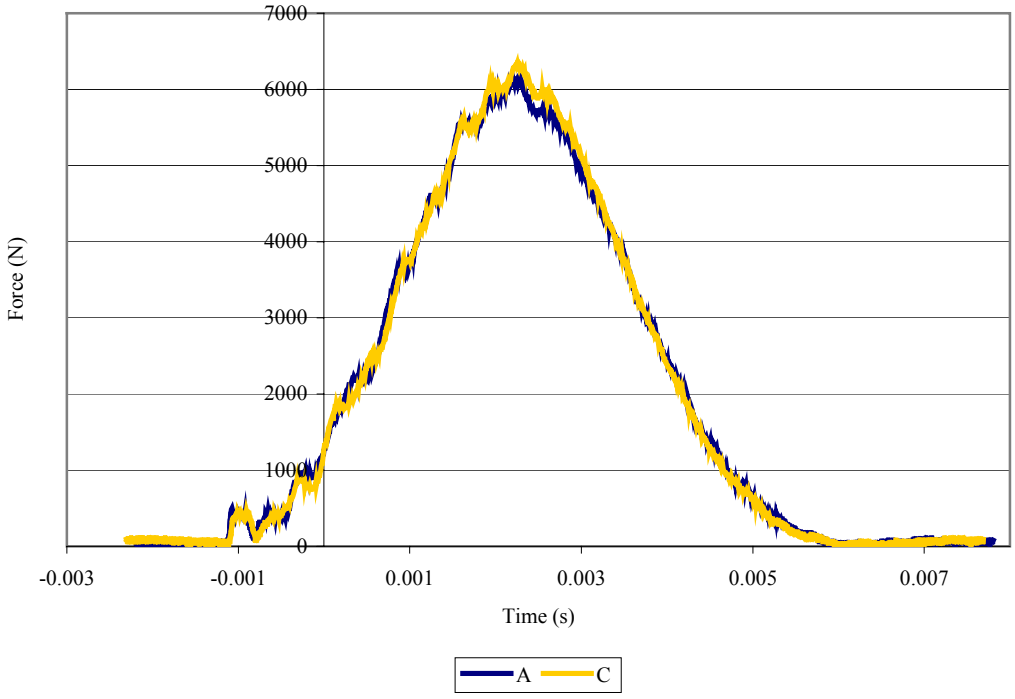

Figure C.9 Force-time plots for panels with 80MPa pre-stress.

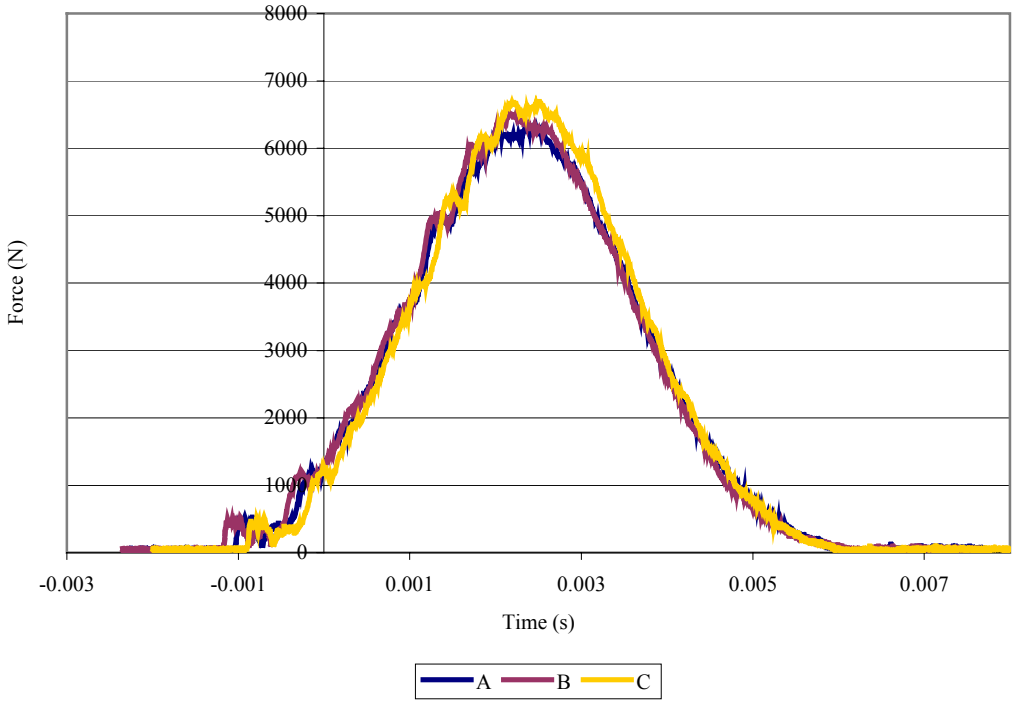

Figure C.10 Force-time plots for panels with 100MPa pre-stress.

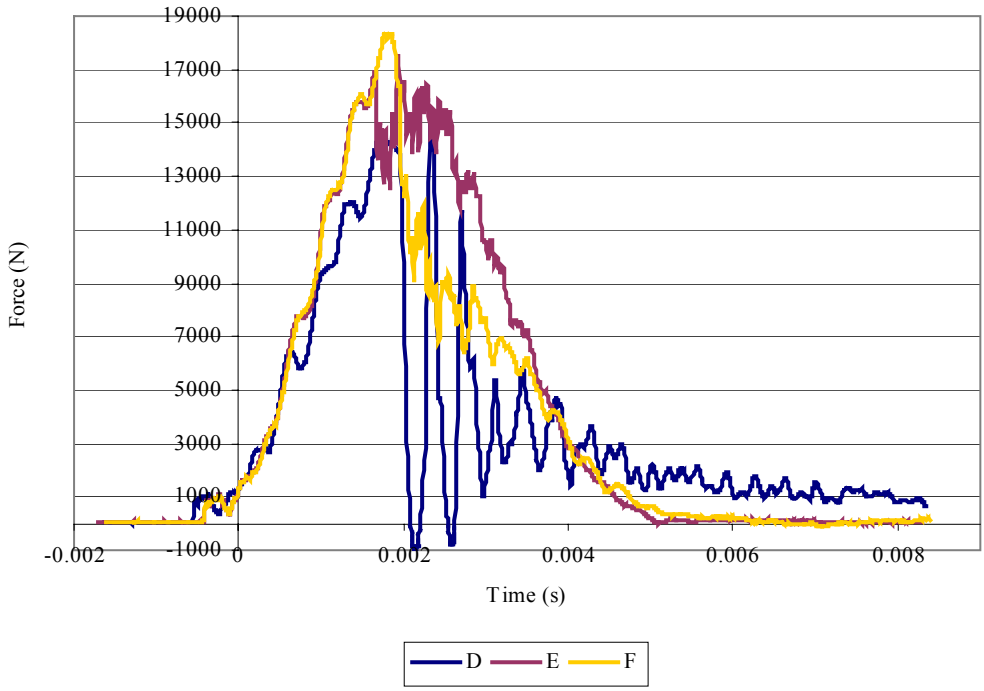

Figure C.11 Force-time plots for panels with 0MPa pre-stress.

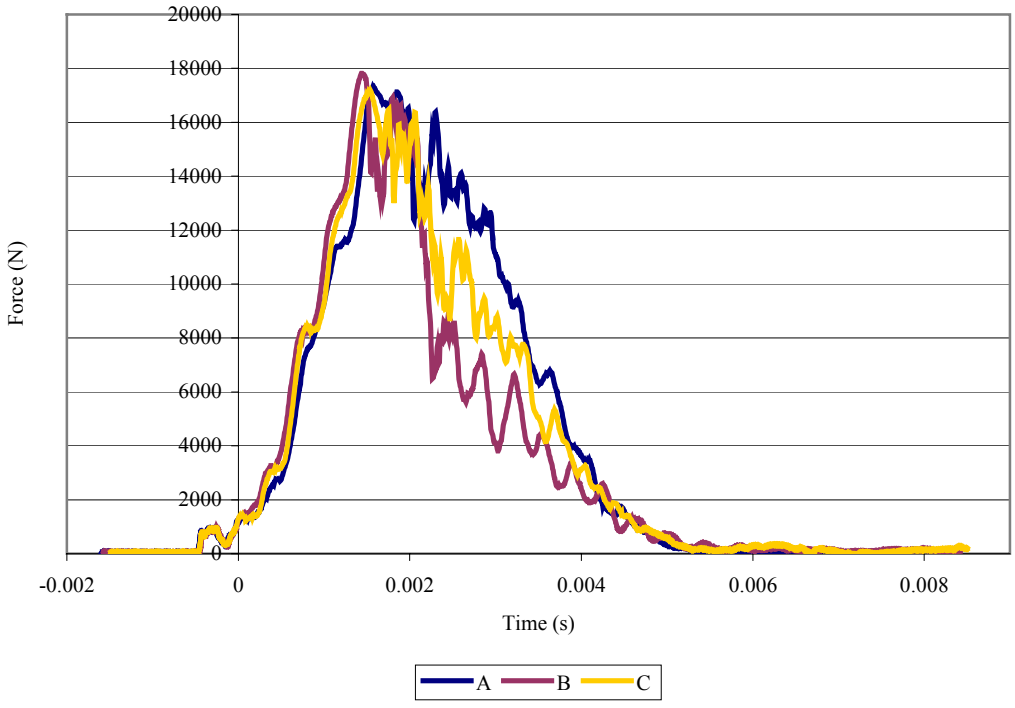

Figure C.12 Force-time plots for panels with 40MPa pre-stress.

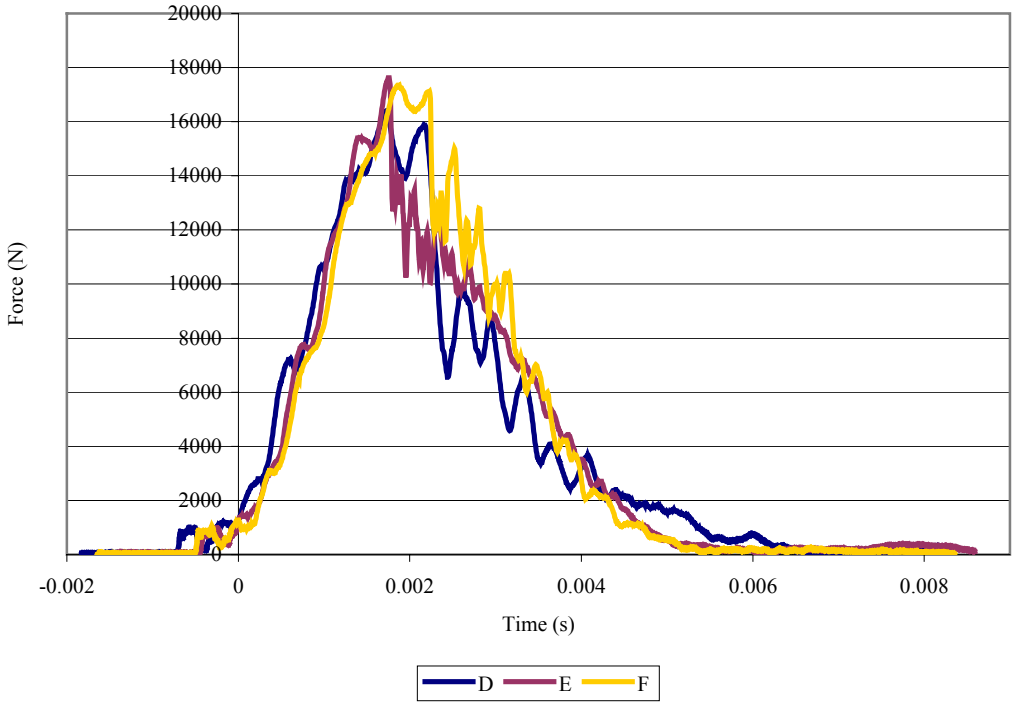

Figure C.13 Force-time plots for panels with 60MPa pre-stress.

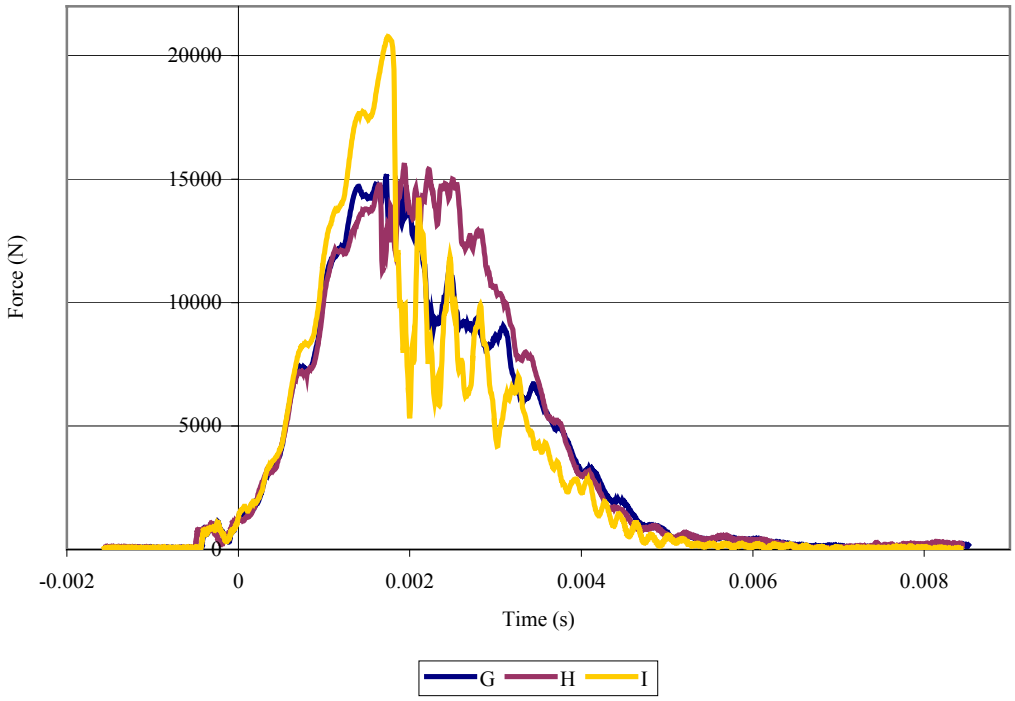

Figure C.14 Force-time plots for panels with 80MPa pre-stress.

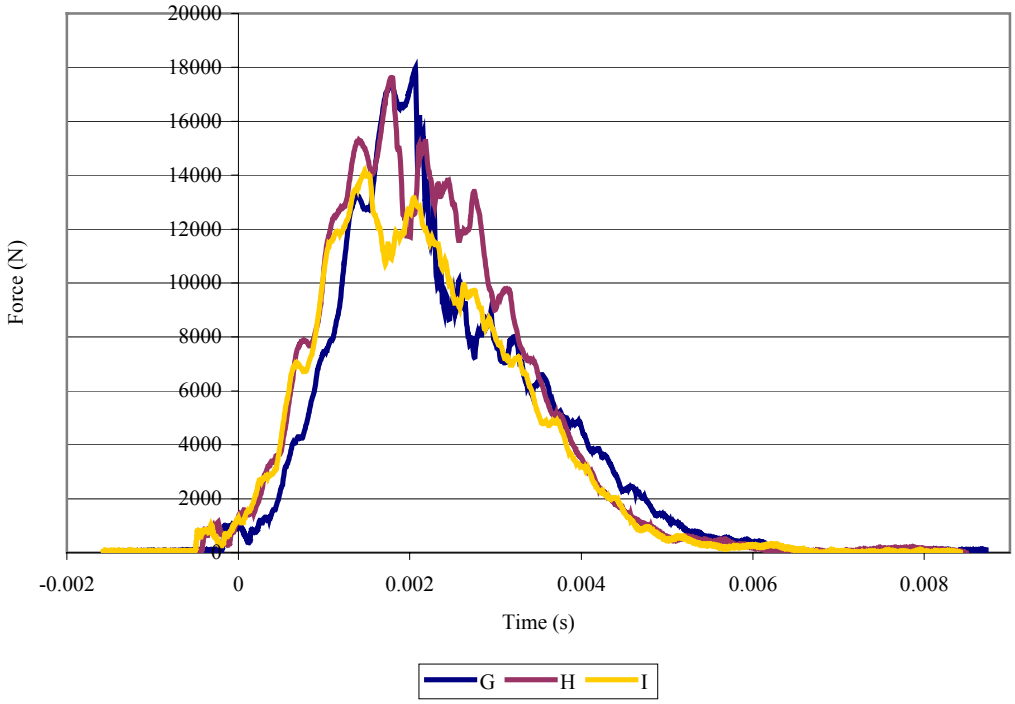

Figure C.15 Force-time plots for panels with 100MPa pre-stress.

APPENDIX D

MICRO-MECHANICAL DERIVATION OF THE THERMAL EXPANSION COEFFICIENTS IN A PLY

A MICRO-MECHANICS APPROACH TO DERIVING THE THERMAL EXPANSION COEFFICIENTS OF A UNIDIRECTIONAL COMPOSITE IN ITS FIBRE DIRECTION AND TRANSVERSE TO THE FIBRE DIRECTION

IN THE FIBRE DIRECTION (11)

This analysis makes two fundamental assumptions. The first is that it assumes strain compatibility, i.e. the overall strain in all materials is the same. The second is that there are no external loads applied to the system, thus the sum of all forces must equal zero.

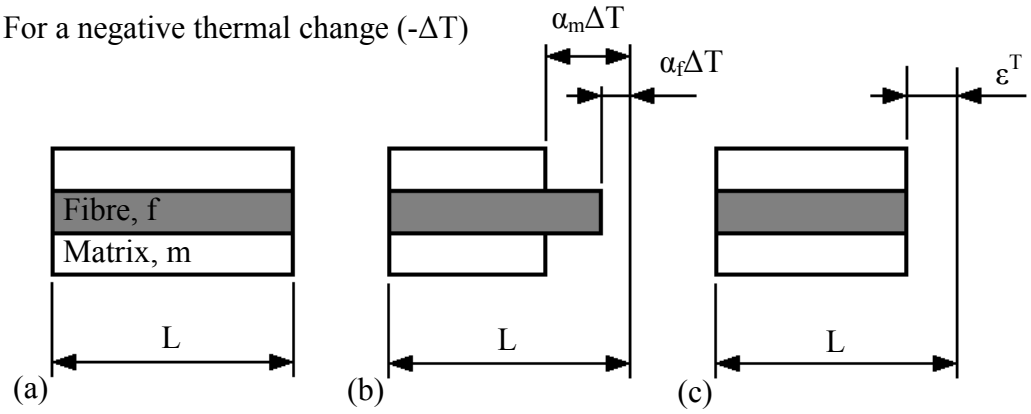

Figure D.1 Concept of Strain Compatibility; (a) original length; (b) actual strains if fibre and matrix did not mutually constrain one another; (c) actual strain in fibre and matrix due to strain compatibility

So, for a given change in temperature ΔT the strain in the fibre (ε_f) and the matrix (ε_m) are respectively

$$\varepsilon_f = \alpha_f \Delta T + \varepsilon_f^T \quad \textbf{(D.1)}$$

$$\varepsilon_m = \alpha_m \Delta T + \varepsilon_m^T \quad \textbf{(D.2)}$$

Where α_f and α_m are the thermal expansion coefficients of the fibres and matrix respectively and ε_f^T and ε_m^T are the strains due to strain compatibility in the fibres and matrix respectively.

Now, considering Hook's Law $E = \frac{\sigma}{\varepsilon}$, we can substitute into Equations (D.1) and (D.2) as follows:

$$\varepsilon_f = \alpha_f \Delta T + \frac{\sigma_f^T}{E_f} \quad \textbf{(D.3)}$$

$$\varepsilon_m = \alpha_m \Delta T + \frac{\sigma_m^T}{E_m} \quad \textbf{(D.4)}$$

Where σ_f^T and σ_m^T are the stresses in the fibre and the matrix respectively due to strain compatibility, and E_f and E_m are the fibre and the matrix Young's moduli respectively.

Knowing that stress is equal to the load applied to a material divided by its cross-sectional area and that the sum of all forces in the system must equal zero, equations (D.3) and (D.4) can be rewritten as follows.

$$\varepsilon_f = \alpha_f \Delta T + \frac{P}{A_f E_f} \quad \textbf{(D.5)}$$

$$\varepsilon_m = \alpha_m \Delta T - \frac{P}{A_m E_m} \quad \textbf{(D.6)}$$

Where P is the applied load and A_f and A_m are the fibre and matrix cross-sectional areas respectively.

Equating (D.5) and (D.6) gives

$$\alpha_f \Delta T + \frac{P}{A_f E_f} = \alpha_m \Delta T - \frac{P}{A_m E_m} \quad \textbf{(D.7)}$$

This can be rearranged to make P the subject

$$P = \frac{A_f E_f A_m E_m (\alpha_m - \alpha_f)}{A_f E_f + A_m E_m} \Delta T \quad \textbf{(D.8)}$$

Since $\frac{A_f}{A_{f+m}} = \frac{V_f}{V_{f+m}}$ and $\frac{A_m}{A_{f+m}} = \frac{V_m}{V_{f+m}}$, where V_f and V_m are the volume fractions of the fibres and the matrix respectively, equation (D.8) can be rewritten as:

$$P = \frac{V_f E_f V_m E_m (\alpha_m - \alpha_f)}{V_f E_f + V_m E_m} \Delta T \quad \textbf{(D.9)}$$

From (D.9), the thermal expansion coefficient for a unidirectional composite in the fibre direction (α_{11}) can be defined as

$$\alpha_{11} = \frac{V_f E_f V_m E_m (\alpha_m - \alpha_f)}{V_f E_f + V_m E_m} \quad \textbf{(D.10)}$$

TRANSVERSE TO THE FIBRE DIRECTION (22)

For the thermal expansion coefficient in the fibre transverse direction (α_{22}) one may assume that the overall strain is as a result of a rule of mixtures of the fibre and matrix thermal strains, coupled with the Poisson effects from the fibre, matrix and composite thermal strain in the fibre direction.

Therefore,

$$\alpha_{22} = \alpha_f V_f + \alpha_f V_f \nu_f + \alpha_m V_m + \alpha_m V_m \nu_m - \alpha_{11} \nu_{12}^c \quad \textbf{(D.11)}$$

Where ν_f, ν_m and ν_{12}^c are respectively the fibre Poisson ratio, the matrix Poisson ratio and the composite in-plane Poisson ratio. The latter, ν_{12}^c, can be calculated from a simple rule of mixtures

$$\nu_{12}^c = \nu_f V_f + \nu_m V_m \quad \textbf{(D.12)}$$

This page is intentionally blank.

APPENDIX E

ANALYSIS OF PRE-STRESSED COMPOSITE LAMINATES USING CLASSICAL LAMINATE ANALYSIS

Analysis of Pre-Stressed Composite Laminates using Classical Laminate Analysis

This analysis is carried out specifically for the 16-ply cross-ply glass epoxy laminates used in this study.

Data Input

fibre pre-stress $pre\_s := 0MPa$

cured ply thickness $t\_ply := 0.125mm$

temperature change $\Delta T := -100K$

Fibre Material Data

Young's modulus $E\_f := 70GPa$

Poisson ratio $\nu\_f := 0.22$

thermal expansion coefficient $\alpha\_f := 4.9 \cdot 10^{-6} K^{-1}$

fibre volume fraction $V\_f := 0.56$

Matrix Material Data

Young's modulus $E\_m := 5GPa$

Poisson ratio $\nu\_m := 0.39$

thermal expansion coefficient $\alpha\_m := 60 \cdot 10^{-6} K^{-1}$

fibre volume fraction $V\_m := 1 - V\_f$ $V\_m = 0.44$

Ply Layup Data

$\theta :=$

$i := 0 .. 15$

Ply Number	Angle (degrees)	Angle (radians)
1	0	0
2	90	1.570796
3	90	1.570796
4	0	0
5	0	0
6	90	1.570796
7	0	0
8	90	1.570796
9	90	1.570796
10	0	0
11	90	1.570796
12	0	0
13	0	0
14	90	1.570796
15	90	1.570796
16	0	0

Derived Material Data

shear modulus of fibre and of matrix

$$G\_f := \frac{E\_f}{2\cdot(1-\nu\_f)} \qquad G\_m := \frac{E\_m}{2\cdot(1-\nu\_m)}$$

$$G\_f = 4.487\times 10^{10}\,\text{Pa} \qquad G\_m = 4.098\times 10^{9}\,\text{Pa}$$

ply Young's moduli $E11 := V\_f\cdot E\_f + V\_m\cdot E\_m$ $\quad E22 := \dfrac{1}{\left(\frac{V\_m}{E\_m}\right)+\left(\frac{V\_f}{E\_f}\right)}$

$$E11 = 4.14\times 10^{10}\,\text{Pa} \qquad E22 = 1.042\times 10^{10}\,\text{Pa}$$

ply Poisson ratio $\nu 12 := V\_f\cdot\nu\_f + V\_m\cdot\nu\_m$ $\quad \nu 12 = 0.295$

ply shear modulus $G12 := \dfrac{G\_m}{V\_m + V\_f\cdot\frac{G\_m}{G\_f}}$ $\quad G12 = 8.344\times 10^{9}\,\text{Pa}$

ply thermal expansion coefficients

$$\alpha 11 := \frac{(\alpha\_f\cdot V\_f\cdot E\_f + \alpha\_m\cdot V\_m\cdot E\_m)}{(V\_f\cdot E\_f + V\_m\cdot E\_m)}$$

$$\alpha 11 = 7.828\times 10^{-6}\,\frac{1}{K}$$

$$\alpha 22 := V\_f\cdot\alpha\_f + V\_m\cdot\alpha\_m + \nu\_f\cdot V\_f\cdot\alpha\_f + \nu\_m\cdot V\_m\cdot\alpha\_m - \nu 12\cdot\alpha 11$$

$$\alpha 22 = 3.774\times 10^{-5}\,\frac{1}{K}$$

Matrix Transformation Matrix

$$m := \cos(\theta) \qquad n := \sin(\theta) \qquad T_i := \begin{bmatrix} (m_i)^2 & (n_i)^2 & 2\cdot m_i\cdot n_i \\ (n_i)^2 & (m_i)^2 & -2\cdot m_i\cdot n_i \\ (-m)_i\cdot n_i & m_i\cdot n_i & (m_i)^2-(n_i)^2 \end{bmatrix}$$

Ply Pre-Stress Strains

$$e\_P := \begin{pmatrix} -pre\_s \cdot \frac{V\_f}{E11} \\ \nu 12 \cdot pre\_s \cdot \frac{V\_f}{E11} \\ 0 \end{pmatrix} \qquad e\_P = \begin{pmatrix} 0 \\ 0 \\ 0 \end{pmatrix}$$

$$\varepsilon\_P_i := (T_i)^{-1} \cdot e\_P \qquad \varepsilon\_P_1 = \begin{pmatrix} 0 \\ 0 \\ 0 \end{pmatrix}$$

Ply Thermal Strains

$$e\_T := \begin{pmatrix} \alpha 11 \cdot \Delta T \\ \alpha 22 \cdot \Delta T \\ 0 \end{pmatrix} \qquad e\_T = \begin{pmatrix} -7.828 \times 10^{-4} \\ -3.774 \times 10^{-3} \\ 0 \end{pmatrix}$$

$$\varepsilon\_T_i := (T_i)^{-1} e\_T \qquad \varepsilon\_T_0 = \begin{pmatrix} -7.828 \times 10^{-4} \\ -3.774 \times 10^{-3} \\ 0 \end{pmatrix}$$

Ply Local Stiffness Matrix

$$delta := 1 - (\nu 12)^2 \cdot \frac{E22}{E11}$$

$$Q11 := \frac{E11}{delta} \qquad Q11 = 4.233 \times 10^{10}\,Pa$$

$$Q12 := \nu 12 \cdot \frac{E22}{delta} \qquad Q12 = 3.139 \times 10^{9}\,Pa$$

$$Q22 := \frac{E22}{delta} \qquad Q22 = 1.065 \times 10^{10}\,Pa$$

$$Q66 := G12 \qquad Q66 = 8.344 \times 10^{9}\,Pa$$

$$q := \begin{pmatrix} Q11 & Q12 & 0 \\ Q12 & Q22 & 0 \\ 0 & 0 & Q66 \end{pmatrix} \qquad q = \begin{pmatrix} 4.233 \times 10^{10} & 3.139 \times 10^{9} & 0 \\ 3.139 \times 10^{9} & 1.065 \times 10^{10} & 0 \\ 0 & 0 & 8.344 \times 10^{9} \end{pmatrix} Pa$$

Ply Global Stiffness Matrix

$$Qbar11_i := Q11\cdot\cos(\theta_i)^4 + 2(Q12 + 2Q66)\sin(\theta_i)^2\cos(\theta_i)^2 + Q22\cdot\sin(\theta_i)^4$$

$$Qbar12_i := (Q11 + Q22 - 4Q66)\sin(\theta_i)^2\cos(\theta_i)^2 + Q12\cdot\left(\sin(\theta_i)^4 + \cos(\theta_i)^4\right)$$

$$Qbar22_i := Q11\cdot\sin(\theta_i)^4 + 2(Q12 + 2Q66)\sin(\theta_i)^2\cos(\theta_i)^2 + Q22\cdot\cos(\theta_i)^4$$

$$Qbar16_i := (Q11 - Q12 - 2Q66)\cdot\sin(\theta_i)\cdot\cos(\theta_i)^3 + (Q12 - Q22 + 2Q66)\cdot\sin(\theta_i)^3\cdot\cos(\theta_i)$$

$$Qbar26_i := (Q11 - Q12 - 2\cdot Q66)\cdot\sin(\theta_i)^3\cdot\cos(\theta_i) + (Q12 - Q22 + 2\cdot Q66)\cdot\sin(\theta_i)\cdot\cos(\theta_i)^3$$

$$Qbar66_i := (Q11 + Q22 - 2Q12 - 2Q66)\sin(\theta_i)^2\cos(\theta_i)^2 + Q66\cdot\left(\sin(\theta_i)^4 + \cos(\theta_i)^4\right)$$

$$Qbar11_1 = 1.065\times 10^{10}\,\text{Pa} \qquad Qbar16_1 = 5.62\times 10^{-7}\,\text{Pa}$$

$$Qbar12_1 = 3.139\times 10^{9}\,\text{Pa} \qquad Qbar26_1 = 1.378\times 10^{-6}\,\text{Pa}$$

$$Qbar22_1 = 4.233\times 10^{10}\,\text{Pa} \qquad Qbar66_1 = 8.344\times 10^{9}\,\text{Pa}$$

$$Qbar_i := \begin{pmatrix} Qbar11_i & Qbar12_i & Qbar16_i \\ Qbar12_i & Qbar22_i & Qbar26_i \\ Qbar16_i & Qbar26_i & Qbar66_i \end{pmatrix} \quad Qbar_1 = \begin{pmatrix} 1.065\times 10^{10} & 3.139\times 10^{9} & 5.62\times 10^{-7} \\ 3.139\times 10^{9} & 4.233\times 10^{10} & 1.378\times 10^{-6} \\ 5.62\times 10^{-7} & 1.378\times 10^{-6} & 8.344\times 10^{9} \end{pmatrix}\text{Pa}$$

Laminate Loads

$$N\_P := t\_ply\cdot\sum_{k=0}^{15} Qbar_k\cdot\varepsilon\_P_k \qquad N\_P = \begin{pmatrix} 0 \\ 0 \\ 0 \end{pmatrix}\frac{kg}{s^2}$$

$$N\_T := t\_ply\cdot\sum_{k=0}^{15} Qbar_k\cdot\varepsilon\_T_k \qquad N\_T = \begin{pmatrix} -8.762\times 10^{4} \\ -8.762\times 10^{4} \\ -1.671\times 10^{-12} \end{pmatrix}\frac{kg}{s^2}$$

$$N := N\_P + N\_T \qquad N = \begin{pmatrix} -8.762\times 10^{4} \\ -8.762\times 10^{4} \\ -1.671\times 10^{-12} \end{pmatrix}\frac{kg}{s^2}$$

Laminate Stiffness and Compliance Matrices

$$A := t\_ply \cdot \sum_{k=0}^{15} Qbar_k \qquad A = \begin{pmatrix} 5.298 \times 10^{7} & 6.279 \times 10^{6} & 5.62 \times 10^{-10} \\ 6.279 \times 10^{6} & 5.298 \times 10^{7} & 1.378 \times 10^{-9} \\ 5.62 \times 10^{-10} & 1.378 \times 10^{-9} & 1.669 \times 10^{7} \end{pmatrix} \frac{kg}{s^2}$$

$$a := A^{-1} \qquad a = \begin{pmatrix} 1.915 \times 10^{-8} & -2.269 \times 10^{-9} & 0 \\ -2.269 \times 10^{-9} & 1.915 \times 10^{-8} & 0 \\ 0 & 0 & 5.992 \times 10^{-8} \end{pmatrix} \frac{s^2}{kg}$$

Laminate Mid-Plane Strains

$$\varepsilon 0 := a \cdot N \qquad \varepsilon 0 = \begin{pmatrix} -1.479 \times 10^{-3} \\ -1.479 \times 10^{-3} \\ 0 \end{pmatrix}$$

Ply Local Resultant Strains and Stresses

$$\varepsilon\_local_i := T_i \cdot \varepsilon 0 \qquad \sigma\_local_i := q \cdot (\varepsilon\_local_i - e\_T)$$

$$\varepsilon\_local_0 = \begin{pmatrix} -1.479 \times 10^{-3} \\ -1.479 \times 10^{-3} \\ 0 \end{pmatrix} \qquad \sigma\_local_0 = \begin{pmatrix} -2.225 \times 10^{7} \\ 2.225 \times 10^{7} \\ 5.985 \times 10^{-10} \end{pmatrix} Pa$$

Ply Internal Stresses and Strain

$$\begin{pmatrix} \varepsilon\_ply11 \\ \varepsilon\_ply22 \\ \gamma\_ply12 \end{pmatrix} := \varepsilon\_local$$

$$\sigma\_m := E\_m \cdot (\varepsilon\_ply11 - \alpha\_m \cdot \Delta T) \qquad \sigma\_m_0 = 2.261 \times 10^{7}\ Pa$$

$$\sigma\_f := E\_f \cdot (\varepsilon\_ply11 - \alpha\_f \cdot \Delta T) + pre\_s \qquad \sigma\_f_0 = -6.922 \times 10^{7}\ Pa$$

Ply Failure Analysis - Maximum Stress Criteria

Ply Strengths (these are measured from test on unidirectional coupons)

$F\_11T := 1.16GPa$

$F\_11C := 700MPa$

$F\_22T := 35.85MPa$

$F\_22C := 71.7MPa$

$F\_12 := 67MPa$

If the above analysis were to be carried out without pre-stress but with thermal effects the resulting strengths below would be the ply strength of a laminate corrected for ply thermal residual stresses. Therefore the improvement with pre-stress should be measured against these and not the ones quoted to the left.

Initial failure occurs in the laminate when the overall laminate loading causes a stress in a ply which exceed any of the above strengths. The mode of failure will be the one for which the stress has exceeded the corresponding strength (i.e. if the ply transverse tensile strength is exceeded first throught in-plane transverse loading of the ply, then this will be the intial failure mode).

The strengths are affected by pre-stress in the following way ...

$$F\_T\_noP := \begin{pmatrix} F\_11T \\ F\_22T \\ F\_12 \end{pmatrix} \qquad F\_T\_P_i := F\_T\_noP - \sigma\_local_i \qquad F\_T\_P_0 = \begin{pmatrix} 1.182 \times 10^9 \\ 1.36 \times 10^7 \\ 6.7 \times 10^7 \end{pmatrix} \text{Pa}$$

$$F\_C\_noP := \begin{pmatrix} -F\_11C \\ -F\_22C \\ F\_12 \end{pmatrix} \qquad F\_C\_P_i := F\_C\_noP - \sigma\_local_i \qquad F\_C\_P_0 = \begin{pmatrix} -6.777 \times 10^8 \\ -9.395 \times 10^7 \\ 6.7 \times 10^7 \end{pmatrix} \text{Pa}$$

Individual Predicted Ply Strengths

$$\begin{pmatrix} F\_11T\_P \\ F\_22T\_P \\ F\_12\_P \end{pmatrix} := \begin{pmatrix} F\_T\_P_0 \end{pmatrix} \qquad \begin{pmatrix} F\_11C\_P \\ F\_22C\_P \\ F\_12\_CP \end{pmatrix} := \begin{pmatrix} -F\_C\_P_0 \end{pmatrix}$$

Predicted Ply Strengths

$F\_11T\_P = 1.182 \times 10^9\ Pa$

$F\_11C\_P = 6.777 \times 10^8\ Pa$

$F\_22T\_P = 1.36 \times 10^7\ Pa$

$F\_22C\_P = 9.395 \times 10^7\ Pa$

$F\_12\_P = 6.7 \times 10^7\ Pa$

Measured UD Ply Strengths

$F\_11T = 1.16 \times 10^9\ Pa$

$F\_11C = 7 \times 10^8\ Pa$

$F\_22T = 3.585 \times 10^7\ Pa$

$F\_22C = 7.17 \times 10^7\ Pa$

$F\_12 = 6.7 \times 10^7\ Pa$

	Present	Temp only	30MPa	50MPa	70MPa	100MPa
F_11T	1.18E+09	1.22E+09	1.23E+09	1.23E+09	1.23E+09	1.24E+09
F_11C	6.78E+08	6.41E+08	6.35E+08	6.31E+08	6.26E+08	6.2E+08
F_22T	13596413	24619481	26592470	27907796	29223122	31196111
F_22C	93953587	82930519	80957530	79642204	78326878	76353889
F_12	67000000	67000000	67000000	67000000	67000000	67000000
Percentage Increase						
	Present	Temp only	30MPa	50MPa	70MPa	100MPa
F_11T	-2.98254	0	0.533836	0.889726	1.245617	1.779453
F_11C	5.66652	0	-1.01424	-1.69039	-2.36655	-3.38078
F_22T	-44.7738	0	8.013934	13.35656	18.69918	26.71311
F_22C	13.29193	0	-2.37909	-3.96514	-5.5512	-7.93029
F_12	0	0	0	0	0	0

$(F\_11T\_P \quad F\_11C\_P \quad F\_22T\_P \quad F\_22C\_P \quad F\_12)$

Analysis of Pre-Stressed Composite Laminates using Classical Laminate Analysis

This analysis is carried out specifically for the 16-ply cross-ply glass epoxy laminates used in this study.

Data Input

fibre pre-stress $pre\_s := 30MPa$

cured ply thickness $t\_ply := 0.125mm$

temperature change $\Delta T := -100K$

Fibre Material Data

Young's modulus $E\_f := 70GPa$

Poisson ratio $\nu\_f := 0.22$

thermal expansion coefficient $\alpha\_f := 4.9 \cdot 10^{-6} K^{-1}$

fibre volume fraction $V\_f := 0.56$

Matrix Material Data

Young's modulus $E\_m := 5GPa$

Poisson ratio $\nu\_m := 0.39$

thermal expansion coefficient $\alpha\_m := 60 \cdot 10^{-6} K^{-1}$

fibre volume fraction $V\_m := 1 - V\_f$ $V\_m = 0.44$

Ply Layup Data

$i := 0 .. 15$

$\theta :=$

Ply Number	Angle (degrees)	Angle (radians)
1	0	0
2	90	1.570796
3	90	1.570796
4	0	0
5	0	0
6	90	1.570796
7	0	0
8	90	1.570796
9	90	1.570796
10	0	0
11	90	1.570796
12	0	0
13	0	0
14	90	1.570796
15	90	1.570796
16	0	0

Derived Material Data

shear modulus of fibre and of matrix

$$G\_f := \frac{E\_f}{2\cdot(1-\nu\_f)} \qquad G\_m := \frac{E\_m}{2\cdot(1-\nu\_m)}$$

$$G\_f = 4.487\times 10^{10}\,\text{Pa} \qquad G\_m = 4.098\times 10^{9}\,\text{Pa}$$

ply Young's moduli $E11 := V\_f\cdot E\_f + V\_m\cdot E\_m$ $\quad E22 := \dfrac{1}{\left(\frac{V\_m}{E\_m}\right)+\left(\frac{V\_f}{E\_f}\right)}$

$$E11 = 4.14\times 10^{10}\,\text{Pa} \qquad E22 = 1.042\times 10^{10}\,\text{Pa}$$

ply Poisson ratio $\nu 12 := V\_f\cdot\nu\_f + V\_m\cdot\nu\_m$ $\quad \nu 12 = 0.295$

ply shear modulus $G12 := \dfrac{G\_m}{V\_m + V\_f\cdot\frac{G\_m}{G\_f}}$ $\quad G12 = 8.344\times 10^{9}\,\text{Pa}$

ply thermal expansion coefficients

$$\alpha 11 := \frac{(\alpha\_f\cdot V\_f\cdot E\_f + \alpha\_m\cdot V\_m\cdot E\_m)}{(V\_f\cdot E\_f + V\_m\cdot E\_m)}$$

$$\alpha 11 = 7.828\times 10^{-6}\,\frac{1}{K}$$

$$\alpha 22 := V\_f\cdot\alpha\_f + V\_m\cdot\alpha\_m + \nu\_f\cdot V\_f\cdot\alpha\_f + \nu\_m\cdot V\_m\cdot\alpha\_m - \nu 12\cdot\alpha 11$$

$$\alpha 22 = 3.774\times 10^{-5}\,\frac{1}{K}$$

Matrix Transformation Matrix

$$m := \cos(\theta) \qquad n := \sin(\theta) \qquad T_i := \begin{bmatrix} (m_i)^2 & (n_i)^2 & 2\cdot m_i\cdot n_i \\ (n_i)^2 & (m_i)^2 & -2\cdot m_i\cdot n_i \\ (-m)_i\cdot n_i & m_i\cdot n_i & (m_i)^2-(n_i)^2 \end{bmatrix}$$

Ply Pre-Stress Strains

$$e\_P := \begin{pmatrix} -pre\_s \cdot \frac{V\_f}{E11} \\ \nu 12 \cdot pre\_s \cdot \frac{V\_f}{E11} \\ 0 \end{pmatrix} \qquad e\_P = \begin{pmatrix} -4.058 \times 10^{-4} \\ 1.196 \times 10^{-4} \\ 0 \end{pmatrix}$$

$$\varepsilon\_P_i := (T_i)^{-1} \cdot e\_P \qquad \varepsilon\_P_1 = \begin{pmatrix} 1.196 \times 10^{-4} \\ -4.058 \times 10^{-4} \\ 0 \end{pmatrix}$$

Ply Thermal Strains

$$e\_T := \begin{pmatrix} \alpha 11 \cdot \Delta T \\ \alpha 22 \cdot \Delta T \\ 0 \end{pmatrix} \qquad e\_T = \begin{pmatrix} -7.828 \times 10^{-4} \\ -3.774 \times 10^{-3} \\ 0 \end{pmatrix}$$

$$\varepsilon\_T_i := (T_i)^{-1} e\_T \qquad \varepsilon\_T_0 = \begin{pmatrix} -7.828 \times 10^{-4} \\ -3.774 \times 10^{-3} \\ 0 \end{pmatrix}$$

Ply Local Stiffness Matrix

$$delta := 1 - (\nu 12)^2 \cdot \frac{E22}{E11}$$

$$Q11 := \frac{E11}{delta} \qquad Q11 = 4.233 \times 10^{10}\,Pa$$

$$Q12 := \nu 12 \cdot \frac{E22}{delta} \qquad Q12 = 3.139 \times 10^{9}\,Pa$$

$$Q22 := \frac{E22}{delta} \qquad Q22 = 1.065 \times 10^{10}\,Pa$$

$$Q66 := G12 \qquad Q66 = 8.344 \times 10^{9}\,Pa$$

$$q := \begin{pmatrix} Q11 & Q12 & 0 \\ Q12 & Q22 & 0 \\ 0 & 0 & Q66 \end{pmatrix} \qquad q = \begin{pmatrix} 4.233 \times 10^{10} & 3.139 \times 10^{9} & 0 \\ 3.139 \times 10^{9} & 1.065 \times 10^{10} & 0 \\ 0 & 0 & 8.344 \times 10^{9} \end{pmatrix} Pa$$

Ply Global Stiffness Matrix

$$Qbar11_i := Q11\cdot\cos(\theta_i)^4 + 2(Q12 + 2Q66)\sin(\theta_i)^2\cos(\theta_i)^2 + Q22\cdot\sin(\theta_i)^4$$

$$Qbar12_i := (Q11 + Q22 - 4Q66)\sin(\theta_i)^2\cos(\theta_i)^2 + Q12\cdot\left(\sin(\theta_i)^4 + \cos(\theta_i)^4\right)$$

$$Qbar22_i := Q11\cdot\sin(\theta_i)^4 + 2(Q12 + 2Q66)\sin(\theta_i)^2\cos(\theta_i)^2 + Q22\cdot\cos(\theta_i)^4$$

$$Qbar16_i := (Q11 - Q12 - 2Q66)\cdot\sin(\theta_i)\cdot\cos(\theta_i)^3 + (Q12 - Q22 + 2Q66)\cdot\sin(\theta_i)^3\cdot\cos(\theta_i)$$

$$Qbar26_i := (Q11 - Q12 - 2\cdot Q66)\cdot\sin(\theta_i)^3\cdot\cos(\theta_i) + (Q12 - Q22 + 2\cdot Q66)\cdot\sin(\theta_i)\cdot\cos(\theta_i)^3$$

$$Qbar66_i := (Q11 + Q22 - 2Q12 - 2Q66)\sin(\theta_i)^2\cos(\theta_i)^2 + Q66\cdot\left(\sin(\theta_i)^4 + \cos(\theta_i)^4\right)$$

$$Qbar11_1 = 1.065\times 10^{10}\,\text{Pa} \qquad Qbar16_1 = 5.62\times 10^{-7}\,\text{Pa}$$

$$Qbar12_1 = 3.139\times 10^{9}\,\text{Pa} \qquad Qbar26_1 = 1.378\times 10^{-6}\,\text{Pa}$$

$$Qbar22_1 = 4.233\times 10^{10}\,\text{Pa} \qquad Qbar66_1 = 8.344\times 10^{9}\,\text{Pa}$$

$$Qbar_i := \begin{pmatrix} Qbar11_i & Qbar12_i & Qbar16_i \\ Qbar12_i & Qbar22_i & Qbar26_i \\ Qbar16_i & Qbar26_i & Qbar66_i \end{pmatrix} \quad Qbar_1 = \begin{pmatrix} 1.065\times 10^{10} & 3.139\times 10^{9} & 5.62\times 10^{-7} \\ 3.139\times 10^{9} & 4.233\times 10^{10} & 1.378\times 10^{-6} \\ 5.62\times 10^{-7} & 1.378\times 10^{-6} & 8.344\times 10^{9} \end{pmatrix}\text{Pa}$$

Laminate Loads

$$N\_P := t\_ply\cdot\sum_{k=0}^{15} Qbar_k\cdot\varepsilon\_P_k \qquad N\_P = \begin{pmatrix} -1.68\times 10^{4} \\ -1.68\times 10^{4} \\ -7.602\times 10^{-13} \end{pmatrix}\frac{kg}{s^2}$$

$$N\_T := t\_ply\cdot\sum_{k=0}^{15} Qbar_k\cdot\varepsilon\_T_k \qquad N\_T = \begin{pmatrix} -8.762\times 10^{4} \\ -8.762\times 10^{4} \\ -1.671\times 10^{-12} \end{pmatrix}\frac{kg}{s^2}$$

$$N := N\_P + N\_T \qquad N = \begin{pmatrix} -1.044\times 10^{5} \\ -1.044\times 10^{5} \\ -2.431\times 10^{-12} \end{pmatrix}\frac{kg}{s^2}$$

Laminate Stiffness and Compliance Matrices

$$A := t\_ply \cdot \sum_{k=0}^{15} Qbar_k \qquad A = \begin{pmatrix} 5.298 \times 10^{7} & 6.279 \times 10^{6} & 5.62 \times 10^{-10} \\ 6.279 \times 10^{6} & 5.298 \times 10^{7} & 1.378 \times 10^{-9} \\ 5.62 \times 10^{-10} & 1.378 \times 10^{-9} & 1.669 \times 10^{7} \end{pmatrix} \frac{kg}{s^2}$$

$$a := A^{-1} \qquad a = \begin{pmatrix} 1.915 \times 10^{-8} & -2.269 \times 10^{-9} & 0 \\ -2.269 \times 10^{-9} & 1.915 \times 10^{-8} & 0 \\ 0 & 0 & 5.992 \times 10^{-8} \end{pmatrix} \frac{s^2}{kg}$$

Laminate Mid-Plane Strains

$$\varepsilon 0 := a \cdot N \qquad \varepsilon 0 = \begin{pmatrix} -1.762 \times 10^{-3} \\ -1.762 \times 10^{-3} \\ 0 \end{pmatrix}$$

Ply Local Resultant Strains and Stresses

$$\varepsilon\_local_i := T_i \cdot \varepsilon 0 \qquad \sigma\_local_i := q \cdot (\varepsilon\_local_i - e\_T)$$

$$\varepsilon\_local_0 = \begin{pmatrix} -1.762 \times 10^{-3} \\ -1.762 \times 10^{-3} \\ 0 \end{pmatrix} \qquad \sigma\_local_0 = \begin{pmatrix} -3.514 \times 10^{7} \\ 1.834 \times 10^{7} \\ 4.934 \times 10^{-10} \end{pmatrix} Pa$$

Ply Internal Stresses and Strain

$$\begin{pmatrix} \varepsilon\_ply11 \\ \varepsilon\_ply22 \\ \gamma\_ply12 \end{pmatrix} := \varepsilon\_local$$

$$\sigma\_m := E\_m \cdot (\varepsilon\_ply11 - \alpha\_m \cdot \Delta T) \qquad \sigma\_m_0 = 2.119 \times 10^{7}\ Pa$$

$$\sigma\_f := E\_f \cdot (\varepsilon\_ply11 - \alpha\_f \cdot \Delta T) + pre\_s \qquad \sigma\_f_0 = -5.906 \times 10^{7}\ Pa$$

Ply Failure Analysis - Maximum Stress Criteria

Ply Strengths (these are measured from test on unidirectional coupons)

$F\_11T := 1.16GPa$

$F\_11C := 700MPa$

$F\_22T := 35.85MPa$

$F\_22C := 71.7MPa$

$F\_12 := 67MPa$

If the above analysis were to be carried out without pre-stress but with thermal effects the resulting strengths below would be the ply strength of a laminate corrected for ply thermal residual stresses. Therefore the improvement with pre-stress should be measured against these and not the ones quoted to the left.

Initial failure occurs in the laminate when the overall laminate loading causes a stress in a ply which exceed any of the above strengths. The mode of failure will be the one for which the stress has exceeded the corresponding strength (i.e. if the ply transverse tensile strength is exceeded first throught in-plane transverse loading of the ply, then this will be the intial failure mode).

The strengths are affected by pre-stress in the following way ...

$$F\_T\_noP := \begin{pmatrix} F\_11T \\ F\_22T \\ F\_12 \end{pmatrix} \qquad F\_T\_P_i := F\_T\_noP - \sigma\_local_i \qquad F\_T\_P_0 = \begin{pmatrix} 1.195 \times 10^9 \\ 1.751 \times 10^7 \\ 6.7 \times 10^7 \end{pmatrix} Pa$$

$$F\_C\_noP := \begin{pmatrix} -F\_11C \\ -F\_22C \\ F\_12 \end{pmatrix} \qquad F\_C\_P_i := F\_C\_noP - \sigma\_local_i \qquad F\_C\_P_0 = \begin{pmatrix} -6.649 \times 10^8 \\ -9.004 \times 10^7 \\ 6.7 \times 10^7 \end{pmatrix} Pa$$

Individual Predicted Ply Strengths

$$\begin{pmatrix} F\_11T\_P \\ F\_22T\_P \\ F\_12\_P \end{pmatrix} := \begin{pmatrix} F\_T\_P_0 \end{pmatrix} \qquad \begin{pmatrix} F\_11C\_P \\ F\_22C\_P \\ F\_12\_CP \end{pmatrix} := \begin{pmatrix} -F\_C\_P_0 \end{pmatrix}$$

Predicted Ply Strengths

$F\_11T\_P = 1.195 \times 10^9\ Pa$

$F\_11C\_P = 6.649 \times 10^8\ Pa$

$F\_22T\_P = 1.751 \times 10^7\ Pa$

$F\_22C\_P = 9.004 \times 10^7\ Pa$

$F\_12\_P = 6.7 \times 10^7\ Pa$

Measured UD Ply Strengths

$F\_11T = 1.16 \times 10^9\ Pa$

$F\_11C = 7 \times 10^8\ Pa$

$F\_22T = 3.585 \times 10^7\ Pa$

$F\_22C = 7.17 \times 10^7\ Pa$

$F\_12 = 6.7 \times 10^7\ Pa$

	Present	Temp only	30MPa	50MPa	70MPa	100MPa
F_11T	1.2E+09	1.22E+09	1.23E+09	1.23E+09	1.23E+09	1.24E+09
F_11C	6.65E+08	6.41E+08	6.35E+08	6.31E+08	6.26E+08	6.2E+08
F_22T	17505946	24619481	26592470	27907796	29223122	31196111
F_22C	90044054	82930519	80957530	79642204	78326878	76353889
F_12	67000000	67000000	67000000	67000000	67000000	67000000
Percentage Increase						
	Present	Temp only	30MPa	50MPa	70MPa	100MPa
F_11T	-1.92472	0	0.533836	0.889726	1.245617	1.779453
F_11C	3.656785	0	-1.01424	-1.69039	-2.36655	-3.38078
F_22T	-28.8939	0	8.013934	13.35656	18.69918	26.71311
F_22C	8.577705	0	-2.37909	-3.96514	-5.5512	-7.93029
F_12	0	0	0	0	0	0

$(F\_11T\_P \quad F\_11C\_P \quad F\_22T\_P \quad F\_22C\_P \quad F\_12)$

Analysis of Pre-Stressed Composite Laminates using Classical Laminate Analysis

This analysis is carried out specifically for the 16-ply cross-ply glass epoxy laminates used in this study.

Data Input

fibre pre-stress $pre\_s := 50MPa$

cured ply thickness $t\_ply := 0.125mm$

temperature change $\Delta T := -100K$

Fibre Material Data

Young's modulus $E\_f := 70GPa$

Poisson ratio $\nu\_f := 0.22$

thermal expansion coefficient $\alpha\_f := 4.9 \cdot 10^{-6} K^{-1}$

fibre volume fraction $V\_f := 0.56$

Matrix Material Data

Young's modulus $E\_m := 5GPa$

Poisson ratio $\nu\_m := 0.39$

thermal expansion coefficient $\alpha\_m := 60 \cdot 10^{-6} K^{-1}$

fibre volume fraction $V\_m := 1 - V\_f$ $V\_m = 0.44$

Ply Layup Data

$i := 0 .. 15$

$\theta :=$

Ply Number	Angle (degrees)	Angle (radians)
1	0	0
2	90	1.570796
3	90	1.570796
4	0	0
5	0	0
6	90	1.570796
7	0	0
8	90	1.570796
9	90	1.570796
10	0	0
11	90	1.570796
12	0	0
13	0	0
14	90	1.570796
15	90	1.570796
16	0	0

Derived Material Data

shear modulus of fibre and of matrix

$$G\_f := \frac{E\_f}{2\cdot(1-\nu\_f)} \qquad G\_m := \frac{E\_m}{2\cdot(1-\nu\_m)}$$

$$G\_f = 4.487\times 10^{10}\,\text{Pa} \qquad G\_m = 4.098\times 10^{9}\,\text{Pa}$$

ply Young's moduli $E11 := V\_f\cdot E\_f + V\_m\cdot E\_m$ $\quad E22 := \dfrac{1}{\left(\frac{V\_m}{E\_m}\right)+\left(\frac{V\_f}{E\_f}\right)}$

$$E11 = 4.14\times 10^{10}\,\text{Pa} \qquad E22 = 1.042\times 10^{10}\,\text{Pa}$$

ply Poisson ratio $\nu 12 := V\_f\cdot\nu\_f + V\_m\cdot\nu\_m$ $\quad \nu 12 = 0.295$

ply shear modulus $G12 := \dfrac{G\_m}{V\_m + V\_f\cdot\frac{G\_m}{G\_f}}$ $\quad G12 = 8.344\times 10^{9}\,\text{Pa}$

ply thermal expansion coefficients

$$\alpha 11 := \frac{(\alpha\_f\cdot V\_f\cdot E\_f + \alpha\_m\cdot V\_m\cdot E\_m)}{(V\_f\cdot E\_f + V\_m\cdot E\_m)}$$

$$\alpha 11 = 7.828\times 10^{-6}\,\frac{1}{K}$$

$$\alpha 22 := V\_f\cdot\alpha\_f + V\_m\cdot\alpha\_m + \nu\_f\cdot V\_f\cdot\alpha\_f + \nu\_m\cdot V\_m\cdot\alpha\_m - \nu 12\cdot\alpha 11$$

$$\alpha 22 = 3.774\times 10^{-5}\,\frac{1}{K}$$

Matrix Transformation Matrix

$$m := \cos(\theta) \qquad n := \sin(\theta) \qquad T_i := \begin{bmatrix} (m_i)^2 & (n_i)^2 & 2\cdot m_i\cdot n_i \\ (n_i)^2 & (m_i)^2 & -2\cdot m_i\cdot n_i \\ (-m)_i\cdot n_i & m_i\cdot n_i & (m_i)^2-(n_i)^2 \end{bmatrix}$$

Ply Pre-Stress Strains

$$e\_P := \begin{pmatrix} -pre\_s \cdot \frac{V\_f}{E11} \\ \nu 12 \cdot pre\_s \cdot \frac{V\_f}{E11} \\ 0 \end{pmatrix} \qquad e\_P = \begin{pmatrix} -6.763 \times 10^{-4} \\ 1.994 \times 10^{-4} \\ 0 \end{pmatrix}$$

$$\varepsilon\_P_i := (T_i)^{-1} \cdot e\_P \qquad \varepsilon\_P_1 = \begin{pmatrix} 1.994 \times 10^{-4} \\ -6.763 \times 10^{-4} \\ 0 \end{pmatrix}$$

Ply Thermal Strains

$$e\_T := \begin{pmatrix} \alpha 11 \cdot \Delta T \\ \alpha 22 \cdot \Delta T \\ 0 \end{pmatrix} \qquad e\_T = \begin{pmatrix} -7.828 \times 10^{-4} \\ -3.774 \times 10^{-3} \\ 0 \end{pmatrix}$$

$$\varepsilon\_T_i := (T_i)^{-1} e\_T \qquad \varepsilon\_T_0 = \begin{pmatrix} -7.828 \times 10^{-4} \\ -3.774 \times 10^{-3} \\ 0 \end{pmatrix}$$

Ply Local Stiffness Matrix

$$delta := 1 - (\nu 12)^2 \cdot \frac{E22}{E11}$$

$$Q11 := \frac{E11}{delta} \qquad Q11 = 4.233 \times 10^{10}\,Pa$$

$$Q12 := \nu 12 \cdot \frac{E22}{delta} \qquad Q12 = 3.139 \times 10^{9}\,Pa$$

$$Q22 := \frac{E22}{delta} \qquad Q22 = 1.065 \times 10^{10}\,Pa$$

$$Q66 := G12 \qquad Q66 = 8.344 \times 10^{9}\,Pa$$

$$q := \begin{pmatrix} Q11 & Q12 & 0 \\ Q12 & Q22 & 0 \\ 0 & 0 & Q66 \end{pmatrix} \qquad q = \begin{pmatrix} 4.233 \times 10^{10} & 3.139 \times 10^{9} & 0 \\ 3.139 \times 10^{9} & 1.065 \times 10^{10} & 0 \\ 0 & 0 & 8.344 \times 10^{9} \end{pmatrix} Pa$$

Ply Global Stiffness Matrix

$$Qbar11_i := Q11\cdot\cos(\theta_i)^4 + 2(Q12 + 2Q66)\sin(\theta_i)^2\cos(\theta_i)^2 + Q22\cdot\sin(\theta_i)^4$$

$$Qbar12_i := (Q11 + Q22 - 4Q66)\sin(\theta_i)^2\cos(\theta_i)^2 + Q12\cdot\left(\sin(\theta_i)^4 + \cos(\theta_i)^4\right)$$

$$Qbar22_i := Q11\cdot\sin(\theta_i)^4 + 2(Q12 + 2Q66)\sin(\theta_i)^2\cos(\theta_i)^2 + Q22\cdot\cos(\theta_i)^4$$

$$Qbar16_i := (Q11 - Q12 - 2Q66)\cdot\sin(\theta_i)\cdot\cos(\theta_i)^3 + (Q12 - Q22 + 2Q66)\cdot\sin(\theta_i)^3\cdot\cos(\theta_i)$$

$$Qbar26_i := (Q11 - Q12 - 2\cdot Q66)\cdot\sin(\theta_i)^3\cdot\cos(\theta_i) + (Q12 - Q22 + 2\cdot Q66)\cdot\sin(\theta_i)\cdot\cos(\theta_i)^3$$

$$Qbar66_i := (Q11 + Q22 - 2Q12 - 2Q66)\sin(\theta_i)^2\cos(\theta_i)^2 + Q66\cdot\left(\sin(\theta_i)^4 + \cos(\theta_i)^4\right)$$

$$Qbar11_1 = 1.065\times 10^{10}\,\text{Pa} \qquad Qbar16_1 = 5.62\times 10^{-7}\,\text{Pa}$$

$$Qbar12_1 = 3.139\times 10^{9}\,\text{Pa} \qquad Qbar26_1 = 1.378\times 10^{-6}\,\text{Pa}$$

$$Qbar22_1 = 4.233\times 10^{10}\,\text{Pa} \qquad Qbar66_1 = 8.344\times 10^{9}\,\text{Pa}$$

$$Qbar_i := \begin{pmatrix} Qbar11_i & Qbar12_i & Qbar16_i \\ Qbar12_i & Qbar22_i & Qbar26_i \\ Qbar16_i & Qbar26_i & Qbar66_i \end{pmatrix} \quad Qbar_1 = \begin{pmatrix} 1.065\times 10^{10} & 3.139\times 10^{9} & 5.62\times 10^{-7} \\ 3.139\times 10^{9} & 4.233\times 10^{10} & 1.378\times 10^{-6} \\ 5.62\times 10^{-7} & 1.378\times 10^{-6} & 8.344\times 10^{9} \end{pmatrix}\text{Pa}$$

Laminate Loads

$$N\_P := t\_ply\cdot\sum_{k=0}^{15} Qbar_k\cdot\varepsilon\_P_k \qquad N\_P = \begin{pmatrix} -2.8\times 10^{4} \\ -2.8\times 10^{4} \\ -1.267\times 10^{-12} \end{pmatrix}\frac{kg}{s^2}$$

$$N\_T := t\_ply\cdot\sum_{k=0}^{15} Qbar_k\cdot\varepsilon\_T_k \qquad N\_T = \begin{pmatrix} -8.762\times 10^{4} \\ -8.762\times 10^{4} \\ -1.671\times 10^{-12} \end{pmatrix}\frac{kg}{s^2}$$

$$N := N\_P + N\_T \qquad N = \begin{pmatrix} -1.156\times 10^{5} \\ -1.156\times 10^{5} \\ -2.938\times 10^{-12} \end{pmatrix}\frac{kg}{s^2}$$

Laminate Stiffness and Compliance Matrices

$$A := t\_ply \cdot \sum_{k=0}^{15} Qbar_k \qquad A = \begin{pmatrix} 5.298 \times 10^{7} & 6.279 \times 10^{6} & 5.62 \times 10^{-10} \\ 6.279 \times 10^{6} & 5.298 \times 10^{7} & 1.378 \times 10^{-9} \\ 5.62 \times 10^{-10} & 1.378 \times 10^{-9} & 1.669 \times 10^{7} \end{pmatrix} \frac{kg}{s^2}$$

$$a := A^{-1} \qquad a = \begin{pmatrix} 1.915 \times 10^{-8} & -2.269 \times 10^{-9} & 0 \\ -2.269 \times 10^{-9} & 1.915 \times 10^{-8} & 0 \\ 0 & 0 & 5.992 \times 10^{-8} \end{pmatrix} \frac{s^2}{kg}$$

Laminate Mid-Plane Strains

$$\varepsilon 0 := a \cdot N \qquad \varepsilon 0 = \begin{pmatrix} -1.951 \times 10^{-3} \\ -1.951 \times 10^{-3} \\ 0 \end{pmatrix}$$

Ply Local Resultant Strains and Stresses

$$\varepsilon\_local_i := T_i \cdot \varepsilon 0 \qquad \sigma\_local_i := q \cdot (\varepsilon\_local_i - e\_T)$$

$$\varepsilon\_local_0 = \begin{pmatrix} -1.951 \times 10^{-3} \\ -1.951 \times 10^{-3} \\ 0 \end{pmatrix} \qquad \sigma\_local_0 = \begin{pmatrix} -4.374 \times 10^{7} \\ 1.574 \times 10^{7} \\ 4.233 \times 10^{-10} \end{pmatrix} Pa$$

Ply Internal Stresses and Strain

$$\begin{pmatrix} \varepsilon\_ply11 \\ \varepsilon\_ply22 \\ \gamma\_ply12 \end{pmatrix} := \varepsilon\_local$$

$$\sigma\_m := E\_m \cdot (\varepsilon\_ply11 - \alpha\_m \cdot \Delta T) \qquad \sigma\_m_0 = 2.024 \times 10^{7}\ Pa$$

$$\sigma\_f := E\_f \cdot (\varepsilon\_ply11 - \alpha\_f \cdot \Delta T) + pre\_s \qquad \sigma\_f_0 = -5.229 \times 10^{7}\ Pa$$

Ply Failure Analysis - Maximum Stress Criteria

Ply Strengths (these are measured from test on unidirectional coupons)

$F\_11T := 1.16GPa$

$F\_11C := 700MPa$

$F\_22T := 35.85MPa$

$F\_22C := 71.7MPa$

$F\_12 := 67MPa$

If the above analysis were to be carried out without pre-stress but with thermal effects the resulting strengths below would be the ply strength of a laminate corrected for ply thermal residual stresses. Therefore the improvement with pre-stress should be measured against these and not the ones quoted to the left.

Initial failure occurs in the laminate when the overall laminate loading causes a stress in a ply which exceed any of the above strengths. The mode of failure will be the one for which the stress has exceeded the corresponding strength (i.e. if the ply transverse tensile strength is exceeded first throught in-plane transverse loading of the ply, then this will be the intial failure mode).

The strengths are affected by pre-stress in the following way ...

$$F\_T\_noP := \begin{pmatrix} F\_11T \\ F\_22T \\ F\_12 \end{pmatrix} \qquad F\_T\_P_i := F\_T\_noP - \sigma\_local_i \qquad F\_T\_P_0 = \begin{pmatrix} 1.204 \times 10^9 \\ 2.011 \times 10^7 \\ 6.7 \times 10^7 \end{pmatrix} \text{Pa}$$

$$F\_C\_noP := \begin{pmatrix} -F\_11C \\ -F\_22C \\ F\_12 \end{pmatrix} \qquad F\_C\_P_i := F\_C\_noP - \sigma\_local_i \qquad F\_C\_P_0 = \begin{pmatrix} -6.563 \times 10^8 \\ -8.744 \times 10^7 \\ 6.7 \times 10^7 \end{pmatrix} \text{Pa}$$

Individual Predicted Ply Strengths

$$\begin{pmatrix} F\_11T\_P \\ F\_22T\_P \\ F\_12\_P \end{pmatrix} := \begin{pmatrix} F\_T\_P_0 \\ \\ \end{pmatrix} \qquad \begin{pmatrix} F\_11C\_P \\ F\_22C\_P \\ F\_12\_CP \end{pmatrix} := \begin{pmatrix} -F\_C\_P_0 \\ \\ \end{pmatrix}$$

Predicted Ply Strengths

$F\_11T\_P = 1.204 \times 10^9\ Pa$

$F\_11C\_P = 6.563 \times 10^8\ Pa$

$F\_22T\_P = 2.011 \times 10^7\ Pa$

$F\_22C\_P = 8.744 \times 10^7\ Pa$

$F\_12\_P = 6.7 \times 10^7\ Pa$

Measured UD Ply Strengths

$F\_11T = 1.16 \times 10^9\ Pa$

$F\_11C = 7 \times 10^8\ Pa$

$F\_22T = 3.585 \times 10^7\ Pa$

$F\_22C = 7.17 \times 10^7\ Pa$

$F\_12 = 6.7 \times 10^7\ Pa$

	Present	Temp only	30MPa	50MPa	70MPa	100MPa
F_11T	1.2E+09	1.22E+09	1.23E+09	1.23E+09	1.23E+09	1.24E+09
F_11C	6.56E+08	6.41E+08	6.35E+08	6.31E+08	6.26E+08	6.2E+08
F_22T	20112301	24619481	26592470	27907796	29223122	31196111
F_22C	87437699	82930519	80957530	79642204	78326878	76353889
F_12	67000000	67000000	67000000	67000000	67000000	67000000
Percentage Increase						
	Present	Temp only	30MPa	50MPa	70MPa	100MPa
F_11T	-1.21952	0	0.533836	0.889726	1.245617	1.779453
F_11C	2.316962	0	-1.01424	-1.69039	-2.36655	-3.38078
F_22T	-18.3074	0	8.013934	13.35656	18.69918	26.71311
F_22C	5.434887	0	-2.37909	-3.96514	-5.5512	-7.93029
F_12	0	0	0	0	0	0

$(F\_11T\_P \quad F\_11C\_P \quad F\_22T\_P \quad F\_22C\_P \quad F\_12)$

Analysis of Pre-Stressed Composite Laminates using Classical Laminate Analysis

This analysis is carried out specifically for the 16-ply cross-ply glass epoxy laminates used in this study.

Data Input

fibre pre-stress $pre\_s := 70MPa$

cured ply thickness $t\_ply := 0.125mm$

temperature change $\Delta T := -100K$

Fibre Material Data

Young's modulus $E\_f := 70GPa$

Poisson ratio $\nu\_f := 0.22$

thermal expansion coefficient $\alpha\_f := 4.9 \cdot 10^{-6} K^{-1}$

fibre volume fraction $V\_f := 0.56$

Matrix Material Data

Young's modulus $E\_m := 5GPa$

Poisson ratio $\nu\_m := 0.39$

thermal expansion coefficient $\alpha\_m := 60 \cdot 10^{-6} K^{-1}$

fibre volume fraction $V\_m := 1 - V\_f$ $V\_m = 0.44$

Ply Layup Data

$i := 0 .. 15$

$\theta :=$

Ply Number	Angle (degrees)	Angle (radians)
1	0	0
2	90	1.570796
3	90	1.570796
4	0	0
5	0	0
6	90	1.570796
7	0	0
8	90	1.570796
9	90	1.570796
10	0	0
11	90	1.570796
12	0	0
13	0	0
14	90	1.570796
15	90	1.570796
16	0	0

Derived Material Data

shear modulus of fibre and of matrix

$$G\_f := \frac{E\_f}{2\cdot(1-\nu\_f)} \qquad G\_m := \frac{E\_m}{2\cdot(1-\nu\_m)}$$

$$G\_f = 4.487\times 10^{10}\,\text{Pa} \qquad G\_m = 4.098\times 10^{9}\,\text{Pa}$$

ply Young's moduli $E11 := V\_f\cdot E\_f + V\_m\cdot E\_m$ $\quad E22 := \dfrac{1}{\left(\frac{V\_m}{E\_m}\right)+\left(\frac{V\_f}{E\_f}\right)}$

$$E11 = 4.14\times 10^{10}\,\text{Pa} \qquad E22 = 1.042\times 10^{10}\,\text{Pa}$$

ply Poisson ratio $\nu 12 := V\_f\cdot\nu\_f + V\_m\cdot\nu\_m$ $\quad \nu 12 = 0.295$

ply shear modulus $G12 := \dfrac{G\_m}{V\_m + V\_f\cdot\frac{G\_m}{G\_f}}$ $\quad G12 = 8.344\times 10^{9}\,\text{Pa}$

ply thermal expansion coefficients

$$\alpha 11 := \frac{(\alpha\_f\cdot V\_f\cdot E\_f + \alpha\_m\cdot V\_m\cdot E\_m)}{(V\_f\cdot E\_f + V\_m\cdot E\_m)}$$

$$\alpha 11 = 7.828\times 10^{-6}\,\frac{1}{K}$$

$$\alpha 22 := V\_f\cdot\alpha\_f + V\_m\cdot\alpha\_m + \nu\_f\cdot V\_f\cdot\alpha\_f + \nu\_m\cdot V\_m\cdot\alpha\_m - \nu 12\cdot\alpha 11$$

$$\alpha 22 = 3.774\times 10^{-5}\,\frac{1}{K}$$

Matrix Transformation Matrix

$$m := \cos(\theta) \qquad n := \sin(\theta) \qquad T_i := \begin{bmatrix} (m_i)^2 & (n_i)^2 & 2\cdot m_i\cdot n_i \\ (n_i)^2 & (m_i)^2 & -2\cdot m_i\cdot n_i \\ (-m)_i\cdot n_i & m_i\cdot n_i & (m_i)^2-(n_i)^2 \end{bmatrix}$$

Ply Pre-Stress Strains

$$e\_P := \begin{pmatrix} -pre\_s \cdot \frac{V\_f}{E11} \\ \nu 12 \cdot pre\_s \cdot \frac{V\_f}{E11} \\ 0 \end{pmatrix} \qquad e\_P = \begin{pmatrix} -9.469 \times 10^{-4} \\ 2.791 \times 10^{-4} \\ 0 \end{pmatrix}$$

$$\varepsilon\_P_i := (T_i)^{-1} \cdot e\_P \qquad \varepsilon\_P_1 = \begin{pmatrix} 2.791 \times 10^{-4} \\ -9.469 \times 10^{-4} \\ 0 \end{pmatrix}$$

Ply Thermal Strains

$$e\_T := \begin{pmatrix} \alpha 11 \cdot \Delta T \\ \alpha 22 \cdot \Delta T \\ 0 \end{pmatrix} \qquad e\_T = \begin{pmatrix} -7.828 \times 10^{-4} \\ -3.774 \times 10^{-3} \\ 0 \end{pmatrix}$$

$$\varepsilon\_T_i := (T_i)^{-1} e\_T \qquad \varepsilon\_T_0 = \begin{pmatrix} -7.828 \times 10^{-4} \\ -3.774 \times 10^{-3} \\ 0 \end{pmatrix}$$

Ply Local Stiffness Matrix

$$delta := 1 - (\nu 12)^2 \cdot \frac{E22}{E11}$$

$$Q11 := \frac{E11}{delta} \qquad Q11 = 4.233 \times 10^{10}\,Pa$$

$$Q12 := \nu 12 \cdot \frac{E22}{delta} \qquad Q12 = 3.139 \times 10^{9}\,Pa$$

$$Q22 := \frac{E22}{delta} \qquad Q22 = 1.065 \times 10^{10}\,Pa$$

$$Q66 := G12 \qquad Q66 = 8.344 \times 10^{9}\,Pa$$

$$q := \begin{pmatrix} Q11 & Q12 & 0 \\ Q12 & Q22 & 0 \\ 0 & 0 & Q66 \end{pmatrix} \qquad q = \begin{pmatrix} 4.233 \times 10^{10} & 3.139 \times 10^{9} & 0 \\ 3.139 \times 10^{9} & 1.065 \times 10^{10} & 0 \\ 0 & 0 & 8.344 \times 10^{9} \end{pmatrix} Pa$$

Ply Global Stiffness Matrix

$$Qbar11_i := Q11\cdot\cos(\theta_i)^4 + 2(Q12 + 2Q66)\sin(\theta_i)^2\cos(\theta_i)^2 + Q22\cdot\sin(\theta_i)^4$$

$$Qbar12_i := (Q11 + Q22 - 4Q66)\sin(\theta_i)^2\cos(\theta_i)^2 + Q12\cdot\left(\sin(\theta_i)^4 + \cos(\theta_i)^4\right)$$

$$Qbar22_i := Q11\cdot\sin(\theta_i)^4 + 2(Q12 + 2Q66)\sin(\theta_i)^2\cos(\theta_i)^2 + Q22\cdot\cos(\theta_i)^4$$

$$Qbar16_i := (Q11 - Q12 - 2Q66)\cdot\sin(\theta_i)\cdot\cos(\theta_i)^3 + (Q12 - Q22 + 2Q66)\cdot\sin(\theta_i)^3\cdot\cos(\theta_i)$$

$$Qbar26_i := (Q11 - Q12 - 2\cdot Q66)\cdot\sin(\theta_i)^3\cdot\cos(\theta_i) + (Q12 - Q22 + 2\cdot Q66)\cdot\sin(\theta_i)\cdot\cos(\theta_i)^3$$

$$Qbar66_i := (Q11 + Q22 - 2Q12 - 2Q66)\sin(\theta_i)^2\cos(\theta_i)^2 + Q66\cdot\left(\sin(\theta_i)^4 + \cos(\theta_i)^4\right)$$

$$Qbar11_1 = 1.065\times 10^{10}\,\text{Pa} \qquad Qbar16_1 = 5.62\times 10^{-7}\,\text{Pa}$$

$$Qbar12_1 = 3.139\times 10^{9}\,\text{Pa} \qquad Qbar26_1 = 1.378\times 10^{-6}\,\text{Pa}$$

$$Qbar22_1 = 4.233\times 10^{10}\,\text{Pa} \qquad Qbar66_1 = 8.344\times 10^{9}\,\text{Pa}$$

$$Qbar_i := \begin{pmatrix} Qbar11_i & Qbar12_i & Qbar16_i \\ Qbar12_i & Qbar22_i & Qbar26_i \\ Qbar16_i & Qbar26_i & Qbar66_i \end{pmatrix} \quad Qbar_1 = \begin{pmatrix} 1.065\times 10^{10} & 3.139\times 10^{9} & 5.62\times 10^{-7} \\ 3.139\times 10^{9} & 4.233\times 10^{10} & 1.378\times 10^{-6} \\ 5.62\times 10^{-7} & 1.378\times 10^{-6} & 8.344\times 10^{9} \end{pmatrix}\text{Pa}$$

Laminate Loads

$$N\_P := t\_ply\cdot\sum_{k=0}^{15} Qbar_k\cdot\varepsilon\_P_k \qquad N\_P = \begin{pmatrix} -3.92\times 10^{4} \\ -3.92\times 10^{4} \\ -1.774\times 10^{-12} \end{pmatrix}\frac{kg}{s^2}$$

$$N\_T := t\_ply\cdot\sum_{k=0}^{15} Qbar_k\cdot\varepsilon\_T_k \qquad N\_T = \begin{pmatrix} -8.762\times 10^{4} \\ -8.762\times 10^{4} \\ -1.671\times 10^{-12} \end{pmatrix}\frac{kg}{s^2}$$

$$N := N\_P + N\_T \qquad N = \begin{pmatrix} -1.268\times 10^{5} \\ -1.268\times 10^{5} \\ -3.445\times 10^{-12} \end{pmatrix}\frac{kg}{s^2}$$

Laminate Stiffness and Compliance Matrices

$$A := t\_ply \cdot \sum_{k=0}^{15} Qbar_k \qquad A = \begin{pmatrix} 5.298 \times 10^{7} & 6.279 \times 10^{6} & 5.62 \times 10^{-10} \\ 6.279 \times 10^{6} & 5.298 \times 10^{7} & 1.378 \times 10^{-9} \\ 5.62 \times 10^{-10} & 1.378 \times 10^{-9} & 1.669 \times 10^{7} \end{pmatrix} \frac{kg}{s^2}$$

$$a := A^{-1} \qquad a = \begin{pmatrix} 1.915 \times 10^{-8} & -2.269 \times 10^{-9} & 0 \\ -2.269 \times 10^{-9} & 1.915 \times 10^{-8} & 0 \\ 0 & 0 & 5.992 \times 10^{-8} \end{pmatrix} \frac{s^2}{kg}$$

Laminate Mid-Plane Strains

$$\varepsilon 0 := a \cdot N \qquad \varepsilon 0 = \begin{pmatrix} -2.14 \times 10^{-3} \\ -2.14 \times 10^{-3} \\ 0 \end{pmatrix}$$

Ply Local Resultant Strains and Stresses

$$\varepsilon\_local_i := T_i \cdot \varepsilon 0 \qquad \sigma\_local_i := q \cdot (\varepsilon\_local_i - e\_T)$$

$$\varepsilon\_local_0 = \begin{pmatrix} -2.14 \times 10^{-3} \\ -2.14 \times 10^{-3} \\ 0 \end{pmatrix} \qquad \sigma\_local_0 = \begin{pmatrix} -5.233 \times 10^{7} \\ 1.313 \times 10^{7} \\ 3.532 \times 10^{-10} \end{pmatrix} Pa$$

Ply Internal Stresses and Strain

$$\begin{pmatrix} \varepsilon\_ply11 \\ \varepsilon\_ply22 \\ \gamma\_ply12 \end{pmatrix} := \varepsilon\_local$$

$$\sigma\_m := E\_m \cdot (\varepsilon\_ply11 - \alpha\_m \cdot \Delta T) \qquad \sigma\_m_0 = 1.93 \times 10^{7}\ Pa$$

$$\sigma\_f := E\_f \cdot (\varepsilon\_ply11 - \alpha\_f \cdot \Delta T) + pre\_s \qquad \sigma\_f_0 = -4.552 \times 10^{7}\ Pa$$

Ply Failure Analysis - Maximum Stress Criteria

Ply Strengths (these are measured from test on unidirectional coupons)

$F\_11T := 1.16GPa$

$F\_11C := 700MPa$

$F\_22T := 35.85MPa$

$F\_22C := 71.7MPa$

$F\_12 := 67MPa$

If the above analysis were to be carried out without pre-stress but with thermal effects the resulting strengths below would be the ply strength of a laminate corrected for ply thermal residual stresses. Therefore the improvement with pre-stress should be measured against these and not the ones quoted to the left.

Initial failure occurs in the laminate when the overall laminate loading causes a stress in a ply which exceed any of the above strengths. The mode of failure will be the one for which the stress has exceeded the corresponding strength (i.e. if the ply transverse tensile strength is exceeded first throught in-plane transverse loading of the ply, then this will be the intial failure mode).

The strengths are affected by pre-stress in the following way ...

$$F\_T\_noP := \begin{pmatrix} F\_11T \\ F\_22T \\ F\_12 \end{pmatrix} \qquad F\_T\_P_i := F\_T\_noP - \sigma\_local_i \qquad F\_T\_P_0 = \begin{pmatrix} 1.212 \times 10^9 \\ 2.272 \times 10^7 \\ 6.7 \times 10^7 \end{pmatrix} \text{Pa}$$

$$F\_C\_noP := \begin{pmatrix} -F\_11C \\ -F\_22C \\ F\_12 \end{pmatrix} \qquad F\_C\_P_i := F\_C\_noP - \sigma\_local_i \qquad F\_C\_P_0 = \begin{pmatrix} -6.477 \times 10^8 \\ -8.483 \times 10^7 \\ 6.7 \times 10^7 \end{pmatrix} \text{Pa}$$

Individual Predicted Ply Strengths

$$\begin{pmatrix} F\_11T\_P \\ F\_22T\_P \\ F\_12\_P \end{pmatrix} := \begin{pmatrix} F\_T\_P_0 \end{pmatrix} \qquad \begin{pmatrix} F\_11C\_P \\ F\_22C\_P \\ F\_12\_CP \end{pmatrix} := \begin{pmatrix} -F\_C\_P_0 \end{pmatrix}$$

Predicted Ply Strengths

$F\_11T\_P = 1.212 \times 10^9\ Pa$

$F\_11C\_P = 6.477 \times 10^8\ Pa$

$F\_22T\_P = 2.272 \times 10^7\ Pa$

$F\_22C\_P = 8.483 \times 10^7\ Pa$

$F\_12\_P = 6.7 \times 10^7\ Pa$

Measured UD Ply Strengths

$F\_11T = 1.16 \times 10^9\ Pa$

$F\_11C = 7 \times 10^8\ Pa$

$F\_22T = 3.585 \times 10^7\ Pa$

$F\_22C = 7.17 \times 10^7\ Pa$

$F\_12 = 6.7 \times 10^7\ Pa$

	Present	Temp only	30MPa	50MPa	70MPa	100MPa
F_11T	1.21E+09	1.22E+09	1.23E+09	1.23E+09	1.23E+09	1.24E+09
F_11C	6.48E+08	6.41E+08	6.35E+08	6.31E+08	6.26E+08	6.2E+08
F_22T	22718656	24619481	26592470	27907796	29223122	31196111
F_22C	84831344	82930519	80957530	79642204	78326878	76353889
F_12	67000000	67000000	67000000	67000000	67000000	67000000
Percentage Increase						
	Present	Temp only	30MPa	50MPa	70MPa	100MPa
F_11T	-0.51431	0	0.533836	0.889726	1.245617	1.779453
F_11C	0.977138	0	-1.01424	-1.69039	-2.36655	-3.38078
F_22T	-7.72082	0	8.013934	13.35656	18.69918	26.71311
F_22C	2.292069	0	-2.37909	-3.96514	-5.5512	-7.93029
F_12	0	0	0	0	0	0

$(F\_11T\_P \quad F\_11C\_P \quad F\_22T\_P \quad F\_22C\_P \quad F\_12)$

Analysis of Pre-Stressed Composite Laminates using Classical Laminate Analysis

This analysis is carried out specifically for the 16-ply cross-ply glass epoxy laminates used in this study.

Data Input

fibre pre-stress $pre\_s := 100MPa$

cured ply thickness $t\_ply := 0.125mm$

temperature change $\Delta T := -100K$

Fibre Material Data

Young's modulus $E\_f := 70GPa$

Poisson ratio $\nu\_f := 0.22$

thermal expansion coefficient $\alpha\_f := 4.9 \cdot 10^{-6} K^{-1}$

fibre volume fraction $V\_f := 0.56$

Matrix Material Data

Young's modulus $E\_m := 5GPa$

Poisson ratio $\nu\_m := 0.39$

thermal expansion coefficient $\alpha\_m := 60 \cdot 10^{-6} K^{-1}$

fibre volume fraction $V\_m := 1 - V\_f$ $V\_m = 0.44$

Ply Layup Data

$i := 0 .. 15$

$\theta :=$

Ply Number	Angle (degrees)	Angle (radians)
1	0	0
2	90	1.570796
3	90	1.570796
4	0	0
5	0	0
6	90	1.570796
7	0	0
8	90	1.570796
9	90	1.570796
10	0	0
11	90	1.570796
12	0	0
13	0	0
14	90	1.570796
15	90	1.570796
16	0	0

Derived Material Data

shear modulus of fibre and of matrix

$$G\_f := \frac{E\_f}{2\cdot(1-\nu\_f)} \qquad G\_m := \frac{E\_m}{2\cdot(1-\nu\_m)}$$

$$G\_f = 4.487\times 10^{10}\,\text{Pa} \qquad G\_m = 4.098\times 10^{9}\,\text{Pa}$$

ply Young's moduli $E11 := V\_f\cdot E\_f + V\_m\cdot E\_m$ $\quad E22 := \dfrac{1}{\left(\frac{V\_m}{E\_m}\right)+\left(\frac{V\_f}{E\_f}\right)}$

$$E11 = 4.14\times 10^{10}\,\text{Pa} \qquad E22 = 1.042\times 10^{10}\,\text{Pa}$$

ply Poisson ratio $\nu 12 := V\_f\cdot\nu\_f + V\_m\cdot\nu\_m$ $\quad \nu 12 = 0.295$

ply shear modulus $G12 := \dfrac{G\_m}{V\_m + V\_f\cdot\frac{G\_m}{G\_f}}$ $\quad G12 = 8.344\times 10^{9}\,\text{Pa}$

ply thermal expansion coefficients

$$\alpha 11 := \frac{(\alpha\_f\cdot V\_f\cdot E\_f + \alpha\_m\cdot V\_m\cdot E\_m)}{(V\_f\cdot E\_f + V\_m\cdot E\_m)}$$

$$\alpha 11 = 7.828\times 10^{-6}\,\frac{1}{K}$$

$$\alpha 22 := V\_f\cdot\alpha\_f + V\_m\cdot\alpha\_m + \nu\_f\cdot V\_f\cdot\alpha\_f + \nu\_m\cdot V\_m\cdot\alpha\_m - \nu 12\cdot\alpha 11$$

$$\alpha 22 = 3.774\times 10^{-5}\,\frac{1}{K}$$

Matrix Transformation Matrix

$$m := \cos(\theta) \qquad n := \sin(\theta) \qquad T_i := \begin{bmatrix} (m_i)^2 & (n_i)^2 & 2\cdot m_i\cdot n_i \\ (n_i)^2 & (m_i)^2 & -2\cdot m_i\cdot n_i \\ (-m)_i\cdot n_i & m_i\cdot n_i & (m_i)^2-(n_i)^2 \end{bmatrix}$$

Ply Pre-Stress Strains

$$e\_P := \begin{pmatrix} -pre\_s \cdot \frac{V\_f}{E11} \\ \nu 12 \cdot pre\_s \cdot \frac{V\_f}{E11} \\ 0 \end{pmatrix} \qquad e\_P = \begin{pmatrix} -1.353 \times 10^{-3} \\ 3.988 \times 10^{-4} \\ 0 \end{pmatrix}$$

$$\varepsilon\_P_i := (T_i)^{-1} \cdot e\_P \qquad \varepsilon\_P_1 = \begin{pmatrix} 3.988 \times 10^{-4} \\ -1.353 \times 10^{-3} \\ 0 \end{pmatrix}$$

Ply Thermal Strains

$$e\_T := \begin{pmatrix} \alpha 11 \cdot \Delta T \\ \alpha 22 \cdot \Delta T \\ 0 \end{pmatrix} \qquad e\_T = \begin{pmatrix} -7.828 \times 10^{-4} \\ -3.774 \times 10^{-3} \\ 0 \end{pmatrix}$$

$$\varepsilon\_T_i := (T_i)^{-1} e\_T \qquad \varepsilon\_T_0 = \begin{pmatrix} -7.828 \times 10^{-4} \\ -3.774 \times 10^{-3} \\ 0 \end{pmatrix}$$

Ply Local Stiffness Matrix

$$delta := 1 - (\nu 12)^2 \cdot \frac{E22}{E11}$$

$$Q11 := \frac{E11}{delta} \qquad Q11 = 4.233 \times 10^{10}\,Pa$$

$$Q12 := \nu 12 \cdot \frac{E22}{delta} \qquad Q12 = 3.139 \times 10^{9}\,Pa$$

$$Q22 := \frac{E22}{delta} \qquad Q22 = 1.065 \times 10^{10}\,Pa$$

$$Q66 := G12 \qquad Q66 = 8.344 \times 10^{9}\,Pa$$

$$q := \begin{pmatrix} Q11 & Q12 & 0 \\ Q12 & Q22 & 0 \\ 0 & 0 & Q66 \end{pmatrix} \qquad q = \begin{pmatrix} 4.233 \times 10^{10} & 3.139 \times 10^{9} & 0 \\ 3.139 \times 10^{9} & 1.065 \times 10^{10} & 0 \\ 0 & 0 & 8.344 \times 10^{9} \end{pmatrix} Pa$$

Ply Global Stiffness Matrix

$$Qbar11_i := Q11\cdot\cos(\theta_i)^4 + 2(Q12 + 2Q66)\sin(\theta_i)^2\cos(\theta_i)^2 + Q22\cdot\sin(\theta_i)^4$$

$$Qbar12_i := (Q11 + Q22 - 4Q66)\sin(\theta_i)^2\cos(\theta_i)^2 + Q12\cdot\left(\sin(\theta_i)^4 + \cos(\theta_i)^4\right)$$

$$Qbar22_i := Q11\cdot\sin(\theta_i)^4 + 2(Q12 + 2Q66)\sin(\theta_i)^2\cos(\theta_i)^2 + Q22\cdot\cos(\theta_i)^4$$

$$Qbar16_i := (Q11 - Q12 - 2Q66)\cdot\sin(\theta_i)\cdot\cos(\theta_i)^3 + (Q12 - Q22 + 2Q66)\cdot\sin(\theta_i)^3\cdot\cos(\theta_i)$$

$$Qbar26_i := (Q11 - Q12 - 2\cdot Q66)\cdot\sin(\theta_i)^3\cdot\cos(\theta_i) + (Q12 - Q22 + 2\cdot Q66)\cdot\sin(\theta_i)\cdot\cos(\theta_i)^3$$

$$Qbar66_i := (Q11 + Q22 - 2Q12 - 2Q66)\sin(\theta_i)^2\cos(\theta_i)^2 + Q66\cdot\left(\sin(\theta_i)^4 + \cos(\theta_i)^4\right)$$

$$Qbar11_1 = 1.065\times 10^{10}\,\text{Pa} \qquad Qbar16_1 = 5.62\times 10^{-7}\,\text{Pa}$$

$$Qbar12_1 = 3.139\times 10^{9}\,\text{Pa} \qquad Qbar26_1 = 1.378\times 10^{-6}\,\text{Pa}$$

$$Qbar22_1 = 4.233\times 10^{10}\,\text{Pa} \qquad Qbar66_1 = 8.344\times 10^{9}\,\text{Pa}$$

$$Qbar_i := \begin{pmatrix} Qbar11_i & Qbar12_i & Qbar16_i \\ Qbar12_i & Qbar22_i & Qbar26_i \\ Qbar16_i & Qbar26_i & Qbar66_i \end{pmatrix} \quad Qbar_1 = \begin{pmatrix} 1.065\times 10^{10} & 3.139\times 10^{9} & 5.62\times 10^{-7} \\ 3.139\times 10^{9} & 4.233\times 10^{10} & 1.378\times 10^{-6} \\ 5.62\times 10^{-7} & 1.378\times 10^{-6} & 8.344\times 10^{9} \end{pmatrix}\text{Pa}$$

Laminate Loads

$$N\_P := t\_ply\cdot\sum_{k=0}^{15} Qbar_k\cdot\varepsilon\_P_k \qquad N\_P = \begin{pmatrix} -5.6\times 10^{4} \\ -5.6\times 10^{4} \\ -2.534\times 10^{-12} \end{pmatrix}\frac{kg}{s^2}$$

$$N\_T := t\_ply\cdot\sum_{k=0}^{15} Qbar_k\cdot\varepsilon\_T_k \qquad N\_T = \begin{pmatrix} -8.762\times 10^{4} \\ -8.762\times 10^{4} \\ -1.671\times 10^{-12} \end{pmatrix}\frac{kg}{s^2}$$

$$N := N\_P + N\_T \qquad N = \begin{pmatrix} -1.436\times 10^{5} \\ -1.436\times 10^{5} \\ -4.205\times 10^{-12} \end{pmatrix}\frac{kg}{s^2}$$

Laminate Stiffness and Compliance Matrices

$$A := t\_ply \cdot \sum_{k=0}^{15} Qbar_k \qquad A = \begin{pmatrix} 5.298 \times 10^{7} & 6.279 \times 10^{6} & 5.62 \times 10^{-10} \\ 6.279 \times 10^{6} & 5.298 \times 10^{7} & 1.378 \times 10^{-9} \\ 5.62 \times 10^{-10} & 1.378 \times 10^{-9} & 1.669 \times 10^{7} \end{pmatrix} \frac{kg}{s^2}$$

$$a := A^{-1} \qquad a = \begin{pmatrix} 1.915 \times 10^{-8} & -2.269 \times 10^{-9} & 0 \\ -2.269 \times 10^{-9} & 1.915 \times 10^{-8} & 0 \\ 0 & 0 & 5.992 \times 10^{-8} \end{pmatrix} \frac{s^2}{kg}$$

Laminate Mid-Plane Strains

$$\varepsilon 0 := a \cdot N \qquad \varepsilon 0 = \begin{pmatrix} -2.424 \times 10^{-3} \\ -2.424 \times 10^{-3} \\ 0 \end{pmatrix}$$

Ply Local Resultant Strains and Stresses

$$\varepsilon\_local_i := T_i \cdot \varepsilon 0 \qquad \sigma\_local_i := q \cdot (\varepsilon\_local_i - e\_T)$$

$$\varepsilon\_local_0 = \begin{pmatrix} -2.424 \times 10^{-3} \\ -2.424 \times 10^{-3} \\ 0 \end{pmatrix} \qquad \sigma\_local_0 = \begin{pmatrix} -6.522 \times 10^{7} \\ 9.222 \times 10^{6} \\ 2.48 \times 10^{-10} \end{pmatrix} Pa$$

Ply Internal Stresses and Strain

$$\begin{pmatrix} \varepsilon\_ply11 \\ \varepsilon\_ply22 \\ \gamma\_ply12 \end{pmatrix} := \varepsilon\_local$$

$$\sigma\_m := E\_m \cdot (\varepsilon\_ply11 - \alpha\_m \cdot \Delta T) \qquad \sigma\_m_0 = 1.788 \times 10^{7}\, Pa$$

$$\sigma\_f := E\_f \cdot (\varepsilon\_ply11 - \alpha\_f \cdot \Delta T) + pre\_s \qquad \sigma\_f_0 = -3.537 \times 10^{7}\, Pa$$

Ply Failure Analysis - Maximum Stress Criteria

Ply Strengths (these are measured from test on unidirectional coupons)

$F\_11T := 1.16GPa$

$F\_11C := 700MPa$

$F\_22T := 35.85MPa$

$F\_22C := 71.7MPa$

$F\_12 := 67MPa$

If the above analysis were to be carried out without pre-stress but with thermal effects the resulting strengths below would be the ply strength of a laminate corrected for ply thermal residual stresses. Therefore the improvement with pre-stress should be measured against these and not the ones quoted to the left.

Initial failure occurs in the laminate when the overall laminate loading causes a stress in a ply which exceed any of the above strengths. The mode of failure will be the one for which the stress has exceeded the corresponding strength (i.e. if the ply transverse tensile strength is exceeded first throught in-plane transverse loading of the ply, then this will be the intial failure mode).

The strengths are affected by pre-stress in the following way ...

$$F\_T\_noP := \begin{pmatrix} F\_11T \\ F\_22T \\ F\_12 \end{pmatrix} \qquad F\_T\_P_i := F\_T\_noP - \sigma\_local_i \qquad F\_T\_P_0 = \begin{pmatrix} 1.225 \times 10^9 \\ 2.663 \times 10^7 \\ 6.7 \times 10^7 \end{pmatrix} \text{Pa}$$

$$F\_C\_noP := \begin{pmatrix} -F\_11C \\ -F\_22C \\ F\_12 \end{pmatrix} \qquad F\_C\_P_i := F\_C\_noP - \sigma\_local_i \qquad F\_C\_P_0 = \begin{pmatrix} -6.348 \times 10^8 \\ -8.092 \times 10^7 \\ 6.7 \times 10^7 \end{pmatrix} \text{Pa}$$

Individual Predicted Ply Strengths

$$\begin{pmatrix} F\_11T\_P \\ F\_22T\_P \\ F\_12\_P \end{pmatrix} := \begin{pmatrix} F\_T\_P_0 \end{pmatrix} \qquad \begin{pmatrix} F\_11C\_P \\ F\_22C\_P \\ F\_12\_CP \end{pmatrix} := \begin{pmatrix} -F\_C\_P_0 \end{pmatrix}$$

Predicted Ply Strengths

$F\_11T\_P = 1.225 \times 10^9\ Pa$

$F\_11C\_P = 6.348 \times 10^8\ Pa$

$F\_22T\_P = 2.663 \times 10^7\ Pa$

$F\_22C\_P = 8.092 \times 10^7\ Pa$

$F\_12\_P = 6.7 \times 10^7\ Pa$

Measured UD Ply Strengths

$F\_11T = 1.16 \times 10^9\ Pa$

$F\_11C = 7 \times 10^8\ Pa$

$F\_22T = 3.585 \times 10^7\ Pa$

$F\_22C = 7.17 \times 10^7\ Pa$

$F\_12 = 6.7 \times 10^7\ Pa$

	Present	Temp only	30MPa	50MPa	70MPa	100MPa
F_11T	1.23E+09	1.22E+09	1.23E+09	1.23E+09	1.23E+09	1.24E+09
F_11C	6.35E+08	6.41E+08	6.35E+08	6.31E+08	6.26E+08	6.2E+08
F_22T	26628189	24619481	26592470	27907796	29223122	31196111
F_22C	80921811	82930519	80957530	79642204	78326878	76353889
F_12	67000000	67000000	67000000	67000000	67000000	67000000
Percentage Increase						
	Present	Temp only	30MPa	50MPa	70MPa	100MPa
F_11T	0.5435	0	0.533836	0.889726	1.245617	1.779453
F_11C	-1.0326	0	-1.01424	-1.69039	-2.36655	-3.38078
F_22T	8.159019	0	8.013934	13.35656	18.69918	26.71311
F_22C	-2.42216	0	-2.37909	-3.96514	-5.5512	-7.93029
F_12	0	0	0	0	0	0

$(F\_11T\_P \quad F\_11C\_P \quad F\_22T\_P \quad F\_22C\_P \quad F\_12)$

APPENDIX F

CALCULATION OF THE PRE-STRESS INDUCED BY THE THERMAL EXPANSION OF THE STEEL FRAME

A one-dimensional analysis of the extent of pre-stress induced by the pre-stressing frame on the fibres in the laminate in one direction as a result of heating the system from ambient to room temperature

Data Input

Temperature Change $\Delta T := 100K$

Steel Frame Data

Young's Modulus $E\_S := 210GPa$

Thermal Expansion Coefficient $\alpha\_S := 12 \cdot 10^{-6} K^{-1}$

Cross-Sectional Area $A\_S := 1712mm^2$ i.e. two 76x38 channel sections

Taken from Steelwork Design Guide for BS 5950: Part 1: 1990

Fibre Data

Young's Modulus $E\_F := 70GPa$

Thermal Expansion Coefficient $\alpha\_F := 4.9 \cdot 10^{-6} K^{-1}$

Cross-Sectional Area $A\_F := 140mm^2$

Due to strain compatibilty the strains in the frame must equal the strain in the fibres, thus:
$\varepsilon = \varepsilon\_S = \varepsilon\_F$.
Also, as there are no external loads being applied the sum of all forces on the system must equal zero, i.e. $\Sigma P = 0$

Strain in Fibres and Steel Frame

$$\varepsilon := \alpha\_F \cdot \Delta T + \frac{\left[A\_S \cdot E\_S \cdot (\alpha\_S - \alpha\_F) \cdot \Delta T\right]}{(A\_S \cdot E\_S + A\_F \cdot E\_F)} \qquad \varepsilon = 1.181 \times 10^{-3}$$

Stress in Fibres

$$\sigma\_F := \frac{\left[A\_S \cdot E\_S \cdot E\_F \cdot (\alpha\_S - \alpha\_F) \cdot \Delta T\right]}{(A\_S \cdot E\_S + A\_F \cdot E\_F)} \qquad \sigma\_F = 4.838 \times 10^{7} Pa$$

Stress in Frame

$$\sigma\_S := \frac{\left[A\_F \cdot E\_F \cdot E\_S \cdot (\alpha\_S - \alpha\_F) \cdot \Delta T\right]}{(A\_S \cdot E\_S + A\_F \cdot E\_F)} \qquad \sigma\_S = 3.956 \times 10^{6} Pa$$

Applied Load

$$P := \frac{\left[A\_F \cdot E\_F \cdot A\_S \cdot E\_S \cdot (\alpha\_S - \alpha\_F) \cdot \Delta T\right]}{(A\_S \cdot E\_S + A\_F \cdot E\_F)} \qquad P = 6.773 \times 10^{3} N$$